Adam Mickiewicz University, Poznan

Faculty of Chemistry

Department of Physical Chemistry and Photochemistry

DARIA LAROWSKA-ZARYCH

Ph. D. Thesis

NON-COVALENT FUNCTIONALIZATION OF GRAPHENE OXIDE WITH PORPHYRIN DYES

Supervisor: Prof. dr. hab. Bronisław Marciniak

Co-supervisor: Prof. UAM dr. hab. Anna Lewandowska-Andrałojć

This thesis was submitted

to the Scientific Board of the Faculty of Chemistry

at the Adam Mickiewicz University

Poznań, 2023

Uniwersytet im. Adama Mickiewicza w Poznaniu

Wydział Chemii

Zakład Chemii Fizycznej i Fotochemii

DARIA LAROWSKA-ZARYCH

Praca doktorska

NIEKOWALENCYJNA FUNKCJONALIZACJA TLENKU GRAFENU BARWNIKAMI PORFIRYNOWYMI

Promotor: Prof. dr hab. Bronisław Marciniak

Promotor pomocniczy: Prof. UAM dr hab. Anna Lewandowska-Andrałojć

Praca przedstawiona Radzie Naukowej Wydziału Chemii
Uniwersytetu im. Adama Mickiewicza w Poznaniu
celem uzyskania stopnia doktora nauk chemicznych

Poznań, 2023

“I have not failed. I’ve just found 10,000 ways that won’t work”.

Thomas A. Edison

Adam Mickiewicz University, Poznan

Faculty of Chemistry

Department of Physical Chemistry and Photochemistry

Acknowledgements

I would like to express my deepest gratitude to **prof. dr. hab. Bronislaw Marciniak** for his guidance, valuable tips and advice throughout the whole period of my Ph.D. work, as well as constant support and encouragement.

„Mentoring is a brain to pick, an ear to listen and a push in the right direction" In terms of these words, I would like to special thanks to **prof. UAM dr. hab. Anna Lewandowska-Andrałojć** without whom I could not have undertaken this journey. Thank you!

Furthermore, I would like to express my warm and sincere thanks to people from Department of Physical Chemistry and Photochemistry for supportive and friendly atmosphere. Special thanks to **dr. Marta Ignasiak-Kciuk**, **dr. Piotr Filipiak** and **prof. UAM dr. hab. Tomasz Pędziński** for their extremely valuable experiences, support and numerous discussions. I would also thank **dr. Franciszek Kaźmierczak** and **dr. Katarzyna Taras-Goślińska** for friendliness and stimulating conversations.

Thanks should also go to **Ewelina Gacka**, **Katarzyna Krancewicz**, **Aleksandra Leśniewicz** and **Aleksander Kolman** for working together and for our scientific adventures. - May the force be with you!

Adam Mickiewicz University, Poznan

Faculty of Chemistry

Department of Physical Chemistry and Photochemistry

Acknowledgements

Thanks of course to my family for their support, especially my parents **Sylwia** and **Dariusz Larowscy**. They gave me love, support and strength to reach for the stars and chase my dreams. I also appreciate all the support I received from my brother, **Michał Larowski**.

My husband **Sebastian Zarych** deserves my wholehearted thanks as well, for understanding, encouragement and emotional support in my many, many moments of crisis .
I dedicate this work to our two-year-old son, **Bruno A. Zarych.**

Table of Contents

List of Abbreviations and Acronyms

AA – ascorbic acid

AFM – atomic force microscopy

AOP - advanced oxidation process

AQE - apparent quantum efficiency

CCG - chemically converted graphene

CR - charge recombination

CT – charge transfer

CTAB - cetrimonium bromide

EA - elemental analysis

ET – electron transfer

FQY - fluorescence quantum yield

GBM – graphene-based material

GC – gas chromatography

GNPs - graphene nanoplates

IFE - inner filter effect

IRF - instrument response function

LFP - laser flash photolysis

NPs - nanopoparticles

rGO – reduced graphene oxide

TA - transient absorption

TAPP - 5,10,15,20-tetra(4-aminophenyl)porphyrin

TCPP – 5,10,15,20-tetraka(4-carboxyphenyl)porphyrin

TCSPC - time-correlated single-photon counting

TEM - transmission electron microscopy

TEOA - triethanolamine

TGA - thermogravimetric analysis

TMAP – 5,10,15,20-tetra(4-trimethylammoniophenyl) porphyrin tetra(p-toluenesulfonate)

TMPyP- 5,10,15,20-tetra(1-methyl-4-pyridino) porphyrin tetra(p-toluenesulfonate)

TPC - transient photocurrent

TPP- 5,10,15,20-tetraphenyl-21,23-dihydroporphyrin

TPPH- 5,10,15,20-tetraka(4-(hydroxyl)phenyl) porphyrin

PET – photoinduced electron transfer

RhB – rhodamine B

1. Purpose of the research

The increasing demand for new safe functional materials with more effective, specific properties is expanding the horizons of current research worldwide. Graphene-based materials (GBM) have attracted interest because of their outstanding properties, such as large surface area, mechanical stability, and optical transmittance. The conjugated aromatic system has made these materials an ideal candidates for application as charge carriers or promoters. Additionally, the oxidized structure of graphene, namely - graphene oxide (GO), which includes various oxygen-based functional groups opens up the possibilities for its functionalization with other materials or molecules. Unlike graphene, GO can form stable aqueous suspensions, which makes it more suitable for some applications e.g. water splitting or dye photodegradation.

One of the promising way to functionalize the GBM is to cover its surface with light-harvesting molecules. An example of such type of molecules is porphyrins, because of their intense absorption in the visible region.[1]

Bringing these two individual components, graphene-based material and porphyrin molecule, into new hybrid materials may lead to important synergies.[2–5] The formation of the hybrid material can be achieved through the formation of covalent bonds between the components of the nanostructure or through non-covalent interactions (electrostatic, hydrogen bonding, van der Waals). In recent years, particular attention has been paid to porphyrin hybrids formed by non-covalent interactions. This interest results from the ease with which they can be prepared and the high efficiency of this process.

Significant interest among the scientific community in the construction of porphyrin- and graphene-based hybrid materials arises among others for possible application in photocatalytic processes. The non-covalent porphyrin/GBM hybrids are promising materials for improving the efficiency of photocatalytic systems such as organic dye photodegradation and hydrogen production systems. Because of the unique properties of GO and porphyrins, hybrid materials composed of these two were reported to be active in photocatalytic reactions and solar energy conversion processes. One of the challenges in increasing the efficiency of photocatalysis is to improve efficiency of charge separation.[6] In this regard, graphene materials are very promising in enhancing formation of the long-lived charge separation state.

However, research in this field lacks of comprehensive studies of the spectroscopic properties of hybrid materials, including both steady-state and time-resolved measurements (absorption and emission). It is believed that complete understanding of the spectroscopic properties of the porphyrin/GBM, including the dynamics of charge transfer, will pave the way to rationalize the design of novel materials for photocatalytic applications. With this as background, there is a need for studies that will provide in-depth understanding of factors affecting spectroscopic properties of porphyrin/GBM hybrids including photoinduced electron transfer. Filling this gap would make it easier and more efficient to design new materials for applications in the photocatalysis area.

2. Introduction and Literature Background

2.1 Graphene and graphene-based materials

Research on the structure of graphene material began in the mid-19th century. The name for this material was proposed in 1962 by Hans Peter Boehm. It was also him who initially characterized its structure using X-ray diffraction.[7]

Graphene was first isolated in 2004 by Andrei Geim and Konstantin Novoselov, who glued adhesive tape to a graphite block and then tore it off. Subsequently the surface of the tape was observed under a microscope. If the graphite layer was too thick, another piece of tape was glued to the tape. The operation was repeated until a single layer of graphene of satisfactory dimensions was obtained. In 2010, Geim and Novoselov received the Nobel Prize for their work on graphene.[7]

Graphene is one of the allotropic varieties of carbon. It is characterized by a two-dimensional lattice composed of carbon atoms with sp^2 hybridization. Carbon atoms form a flat (single-layer), hexagonal structure (***Figure 1***). It is a perfectly flat structure, and corrugations of the structure can only occur as a result of thermal fluctuations. The distances between carbon atoms are 0.0142 nm[8–11] (***Table 1***).

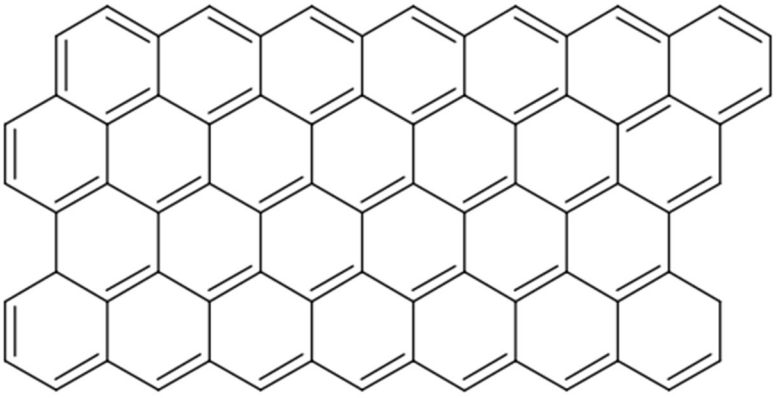

Figure 1 *Structure of graphene*

Graphene is often referred to as the strongest and thinnest material in the world. Even with such a strength, it is relatively flexible and thus can form different allotropes, such as carbon nanotubes, nanohorns, and fullerenes.[12–17] The band structure of graphene shows amazing conductivity and electron mobility (***Table*** **1**).

Table 1 *Exemplary graphene properties*

Property		Ref
electron mobility[1]	~200000–250000 $cm^2\ V^{-1}\ s^{-1}$	[18]
thermal conductivity	~5000 $W\ m^{-1}\ K^{-1}$	[7,19]
carbon-carbon bond length	0.0142 nm	[8]
electrical conductivity[2]	$6 \times 10^8\ S\ m^{-1}$	[20,21]

1 – at room temperature, 2- depends on the reduction technique

For the last almost 20 years, graphene and graphene-based materials have been a popular research topic because of their unique properties and various possible modification. The graphene-based materials were studied in various areas such as sensors, electronic and biomedical devices or water purification treatment (***Scheme 1***). Another important field of application of these materials is photocatalysis. The band structure of graphene shows amazing conductivity and electron mobility. When the superior conductivity of graphene is considered, its use as an electron acceptor and transporter provides an ideal way to design new dye-sensitized photocatalysts. However, graphene sheets are hydrophobic and tend to aggregate due to strong π-π interactions, which may limit their application for example in water splitting or dye photodegradation.

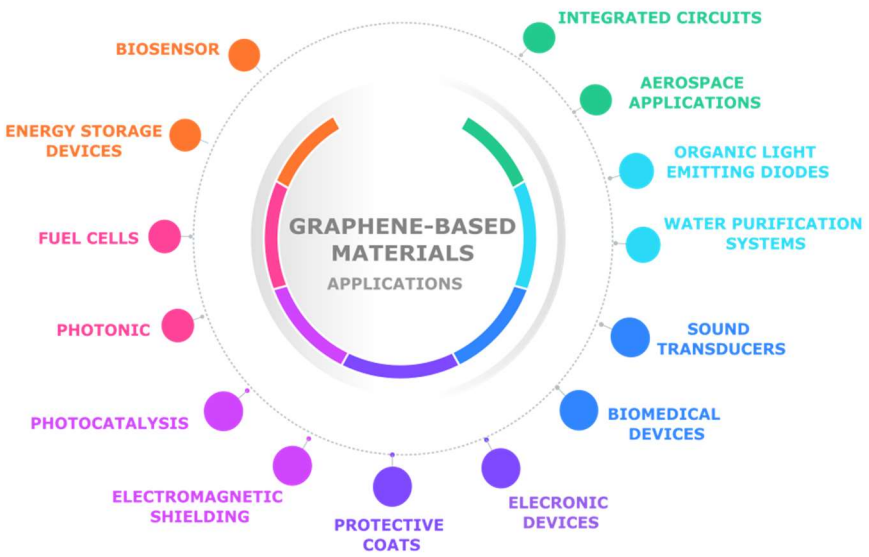

Scheme 1 *Exemplary applications of graphene-based materials*[7,22–33]

2.1.1 Graphene oxide and reduced graphene oxide

Graphene oxide (GO) is one of the most important forms of graphene which is a solution-dispersible[34], and it is commonly produced by chemical exfoliation of graphite through strong oxidization. It is widely considered as an individual 2D sheet (with a height of 0.8 to 1.0 nm)[35,36] of covalently bonded carbon atoms and is rich with oxygen functional groups (e.g. hydroxyl, epoxide, and carbonyl groups). The exact structure of GO has been the subject of debate for many years.[37] The most widely accepted structural model of GO is the Lerf–Klinowski model (***Scheme* 2**).[38] In this model the basal plane of GO is covalently surrounded by hydroxyl and epoxy groups, while at the edges of the sheets mainly carboxylic groups are found[39,40] (***Scheme* 2**). Therefore, GO contains aromatic (sp^2) and aliphatic (sp^3) domains which further expands the types of interactions that can occur with its surface. All of these functional groups present in the GO make it hydrophilic in nature, while the graphite and graphene are hydrophobic in nature. GO can be easily dispersed in water and other polar solvents (DMF, THF) to form stable colloidal suspensions[36,41] Formation of stable dispersion in water make GO suitable for applications in the photocatalytic processes that requires aqueous environment.[36]

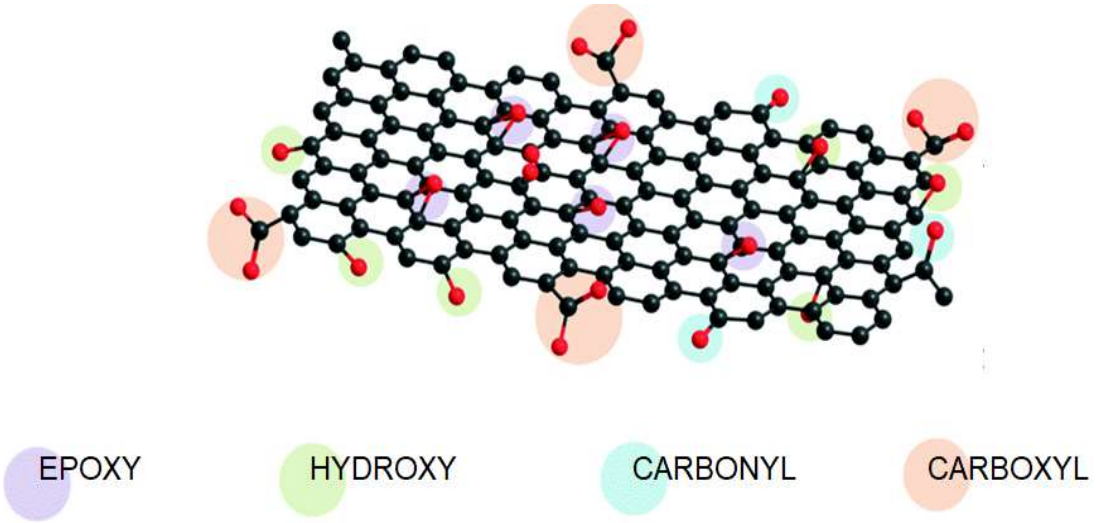

Scheme 2 *Schematic structure of GO*

The Hummer's method is the most commonly used method for the synthesis of graphene oxide. In brief, this method is based on oxidizing powdered graphite with $KMnO_4$.[42]

The GO material can be treated with a reducing agent – e.g. ascorbic acid (AA)[43] or hydrazine[41,44,45] to remove the oxygen functional groups and restore some of the aromaticity. Through this process, it is possible to obtain reduced graphene oxide (rGO).

Functionalization of GO

The wide interest in graphene and graphene-based materials results from the fact that they can be functionalized with organic molecules to obtain new graphene-based nanomaterials with different properties from pristine graphene-based material.[46] The modification of graphene oxide can be both covalent and non-covalent in nature[47,48] (***Scheme* 3**). Covalent linkages rely on the formation of covalent bond e.g amide or ester between functional groups of GO and organic molecule. The non-covalent chemical modification of graphene oxide with organic molecules is based on the molecular interactions, such as electrostatic attraction, π-π stacking and hydrogen bonding between graphene oxide and organic molecules. The great advantage of the latter strategy is that it can combine the unique properties of the chromophore and graphene oxide.[49] Furthermore, the synthesis is facile, that is it requires only mixing of the organic molecule solution with a dispersion of graphene oxide with the aid of stirring or ultrasonication.

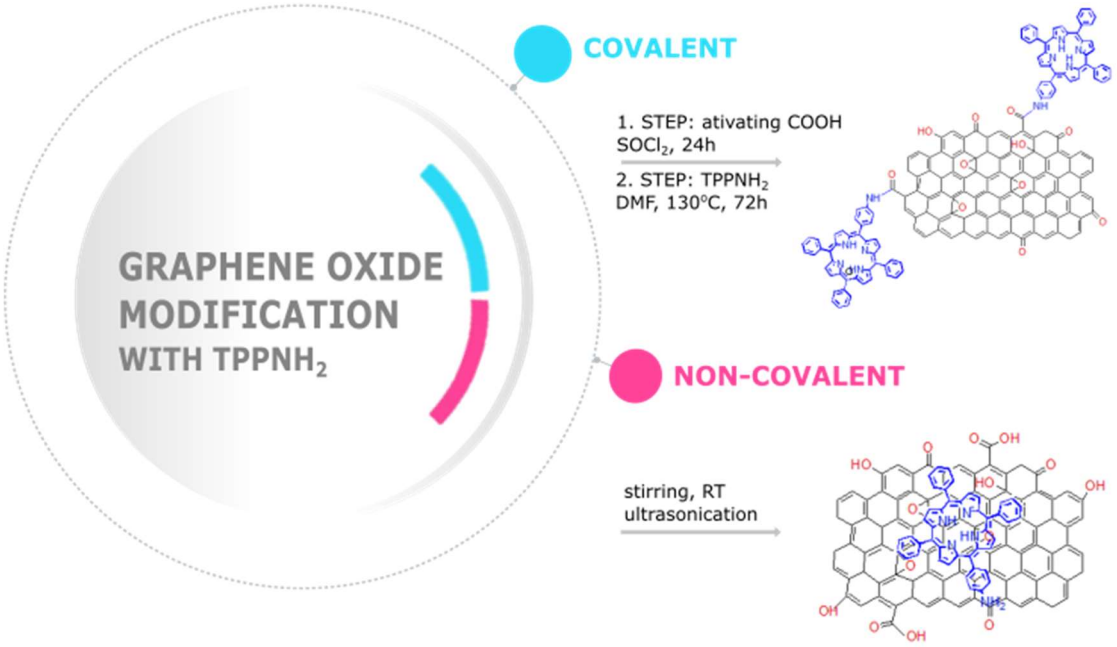

Scheme 3 *Schematic illustration of the preparation of GO with covalently and non-covalently linked porphyrin. Conditions for covalent functionalization were taken from*[50]

Non-covalent functionalization

Graphene-based materials can participate in various types of non-covalent interactions, including hydrogen bonding, electrostatic attraction, and π-π bonding, which are important for their functionalization.[51] Usually π–π interactions with GO occur for organic molecules and polymers with extensive aromatic systems. Van der Waals forces are formed between graphene and GO with the same type of characteristics as for π–π interactions but the functionalizing entities should have a hydrophobic character.[49] While planar graphene sheets readily interact via π–π with other aromatic planar molecules, this ability is weakened in rGO and GO compared to pristine graphene. Two types of π–π interactions can occur between the electron-rich and electron-poor regions of GBM, which influence their interaction with other molecules or nanomaterials: face-to-face and edge-to-face arrangement. Hydrogen-bond formation and electrostatic interactions can also occur between GBM and other molecules due to differences in the overall charges and intermolecular distance. The oxygen functionalities on the surface and edges of GO induce ionic interactions and hydrogen bond formation. The pK_a of GO is around 4.0 which means that under neutral pH carboxyl groups dissociate and GO has a negative charge.[52] This property allows for electrostatic interactions with positively charged particles These non-covalent bonds do not interfere with the π system of the graphene-based materials, and hence the properties offered by the unique sp^2 hybrid planar structure is maintained.

2.2 Introduction to porphyrins

Porphyrins and metalloporphyrins are of particular interest in many areas (***Scheme* 4**) because of their photophysical, photochemical, and electrochemical properties. They are well-known for their excellent photoactive properties.[53] Porphyrin structure is based on the four pyrole rings connected to each other. The rings are connected by methine bridges and form a closed aromatic structure. The structure of all compounds belonging to the porphyrin group is based on the structure of the simplest of them, porphyrin (***Figure 2***). Metalloporphyrins are analogous to porphyrins, but with a central metal ion incorporated within their structure. The formation of metalloporphyrins involves replacing two hydrogen atoms in the porphine core with a positively charged metal ion.

Compounds containing Fe, Co, Zn, and Ni ions are among the most well-known metalloporphyrins.[54–58]

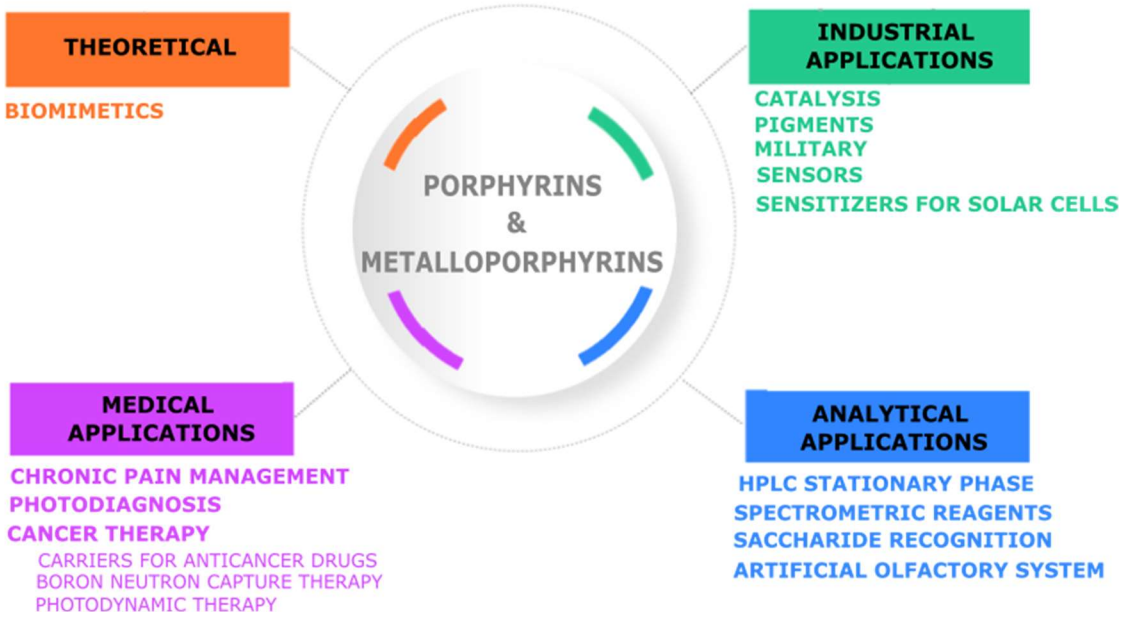

Scheme 4 *Exemplary applications of porphyrins and metalloporphyrins*

Porphyrins are very reactive compounds that are involved in a number of chemical transformations. Metallated porphyrins participate in a variety of reactions, including oxidation/reduction reactions[55,56], sulfur and nitrogen reduction reactions[59], methane production[54], methyl group transfer[60], and light-harvesting reactions.[61,62]

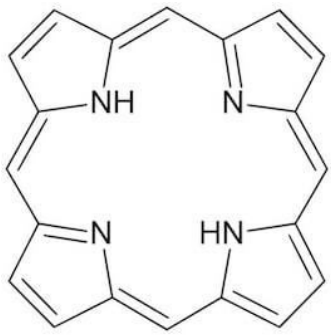

Figure 2 *The structure of porphyrin*

Porphyrins play also a special role in many biological reactions. Heme porphyrins (containing an iron atom) are very common in nature and have many functions: from the storage and transport of O_2 (myoglobin, hemoglobin), through the transport of electrons (cytochrome b, cytochrome c) to the activation and operation of O_2 (cytochrome P450,

cytochrome oxidase). Related macromolecules have been detected, including chlorophylls (containing a magnesium atom), pheophytin (not containing a metal atom), and vitamin B12 (containing cobalt) in plant and animal organisms.

Various substituents can be attached to porphyrins to modify their properties, with substitution possible at either the β or meso position (***Scheme* 5**). They can be designed to exhibit specific molecular properties such as absorption in the visible range and redox potential.

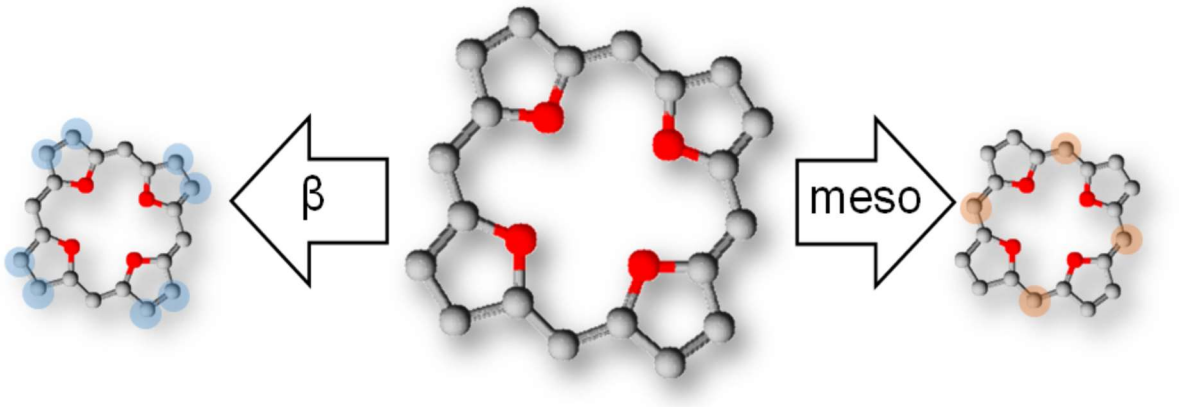

Scheme 5 *Representation of the β and meso positions in free-base porphyrin*

Most porphyrins are water-insoluble compounds which limits their potential applications in some processes such as water splitting or photodegradation of water pollutant. However the introduction of the hydrophilic groups (such as carboxylates, sulfonic acids, quaternary pyridinium, ammonium groups into the ring) can increase the solubility of the compounds in water. The charge of the substituent can determine whether water-soluble porphyrins are cationic or anionic.

2.2.1 Spectroscopy properties

The porphyrin family of compounds possesses a distinct electronic structure that leads to a complex absorption spectrum. Porphyrins absorb light in the visible range. The example of the absorption spectrum of the porphyrin is shown in ***Figure 3***.

The explanation for the origin of the absorption spectra of porphyrin was proposed by Gouterman.[63,64] He presented the theory of the "four orbitals" in unison, in which the absorption bands in the porphyrin system appear as a result of transitions between two HOMO orbitals and two LUMO orbitals of the molecule (***Figure* 4**). The relative energies

of these transitions are affected by the specific identities of the metal center and the substituents on the ring. The HOMOs were calculated to be an a1u and an a2u orbital, while the LUMOs were calculated to be a degenerate set of eg orbitals.64 Transitions between these orbitals gave rise to two excited states. Through orbital mixing, these two states are split in energy, resulting in a higher energy state with greater oscillator strength, which generates the Soret band, and a lower energy state with lower oscillator strength, producing the Q-bands.

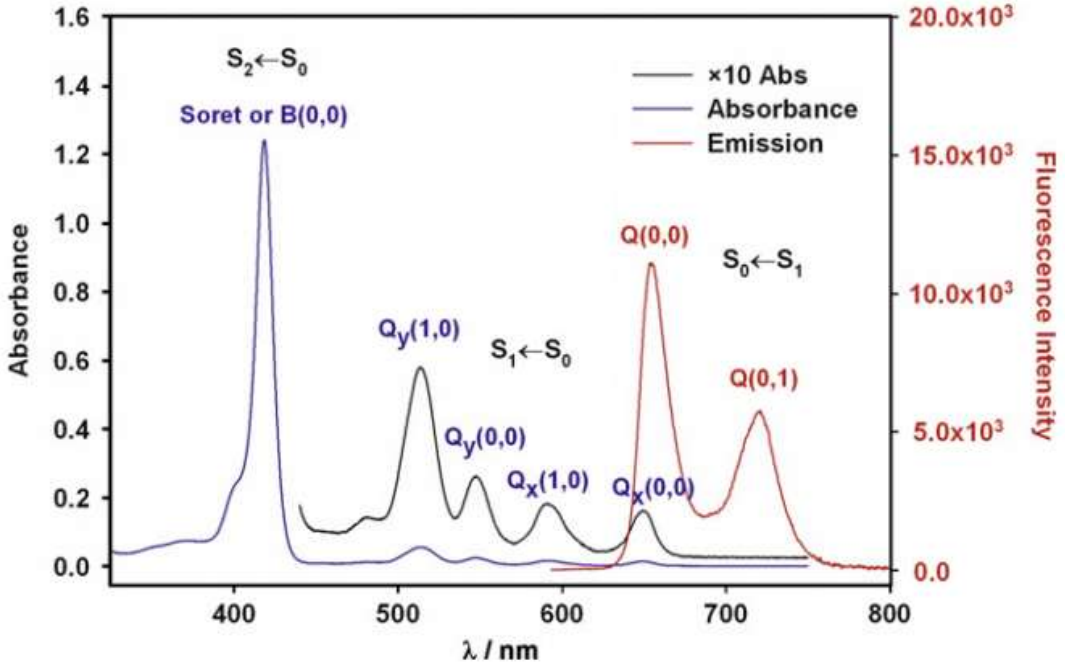

Figure 3 *Absorption and emission spectra of porphyrin on the example of TPP porphyrin. The TPP concentrations were 5 μM and 0.5 μM for absorbance and fluorescence measurements, respectively. Adapted from ref [65] with permission from Elsevier (2008)*

It has been well documented that changes in the conjugation pathway and symmetry of a porphyrin can affect its UV-Vis absorption spectrum.[63,64,66]

The porphyrin absorption spectrum can be divided into two regions. The first involves the transition from the ground state to the second excited state ($S_0 \rightarrow S_2$) and the corresponding band is called the Soret or B band. The absorption range is between 380 and 500 nm, depending on the substitution. The second region consists of a series of much weaker bands in the visible region - Q bands at longer wavelengths (500-700 nm), which are associated with transitions from S_0 to S_1. Porphyrins are known for their high molar

absorption coefficient in the Soret band region, typically ranging from 10^4-10^6 dm^3 mol^{-1} cm^{-1}.

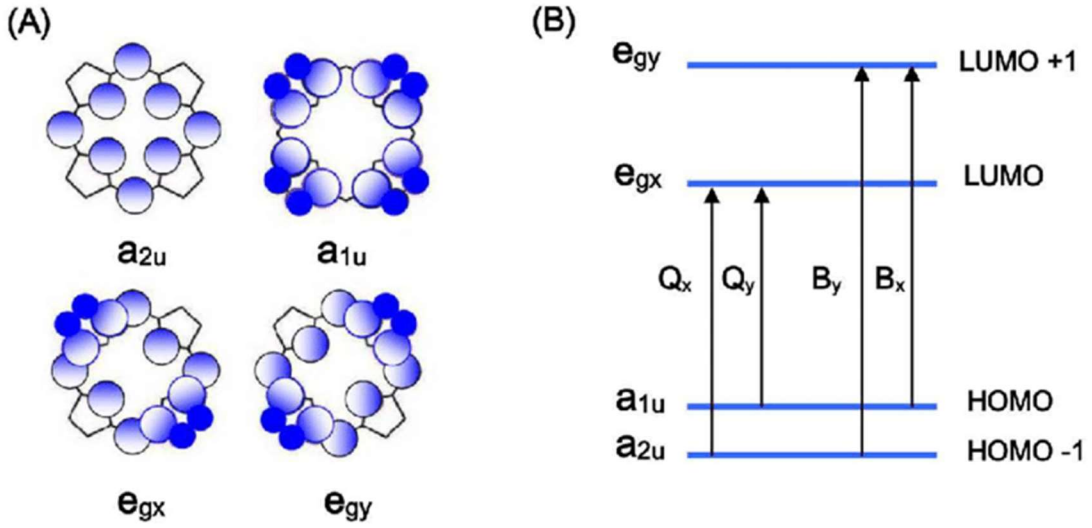

Figure 4 *Porphyrin HOMOs and LUMOs. (A) Representation of the four Gouterman orbitals in porphyrins. (B) Drawing of the energy levels of the four Gouterman orbitals after the symmetry is reduced from D_{4h} to C_{2V}. Adapted from ref [66]*

Porphyrins and their derivatives exhibit a strong characteristic red fluorescence, which is detectable even in the case of trace amounts of these molecules. Excitation from the ground state S_0 to any excited state leads to a very rapid radiation-free transition to the lowest ground state S_1. Fluorescence is generated from the S_1 state. The emission spectra have two emission bands Q(0,0) and Q(0,1).[67] Porphyrins are characterized by moderate fluorescence quantum yields, typically ~0.1.[68]

2.2.2 Aggregation of porphyrin molecules

Porphyrins and their analogues tend to self-aggregate, which is facilitated by a flat, wide, and electron-rich surface.[69]

Porphyrin aggregates also play specific roles in nature namely in photosynthetic plants and in organisms and have potential uses as nonlinear optical materials.[69] In fact, much of the development in molecular electronics has been derived from attempts to mimic the highly efficient electron and energy transfer processes that take place in the light-harvesting complexes and reaction centers of photosynthetic organisms.[70]

A variety of factors can influence the extent of self-association, including the nature of the porphyrin itself (metal ion, number, and structure of peripheral groups), as well as external variable such as ionic strength, pH, solvent nature, and temperature, among others.

According to Kasha's exciton theory, J-aggregates are formed when the transition dipole moments of monomer molecules are aligned parallel to the line that joins the molecular centers in the aggregate ("head-to-tail")[69] (***Figure 5***). In contrast, in the case of H-aggregates, the transition dipole moments of the monomer molecules are perpendicular to the line of centers ('face-to-face'). It is generally accepted that a red-shift in the electronic absorption spectra relative to that of the monomer is a proof of the J-aggregate, whereas a blue shift is an evidence of the H-aggregates.[69]

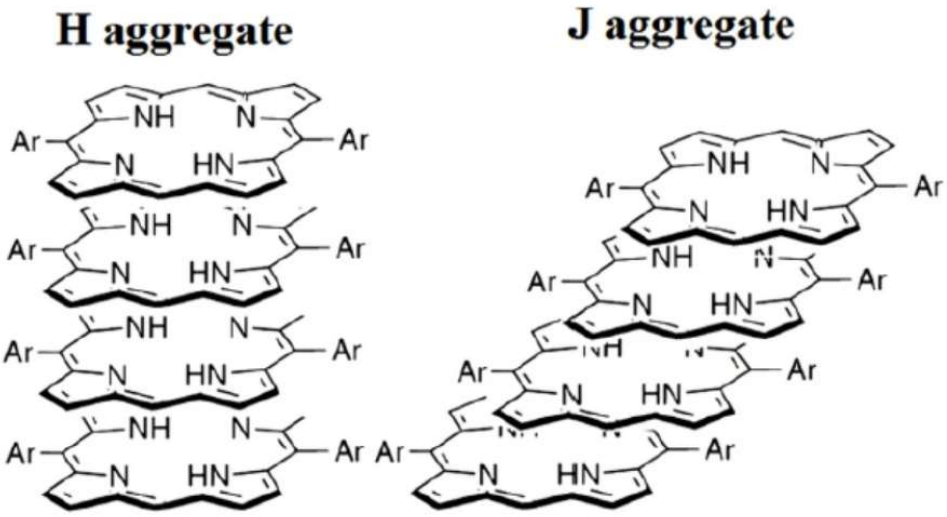

Figure 5 *Schematic illustration of H-type and J-type aggregate. Adapted from ref [71]*

2.3 Non-covalent functionalization of graphene oxide with porphyrins

The non-covalent functionalization of GO with porphyrin derivatives is an attractive approach, as it allows for the introduction of porphyrin molecules without affecting the desirable properties of GO.[72] This approach also extends the light absorption of the material into the visible region, making it a promising option for various applications. The graphene-based materials, and therefore also graphene oxide, can be chemically modified with porphyrin molecules *via* covalent and non-covalent functionalization. As mentioned earlier, the non-covalent method is the simplest approach for

functionalizing graphene-based materials. Facile synthesis (i.e., requires only the mixing of a dye solution with a dispersion of the graphene-based material)[73–76] has the advantage of high yield and preserving the main properties of each component. The porphyrin structure can influence on the strength of the interaction with graphene-based material. A straightforward way to confirm the successful adsorption of porphyrin onto the GO surface is by measuring the UV-Vis spectra of the supernatant obtained after the centrifugation process.[73,74] When only a minor peak attributed to the porphyrin is detected in the suspension it can be concluded that the porphyrin-graphene oxide nanocomposite has been successfully isolated as the precipitate. One disadvantage of this approach is the low weight content of porphyrin in the hybrid material, especially for neutral porphyrins, where the assemblies primarily rely on π–π stacking.[73,74,77]

Nanomaterials that combine porphyrin molecules and GO represent a new type of photocatalysts. Both of these groups have certain limitations in photocatalysis and cannot be used efficiently as a single photocatalyst. Porphyrin molecules tend to be relatively unstable under light illumination while also exhibiting inefficient charge separation. Furthermore, they cannot be easily regenerated through processes such as centrifugation, limiting their potential for reuse.

Although GO material has a number of desirable properties its weak absorption in the visible region limits its application as a photocatalyst. However, by combining GO with porphyrin molecules to form hybrids, it is possible to overcome these limitations and enhance the photocatalytic performance (***Scheme* 6**).

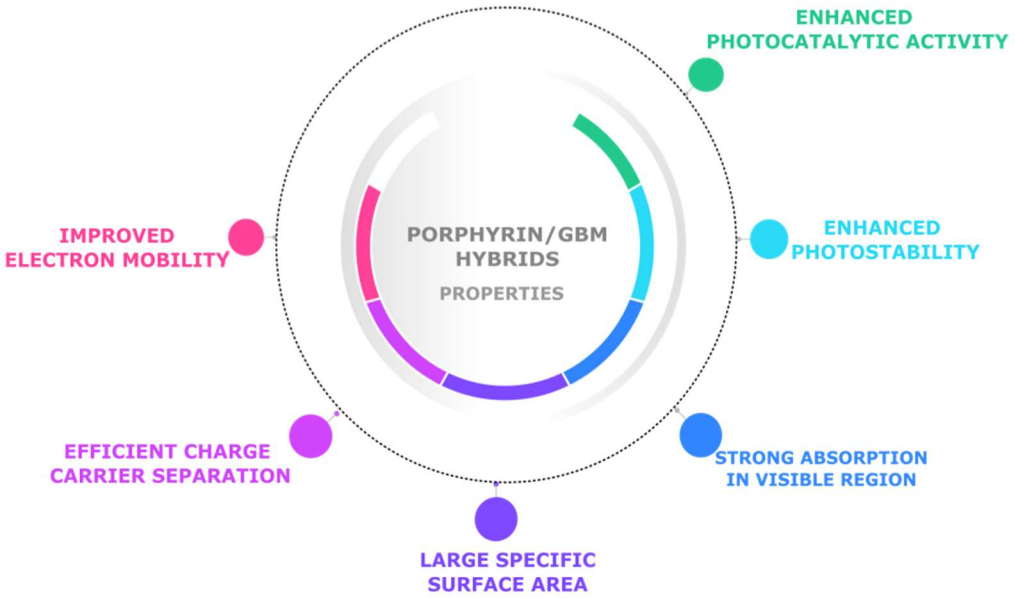

Scheme 6 *The properties of hybrid materials (porphyrin/GBM)*

The first report on the non-covalent interactions of chemically converted graphene (CCG) functionalized with cationic porphyrin TMPyP (***Figure 6***) was published in 2009.[78] Due to deprotonation of the residual carboxyl groups, the CCG surface in the aqueous dispersion carries a negative charge, while TMPyP is a positively charged porphyrin, CCG and TMPyP can be assembled through a combination of electrostatic and π-π stacking interactions. To date, several graphene-based materials derived from cationic porphyrins have been reported.[75,78–82] Wojcik *et al.* proved that the positively charged porphyrin TMPyP non-covalently interacts with reduced graphene oxide through electrostatic and π–π stacking interactions.[80] The authors presented results of femtosecond transient absorption and photoelectrochemical measurements, which clearly indicated the occurrence of photoinduced electron transfer in TMPyP/rGO nanohybrids.[80] Wang *et al.* formed a non-covalent hybrid between water-soluble cationic TMAP (***Figure 6***) and GO at pH 2.[75] The porphyrin/GO nanohybrid exhibited a fast and reversible on/off photocurrent upon exposure to white light, suggesting efficient charge transfer from the TMAP moieties to GO The nanohybrid showed that porphyrin acts as an energy-absorbing and electron-transferring antenna, and GO serves as an efficient electron acceptor of the system. Thus, it is a potential candidate for photovoltaic devices and light-harvesting applications.

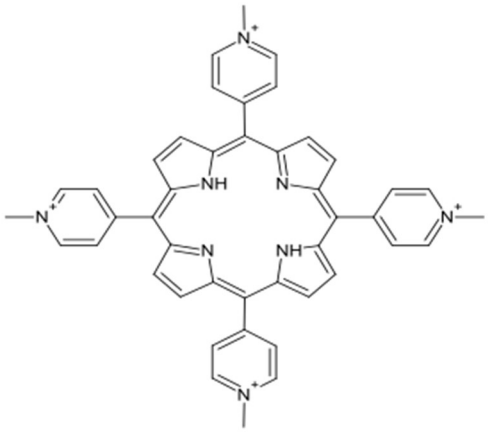

TMPyP
5,10,15,20-tetra(1-methyl-4-pyridinio)porphyrin

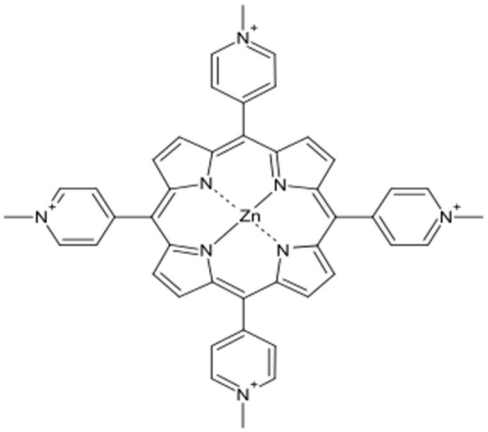

ZnTMPyP
Zinc (II) 5,10,15,20-tetra(1-methyl-4-pyridinio)-

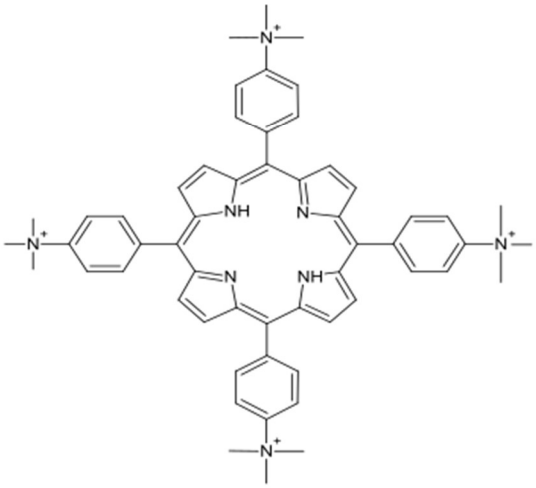

TMAP
5,10,15,20-tetra(4-trimethylammoniophenyl)-
-porphyrin

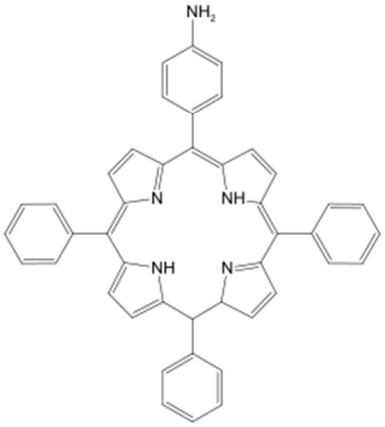

TPPHNH2
5,10,15,20-tetra(4-sulfonatophenyl)porphyrin

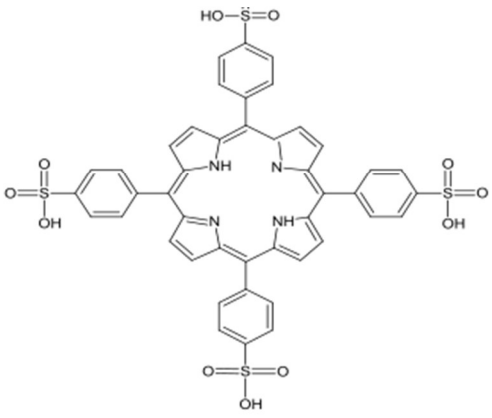

TSPP
5,10,15,20-tetra(4-sulfonatophenyl)porphyrin

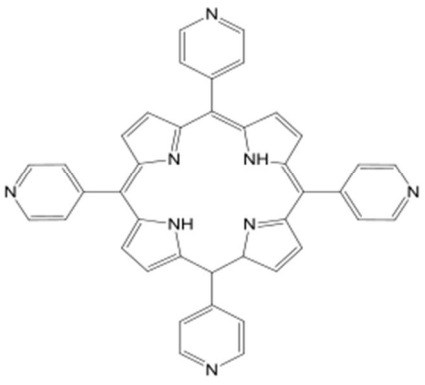

TPP
5,10,15,20-tetra(4-pirydyl)porphyrin

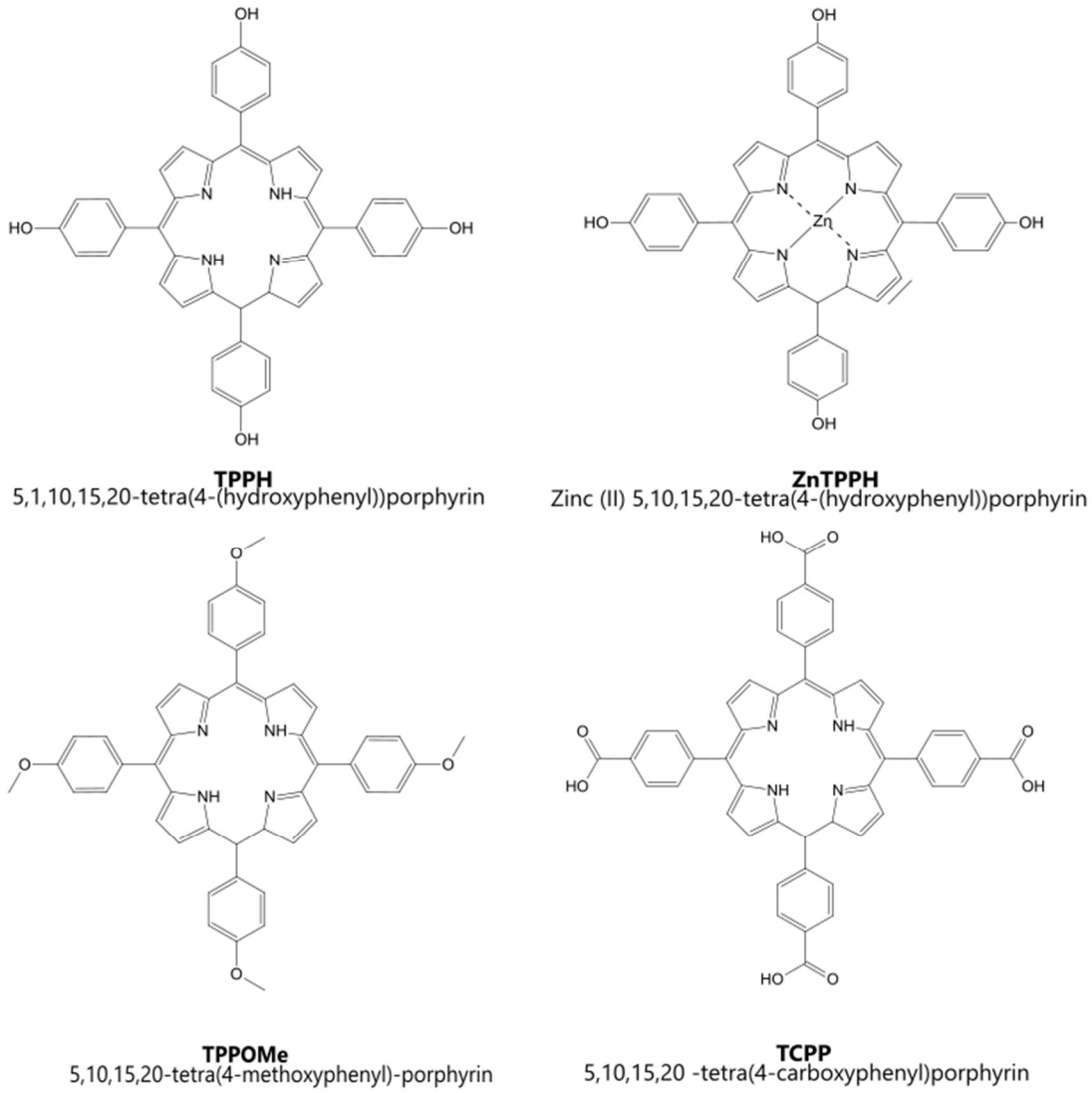

Figure 6 *Structural formulas and names of the porphyrins described in Chapter 2*

It was also shown that the TMAP/GO composites can facilitate the incorporation of iron(III) ions into the porphyrin moieties, and thus can be used as an optical fluorescence probe for the detection of iron (III) ions in samples.[83]

In 2009, Xu *et al.* published an article describing the absorption and emission properties of the two prepared hybrids: TMPyP/CCG and TMAP/CCG.[78] The formation of these hybrids is primarily attributed to the π-π and electrostatic interactions between the negatively charged CCG surface and the positively charged cationic porphyrin. The TMPyP/CCG material was found to act as an optical probe for the detection of Cd^{2+} ions.

Furthermore, non-covalent interaction of the TSPP (***Figure 6***) and TMAP hybrids with GO were reported.[82] The porphyrin molecules TSPP possess a negative charge owing to the sulfonate groups present, while the TMAP molecule bears a positive charge. The presence of a charge on the porphyrin molecule resulted in the appearance of electrostatic repulsion between TSPP, or attraction between TMAP and GO.

There are limited studies available that discuss results obtained from femtosecond transient absorption or photocurrent measurements, which could be excellent evidence for electron transfer in investigated hybrid systems.[73–75,79–81,84,85] Therefore comprehensive studies that explore the effect of the porphyrin and GBM structure on the properties of their nanohybrids are highly necessary.

2.3.1 Spectroscopic properties of porphyrin-GBM hybrids

Ground state interaction

The titration method followed by UV-Vis absorption measurements is an often applied technique for monitoring the ground state interaction between the porphyrin and GBM. One common approach is to measure UV-Vis spectra while keeping the porphyrin concentration constant and varying the GBM concentration. During the titration process reported by Xu *et al.*, for TMPyP and CCG the intensity of the Soret band attributed to porphyrin gradually decreased and a new red-shifted Soret band appeared.[78] The shift of the Soret band was about 37 nm. Furthermore, an isosbestic point was observed at 429 nm. By subtracting from the UV-Vis spectra the contribution of the absorption from the CCG dispersion, a spectrum that corresponds to TMPyP adsorbed on the CCG sheet was isolated. The UV-Vis spectra of the TMPyP/CCG complex were characterized by a bathochromic shift (37 nm), a broader half-bandwidth, and a weaker extinction compared to that of the free TMPyP in solution. The alterations in the UV-Vis spectra of porphyrins upon the addition of GBM have been documented in several porphyrin/GBM systems, and these findings are compiled in ***Table 2***. The authors attributed this shift to the flattening of the porphyrin molecule. To determine the role of the electrostatic attraction for the ground state interaction between the porphyrin and CCG, the cationic TMPyP was replaced with anionic TPPS. In that case, no appreciable changes in the UV-Vis spectra of TPPS were observed upon the addition of CCG. Bajjou et. al. also reported that the position of the Soret band of the TPPS is not affected by the presence of rGO.[86] While cationic porphyrins such as TMPyP, exhibited absorption

spectral changes in the presence of GBM, such behaviour was not detected for TPP.[79] This indicates the importance of the positive charge of the chromophore for the occurrence of a strong interaction between porphyrin in the ground state and GBM, which is reflected by the changes in the electronic configuration of the ground state of porphyrin.

Gacka *et al.* studied the influence of pH on the strength of the interaction between TPPH and GO.[73] One interesting aspect of this study was that the TPPH molecule's total charge varies from negative (-4) to neutral, and positive (+2) depending on the pH of the solution, which is due to the protonation of the imino nitrogens and deprotonation of the –OH groups. Therefore, the strength of the electrostatic interaction between TPPH and GO was modulated by the change in pH. The outcome of this investigation was that both neutral TPPH and cationic $TPPH^{2+}$ molecules can be assembled on the surface of GO, but a stronger interaction with GO was demonstrated for $TPPH^{2+}$. For negatively charged $TPPH^{4-}$ no appreciable changes in the UV-Vis spectra were registered in the presence of GO. Furthermore, after centrifuging the suspension, nearly all of the porphyrin remained in the supernatant. The authors concluded that the interaction between $TPPH^{4-}$ and GO was largely suppressed. Additionally, the authors complemented the spectroscopic results with theoretical calculations, which provided further evidence for a stronger interaction between cationic $TPPH^{2+}$ and GO in comparison to neutral TPPH. The interaction energies were found to be -22.4 kcal mol^{-1} and -58.0 kcal mol^{-1} for TPPH/GO and $TPPH^{2+}$/GO, respectively. Furthermore, the center-to-center distance between $TPPH^{2+}$ and GO was found to be 4.40 Å compared to 4.55 Å obtained for the nanohybrid TPPH/GO.

For cationic porphyrins, the electrostatic interactions with GBM are the main driving force for the assembling of the hybrid. For neutral porphyrins, the main types of interaction are π-π interactions and hydrogen bonding. Gacka *et al.* compared the interaction of TPPH and meso-tetra(4-methoxyphenyl)porphyrin (TPPOMe) with GO. By replacing the OH groups with the methoxy group, the hydrogen bonding between TPPOMe and GO was suppressed.[73] Using the titration method followed by absorption spectra, it was determined that the strength of the interaction of the porphyrin TPPOMe with GO was comparable to that of TPPH and GO. Therefore, it was concluded that π-π

stacking interaction is required to efficiently form nanoassemblies with GO by simply mixing the solutions of both components.

Table 2 *Exemplary absorption properties of the free porphyrins and porphyrins adsorbed non-covalently on GBM*

Porphyrin	GBM	Solvent	λ_{max} of free porphyrin	λ_{max} of nanohybrid	Shift of the Soret band	Isosbestic point	Ref.
TMPyP	CCG	H_2O	421 nm	458 nm	37 nm	429 nm	[78]
TMAP	CCG	H_2O	411 nm	436 nm	35 nm	416 nm	[78]
TMPyP	rGO	H_2O	422 nm	452 nm	30 nm	442 nm	[80]
TPPH	rGO	EtOH	420 nm	448 nm	28 nm	-	[76]
CoTPP	rGO	DMF	415 nm	433 nm	18 nm	420 nm	[87]

Ge *et al.* studied the effect of the functional groups linked on the peripheries of the porphyrin on the combination mode of porphyrin and GO, and also on the spectroscopic properties of porphyrin/GO composites.[88] To investigate the role of porphyrin peripheries on their interaction with GO, three porphyrins with varying numbers of hydroxyl groups in the substituent were selected for the study. The results revealed that the binding strength between the GO and the porphyrins is on the order of TPPH/GO > TPPOH/GO > TPP/GO (***Figure 7***). The authors stated that in the case of TPPH, the hydroxyl substituents and the TPPH core have a cooperative effect on the assembling of the TPPH/GO hybrid, enabling the flattening of the TPPH on the surface of GO. For the TPP porphyrin, the π-π interaction is the only one that could operate with GO. The weak interaction observed between TPP and GO was attributed to hydroxyl and epoxy functional groups on GO sheets that prevented TPP molecules from efficiently loading on the surface of GO and close contact between the moieties.

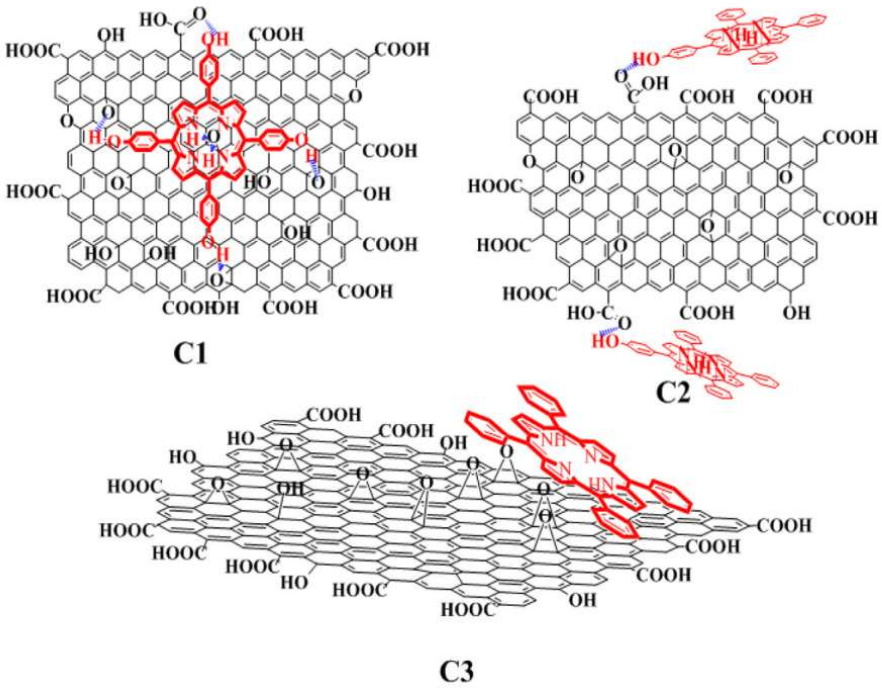

***Figure** 7 Structural schemes of (C1) THPP/GO, (C2) TPPOH/GO, (C3) TPP/GO. Adapted from ref [88] with permission from Elsevier (2015)*

Excited state interaction

The primary goal of constructing porphyrin/GO is to facilitate photoinduced processes and enhance the efficiency of photocatalytic systems, such as organic dye photodegradation systems. Therefore, the ability of GBM to interact with the excited states of porphyrins has attracted the attention of scientists over the past 10 years.[2,89–91]

The emission of the excited porphyrin molecules serves as a great probe for monitoring the interactions between the components of the obtained hybrids. Nevertheless, steady-state emission spectroscopy of graphene-based materials hybrids can be challenging. Typically, in these studies, the fluorescence intensity of the free porphyrin is compared with the fluorescence in the presence of GBM, which acts as the quencher. The fluorescence intensity can be reduced by the presence of any species that is capable of absorbing a portion of the excitation energy. Corrections for absorption of part of the excitation light by GBM should be taken into account by applying the appropriate equation for the inner filter effect (*vide infra*).[92] It is also possible to absorb by GBM part of the radiation emitted by porphyrin a phenomenon known as reabsorption. It is extremely important especially for hybrid materials for which interaction between

porphyrin and GBM is not strong and a higher concentration of GBM is needed to observe efficient emission quenching. Often these corrections are not considered, which can lead to incorrect data analysis and incorrect conclusions. Gacka *et al.* calculated that the correction factor for GO absorption of the excitation light for the emission study of neutral TPPH was as high as 24% for 0.018 mg mL^{-1} of GO.[73] In addition to correcting for the absorption of the excitation light by GBM it is also crucial to match the absorbances at the excitation wavelength to accurately analyze the emission data. Otherwise, the decrease in porphyrin fluorescence intensity after the addition of GBM could be due to changes in porphyrin absorbance at the excitation wavelength, rather than fluorescence quenching. Several studies have reported a reduction in porphyrin fluorescence intensity upon interaction with GBM.[73,74,80,81,93] For example, Masih *et al.* reported that for ZnTMPyP the quenching efficiency was 50% at a graphene carboxylate concentration of 5.7×10^{-3} mg mL^{-1} [94], and Wojcik *et al.* measured a 50% emission quenching efficiency of TMPyP at an rGO concentration of 8×10^{-4} mg mL^{-1}.[80] To quench 39% of the emission of neutral porphyrins ZnTPPH a GO concentration of 1.0×10^{-2} mg mL^{-1} was required.[95] Some studies have reported no emission quenching was observed for neutral porphyrins in the presence of GBM such as in TPP/GC composites[79] or TPP with GO. For anionic TPPS the emission intensity was only slightly decreased in the presence of CCG.[78] By comparison of various reports it can be noticed that cationic porphyrins require a much lower concentration of GMB material for the emission to be quenched efficiently compared to neutral porphyrins. In general, electrostatic interaction between cationic porphyrin and negatively charged graphene-based material enhances the quenching of the porphyrin emission,[94,96] compared to the neutral porphyrin where the interaction with graphene-based material is attributed mainly to π-π stacking interactions.[77,88,94] Careful comparison of the quenching efficiency performed under the same conditions allows for the assessment of the interaction strength for various porphyrin-GBM hybrids.

The strength of the interaction for TPPH, TPPOH, and TPP porphyrins with GO was compared via calculation of the apparent binding constant based on the Stern-Volmer type equation.[88] The binding constants were found to be 128.35 mL mg^{-1}, 5.39 mL mg^{-1} and 0.39 mL mg^{-1}, respectively. On this basis, the authors concluded that TPPH has the strongest interaction with GO.

Based solely on the steady-state emission measurements of porphyrins in the presence of GBM, the quenching mechanism can not be unambiguously determined. However, the observed decrease in the emission in the presence of GO is commonly related to electron or energy transfer mechanisms, while alternative mechanisms are often neglected.[76,94,97] Surprisingly contribution of the static quenching in the emission quenching experiments is rarely discussed.

Few authors analyzed emission quenching experiments in terms of Stern-Volmer equations in order to determine the contribution of static and dynamic quenching.[98–100]

Static and dynamic rate constants were determined from the following equation:

$$\frac{F_0}{F} = 1 + (K_D + K_S)[GO] + K_D K_S [GO]^2 \quad (1)$$

where, F_0 and F represent the fluorescence intensities of the fluorescent substance in the absence and in the presence of the quencher concentration of [GO] and K_D and K_S are the dynamic and static quenching constants, respectively.[85]

It was found for example that for systems CoTPP/rGO[99], TPPH/GO[98] and TCPP/GO[98] K_s is much larger than K_d. It was concluded that the observed quenching of the emission is mainly related to the static quenching. In other words, the formation of the non-fluorescent complex already in the ground state was the primary cause of the decrease in fluorescence intensity. In other studies, the contribution of the static quenching mechanism to the decrease in emission intensity was determined based on the time-resolved emission.[73,95]

The conversion of light energy through photocatalytic processes begins with the photoinduced generation of energy-rich electrons. Therefore, the PET process in these hybrid materials plays a key role in terms of their possible photocatalytic activity. Examining photoinduced transient species with appropriate time-resolved spectroscopy is crucial for unraveling the excited-state interactions. Femtosecond transient absorption measurements are a useful tool to probe the possibility of PET in hybrid materials.[73,79,80,95] However, to date, only a few studies have incorporated results obtained from femtosecond transient absorption spectroscopy.[73,79–81,84,95] Solid evidence for the PET process in porphyrin-GBM hybrid was provided for the first time in 2010.[80] The authors assembled non-covalently positively charged TMPyP with reduced graphene oxide *via* electrostatic and π–π stacking interactions. By applying femtosecond transient absorption

measurements it was found that the singlet excited state of TMPyP adsorbed on rGO film decays faster compared to TMPyP adsorbed on SiO_2. Furthermore, the decay of the singlet excited state of TMPyP was followed by the formation of a longer-living product with an absorption maximum around 515 nm which was attributed to the porphyrin radical cation. A calculated negative value for the free energy of ET indicated the photoinduced electron transfer from photoexcited porphyrin to rGO was thermodynamically feasible. Other evidence for the interaction between the excited state of TMPyP and rGO was obtained from the photocurrent measurements. A small but noticeable photocurrent density was observed for the TMPyP/rGO hybrid, which was higher than that obtained for rGO alone. The low yield of the photocurrent density was attributed to the inefficient charge separation within the TMPyP/rGO hybrid.

Aly *et al.* tested three porphyrins with different substituents and redox properties to correlate those properties with the electron injection process to the carboxylate graphene (GC).[79] The presence of GC, did not influence the excited state dynamics of neutral porphyrin – TPP. In contrast, the transient absorption spectra of two cationic porphyrins TMPyP and TMAP measured in the presence of the same graphene-based material exhibited much faster dynamics in addition to the changes in spectral features. Interestingly, a new spectral band in the region from 500-600 nm assigned to the porphyrin radical cation was detected immediately after the femtosecond laser pulse. The very fast PET process occurs from the porphyrin excited state to GBM. Such efficient and fast ET for TMPyP and TMAP was attributed to the strong electrostatic interaction between cationic porphyrin and GC which was explained by close contact of the two species prior to excitation The same group extended their studies to non-covalent functionalization of Zn-metallated cationic porphyrin ZnTMPyP with GC with the ultimate goal of the construction of hybrid material with long-lived charge separation state.[81] Ultrafast transient absorption (TA) spectroscopic measurements were performed with the non-covalent ZnTMPyP with varied GC concentration. When a higher concentration of GC is added, the dynamics of the TA have changed and a spectral feature in the range of 650–750 nm attributed to the $ZnTMPyP^{\bullet+}$ radical cation has been developed. The radical cation of ZnTMPyP was detected within the temporal resolution of the equipment, indicating that the ET from Zn porphyrin to GC occurs ultrafast. However, similar to studies for TMPyP and TMAP, the $ZnTMPyP^{\bullet+}$ and GC radical ion pair recombined back to the initial state, with time constants of 20.18 ps (***Scheme* 7**).

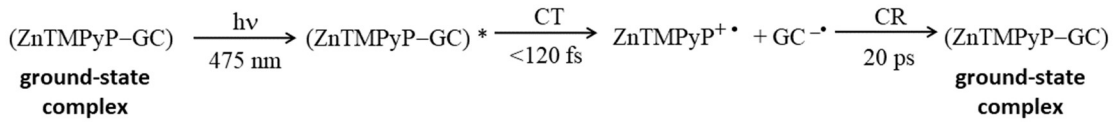

***Scheme** 7 Excited state dynamics of ZnTMPyP-GC (CT- charge transfer, CR -charge recombination). Adapted from ref [81] with permission from the PCCP Owner Societies (2015)*

Most studies have focused on investigating the effect of GBM on the singlet state dynamics of porphyrins. while only a few studies explored the impact of GBM on the triplet state of porphyrins.[95,101]

It was reported that the lifetime of the triplet excited state of porphyrin increases in the presence of GO.[95,101] Gacka et. al. proposed that the enhancement of the porphyrin lifetime is due to the decrease of the radiationless rate constant which is the result of suppressing the free rotation of the hydroxyphenyl rings.[95] There are few reports which relate the triplet excited states decay to the ground state via radiationless mechanisms with the ease of flipping and twisting of conformational free meso-phenyl rings around the core of the porphyrin.[102,103]

2.4 Application of non-covalent nanohybrids Porphyrin/GBM in photocatalysis

Non-covalent porphyrin/GBM hybrids has been tested as photocatalysts, mainly in photocatalytic hydrogen evolution and pollutants (dyes, pharmaceuticals) degradation systems. Exemplary hybrids with their application are summarized in ***Table** 3*.

***Table 3** Exemplary porphyrin/GBM with their application in photocatalysis*[104]

	Co-catalyst	Application	Experimental conditions	Activity	Ref
TPPH/rGO	Pt NPs	hydrogen evolution	Xe lamp 150 W, TEOA	1060 μmol g^{-1} h^{-1} AQE=1.7%	[76]
			Xe lamp 150 W, CTAB,TEOA	2240 μmol g^{-1} h^{-1} AQE=3.6%	[76]
			Xe lamp 150 W (λ > 420 nm) TEOA	138 μmol g^{-1} h^{-1} H_2	[76]
ZnTMPyP/rGO	MoS_2	hydrogen evolution	300 W Xe lamp (λ > 420 nm) TEOA	2560 μmol g^{-1} h^{-1} AQE = 15.2 % 420 nm	[105]
TCPP/GNPs		degradation of RhB	1500 W Xe lamp (λ > 400 nm)	k=7.3× 10^{-3} min^{-1}	[106]

			[RhB]=5mg L^{-1} [photocatalyst]= 5mg L^{-1}		
TCPP/GNPs		degradation of RhB and MB	1500 W Xe lamp (λ > 400 nm) [RhB] = 5 mg L^{-1} [photocatalyst]= 5mg L^{-1}	k=15.8×10^{-3} min^{-1} for MB k=6.5× 10^{-3} min^{-1} for MO	[107]
TMPyP/GO		simultaneous degradation of MB and MO	150 W Xe lamp, (λ > 420 nm) [mixed dyes] = 9.0 × 10^{-4} M [photocatalyst] = 500 mg L^{-1}	k = 3.9 ×10^{-2} min^{-1} for MO k = 1.1 ×10^{-2} min^{-1} for MB	[108]

The first report on the application of porphyrin/GBM for photocatalytic hydrogen production was published by Zhu *et al.*[76] The TPPH/rGO composite show photocatalytic activity in composite with Pt nanoparticles as a co-catalyst. The photocatalytic activity of the TPPH/rGO/Pt nanocomposite in the production of hydrogen was found to be significantly improved compared to the TPPH-functionalized Pt colloid or Pt-modified rGO. The evident improvement in H_2 production for TPPH/rGO/Pt could be attributed to the efficient electron transfer from photoexcited TPPH to Pt nanoparticles through rGO sheets. Here, rGO acts as a solid-state electron mediator, facilitating charge separation and suppressing the recombination of photoexcited electron−hole pairs in the TPPH/rGO nanocomposite.[104] The total amount of H_2 evolved under 5h UV−Vis light irradiation using various photocatalysts: P25−TiO_2, rGO/Pt, TPPH/Pt and TPPH/rGO/Pt is shown in ***Table* 4**.

Table 4 *Comparison of the H_2 evolved under 5h UV−Vis light irradiation using various photocatalysts: P25−TiO_2, rGO/Pt, TPPH/Pt and TPPH/rGO/Pt (given in mmol g^{-1})*[76]

Catalyst	P25-TiO_2	rGO/Pt	TPPH/Pt	TPPH/rGO/Pt	TPPH/rGO/Pt with CTAB[1]
amount of H_2 (mmol g^{-1})	1.52	0.89	2.74	5.29	11.2 (0.69[2])

Reaction conditions: mcatalyst = 1 mg, rGO:TPPH = 2:1, [Pt] = 5 wt %, pH = 9, [TEOA] = 10 vol %, [surfactant] = 2 mg, T = 298 K, Xenon lamp (150 W); 1- [CTAB]=2mg; 2- under visible light (λ>400) irradiation

The addition of CTAB to the photocatalytic system enabled further improvement of catalytic activity and its stability by preventing aggregation of the TPPH/rGO/Pt nanocomposite (increase in AQE from 1.7% to 3.6%). Under UV-Vis light irradiation for TPPH/rGO/Pt nanocomposite in the presence of surfactant the determined hydrogen evolution rate was 1060 μmol g^{-1} h^{-1} and under visible light (λ>400) irradiation it equals

138 μmol g^{-1} h^{-1}. It was proposed that the light-driven proton reduction by TPPH/rGO/Pt nanocomposite occurs in the following steps: 1) excitation of the TPPH molecules adsorbed on the rGO surface upon UV-Vis light irradiation, 2) PET from the excited state of TPPH to rGO, 3) electron transfer from the rGO to the Pt nanoparticles adsorbed on the rGO surface where the water molecules accept the electrons to form hydrogen, and 4) restoration of the TPPH ground state by accepting electrons from the triethanolamine (TEOA).

Yuan *et al.* constructed a noble metal-free system consisting of MoS_2/reduced graphene oxide (MoS_2/rGO) catalyst and cationic porphyrin ZnTMPyP as a photosensitizer, which was tested toward photocatalytic H_2 production under visible light irradiation[105] (***Figure* 8**). The ZnTMPyP/MoS_2/rGO showed the highest H_2 evolution rate of 2.56 mmol h^{-1} g^{-1} at pH 7 when the ratio of MoS_2 to rGO was 5:1 (***Figure* 8**B). An AQY of 15.2% at 420 nm was observed under optimized reaction conditions. By monitoring the photoluminescence decay, it was found that the excited state lifetime of ZnTMPyP decreased with increasing rGO contents in the MoS_2/rGO composites. On the basis of the steady-state and time-resolved emission experiments, the authors concluded that after photoexcitation of the ZnTMPyP electron transfer to the rGO surface occurred. Because the oxidation potential of the singlet excited state of ^{1}ZnMPyP* (-1.09 V vs NHE) is more negative than the rGO/rGO$^{\bullet-}$ redox potential (-0.16 V vs. NHE), the electron transfer from the excited state of ^{1}ZnTMPyP* to rGO is thermodynamically feasible. Furthermore, the redox potential of the rGO/rGO$^{\bullet-}$ couple is more negative than the conduction band of MoS_2 nanosheets (-0.13 V vs. NHE). Therefore, there should be enough driving force for further electron transfer from rGO to MoS_2. The edges of MoS_2 crystallites can act as active sites for the evolution reaction of H_2 once they are reduced with the electrons from rGO. The oxidized ZnTMPyP can be regenerated by reduction with TEOA. In summary, in the ZnTMPyP/MoS_2/rGO composite, the rGO acted as a conductive electron transport bridge, which enhanced the efficiency of the electron transfer from the photoexcited photosensitizer (porphyrin) to MoS_2, thus resulting in the increased photocatalytic efficiency of the whole system.

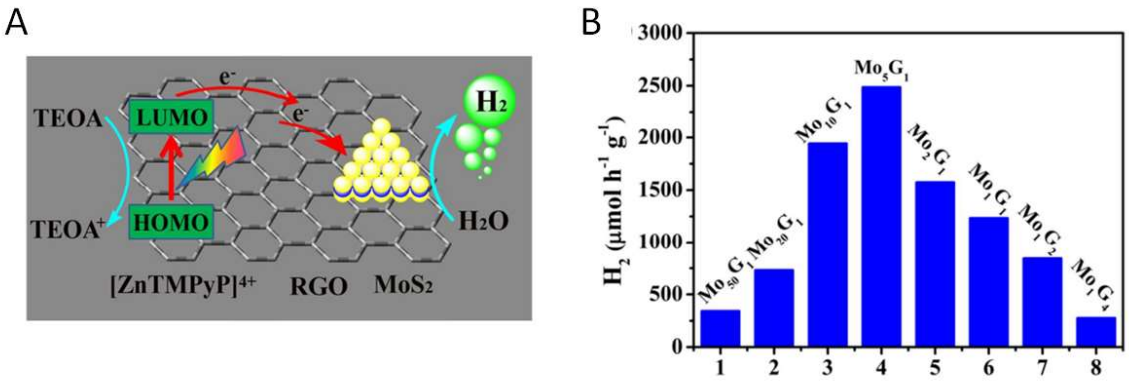

Figure 8 *A) Proposed mechanism for photocatalytic H_2 generation in $ZnTMPyP^{4+}$-MoS_2/rGO-TEOA system under visible light irradiation (numbers 1-8 are the designations of subsequent samples). B) Photocatalytic H production upon visible light irradiation (λ>420 nm) of aqueous solutions containing 0.2 mM ZnTMPyP, 0.2 M TEOA and 40 mg various MoS_2/rGO catalysts at pH 7. Adapted from [105] with permission from American Chemical Society (2017)*

Photocatalytic degradation has attracted a great deal of attention for its simplicity, efficiency, low cost, and low secondary pollution. Concerning photocatalysts for the degradation of organic pollutants, numerous UV-light-driven photocatalytic species have been developed. However, considering energy utilization and savings, research focusing on the development of visible light-energized photocatalysts is an important issue to be explored intensively and extensively. Visible-light-driven photocatalysts have become one of the hot topics in the field of organic pollutant photodegradation. Without a doubt, sunlight is by far the energy source with the highest energy potential in the world. Almost 47% of the solar spectrum is visible light (400 nm< λ<700 nm) that can, and should, be used in the treatment of dyes and organic pollutants.

La *et al*. reported the facile fabrication of well-dispersed TCPP nanorods on the surface of graphene nanoplates (GNPs) by surfactant-assisted (CTAB) self-assembly.[106] The resulted TCPP nanorods with an average diameter of 50 nm and a length of ~250 nm were uniformly distributed on the surface of the GNPs. Obtained hybrid materials displayed significant changes in the UV-Vis spectrum. Compared to the Soret band of monomeric TCPP molecules, the TCPP/GNPs hybrids exhibited a distinct (8 nm) bathochromic shift of the Soret band from 416 nm observed for the monomer to 424 nm registered for the porphyrin nanorods along with a slight red-shift of the Q-bands. Based

on these spectral changes it was suggested that most of the TCPP molecules in supramolecular assemblies fabricated with the assistance of CTAB and GNPs follow a J-type aggregation pattern. Additionally, emission spectra revealed changes in the number of peaks and their position together with a significant decrease in the emission intensity upon self-assembly of TCPP on GNPs. The prepared hybrid shows enhanced photocatalytic performance compared to that of free-standing TCPP nanorods under visible light irradiation, because of the improved charge separation and charge transfer with the introduction of GNPs. In the presence of GNPs-supported TCPP aggregates the RhB degradation reached 80%, after 3 hour of irradiation, with a photodegradation rate constant of ca. 7.3×10^{-3} min^{-1} (***Figure 9***). The role of graphene was attributed to an enhancement in charge separation, achieved by suppressing the recombination of electron-hole pairs that are generated during porphyrin irradiation. This phenomenon contributes to an increase in the lifetime of the charge carriers.

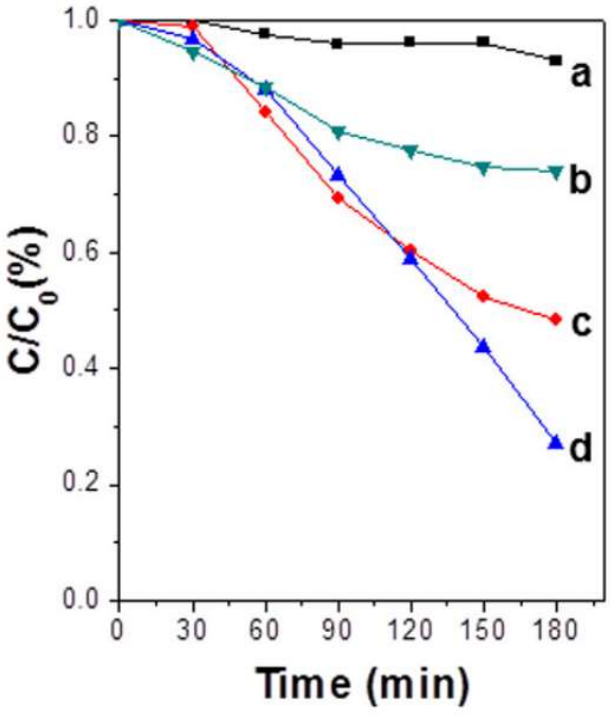

Figure 9 *Photocatalytic performance for RhB degradation of a) control without catalyst, b) GNPs, c) free standing TCPP nanorods, d) GNPs-supported TCPP nanorods. Adapted from ref [106] with permission form Wiley (2016)*

It has been shown that the fabrication of TCPP nanorods/GNPs can be achieved also with support of the arginine.[107] The porphyrin nanofibers, which had a diameter ranging from

50 to 200 nm and a length of several micrometers, were densely and uniformly distributed on the GNPs surface. Compared to the CTAB-assisted self-assembly of TCPP with GNPs, the presence of arginine helped to prepare elongated aggregates of TCPP on graphene, with nanofibers on the micron length scale. The UV-Vis spectra of such prepared hybrids showed a Soret peak at 420 nm, which was 6 nm shifted in comparison to the Soret absorption band of monomeric TCPP. Moreover, one strong peak at 666 nm along with three relatively weak peaks in the Q-band region was registered. The emission spectra exhibited weak and broad emission peaks at 686 nm and 730 nm, whereas the TCPP monomer emitted at 655 and 714 nm. The authors explained the appearance of new emission peaks by the coupling arising from the spatial packing of the TCPP porphyrins, while the decrease in the emission intensity by the quenching effect of graphene, suggesting an efficient photoinduced process. The TCPP nanofibers/GNP exhibited a remarkable photocatalytic performance toward the degradation of RhB. The dye was completely removed after 150 minutes of visible light irradiation. The prepared hybrid material also exhibited high photocatalytic activity towards MO degradation (80% after 180 minutes). The mechanism underlying the photocatalytic performance of TCPP nanorods/GNP hybrids involves the excitation of electrons from the TCPP valence band to the conduction band (CB) when exposed to visible light, which leads to the generation of e^-/h^+ pairs. The photoexcited electrons present in the CB can then be transferred to the graphene sheets. Therefore, the generated electron-hole pairs are efficiently separated. This way, the presence of graphene sheets improves the efficiency of the charge separation. The reaction between holes and H_2O or OH^- produces hydroxyl radicals $OH^\bullet$ which can oxidize the dye molecule. On the other hand, oxygen can be reduced by electrons accumulated on the graphene sheet to form $O_2^{\bullet-}$, which can also react with RhB.

El-Shafai *et al.* using the self-assembly method fabricated another hybrid material composed of cationic porphyrin TMPyP and GO.[108] The obtained TMPyP/GO hybrid shows high photocatalytic activity towards the simultaneous degradation of MB and MO in water under visible light irradiation. The degradation rate constants were found to be 0.039 and 0.011 min^{-1}, respectively for MO and MB.

The presented literature examples of Por/GBM systems applications in photocatalysis clearly show that this is an important topic that still arouses the interest of scientists.

Further research in this direction is still necessary to achieve higher efficiency and a better understanding of the factors that affect the activity of the Por/GBM systems.

3. Aim of work

Although worldwide interest in the development of porphyrin and graphene-based composite materials resulted in numerous publications, there are no comprehensive studies that combine detailed steady-state and time-resolved spectroscopic measurements with the characterization of the morphology and structure of the graphene-based hybrid materials. In many reports on graphene-based materials, the interaction of GBM with dyes was marked only by fluorescence quenching of organic molecules and/or photocurrent measurements.[76,94] While the fluorescence quenching observed suggests a strong interaction between porphyrin and graphene, it does not provide insight into the mechanism of the quenching process, whether it involves energy transfer or electron transfer. It is important to consider the possibility of static quenching as a contributing factor to the observed decrease in fluorescence intensity. Furthermore, any quantitative analyses of emission data for graphene-based materials should account for potential light absorption and scattering by GO. Porphyrins with their strong absorption in the visible region, are frequently used as photosensitizers in both natural and synthetic systems.[109] However, their hydrophobic nature, the low photostability of the porphyrins themselves, and the presence of strong π–π interactions between the rigid macrocyclic molecules lead to aggregation which may limit their applications.[110,111] Moreover, porphyrin molecules alone do not form long-lived charge separation states.

The remarkable properties of graphene, including high optical transmittance, large specific surface area, and a conjugated aromatic system, have made it an ideal candidate for applications as charge carriers or promoters. However, due to its low solubility in aqueous media, its hydrophilic derivative, graphene oxide (GO), can form stable aqueous suspensions, making it more suitable for use in some photocatalytic processes.

Structural engineering is an indispensable strategy to prepare high-performance materials by integrating different components to make full use of their advantages. Therefore the main aim of this study was to synthesize hybrid systems composed of GBM and porphyrins and to conduct a detailed analysis of their properties in terms of potential application in photocatalysis. The research included photochemical and photophysical characterization of selected porphyrins or metalloporphyrins and their nanohybrids with graphene oxide (or reduced graphene oxide). The research was focused on determining the factors that influence on the strength of the interaction between the components of the

nanohybrid. Moreover, important an aspect of this work was to confirm whether the phenomenon of photoinduced electron transfer from the excited state of porphyrin molecule to a graphene oxide sheet occurs in the obtained nanostructures. In the literature, the number of techniques applied for the determination of the spectroscopic properties of the porphyrin/GBM is usually limited, and therefore in-depth understanding of the key factors affecting the properties of those materials, including the efficiency of the PET is still ambitious.

Hence, there is a need for detailed studies that can analyze the spectroscopic properties of different Por/GBM composites to reveal the factors that favor the strong interaction between the components in their ground state and photoinduced electron transfer. Such an analysis would be essential for the rational design of highly efficient materials for photocatalytic applications.

The research presented in this thesis aims to address this need by conducting comprehensive spectroscopic measurements (combined steady-state and time-resolved absorption and emission measurements) and data analyses that could be beneficial for other scientists.

The main specific objectives of the thesis are:

1. synthesizing and characterizing of novel nanohybrids based on GBM (GO and rGO) and porphyrins,

2. correlating the structure of the porphyrin (anionic, neutral, cationic, free-base, or metalated) with its interaction in the ground and excited states with GBM,

3. comparing of the spectroscopic properties of the free porphyrins and porphyrins adsorbed on the GBM surface,

3. determining the effect of GBM oxidation level on the spectroscopic properties of the porphyrins,

4. establishing the effect of pH on the formation of the hybrid materials.

4. Methods of measurements

4.1 The compounds used in the doctoral dissertation

Graphene-Based Materials

Graphene oxide was either purchased from Abalonyx or received from Graphene Laboratory at the *Warsaw University of Technology*. The rGO was obtained by a chemical reduction of the GO with the use of ascorbic acid.

Porphyrins

Throughout the research, six porphyrins were employed, their structural formulas, names, and abbreviation are presented in ***Figure* 10**. TMPyP and its zinc (II) derivative – ZnTMPyP have been synthesized and delivered in cooperation with Senge Group at Trinity College Dublin, Ireland. The TMAP and TSPP porphyrins were purchased from Sigma Aldrich, while TAPP was purchased from Porphyrin System.

The solvents used for the measurements of the UV-Vis spectra of individual porphyrins are summarized in ***Table* 5**.

Table 5 *Solvents used for preparing solutions of different porphyrins*

Porphyrin	Solvent
TMAP	water[1]
TPP	methanol[2]
TMPyP	water
ZnTMPyP	water
TAPP	ethanol[3]-water (1:2 v/v)
TSPP	water

1- obtained using the Simplicity cleaning system,18MΩcm; 2- Sigma-Aldrich, HPLC grade; 3J.T.Beaker, HPLC grade

Solvents and Other compounds

2% colloidal solution of SnO_2 and RhB, acsorbic acid were purchased from Alfa Chemicals and Sigma-Aldrich, respectively. Anhydrous DMF was purchased from Sigma-Aldrich

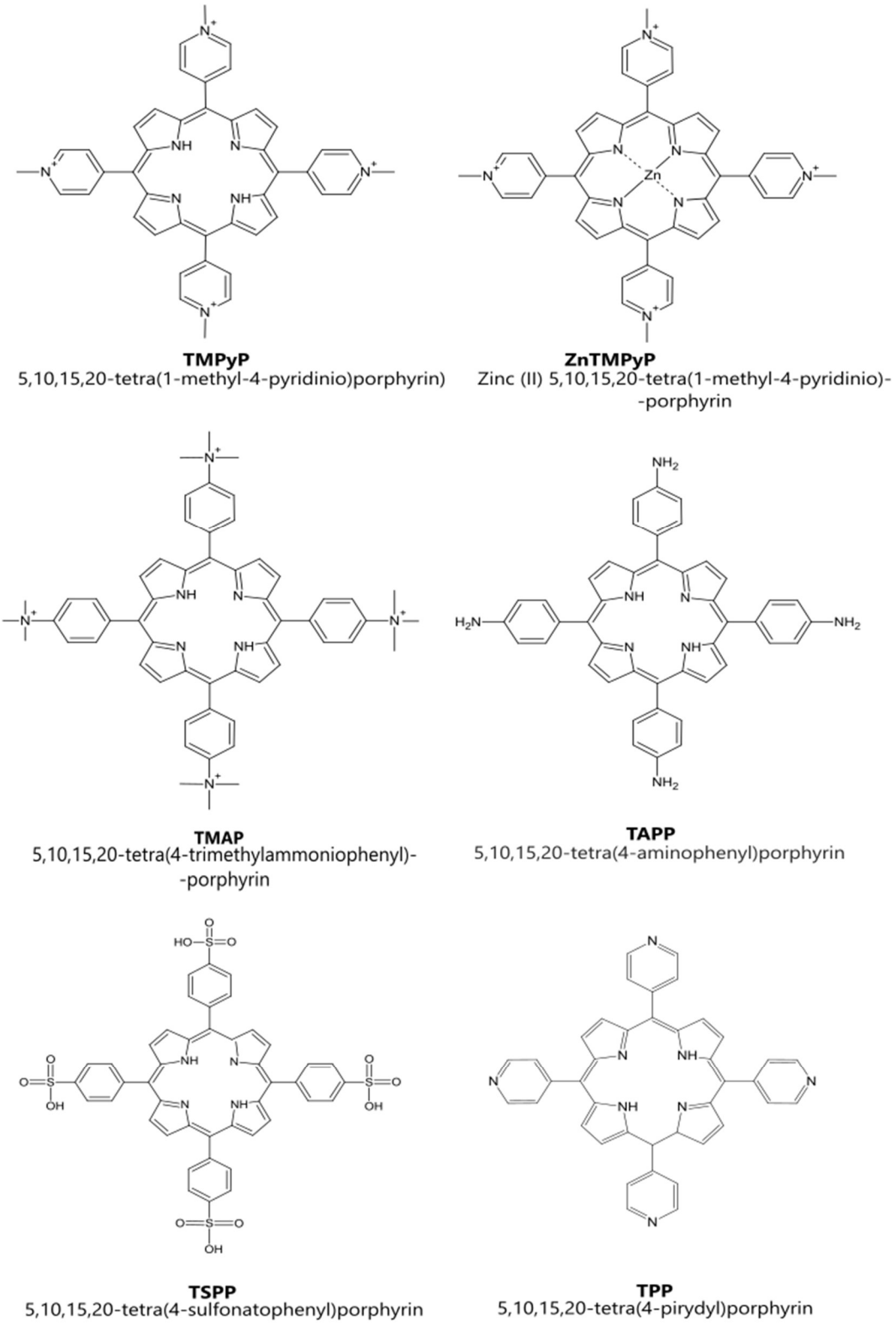

Figure 10 *Structural formulas and names of the investigated porphyrins*

4.2 UV-Vis absorption measurements

Absorption spectroscopy refers to spectroscopic techniques that measure the absorption of radiation, due to its interaction with a sample. It measures the absorbance of light by a compound as a function of the wavelength or frequency in the UV-Vis range. The irradiation light used to excite the sample covers the UV range (180^{112}/200^{113} nm - 400 nm) and the visible range (400 nm - 750 nm). Every molecule has its characteristic frequencies of electromagnetic radiation that it can absorb, which leads to a reduction in the intensity of the electromagnetic radiation as it passes through the sample. When a molecule absorbs a photon from the ultraviolet-visible (UV-Vis) range, it is excited from the ground state (low-energy state) to the electronic excited state (high-energy state). That is, an electron is promoted from the highest-occupied molecular orbital (HOMO) to the lowest-unoccupied molecular orbital (LUMO) of the molecule (***Figure* 11**). The energy difference between the highest occupied molecular orbital (HOMO) and the lowest unoccupied molecular orbital (LUMO) determines the wavelengths of electromagnetic radiation that a molecule can absorb. A molecule can absorb radiation of a specific wavelength when the energy difference between HOMO and LUMO matches the energy of the radiation. Thus, molecules with smaller HOMO-LUMO energy gaps absorb longer wavelengths of light, while those with larger energy gaps absorb shorter wavelengths, since they require more energy to be excited.

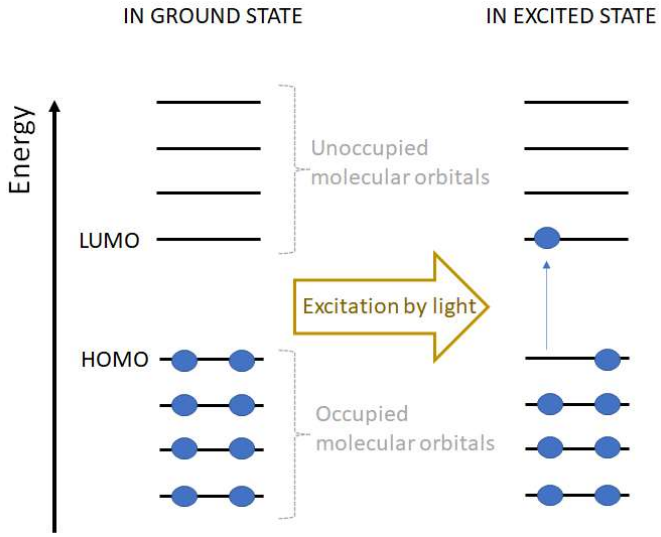

Figure 11 *Diagram illustrating the HOMO and LUMO orbitals of a molecule. (Each circle represents an electron in an orbital): when electromagnetic radiation with sufficient energy is absorbed by an electron in the HOMO, it transitions to the LUMO*

Spectrophotometers are used to obtain the absorption characteristics of a given substance. The absorption spectrum is displaying the relationship between the absorbance and the wavelength of the incident light. Analysis of the absorption spectra is based on two Lambert-Beer laws, which are one of the fundamental laws of absorption. The first Beer's law states that absorption is proportional to the number of absorbing molecules, and therefore depends on the concentration of the sample. Lambert's law also states that the fraction of radiation absorbed is independent of the intensity of the radiation.

***Figure* 12** illustrates a schematic representation of the concept of measuring the sample absorption. Suppose that the solvent absorption coefficient is equal to zero. In that case, according to the Beer-Lambert law, the monochromatic radiation (λ) beam after passing through a homogeneous solution of a substance with a concentration of *c* is weakened according to the equation:[112]

$$I = I_0 \times 10^{-\varepsilon l c} \tag{2}$$

where:

I – the intensity of transmitted light [Einstein dm^{-3} s^{-1}]; I_0– intensity of incident light, [Einstein dm^{-3} s^{-1}]; ε – molar absorption coefficient at wavelength λ [M^{-1} cm^{-1}]; l– length of the light path through the cell [cm]; c– sample concentration [M].

A substance's ability to absorb light at a specific wavelength λ is quantified by its molar absorption coefficient, with higher values indicating greater absorption. Additionally, absorbance (A) can be expressed as:

$$A = log \frac{I_0}{I} = \varepsilon l c \tag{3}$$

According to the Beer-Lambert law (3), the absorption of radiation at wavelength λ depends on:

• the path length

• the concentration of absorbing species (chromophores)

• the molar absorption coefficient.

The electronic absorption spectrum shows the relation between A or ε and the wavelength of light. According to the Beer-Lambert law, the absorption of the sample increases

linearly with the increase of the concentration of the sample. An absorption spectrum is a characteristic feature of a particular chromophore. The wavelength of maximum absorption for each band, along with the accompanying molar absorption coefficient, must be determined in order to provide a comprehensive description of the spectrum.

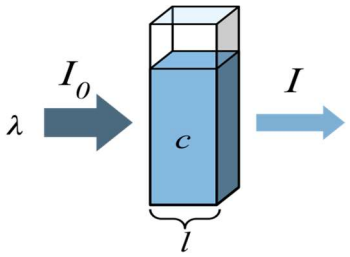

Figure 12 *Schematic representation of the concept of sample absorption measurement (I_0 is the intensity of incident light at wavelength λ*

The absorption of UV-Vis radiation in organic molecules is restricted to functional groups that contain valence electrons of low excitation energy. The valence electron can generally occupy three types of molecular orbitals: single, double, or triple bonds bonding orbitals, and non-bonding orbitals (lone pair electrons). ***Figure* 13** displays the arrangement of the electronic orbitals in terms of their respective energy. The σ bonding orbitals have lower energy than the π bonding orbitals, which have lower energy than the non-bonding orbitals. The absorption of electromagnetic radiation enables an electron to transition from a bonding or non-bonding orbital into one of the empty anti-bonding orbitals.

Most of the observed transitions in the UV-Vis region involve transitions π→π*, n→π* and n→σ*.

The Cary 100 UV-Vis two-beam spectrophotometer and quartz cells (different path lengths, 2 mm to 10 mm) were used to measure the absorption spectra of the compounds at room temperature. The list of the investigated porphyrins and solvents used for the measurements of the UV-Vis spectra of individual porphyrins is summarized in ***Table* 5**.

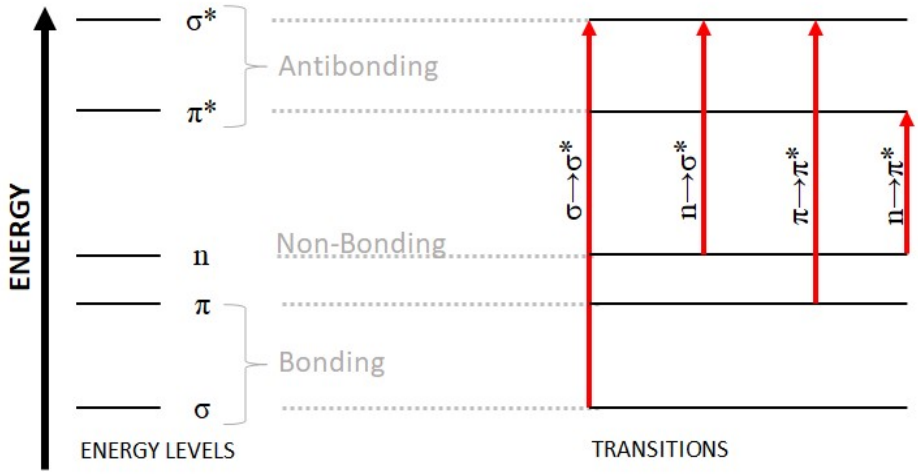

Figure 13 *Diagram of electronic transitions in UV-Vis spectroscopy of organic chromophores*

4.3 Fluorescence measurements

Fluorescence is a spectroscopic technique complementary to UV-Vis absorption. The emission of light by a substance that has absorbed light or other electromagnetic radiation is known as fluorescence. It is a form of luminescence. The emitted light has a longer wavelength, and therefore a lower photon energy, than the absorbed radiation. Moreover, the same orbitals are involved as in absorption spectroscopy. Fluorescence spectroscopy is primarily concerned with electronic and vibrational states. Generally, the species being examined has a ground electronic state (a low energy state) of interest, and an excited electronic state of higher energy (as mentioned in **4.2 UV-Vis absorption measurements**). Multiple vibrational states are found within each electronic state.

The absorption of a photon by a molecule results in the movement of an electron from the highest occupied molecular orbital (HOMO) to the lowest unoccupied molecular orbital (LUMO). From the sublevels, energy loss occurs in a nonradiative way, which is called 'vibrational relaxation'. After reaching the lowest vibrational level of the excited state, the molecule can emit a photon and return to the ground state or to a vibrationally excited ground state. Alternatively, the molecule may decay back to the ground state through the emission of heat or, in some cases, by means of a photochemical reaction.

Overall, this indicates that the photon that eventually gets released has less energy and a longer wavelength than the photon that was initially absorbed. The diagram used to describe this process is called the Jablonski diagram, shown in ***Figure* 14**.

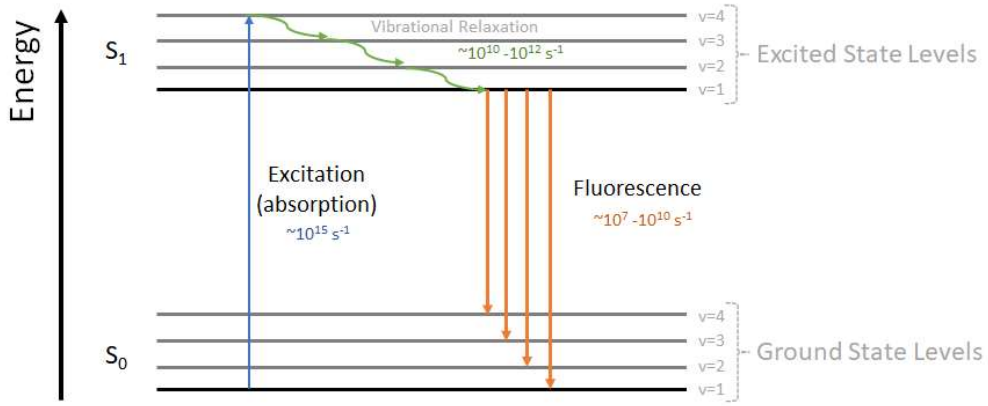

Figure 14 *Fluorescence, shown in this Jablonski diagram, involves emitting a photon of lower energy than the initially absorbed photon. The diagram is read from the left to the right: absorbance (blue) occurs first, then vibrational relaxation (green), and then fluorescence (orange)*

In fluorescence spectroscopy, the Stokes shift is the difference between the spectral position of the maximum of the absorption band and the maximum of the fluorescence emission and can be expressed in either wavelength or wavenumber units, as shown in ***Figure* 15**.[114]

Stokes shift:

$$\Delta\lambda = \lambda_f^{max} - \lambda_a^{max} \tag{4}$$

It should be noted that the wavenumber Stokes shift expression written above is only an approximation, since it assumes that the wavenumber maxima are at the same position as the wavelength maxima, which is not strictly true. When fluorescence spectra are converted from a wavelength scale to a wavenumber scale, the positions of the maxima slightly shift, since the spectral bandpass of the measurement is constant in wavelength but not in wavenumber.

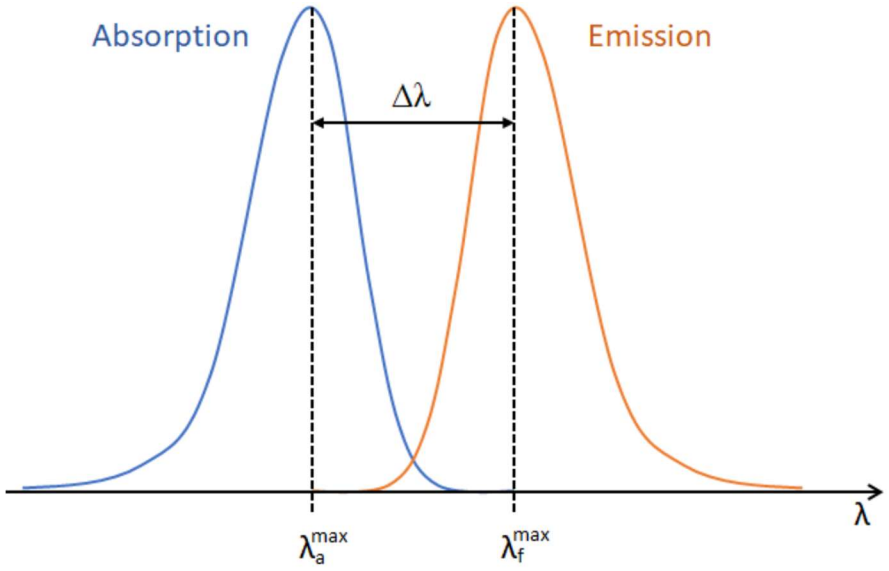

Figure 15 *Definition of the Stokes shift (Δλ)*

The Stokes shift can be explained by the Perrin-Jablonski diagram which depicts the process as an initial excitation to a higher vibrational level of the S_1, followed by a rapid non-radiative decay to the vibrational ground state of the S_1 (***Figure* 14** – green arrows). As a result, the energy of the emitted fluorescence is lower than that of the absorbed photon, causing it to have a longer wavelength.

Following photon absorption, an excited state molecule with an electron at a high-energy vibrational level within an excited electronic state might simply re-emit a photon of exactly the same wavelength as the one that was absorbed. However, the excited electron is much more likely to relax into the lowest vibrational state within the excited electronic state. Thus, if the excited fluorophore dissipates some of that initial excitation energy as heat, it will quickly undergo relaxation to the lowest vibrational energy level of the excited state. An important consequence of this rapid internal conversion is that all subsequent relaxation pathways (fluorescence, non-radiative relaxation, intersystem crossing, etc.) proceed from the lowest vibrational level of the excited state (S_1). Typically, when returning to the ground state (S_0), the transition occurs to a higher vibrational level, which then undergoes vibrational relaxation to reach thermal equilibrium. The probability of returning of the electron to a particular vibrational energy level in the ground state is similar to the probability of this electron's position in the ground state before excitation. This concept, known as the mirror image rule, is illustrated in ***Figure* 16**. The emission transitions (orange lines) from the lowest vibrational energy

level of the excited state back to various vibrational levels in the ground state. The resulting emission spectrum (orange band) is a mirror image of the absorption spectrum displayed for the hypothetical chromophore.

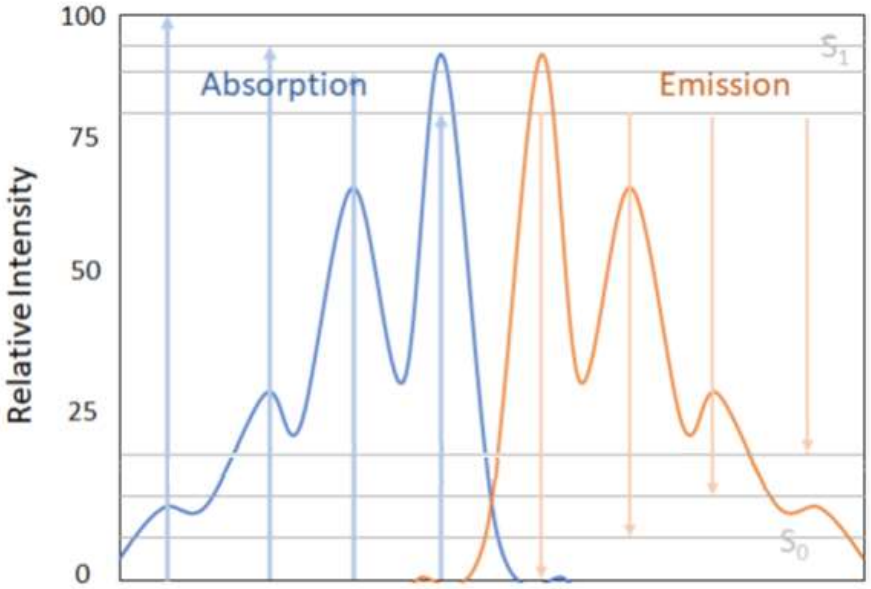

Figure 16 *Schematic representation of the mirror image rule*

In brief, a spectrofluorometer that allows for fluorescence measurement is composed of high intensity light source, excitation and emission monochromators, a sample holder, and a detector connected to the computer (***Figure* 17**).

Measurements of the fluorescence spectra of the studied porphyrins and their hybrids with GO and rGO and GO/rGO itself were conducted using the LS 50B spectrofluorometer (Perkin Elmer). Emission spectra were measured in quartz cells with 10 mm optical lengths in solutions with absorbances at the excitation wavelength not higher than 0.1.

A plot of emission against wavelength for any given excitation wavelength is known as the emission spectrum. To ensure the emission data obtained are reliable and credible, a few rules should be followed:

- the absorption properties should be established before the excitation wavelength is selected.
- excitation spectra are recorded to establish the origin of the emission and to detect the presence of impurities.

- low absorbance (<0.1) should be used at excitation wavelengths to ensure uniform excitation of the sample.
- self-absorption should be recognized to avoid inner filter effects type I and II. (see: **4.3.2 Inner filter effect I and II**)
- possible contributions from the static quenching mechanism (see: **4.3.1 Static and dynamic quenching**) should be evaluated by combining steady-state and time-resolved fluorescence measurements.

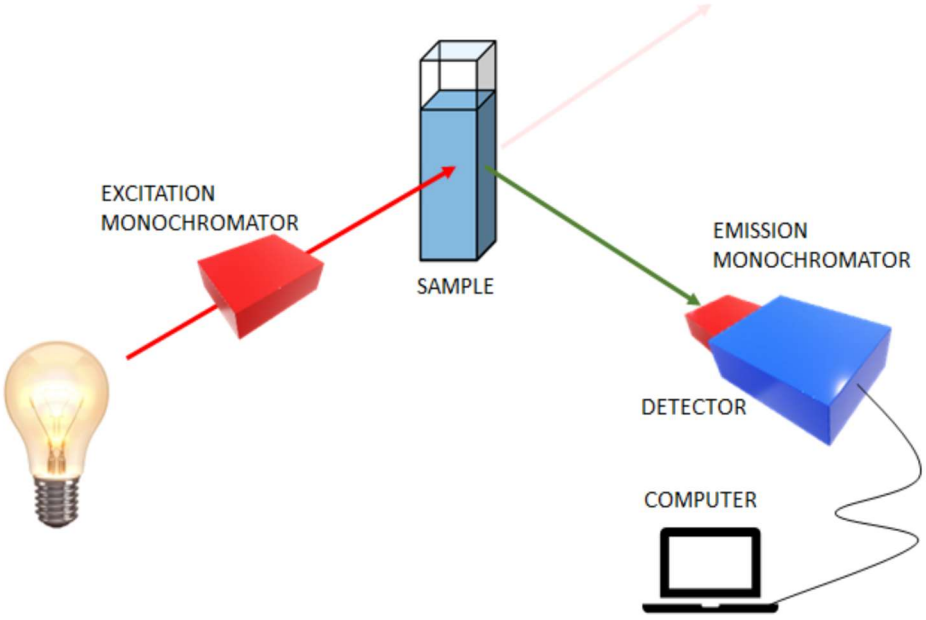

Figure 17 *Schematic representation of the spectrofluorometer*

4.3.1 Static and dynamic quenching

Quenching refers to a physicochemical process that decreases the intensity of the fluorescence of a sample. It can result from various phenomena, including excited-state reactions, energy transfer, complex formation, and collisional quenching is a competing process that reduces the quantum yield of fluorescence. The quenching can occur *via* static or dynamic mechanism (***Table 6***).

Table 6 *Comparison between static quenching and dynamic quenching*

	Dynamic Quenching	Static Quenching
Influence of the increase of the temperature	quenching rate increases	quenching rate decreases
Excited state lifetime	shortening of the excited state lifetime	no change in the excited state lifetime
Absorption spectrum of fluorophore	unchanged	can be distorted

For dynamic (collisional) quenching, the Stern-Volmer equation holds:

$$\frac{I_{f0}}{I_f} = 1 + K_D[Q] = 1 + k_q\tau_0[Q] \quad (5)$$

where:

I_{f0}- intensity of the emission without a quencher; I_f – intensity of the emission with a quencher; K_D – Stern-Volmer constant [M^{-1}]; k_q – bimolecular rate constant [M^{-1} s^{-1}]; τ_0 - lifetime of the excited emissive state without presence of a quencher [s]; [Q] – concentration of a quencher [M].

For dynamic quenching, the I_{f_0}/I_f value is the same as the ratios of the fluorescence quantum yields (ϕ_{f0}/ϕ_f) and excited state lifetimes (τ_0/τ) (**Equation 6.**).

$$\frac{I_{f_0}}{I_f} = \frac{\Phi_{f_0}}{\Phi_f} = \frac{\tau_0}{\tau} \quad (6)$$

where: τ_0 - lifetime of the excited emissive state in the absence of a quencher [s]; τ - lifetime of the excited emissive state with presence of a quencher [s]; ϕ_0 – quantum yield of fluorescence in the absence of a quencher; ϕ - – quantum yield of fluorescence with presence of a quencher.

Static quenching occurs when a fluorophore and quencher molecule form a complex in the ground state, which is nonfluorescent. Therefore, the observed fluorescence can occur only from the uncomplexed molecule. In this type of quenching, the properties

of the excited state of the uncomplexed molecule remain unaltered, and hence the excited state lifetime remains unchanged. There exists an equilibrium between a molecule bound to the quencher and the free molecule (M) and the quencher (Q) as described below, with an equilibrium constant for the static quenching K_s:

$$M + Q \rightleftarrows (M:Q) \qquad K_S = \frac{[M:Q]}{[M][Q]} \tag{7}$$

Static quenching can be described by the equation:

$$\frac{I_{f_0}}{I_f} = 1 + K_S[Q] \tag{8}$$

Interestingly, for static quenching, the dependence of I_{f_0}/I_f on [Q] is also linear therefore based solely on the steady-state measurements dynamic and static quenching cannot be distinguished. However, for static quenching, excited state lifetimes do not change and $\tau_0/\tau=1$.Very often, a molecule can be quenched by through both mechanisms: static and dynamic, which leads to the modified Stern-Volmer(**Equation 9.**):

$$\frac{I_{f_0}}{I_f} = (1 + K_S[Q])(1 + K_D[Q]) \tag{9}$$

The existence of static quenching can be easily identified by the upward curvature of the plot of I_{f_0}/I_f against [Q].

4.3.2 Inner filter effects I and II

The inner filter effect (IFE) is widely regarded as one of the most common phenomena in fluorescence spectroscopy that can impact spectral measurements and data analysis.[92,115] The fluorescence intensity may be affected by species present in the solution that can absorb a portion of the excitation energy. This is particularly critical when added quencher absorbs light at the excitation wavelength. In this case, to correct the observed fluorescence intensities, the equation for the inner filter effect I (IFE I) luore be applied. (**Equation 10**.)

$$I_f^{corr} = I_f^{obs} \frac{A_{D+Q}}{A_D} \left(\frac{1-10^{-A_D}}{1-10^{-A_{D+Q}}}\right) \tag{10}$$

Where: I_f^{obs}, I_f^{corr} – the intensities of fluorescence observed and corrected for the absorption of the exciting light by the quencher, respectively; A_D – the absorbance of the absorber at the excitation wavelength; A_{D+Q}– total absorbance of the absorber and quencher at the excitation wavelength.

Reabsorption of the emitted light by the added quencher can also reduce the measured fluorescence intensity. This situation is called Inner Filter Effect II (IFE II). The inner filter effect II should be taken into account when the absorption and fluorescence spectra of the quencher and fluorophore overlap. The presence of IFE II can be identified by the change in the shape of the fluorescence spectrum. This is because when the concentration of the quencher changes, its ability to absorb the emitted light also changes. To take this effect into account, the absorbance spectrum of the quencher should be measured and subsequently used to compute the correction factor. Then the correction to the fluorescence intensity can be calculated from **Equation 11**.:

$$I_f^{corr} = \frac{I_f^{obs}}{10^{-\varepsilon_Q c_Q l'}} \tag{11}$$

Where: I_f^{obs}, I_f^{corr} – the intensities of the fluorescence intensities observed and corrected for the absorption of the emitted light by the quencher, respectively; ε- molar absorption coefficient of the quencher at the monitored emission wavelength; l' – effective path length for the reabsorption of fluorescence.

4.3.3 Determination of fluorescence quantum yield

Fluorescence quantum yield (FQY) is defined as the ratio of the number of photons emitted to the number of photons absorbed by the substance. FQY can be determined using the standard substance, i.e. a substance with a well-known fluorescence quantum efficiency. Standard samples should have a fluorescence band in the same spectral range as that of the investigated sample. Furthermore, the absorbance for both should be comparable and small (A<0.1). If the studied and standard samples are excited with the light with the same wavelength, the following equation can be applied to calculate the fluorescence quantum yield (**Equation 12.**).

$$\Phi_f^x = \frac{S_x}{S_{st}} \frac{A_{st}^\lambda}{A_x^\lambda} \Phi_f^{st} \frac{n_x^2}{n_{st}^2} \quad (12)$$

Where: Φ_f^x- luorescence quantum yield of a sample x; S_x, S_{st}- integrated fluorescence intensity (area under the spectrum) for sample x and standard sample, respectively; $A_x^\lambda, A_{st}^\lambda$ – absorbance at the excitation wavelength (λ) for sample x and standard sample, respectively; Φ_f^{st}- fluorescence quantum yield of the standard sample; n_x, n_{st} – refractive index for sample x solvent's and standard sample solvents's, respectively.

If the measurements for the sample and the standard sample are conducted in the same solvent, the part of the equation that contains refractive indexes equals one and can be omitted.

4.4 Time-correlated single-photon counting

Time-correlated single-photon counting (TCSPC) was performed to determine the lifetime of the singlet excited state of the sample. The sample is excited by ultra-fast impulses. The TCSPC method records the time between an exciting pulse and the arrival of an individual photon that was emitted to the detector – interval time (***Figure* 18**A). The interval time is measured for each measurement cycle. Conditions of the measurement should be selected carefully to ensure a nearly zero probability of registering more than one photon in a cycle.

The schematic results obtained for TCSPC measurements are presented in histogram form. The histogram shows the number of photons as a function of the time between excitation and emission (***Figure* 18**B).

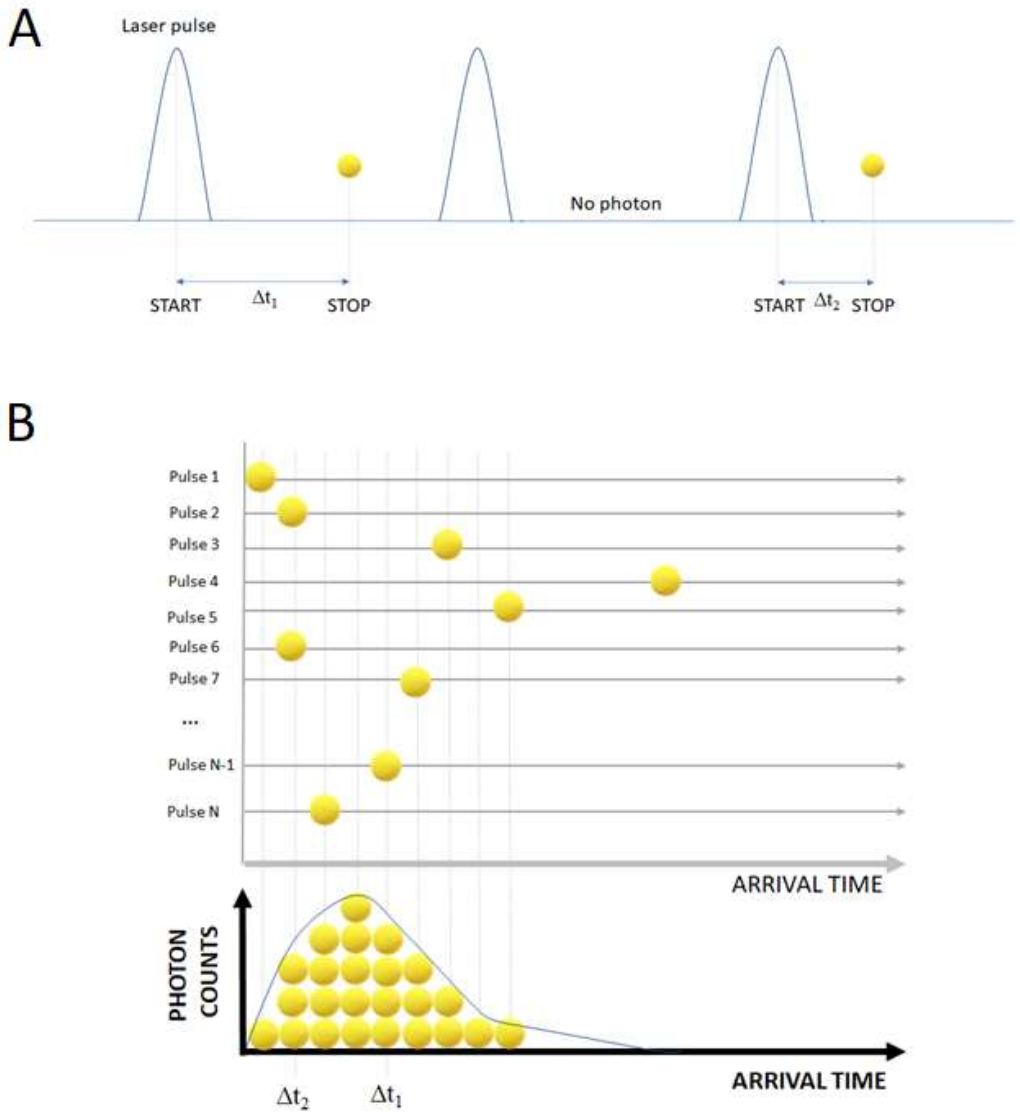

Figure 18 *The principle of measuring fluorescence decay using the TCSPC method. (A) Measurements of the interval between the exciting pulse and the emitted photon, and (B) the final histogram resulting from the TCSPC measurements*

Monoexponential decay can be described with the following mathematical equation:

$$I(t) = \alpha \exp\left(-\frac{t}{\tau}\right) \tag{13}$$

I(t) is the fluorescence intensity at time t, and α and τ are the pre-exponential factors and the decay time, respectively.

However, in the case of multiexponential decay equation (14) is applied:[116]

$$I(t) = \sum_i \alpha_i \exp\left(-\frac{t}{\tau_i}\right) \quad (14)$$

The TCSPC method was used to measure the fluorescence lifetimes of porphyrins and their nanohybrids with GBM. Emission lifetimes were measured using the FluoTime300 high-performance fluorescence spectrometer (PicoQuant) operating in time-correlated single-photon counting mode. Different sub-nanosecond pulsed LEDs were used to excite the investigated samples with appropriate wavelengths (405 or 440 nm). Light-scattering Ludox solution (colloidal silica) was used to obtain the instrument response function (IRF). All samples were measured in quartz cells with a path length of 10 mm. Easy Tau software was used to fit the model functions (one- or two-exponential decays) to fit the experimental data, with appropriate correction for the instrument response.

4.5 Femtosecond transient absorption spectroscopy

Femtosecond transient absorption (TA) spectroscopy measurements allow for monitoring of processes occurring on the picoseconds to a few nanosecond time scale (i.e., singlet excited state lifetime, electron transfer and energy transfer). The method can be applied to obtain transient absorption spectra of short-lived individuals (excited states, products of charge transfer) and the kinetics of their formation and disappearance.

The TA technique is a pump-probe technique in which two laser beams are used. ***Figure 19*** and

Figure 20 present a concept of the method and the experimental setup. First beam a monochromatic energetic pump pulse that triggers the photoexcitation of the sample and a weak (broad or monochromatic) probe pulse, which monitors the absorbance changes caused by excitation. The pump pulse is resonant with the electronic transition of the photosystem. Thus, the pulse induces the transition of a certain amount of molecules to their excited states by a vertical Franck-Condon transition.

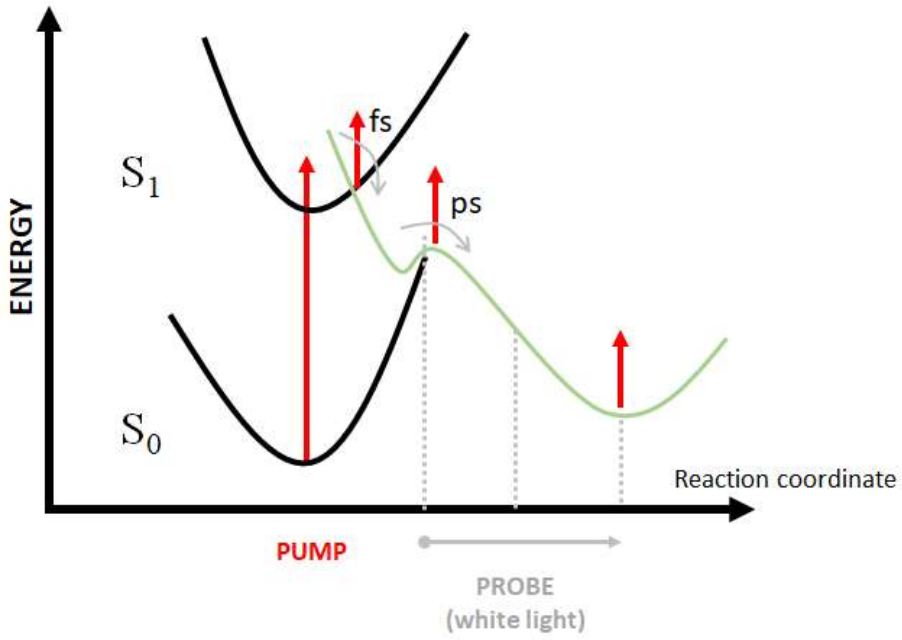

Figure 19 *Principle of femto-TA*

Additionally, the probe beam is separated, in front of the measuring cell, into its two replicas. One is a probing beam (which passes through the excitation area of the sample), whereas the other is a reference beam which passes through the unexcited area. This approach allows to significantly reduce the impact of laser power fluctuations on the measured spectra, and consequently allows the measurement of reliable spectra with much smaller absorbance values.

A transient absorption spectrum is a graph of the dependence of the absorption change on the wavelength. ΔA is the difference between sample absorption before excitation and after excitation after a certain time delay. It is obtained by measuring the spectral intensities of the probe beam for different pump-probe delays. The following equation defines it:

$$\Delta A(\tau, \lambda) = log \frac{I_0(\lambda)}{I(\tau,\lambda)} \tag{15}$$

Where: ΔA – difference between sample absorption and ground and excited state or reaction product ; $I_0(\lambda)$ – the intensity of the probe pulse, measured in front of the

sample; I- the intensity of the probe pulse passing through the sample, measured after the τ time from the moment of excitation.

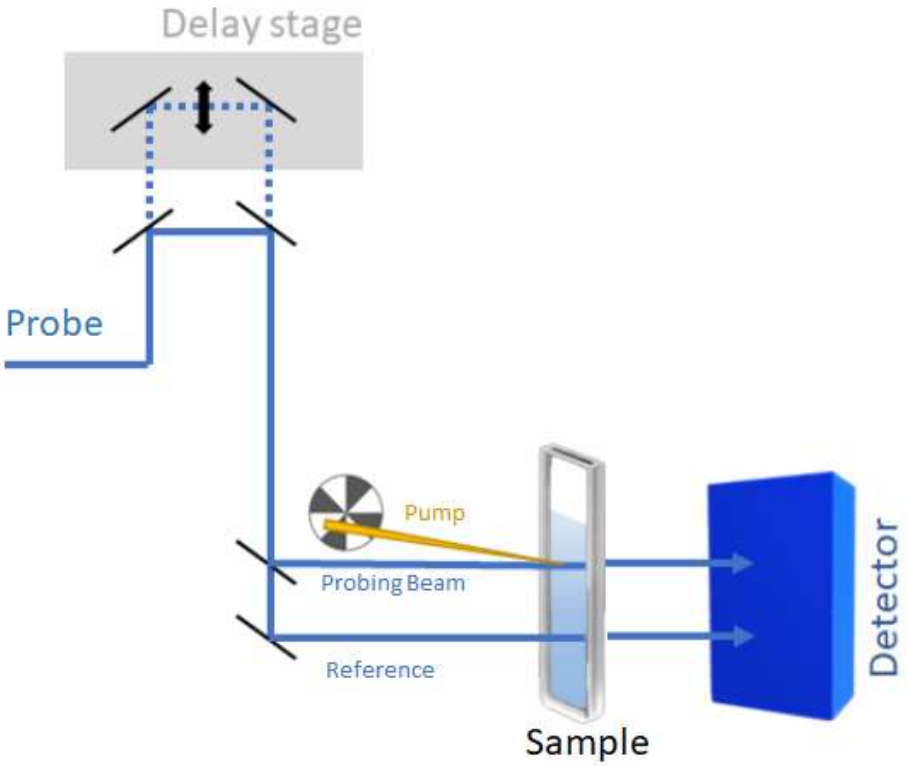

Figure 20 *Schematic representation of the transient absorption technique (two-beam method)*

Femtosecond transient absorption experiments were conducted using a Solstice Ti:sapphire regenerative amplifier from SpectraPhysics, combined with a Helios (Ultrafast Systems) optical detection system. The fundamental output of the Solstice system (800nm) was split the fundamental output of Solstice system (800nm) into two beams: a pump (95%) and a probe (5%). The pump beam was directed through the TOPAS-Prime (SpectraPhysics) automated optical parametric amplifier to obtain the desired excitation wavelength in the range of 290-2600 nm. The probe beam was directed to the Helios: a CCD-based pump-probe TA spectrometer (Ultrafast Systems LLC) with an optical delay line that allows regulation of an appropriate delay time between the pump and the probe (up to 3.2 ns). The white-light continuum was generated from the 5% of the fundamental beam by passing it through the sapphire or calcium fluoride crystal and was used to detect the transients.

Femtosecond transient absorption measurements were used to investigate cationic porphyrins and their nanohybrids with GO. All samples were prepared in quartz cells with a 2 mm path were used. During the measurement, the sample was stirred continuously.

4.6 Nanosecond flash photolysis

Nanosecond laser flash photolysis (LFP) is a technique that enables the study of events that occur on a timescale from a few nanoseconds to milliseconds. A sample is first excited by a strong nanosecond pulse (pump pulse) of light from a pulsed laser. The pump pulse leads to an increase in the population of the excited state molecules. The change in absorption of the sample is recorded over time by temporal analysis of the transmitted probe pulse. This method allows for the study of the decay of the triplet excited states of molecules and short-lived species (i.e., as unstable radical intermediate products).

LFP experiments were conducted using an Nd:YAG laser for excitation (SpectraPhysics) and a pulsed xenon lamp to probe the excited sample. The setup additionally has a monochromator and a photomultiplier tube to detect and convert the acquired signal. The step-scan method recorded transient decays at individual wavelengths, and a step distance was equal to 10 nm. The samples for the LFP measurements were deoxygenated with argon (high purity) for 15 minutes prior to measurements. Rectangular quartz cells (1 cm x 1 cm) were used in the experiments.

4.7 Fourier-transform infrared spectroscopy

Fourier-Transform Infrared Spectroscopy (FTIR) is a type of infrared spectroscopy that involves passing infrared radiation through a sample. When the radiation interacts with the sample, some of it is absorbed The absorbed energy in the infrared region corresponds to the oscillation energy of the molecules which can cause bonds to stretch or bend (***Figure* 21**). It is called stretching or bending vibration. The IR light is absorbed when the frequency matches the frequency of a particular vibrational mode.

The presence of the various bonds in the sample can be identified by the presence of the characteristic frequencies for the bond vibration. According to the selection rules for IR vibrations the vibrations are active only when the dipole moment of the molecule changes during the absorption.

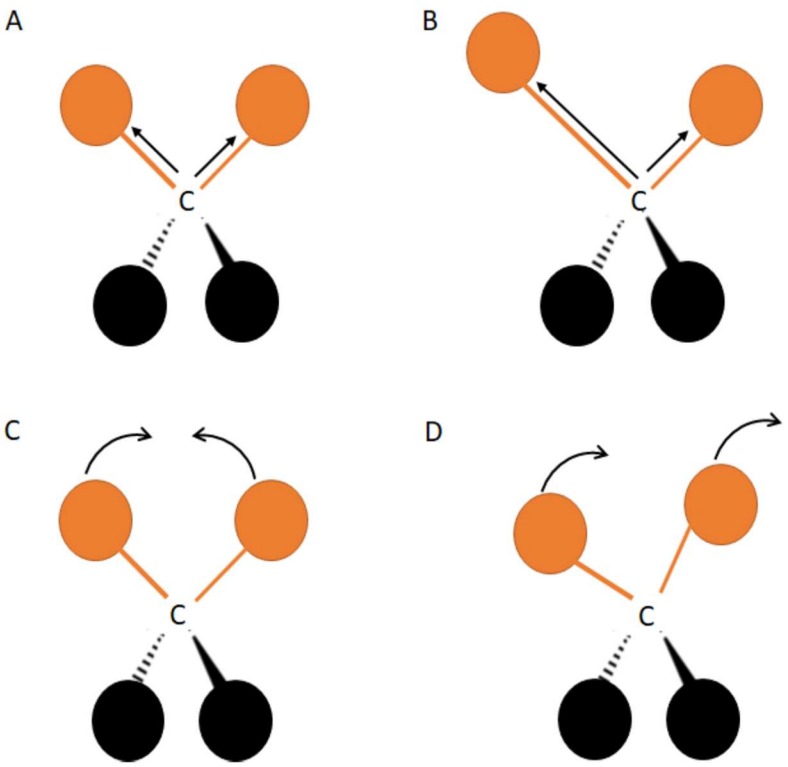

Figure 21 *Examples of different types of vibration modes: A) symmetric stretching, B) asymmetric stretching, C) scissoring, and D) rocking*

The obtained FTIR spectrum can be depicted as a dependence of transmittance (expressed in %) on the wavenumber. It is a "molecular fingerprint" of a sample, and there are no two molecular structures with identical IR spectra. Infrared spectroscopy is a useful tool for identifying unknown materials, assessing the quality or consistency of a sample, and determining the number of components in a mixture.

***Figure* 22** presents a schematic representation of the FTIR technique. Infrared radiation is emitted from the source and passes through an aperture that controls the amount of energy that reaches the sample. The beam enters the interferometer. This part of the FTIR setup is employed to make the simultaneous measurement for all possible IR frequencies. The interferometer produces a special type of signal that has all frequencies 'encoded' into it. Then, the beam reaches the sample, where it is transmitted through or reflected off, depending on the type of analysis. In this place, specific frequencies of energy for the material are absorbed. Finally, the beam passes to the detector for the final measurement. The detectors are designed to measure unique interferogram signals.

The signal is digitized, sent to the computer, and treated by the Fourier transformation procedure.

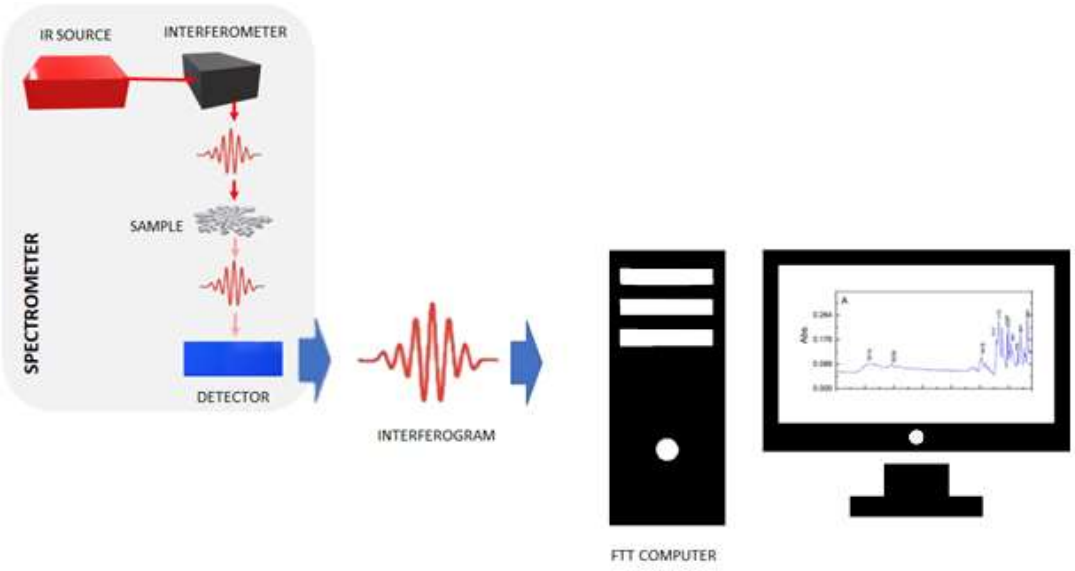

Figure 22 *Schematic representation of the FTIR technique*

The FTIR method was used to confirm the successful functionalization of GO or rGO with porphyrins. It was realized by a qualitative comparison of the GO/rGO FTIR spectrum with the spectrum obtained for the hybrid. Samples for FTIR measurements were prepared as a pellet of the investigated hybrid with KBr. The hybrid was previously centrifuged from the solution (12000 rpm, 45 minutes) and dried at 80°C throughout the night. The pellet contains approximately 0.5% w/w of the investigated substance.

4.8 Elemental analysis

Elemental analysis (EA) is a method that allows the investigation of the elemental composition of the substance. A fixed amount of investigated substance is used to carry out the experiment. The EA can be both, quantitative, and qualitative. Qualitative EA gives information on which chemical elements are present in the sample. Quantitative EA shows the amount of each element in the investigated sample/compound.

The most common EA is the CHNS/O version, which is based on the combustion of the sample. Upon combustion, the sample generates gases based on elements C, H, N, and S. These combustion products are detected using gas chromatography, which allows the

elemental composition to be quantified in the sample. C, H, N and S can be determined simultaneously, while O can be analyzed in a second step by pyrolysis.

***Figure* 23** is a schematic representation of the EA technique. The sample is introduced into the combustion chamber with various reductive and catalytic zones to convert compounds to gases, such as CO_2, H_2O, SO_2, and N_2. Gas chromatography is then used to separate them. Gases are quantified with a thermal conductivity detector to determine the carbon, hydrogen, and nitrogen percentage in the sample.

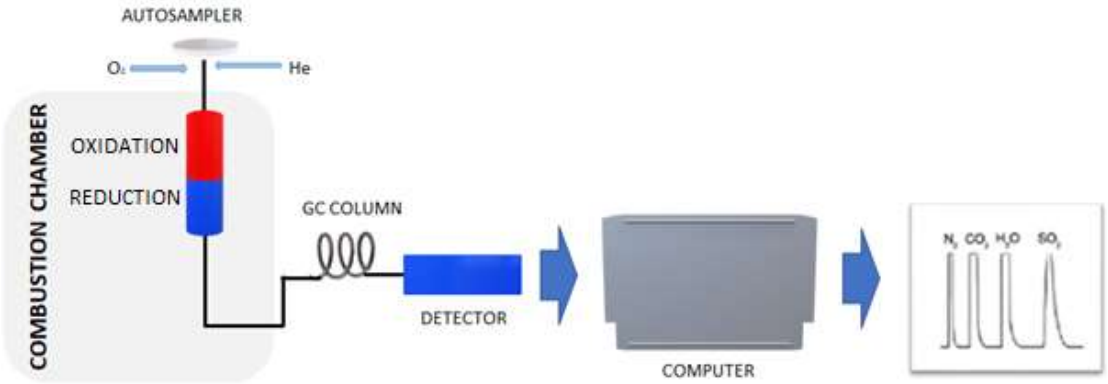

***Figure 23** Schematic representation of the EA technique*

Elemental analysis measurements were obtained using a Thermo ScientificFlash 2000 CHNS/O analyzer. The samples for the EA measurements were prepared by weighing the fixed amount of the investigated samples (minimum 5 mg per sample). The samples were prepared as pure and dried powder. Then 8 mg of V_2O_5 were added. V_2O_5 is used as an oxidation catalyst. An oxidation catalyst is used to complete the oxidation of the sample, and a reduction catalyst is used to perform any required reduction and remove any excess oxygen.

4.9 Thermogravimetric analysis

Thermogravimetric analysis (TGA) is an analysis method that allows to determine the thermal stability of the substance. Measurement is based on the determination of the loss of the sample mass with the temperature increase. Through the TGA, physical phenomena such as second-order phase transitions, vaporization, desorption, etc., and chemical phenomena such as decomposition, dehydration, etc., can be studied. The TGA analyzer

can also be connected to an FTIR spectrometer, a mass spectrometer, or a gas chromatograph.

***Figure* 24** presents schematically the TGA technique. The fixed amount of the investigated sample is placed in the platinum basket, and the basket is placed in a holder and then in a heating tube. The temperature in the tube changes in a fixed temperature range with a fixed step. The sample mass is continuously monitored and measured over time thanks to a built-in balance.

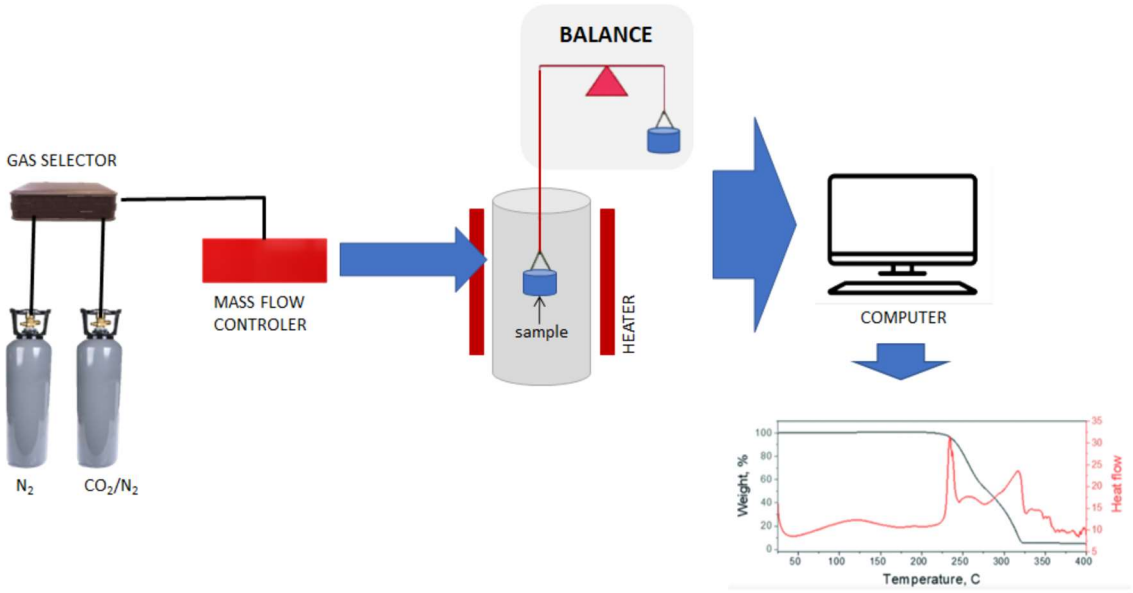

***Figure 24** Schematic representation of the TGA technique*

Porphyrin samples, GO and rGO, and their hybrids were investigated by a thermogravimetric analyzer (Mattler Toledo TGA/DSC3+). Measurements were carried out in an argon atmosphere from room temperature to 900°C with a step equals to 10°C/min.

All samples used for the TGA measurements were dried powdered.

4.10 Atomic force microscopy

Atomic force microscopy (AFM) is a high-resolution non-optical imaging technique. It is a powerful tool for surface analysis. AFM allows accurate and non-destructive measurements of the various properties (topographical, electrical, magnetic, chemical, optical, mechanical, etc.) of a sample surface in air, liquids, or ultra-high vacuum.

Measurement is accomplished by scanning the surface with a sharp tip using a feedback loop to adjust the parameters needed to image a surface in a raster pattern. AFM does not require a conducting sample, and atomic forces are used to map the tip-sample interaction. The AFM tip is usually made of silicon or silicon nitride and is integrated near the free end of a flexible AFM cantilever. AFM demonstrated resolution on the order of fractions of a nanometer, more than 1000 times better than the optical diffraction limit.

Atomic force microscopy images were recorded on an Agilent5500 AFM instrument. Samples for the AFM measurements were prepared by dropping diluted aqueous suspensions onto a mica surface and drying them in air.

4.11 Transmission electron microscopy

Transmission electron microscopy (TEM) is a microscopy technique in which a beam of electrons is transmitted through a specimen to form an image. Transmission electron microscopes operate on many of the same optical principles as the light microscope. However, they are capable of imaging at a significantly higher resolution than light microscopes, owing to the smaller de Broglie wavelength of electrons. This increased resolution allows to study the surface and structure of biological samples (organelles, viruses and macromolecules). The analysis of metallic materials allows for the observation of their structure, interfacial boundaries, crystallographic structure, chemical bonds, or arrangement of atoms.

TEM employs a high-voltage electron beam in order to create an image. An electron gun at the top of a TEM emits electrons that travel through the vacuum tube of the microscope. Rather than having a glass lens focusing the light (as in the case of light microscopes), the TEM employs an electromagnetic lens which focuses the electrons into a very fine beam. This beam then passes through the specimen, which is very thin, and the electrons either scatter or hit a fluorescent screen at the bottom of the microscope. An image of the specimen appears on the screen with its parts displayed in different shades according to its density. This image can then be studied directly within the TEM or photographed.

Porphyrin structures in aqueous dispersion were imaged in EM 912 (Zeiss) Transmission Electron Microscope after placing drops of dispersion onto copper grids, firmware of 200 mesh, and leaving the liquid to dry in air at room temperature.

4.12 Transient photocurrent

The transient photocurrent (TPC) measurement technique is used to study the time-dependent (on a microsecond time scale) extraction of charges generated by the photovoltaic effect. The measurement of TPC is realized by irradiation of the cell. The cell consists of a working electrode (investigated sample), a counter electrode, a reference electrode, and an electrolyte. A pulsed light source treats the investigated sample. There are two ways to measure TPC: in a “light on” and a “light off” position. In a ‘light on’, the signal is recorded as soon as the excitation pulse is switched on, allowing to observe the build-up of charges on the electrode after the start of excitation. ’Light off’ measurements show how the decay of the after the pulse is switched off. Performing several on-off cycles allows to check the repeatability of the process. The time between switching the irradiation on/off can be fixed.

The electrochemical workstation (Keithley model 617 programmable electrometer) was used to conduct photoelectrochemical activities. The 0.1 M LiI acetonitrile solution was used as an electrolyte. Experiments were performed using a three-electrode quartz cell. The saturated calomel electrode was the reference electrode, a platinum electrode was used as the counter electrode, and the electrodes with investigated samples acted as the working electrodes. The photocurrents of the working electrodes with and without irradiation were measured at 0 V using a fiber optic illuminator as the light source. The irradiation was switched on and off in 30-second periods to measure the light and dark current responses.

The samples used for the transient current photovoltaic (TCP) experiments, specifically the working electrodes, were prepared by depositing a layer of SnO_2 on a fluorine-doped tin oxide (FTO) glass electrode using the doctor-blading method. The deposited sample was then thermally treated under an air atmosphere. The prepared samples were coated with GO by electrophoretic deposition. The GO - SnO_2 - FTO electrodes were left overnight in the porphyrin baths (60 μM) and dried in air to achieve porphyrin functionalization on their surface.

5. Results and Discussion

5.1 Characteristics of 2D materials used in work

In this work, two types of 2D materials were employed namely – graphene oxide and reduced graphene oxide. Graphene oxide, received from Graphene Laboratory, was prepared by oxidizing graphite powder using a modified Hummers' method.[117] The experiments were carried out using the GO material, which also served as the starting material for obtaining rGO through its chemical reduction using ascorbic acid (***Appendix* 1**). The GO dispersions in water were stable and displayed a yellow-brown colour. The aqueous rGO dispersions exhibited a noticeable showed a distinct colour change from yellow-brown to black upon reduction with ascorbic acid (inset of ***Figure* 25**).

The UV-Vis spectra of the GO and rGO suspensions are shown in ***Figure* 25**. The absorption spectra of GO have been reported previously in a number of publications.[43,118,119] A sharp peak at ~230 nm is due to to π–π* transition of aromatic C=C bonds in an aromatic ring, while the broad shoulder peak at 300 nm was attributed to the n-π* transition of carbonyl groups.[119,120] The intensity and position of these two peaks may vary from sample to sample. [121,122] The progress of GO reduction can be monitored by UV–Vis spectroscopy. The C=C peak position of the rGO synthesized at different reduction times is shown in ***Figure* 26**. As the reduction time increased, the red-shift of the λ_{max} peak and the disappearance of the shoulder peak were observed. These changes indicate the restoration of double bond conjugation in the rGO sheets and the concurrent simultaneous removal of oxygen functionalities, respectively (***Figure* 26**).[123] In the case of 2D materials used, signature peaks of GO disappeared and the spectrum is red-shifted with a maximum at 259 nm. Also, the absorption background between 260 and 800 nm increases obviously. All of that indicates an increase of the degree of sp^2 conjugation by a regeneration of the sp^2 π-conjugated network.[124]

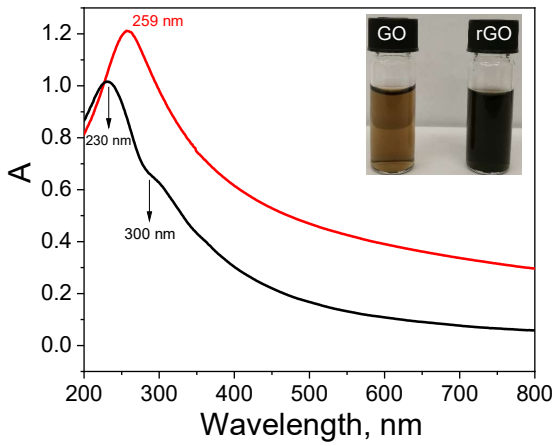

Figure 25 *UV-Vis spectra of the aqueous solution of GO (black) and rGO (red). The inset is an image of GO and rGO suspensions*

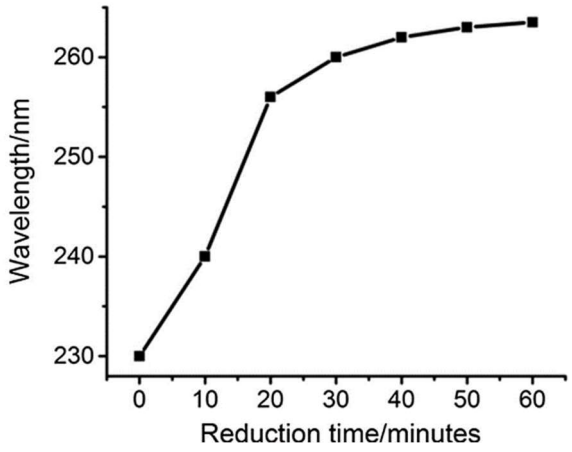

Figure 26 *The C=C peak position shifting of rGO synthesized at different reduction times. Adapted from ref*[43] *with permission from Elsevier (2018)*

The obtained materials were characterized by X-ray photoelectron spectroscopy (XPS) (***Figure*** **27**A), TGA (***Figure*** **27**B) and FTIR (***Figure*** **28**). XPS provides important information on the chemical and electronic state of the element present on the surface and, in that case, is useful for investigating the efficiency of the reduction by the ascorbic acid. In ***Figure*** **27**A are reported the C1s XPS spectra of GO and rGO. On the XPS spectrum of graphene oxide, a high degree of oxidation is clearly visible. On the other hand, the C1s spectrum of rGO shows the same peak, but in this case, the intensity peaks relative to the oxygen functional groups are much weaker, demonstrating efficient oxygen removal. The C/O ratio of rGO is improved from 2.2 to 4.1 of GO showing that a large

amount of the oxygen-containing groups are successfully removed from GO after reduction.

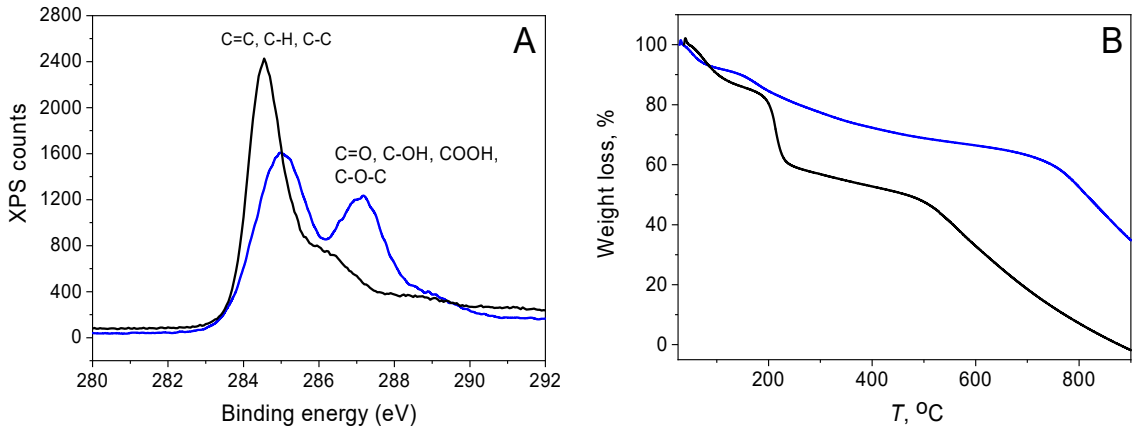

Figure 27 *A) The C1s scan XPS spectra of the GO (black) and rGO (blue) samples; B) TGA curves of GO (black) and rGO (blue)*

The confirmation for the successful reduction of GO was derived from TGA. ***Figure* 27**B shows the TGA curves of GO and rGO. The mass loss of about 16% from room temperature to 180 °C for GO can be ascribed to the loss of adsorbed water. The mass loss of approximately 24% at 215 °C was related to the decomposition of unstable oxygen functional groups. In the case of rGO, no sharp mass loss at 215 °C was observed.

Consistent with the XPS analysis, the FTIR spectra (***Figure* 28**B) clearly show the effective chemical reduction of GO. As shown in ***Figure* 28**B, the peaks attributed to C=O in carboxylic acid and carbonyl moieties (υC=O at 1622 cm^{-1}), C–OH (υC–OH at 1380 cm^{-1}) and the broad peak around 3400 cm^{-1} attributable to the C–OH stretching vibrations of a hydroxyl group decrease dramatically in the transition from GO to rGO. This implies a partial reduction of GO. The spectrum of GO shows a lot of functional groups present in the structure (***Figure* 28**). Skeletal vibrations of the C=C bonds in graphitic structures overlapped with the vibrations of the O−H bonds in the water molecules present in the GO sample. Additionally, there are shown peaks around: 1156 cm^{-1} (stretching vibrations of the C−O bonds) and 1040 cm^{-1} (stretching vibrations of the C−O-C bonds in the epoxy groups).

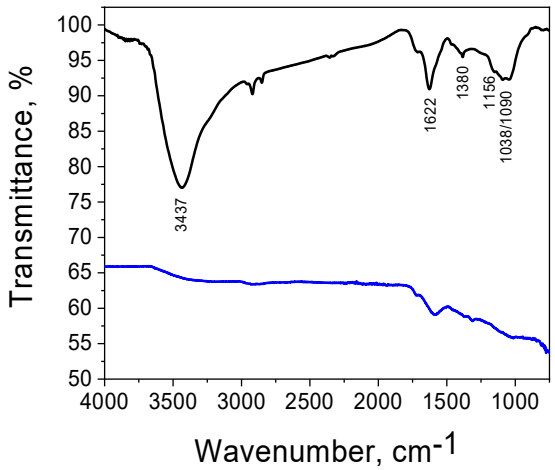

Figure 28 *The FTIR spectra of GO (black) and rGO (blue)*

The GO sheets were imagined by AFM (***Figure* 29**). The obtained results allowed to estimate their lateral sizes to be 1-2 μm with an average thickness of 0.9 nm what is in great agreement with literature[125] (***Figure* 30**).

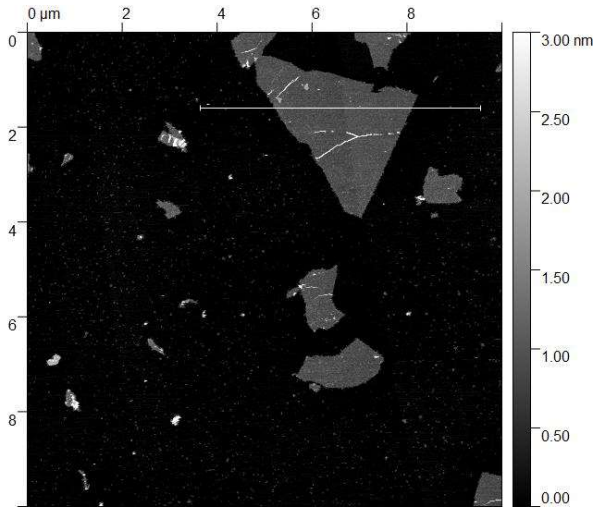

Figure 29 *A representative AFM image of the GO sheets collected from GO dispersion in water*

Moreover, oxidation level, flakes size, and number of layers of GO sheets may vary depending on the conditions of their preparation. Gacka *et al.* demonstrated that there is a correlation between the size/ number of graphene oxide flakes and the photocatalytic activity of GO. They evaluated the effect based on the photocatalytic hydrogen production in a system containing eosin Y as a sensitizer, triethanolamine as a sacrificial electron donor, and $CoSO_4$ as a precatalyst.[126] It was found that too long ultrasound

treatment had a negative impact on the GO enhancement of hydrogen production which was related to fragmentation of GO flakes. The photocatalytic system produced the highest amount of H_2 when graphene oxide occurs as monolayers, and the efficiency becomes lower with the decreasing GO sheet size.

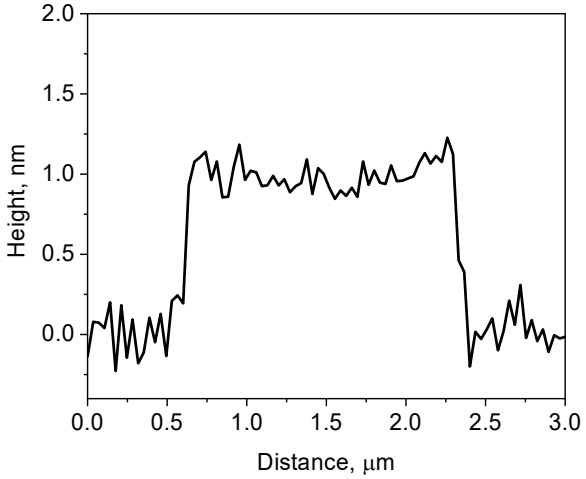

Figure 30 *A thickness distribution histogram for GO sheet*

The ionic strength and pH are vital factors affecting the aggregation of GO sheets. According to the new aggregation model[127], one can quantitatively predict the aggregation behaviour of GO sheets under different ionic strengths and pH values. The stability of GO sheets depends on the equilibrium between the van der Waals attraction and the electrostatic repulsion. The electrostatic repulsion between the adjacent GO sheets mainly stems from the deprotonated oxygen functional groups such as the carboxylic group. Therefore, the pH value of the GO dispersion is the key to the stabilization of the GO sheets because it largely influences the surface charge density of GO. It is known that both (multilayered) graphite oxide and (single-layered) graphene oxide dispersions tend to coagulate under highly acidic conditions as a result of the loss of surface charge.[128,129] The pK_a of GO is around 4.0 which means that under low pH most of its carboxyl groups are protonated[52], which may affect non-covalent interaction with different molecules.

The conduction band edge of GO, used in the conducted considerations and calculations, was taken from the literature and was found to be equal to -0.55 V vs. NHE.[130]

5.2 Cationic porphyrins

5.2.1 TMPyP and its zinc derivative ZnTMPyP

Two noncovalent porphyrin/graphene oxide nanohybrids were synthesized by mixing the solution of the cationic porphyrin TMPyP or its zinc(II) derivative (ZnTMPyP) with a graphene oxide suspension, followed by their spectroscopic characterization. These nanohybrids were investigated for their potential use in RhB photodegradation. The structures of TMPyP and ZnTMPyP are shown in ***Figure* 10** (Chapter **4.1 The compounds used in the doctoral dissertation**). The nanohybrids were comprehensively compared focusing on their spectroscopic and photocatalytic properties. The main objective of this work was to determine whether the presence of a Zn(II) atom in the porphyrin core affects the photocatalytic activity of the nanohybrid toward RhB degradation (***Scheme* 8**).

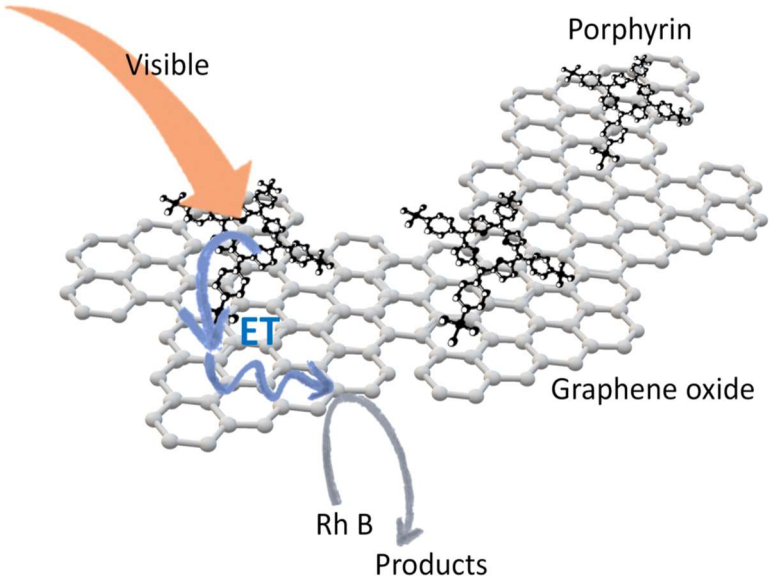

Scheme 8 *Illustration of the concept of RhB photodegradation in the system containing the non-covalent Por/GO hybrid*

5.2.1.1. Steady-state absorption properties

TMPyP is a water-soluble porphyrin with four N-methylpyridyl substituents in the meso positions. At neutral pH, TMPyP carries a charge of +4. Under strongly acidic conditions the protonation of imino nitrogens increases the overall charge to +6. Based on acid-base

titration, the pK_a of the protonation of imino nitrogens in the porphyrin core was determined to be 1.2 (***Figure* 31**).

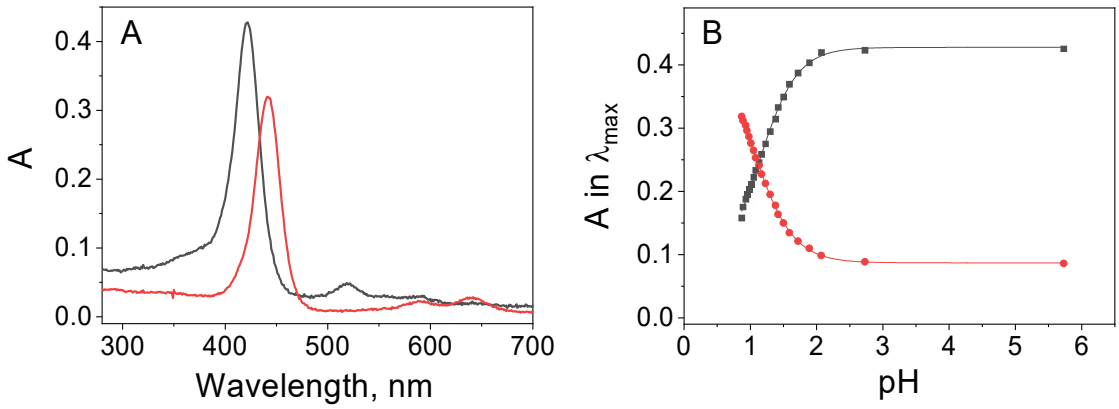

Figure 31 *A) UV-Vis absorption spectra registered for TMPyP solution (2.3 μM) at neutral (pH 7.0) (black) and acidic condition (pH 1.0) (red) B) Fitting of Boltzmann function to the dependence of the absorbance at 421 nm (red) and 442 nm (black) as a function of pH*

ZnTMPyP has been obtained through the metalation of the porphyrin core with Zn(II) and resulting in a molecule that can exists only as a cation with +4 charge.

Porphyrins are prone to aggregation, which affects their spectroscopic properties. However, for $TMPyP^{4+}$ and $ZnTMPyP^{4+}$, because of Columbic repulsion between the cationic porphyrin molecules, aggregation is not likely.[131]

The absorption spectra for both $TMPyP^{4+}$ and $ZnTMPyP^{4+}$ were compared in a water solution under neutral conditions (***Figure* 32**). The spectra exhibited characteristic bands expected for porphyrin molecules, that is, the Soret and Q-bands. The UV-Vis spectrum obtained for $TMPyP^{4+}$ exhibited a Soret band with a maximum at ca. 422 nm and four less intense Q-bands at ca. 518, 555, 584, and 642 nm. The Zn(II) intersection into the porphyrin ring caused a 15 nm red-shift of the Soret band along with a decrease in the molar absorption coefficient. The shift of the Soret band can be explained by the fact that the zinc metalloporphyrin is a closed-shell ion, in which zinc-based orbitals have low energy. This reduces the energy gap between the HOMO and LUMO levels of the porphyrin ring.[66] In addition, the UV-Vis spectrum of ZnTMPyP poses two Q-bands,at 566 and 613 nm. The decrease in the number of bands can be attributed to the increase in

the symmetry (from D_{2h} to D_{4h}) of the porphyrin ring which is consistent with the reported spectra of porphyrin and analogous metalloporphyrin.[66]

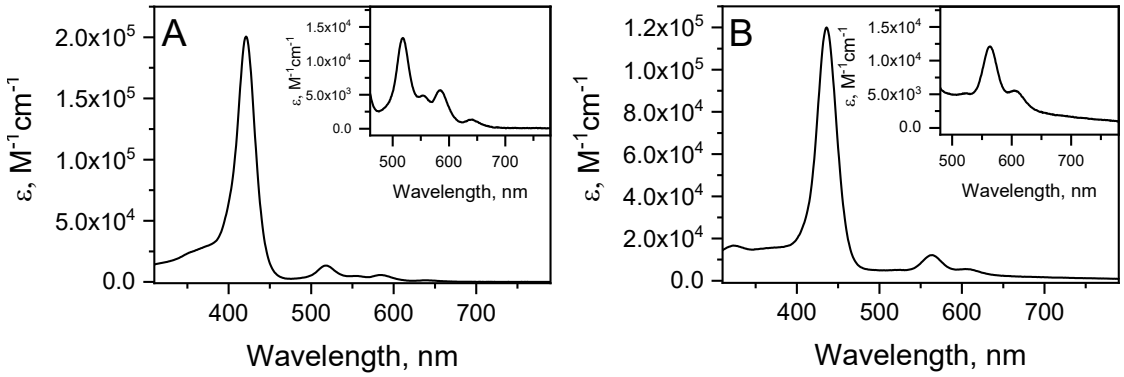

Figure 32 *Absorption spectra of: A) $TMPyP^{4+}$ and B) $ZnTMPyP^{4+}$ in water (inset: Q-band region of the same spectra)*

The molar absorption coefficients were calculated based on the absorbance value of the porphyrin solutions with known concentration, and were equal to $\varepsilon_{422} = 2.0 \times 10^5$ $M^{-1}\,cm^{-1}$ and $\varepsilon_{437} = 1.2 \times 10^5$ $M^{-1}\,cm^{-1}$ for $TMPyP^{4+}$ and $ZnTMPyP^{4+}$, respectively.

Steady-state absorption measurement in the presence of GO

A titration experiment was conducted to estimate the ground state interaction between porphyrin molecules and graphene oxide surfaces. 3 mL of each porphyrin ($TMPyP^{4+}$ or $ZnTMPyP^{4+}$) solutions were placed in a quartz cuvette with a 10 mm light path and titrated with an aqueous solution of GO with a fixed concentration, i.e., 0.2 mg mL^{-1}.

The optical absorption spectra of the series $TMPyP^{4+}$/GO nanohybrid suspension obtained during the titration experiment are shown in ***Figure* 33**A. The GO solution was gradually added to the 1.0 μM aqueous solution of $TMPyP^{4+}$. The addition of GO caused a significant change in the UV-Vis spectra of the porphyrin. The Soret band at 422 nm disappeared, and a new red-shift band at ca. 440 nm was formed simultaneously. The new band can be assigned to the increasing concentration of $TMPyP^{4+}$ porphyrin molecules absorbed on the GO surface. The absorbance at 440 nm increased linearly with the added GO dispersion and reached a maximum for a concentration as low as 6.7 μg mL^{-1}. The clear isosbestic point observed at 434 nm indicates a clear transformation from the free porphyrin to the porphyrin adsorbed on the GO surface.

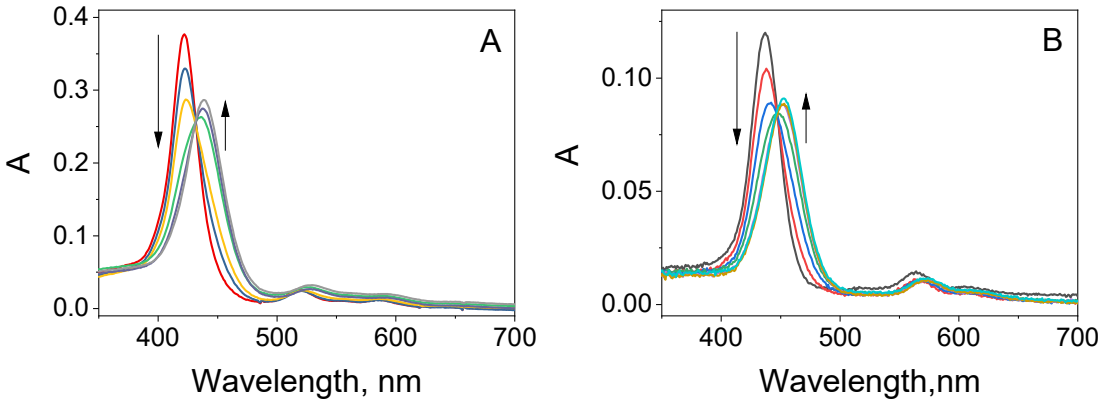

Figure 33 *A) Absorption spectra recorded during the addition of a different amount of aqueous solution of GO (concentration of a stock solution: 0.2 mg mL^{-1}) to: A) 1.9 μM aqueous TMPyP^{4+} solution, B) 1.0 μM aqueous ZnTMPyP^{4+} solution. The spectra are corrected for the GO absorption*

The analogous experiment was carried out for ZnTMPyP^{4+}. ***Figure*** **33**B shows the UV-Vis spectra of the ZnTMPyP^{4+}/GO nanohybrid series recorded during the addition of an aqueous suspension of GO (0.2 mg mL^{-1}) to an aqueous solution of 1.0 μM ZnTMPyP^{4+}. A bathochromic shift of the Soret band position by 16 nm was observed together with the appearance of an isosbestic point at 447 nm. Observed changes provide evidence of an interaction between porphyrin molecules in their ground state and GO surface.

In both cases, the formation of a hybrid resulted in a decrease in the molar absorption coefficient of the porphyrin adsorbed on the GO surface. The molar absorption coefficients obtained for porphyrin/GO nanohybrids are still high and equal to $\varepsilon_{440} = 1.2 \times 10^5$ M^{-1} × cm^{-1} for TMPyP^{4+}/GO and $\varepsilon_{453} = 0.8 \times 10^5$ M^{-1} cm^{-1} for ZnTMPyP^{4+}/GO (***Table 7***).

The bathochromic shifts observed during both nanohybrid formation processes could be explained by at least two mechanisms: (1) J-aggregation of the porphyrin molecules and (2) porphyrin molecule flatten ring. The first possibility is unlikely because under experimental conditions, i.e. pH equals 6.2, the porphyrins exist as +4 cation (four positive charges at the meso substituents). However, it was reported that TMPyP^{4+} in water exist as a monomer at lower concentrations (~10^{-5} M), with higher concentrations it exists as a dimer.[131,132] The formation of the higher aggregates of the TMPyP^{4+} may

be prevented by the electrostatic repulsion between $TMPyP^{4+}$ dimer and monomer at the concentrations below 1×10^{-2} M.[132] The clear isosbestic point during titration (***Figure 33***, ***Table 7***) and the linear dependence of the absorbance at the maximum of the Soret band on the GO concentration (***Figure 34***) suggest that the obtained material has a precisely defined structure. In addition, only a slight broadening of the Soret band was observed for the adsorbed porphyrin.

Table 7 *Summary of the absorption properties of $TMPyP^{4+}$ and $ZnTMPyP^{4+}$ in water as a free molecule and adsorbed on the surface of GO*

Porphyrin	Free porphyrin molecule		Adsorbed on GO		Isosbestic point (nm)
	λ_{max} (nm)	$\varepsilon(\lambda_{max})$ (M^{-1} cm^{-1})	λ_{max} (nm)	$\varepsilon(\lambda_{max})$ ($M^{-1}\times cm^{-1}$)	
$TMPyP^{4+}$	422	2.0×10^5	440	1.2×10^5	434
$ZnTMPyP^{4+}$	437	1.2×10^5	453	0.8×10^5	447

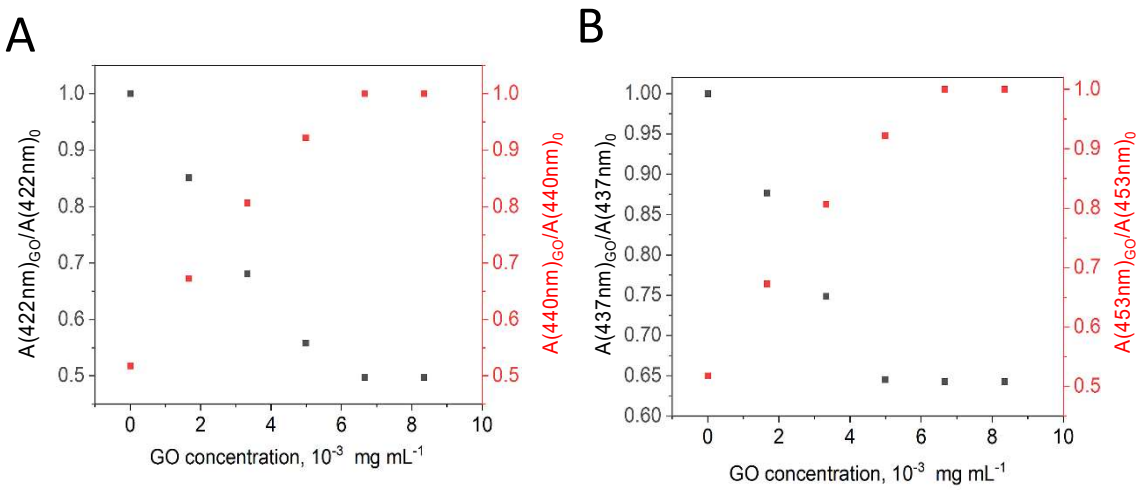

Figure 34 *Dependence of the absorbance changes as a function of GO concentration added to porphyrin solution for A) $TMPyP^{4+}$, B) $ZnTMPyP^{4+}$. The subscripts 0 and GO refer to samples without and with the addition of GO, respectively*

In addition, the AFM measurements were useful tools to investigate the morphology of the porphyrin/GO nanohybrids in more detail. The AMF images obtained provided solid evidence for the molecular assembly of cationic porphyrins on GO sheets. As mentioned in **5.1 Characteristics of 2D materials used in work**, individual sheets of non-functionalized GO in pH 6.2 are 1-2 μm lateral sizes. The GO was present as a single sheet with an apparent thickness of ca. 0.9 nm.[125] The depth profiles obtained for both nanohybrids ($TMPyP^{4+}$/GO and $ZnTMPyP^{4+}$/GO) showed additional jumps of ca. 1 nm (***Figure 35***). Assuming that the thickness of one TMPyP molecule is ca. 0.5 nm (considering the rotation of pyridinium rings to a more flat position, parallel to the planes of porphyrin rings)[70], it can be concluded that the porphyrin molecules were adsorbed on the GO sheets as single molecules, not aggregates.

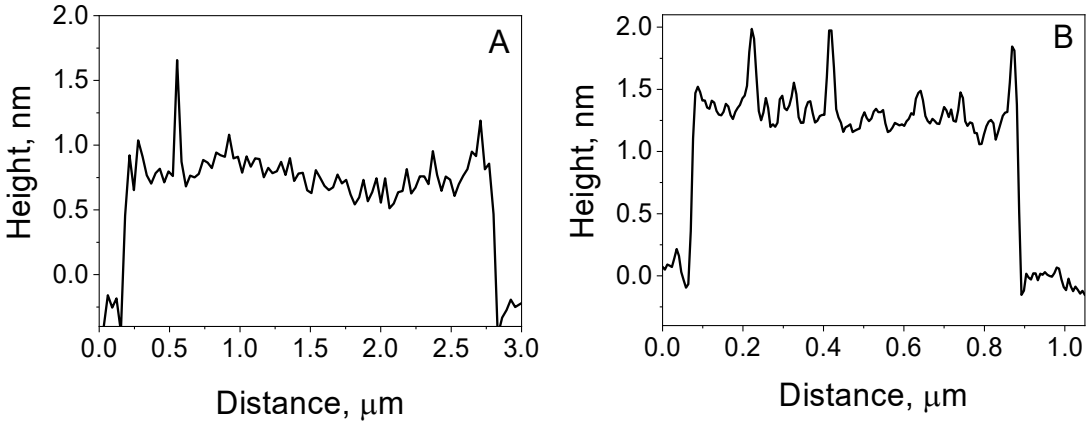

Figure 35 *AMF depth profile of A) $TMPyP^{4+}$/GO and B) $ZnTMPyP^{4+}$/GO*

A possible explanation for the observed red-shifts of the Soret bands in the $TMPyP^{4+}$/GO and $ZnTMPyP^{4+}$/GO nanohybrids is related to the flattening of the porphyrin molecule once it is adsorbed on the GO sheet. This concept was discussed earlier in the literature for similar cationic nanohybrids of $TMPyP^{4+}$ and rGO or chemically converted graphene (CCG) and neutral TPPH or ZnTPPH with GO.[73,78,80,95] Previous theoretical calculations showed that only a 30° change in the orientation of the meso-substituents toward the porphyrin core can lead to a bathochromic shift of the Soret band by as much as 30 nm.[133] Theoretical calculations for neutral porphyrin have provided evidence for the flattening of the ZnTPPH and TPPH upon adsorption on graphene oxide. The interaction of ZnTPPH and TPPH with GO causes twisting of the side rings relative to the porphyrin core from about 60° to 45° and 39° for ZnTPPH and TPPH, respectively.[73,95] Moreover, the experimentally observed Soret band red-shift of 16 nm for the ZnTPPH adsorbed

on the GO surface was well reproduced in theory.[95] The slightly smaller red-shift observed for $ZnTMPyP^{4+}$ in comparison to $TMPyP^{4+}$ upon adsorption on GO (***Figure* 33**, ***Table* 7**) can be attributed to the less profound flattening of the $ZnTMPyP^{4+}$ as observed previously for the TPPH and ZnTPPH.[73,95]

The titration of the aqueous graphene oxide solution with porphyrin solutions was used to estimate the maximum amount o porphyrin that can be attached to the surface of graphene oxide sheets (***Figure* 36**). To the GO solution with a fixed concentration, different amounts of porphyrins solutions were gradually added. For small concentrations, the maximum position of the Soret band corresponded to the porphyrin adsorbed on the surface of GO. With a small amount of porphyrin, all molecules were adsorbed on the GO sheet. However, with an increasing concentration of $TMPyP^{4+}$ and $ZnTMPyP^{4+}$ Soret band shifted to the lower wavelength, and above 6.42 μM the absorbance of the Soret band attributed to free porphyrins began to contribute to the absorption spectra. The maximum amount of $TMPyP^{4+}$ in $TMPyP^{4+}$/GO is less than 5% (% w/w), while nearly 0.11 mg of $ZnTMPyP^{4+}$ can be adsorbed on 1 mg of GO surface (9.9%, % w/w). The assumption that porphyrin molecules do not cover the whole surface of GO seems legitimate on the basis of AFM data.

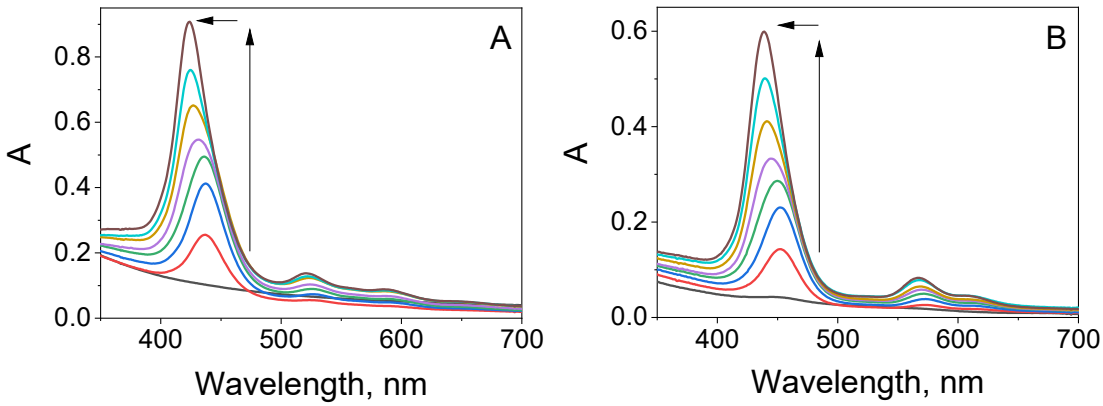

Figure 36 *A) Absorption spectra recorded during the addition of an aqueous solution of $TMPyP^{4+}$ (0-15 μM) to 0.13 mg mL^{-1} GO in H_2O (3 mL). B) Absorption spectra recorded during the addition of an aqueous solution of $ZnTMPyP^{4+}$ (0-15 μM) to 0.05 mg mL^{-1} GO in H_2O (3 mL)*

Spectroscopic results demonstrated that the interaction between GO and porphyrins ($TMPyP^{4+}$ and $ZnTMPyP^{4+}$) was already profound in the ground state and that the

fabrication of the new hybrid materials is limited simply to the combination of two solutions containing porphyrin and GO.

The newly obtained cationic porphyrin/GO materials were isolated by a centrifugation experiment controlled by absorption spectroscopy. The UV−Vis spectra of the suspension of the nanohybrids $TMPyP^{4+}$/GO and $ZnTMPyP^{4+}$/GO before and supernatants after the centrifugation are shown in ***Figure 37***. Based on the minor peak attributed to porphyrin in the UV−Vis of the supernatant, it was concluded that nearly the entire amount of nanohybrids was collected successfully as a precipitate. A strong interaction of porphyrins with GO can be explained by the coulombic attraction between cationic $TMPyP^{4+}$ and $ZnTMPyP^{4+}$ and negatively charged GO.

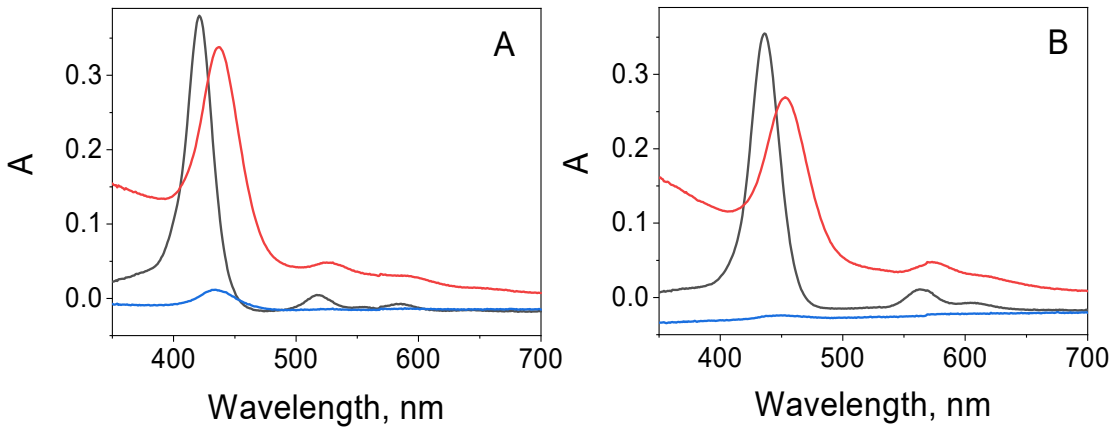

Figure 37 *Absorption spectra of: A) aqueous solutions of free $TMPyP^{4+}$ (black), $TMPyP^{4+}$ with the addition of GO suspension (red) and spectrum of the supernatant after centrifuging (blue), B) aqueous solutions of free $ZnTMPyP^{4+}$ (black), $ZnTMPyP^{4+}$ with the addition of GO suspension (red) and spectrum of the supernatant after centrifuging (blue)*

5.2.1.2 Steady-state and time-resolved emission

To investigate the interactions of the excited state of the porphyrin molecules with GO, photoluminescence spectroscopy was applied. As discussed previously, the absorption spectra of $TMPyP^{4+}$ and $ZnTMPyP^{4+}$ change after adding graphene oxide to the solution. Therefore, the solutions were excited at the isosbestic points (***Table 7***) to maintain the same absorbance at the excitation wavelength during all measurements. It was essential for quantitative analysis of the data. An increase in the amount of GO in the sample results

in a decrease in the fluorescence intensity of the porphyrin. The emission spectra of several porphyrin/GO (different in the amount of GO) hybrids are shown in ***Figure* 38**. To compare the efficiency of both porphyrins' fluorescence quenching by GO, the emission spectra presented were depicted for the same amount of added GO (0.19 μg mL^{-1}). The quenching efficiency for the GO concentration of 0.19 μg mL^{-1} was calculated to be 17% and 50% for $TMPyP^{4+}$ and $ZnTMPyP^{4+}$, respectively. To quench 50% of the TMPyP emission intensity, a concentration of GO equal to 0.42 μg mL^{-1} was required (***Figure* 39**).

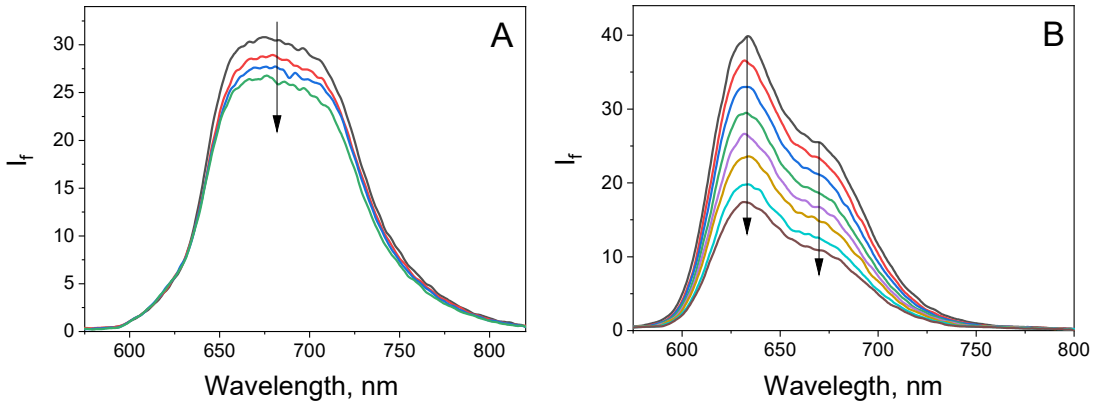

Figure 38 *A) Quenching of the fluorescence of: A) 0.50 μM $TMPyP^{4+}$ in H_2O recorded during the addition of an aqueous suspension of GO (0 -0.19 μg mL^{-1}); λ_{ex}= 434 nm; B) 0.16 μM $ZnTMPyP^{4+}$ in H_2O recorded during the addition of an aqueous suspension of GO (0 -0.19 μg mL^{-1}), λ_{ex}= 447 nm*

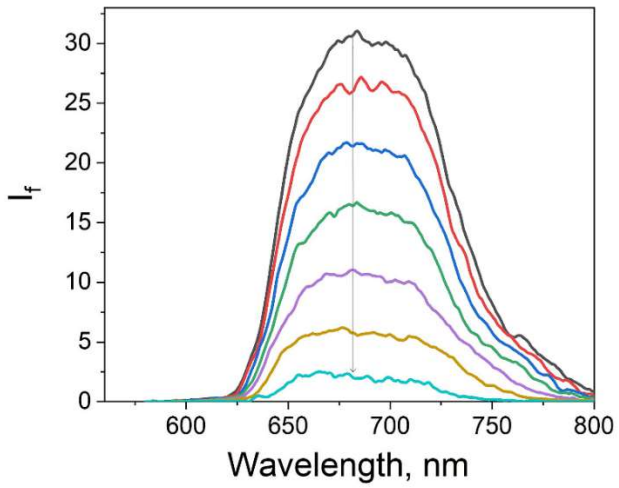

Figure 39 *Quenching of the fluorescence of 0.50μM $TMPyP^{4+}$ in H_2O recorded during the addition of an aqueous suspension of GO (GO concentration in solution 0- 0.98 μg mL^{-1}), λ_{ex}= 434 nm*

The lower quenching efficiency of $TMPyP^{4+}$ by GO provides the information that the interaction with this porphyrin is weaker compared to its zinc(II) derivative. On the basis of the emission measurements in the presence of GO, the quenching mechanism cannot be specified. To explain the origin of the observed decrease in the emissions intensity of both $TMPyP^{4+}$ and $ZnTMPyP^{4+}$ in the presence of GO, it is necessary to consider the mechanisms of dynamic and static quenching. In the case of dynamic quenching, the shortening of the fluorescence lifetime of the porphyrin in the presence of GO should be detected. In contrast, the fluorescence lifetime is expected to remain unchanged for the static quenching. (see: **4.3.1 Static and dynamic quenching**) To determine which mechanism is responsible for the observed decrease of the porphyrin's fluorescence intensity upon GO addition, the time-correlated single-photon counting technique was applied.

The fluorescence decay profiles of $TMPyP^{4+}$ and $ZnTMPyP^{4+}$ recorded in the presence and absence of GO were presented in the ***Figure 40***. The fluorescence lifetime extracted from the fluorescence decays for $ZnTMPyP^{4+}$ and $TMPyP^{4+}$ in the absence of GO was found to be approximately 1.3 ns and 5.7 ns (which is in line with previous literature reports[80,83,134]), respectively. With increasing concentration, no change in the fluorescence decay kinetics of both porphyrins was observed. The lack of a detectable

change in the fluorescence lifetime of the free porphyrins excludes dynamic quenching of the singlet excited state of porphyrins by GO. Comprehensive analysis of the emission quenching (steady-state and time-resolved) led to the conclusion that observed fluorescence quenching was attributed to the static quenching of the porphyrin by GO.

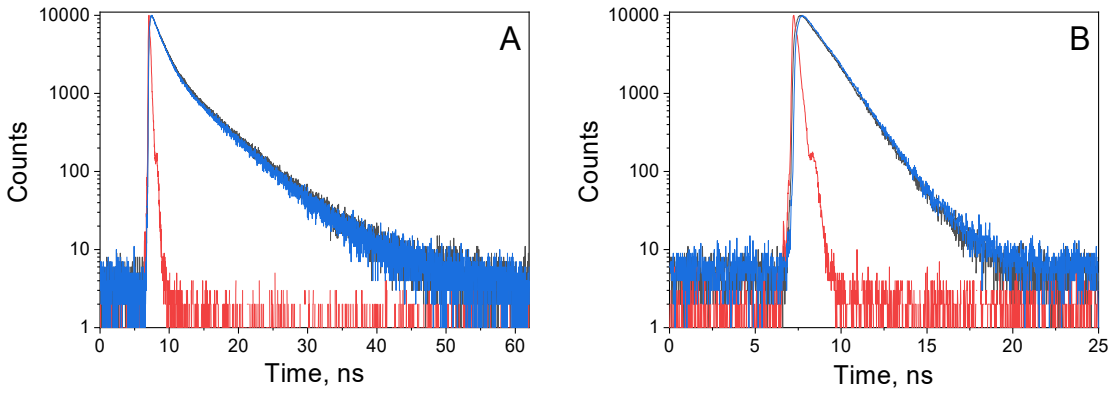

Figure 40 *Decay of A) $TMPyP^{4+}$ fluorescence recorded in the absence (black) and presence (blue) of GO (0.49 μg mL^{-1}), prompt (red); λ_{ex} = 440 nm, λ_{em} = 693 nm, B) $ZnTMPyP^{4+}$ fluorescence recorded in the absence (black) and presence (blue) of GO (0.19 μg mL^{-1}), prompt (red); λ_{ex} = 440 nm, λ_{em} = 650 nm*

Based on the comparison of the UV-Vis absorption spectra emission from the nanohybrid material is expected to be red-shifted compared to the emission of free porphyrin molecules. However, no change in the position and shape of the peaks in the emission spectra was observed after adding GO to the $TMPyP^{4+}$ or $ZnTMPyP^{4+}$ solution (***Figure* 41**).

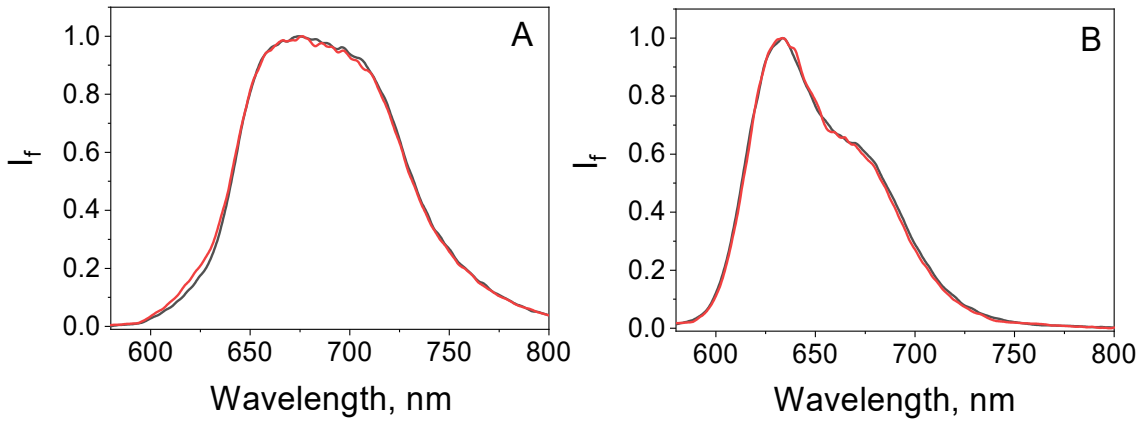

Figure 41 *Normalized fluorescence spectra of: A) $TMPyP^{4+}$ solution (black) and in the presence of GO (0.72 μg mL^{-1}) (red), λ_{ex}=434 nm; B) $ZnTMPyP^{4+}$ solution (black) and in the presence of GO (0.13 μg mL^{-1}) (red), λ_{ex}=447 nm*

Furthermore, the fluorescence excitation spectrum recorded for $TMPyP^{4+}$ and $ZnTMPyP^{4+}$ solutions after the addition of GO matched the absorption spectrum of the free porphyrins (***Figure* 42**). On the basis of the above observations, it can be concluded that the investigated nanohybrid is not an emissive complex.

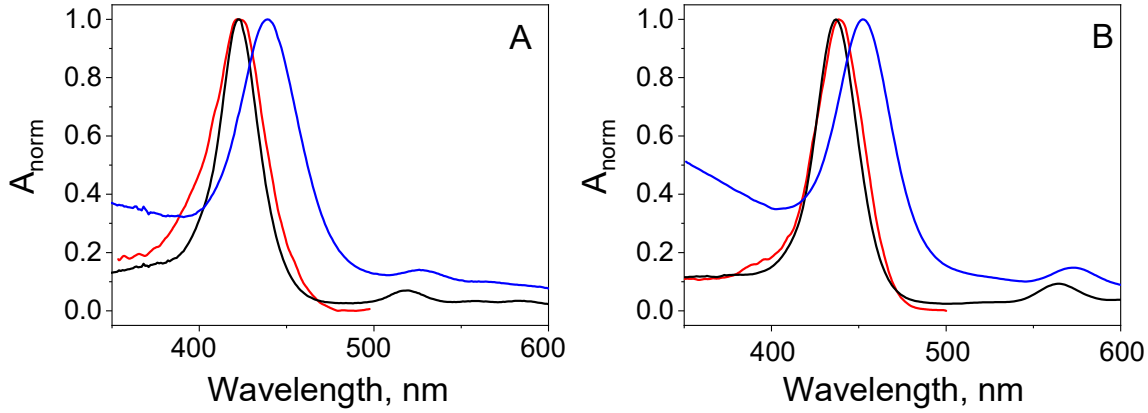

Figure 42 *A) Normalized fluorescence excitation spectrum of the mixture of $TMPyP^{4+}$ (1.2 μM) and GO (6.67 μg mL^{-}) λ_{ex}=434 nm (red), absorption spectra of $TMPyP^{4+}$ (1.0 μM) in the absence of GO (black) and with the presence of GO (6.67 μg mL^{-1}) (blue). B) Normalized fluorescence excitation spectrum of the mixture of $ZnTMPyP^{4+}$ (1.5 μM) and GO (6.67 μg mL^{-1}) λ_{ex}=447 nm (red) and absorption spectra of $ZnTMPyP^{4+}$ (1.0 μM) in the absence of GO (black) and with the presence of GO (6.67 μg mL^{-1}) (blue)*

5.2.1.3 Femtosecond TA Spectroscopy

The lack of measurable emission from the complexes ZnTMPyP^{4+}/GO and TMPyP^{4+}/GO indicates that there is a possibility of a very rapid deactivation process of the excited state, such as an energy or electron transfer. This process could be responsible for the quenching of the singlet excited state ($^1S^*$) of porphyrins. The free energy of the ET was calculated by applying the Rehm-Weller equation.[135,136] The value of this free energy gives information on whether an ET process from the singlet excited state ($^1S^*$) of the porphyrin to GO is thermodynamically feasible. The value of the 0-0 transition energy was estimated (***Table* 8**), based on the fluorescence results of free porphyrins. The oxidation potentials were taken from the literature.[137] The conduction band edge of GO was taken from the literature and was found to be equal to -0.55 V vs. NHE.[130] Using these values, the free energy of the electron transfer from the singlet excited state of ZnTMPyP^{4+} and TMPyP^{4+} to GO was estimated to be -0.11 eV and 0.02 eV, respectively (***Table* 8**). The negative value of the free ET energy for ZnTMPyP (-0.11eV) and the slightly positive value for TMPyP (0.02 eV) indicate that photoinduced electron transfer could possibly take place in both cases.

Table 8 *Zero-zero transitions of the singlet excited state of TMPyP^{4+} and ZnTMPyP^{4+}, their oxidation potentials, and estimated driving force of the electron transfer reaction values*

Porphyrin	$E_{0\text{-}0}$ (eV)	E_{ox} (V vs. NHE)	E^*_{ox} (V vs. NHE)	G_{ET} (eV)
TMPyP	2.07	1.54	-0.53	0.02
ZnTMPyP	2.08	1.42	-0.66	-0.11

Ultrafast TA spectroscopy was applied as a helpful tool to monitor the influence of GO on the deactivation pathways of the singlet excited state ($^1S^*$) of porphyrins. Experiments were performed for both porphyrins (TMPyP^{4+} and ZnTMPyP^{4+}) and their nanohybrids with GO.

Figure 43 presents transient absorption spectra for the TMPyP^{4+} and TMPyP^{4+}/GO nanohybrid measured at different time delays. The transient absorption spectra for TMPyP^{4+} measured immediately after the laser pulse exhibited an intense signal ca. 450-500 nm, which is typical for $^1S^*$ of porphyrins.[79,80] In addition, bleaching of the Q-bands at ca. 518, 555, 584, and 643 nm can be observed.

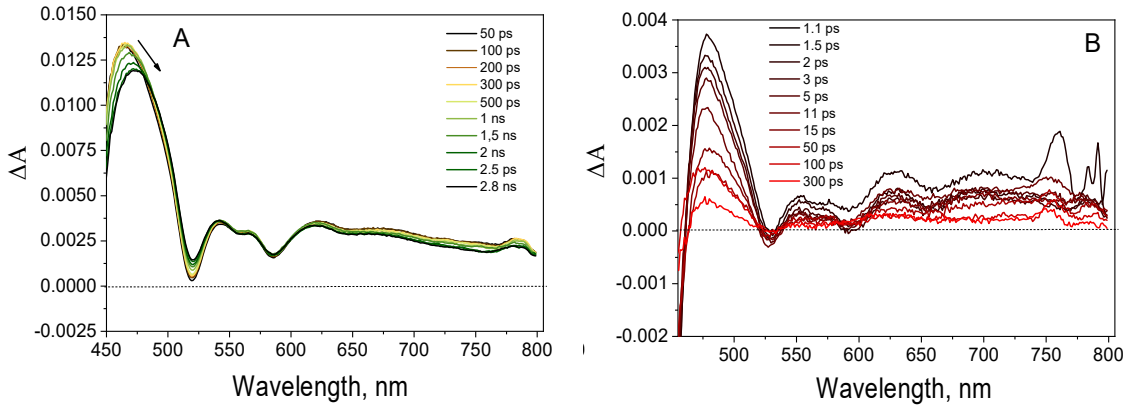

Figure 43 *Transient absorption spectra measured at different time delays for A) $TMPyP^{4+}$ (5.0 μM) and B) $TMPyP^{4+}$/GO (porphyrin concentration 5.0 μM, GO concentration 10 μg mL^{-1}) in water following the 422 nm laser excitation for A) and 437 nm laser excitation for B). Transient absorption spectra in B) were corrected for the contribution from GO itself*

The positions of these signals match the positions of the Q-band of the $TMPyP^{4+}$ in the ground state (**Figure 32**). Transient absorption kinetics were found to be biexponential. The transient spectra showed two components: a fast one (16 ps) and a slower one (3.8 ns) (value with the error since the whole time window of the experiment is 2.8 ns). The fast component can be assigned to an excited state conformational change or a vibrational cooling path through the relaxation of excess energy from the solute to the solvent.[138–140] However, the slow component is attributed to the decay of ^1S (***Figure* 44**). The decay of $^1S^*$ is related to formation of the triplet state, which has a similar transient spectrum.[81,141] After the addition of GO to $TMPyP^{4+}$, the transient absorption spectra after correction for the transient absorption of GO itself (***Figure* 43**B) showed almost no difference compared to the spectra recorded for the unbound $TMPyP^{4+}$ (***Figure* 43**A). Only the position of the bleach signal changed from 520 nm to 528 nm, which is in agreement with the ground-state absorption spectra of the nanohybrid. No appreciable increase in the absorption above 600 nm was observed, which could indicate the presence of a TMPyP radical cation.[80]

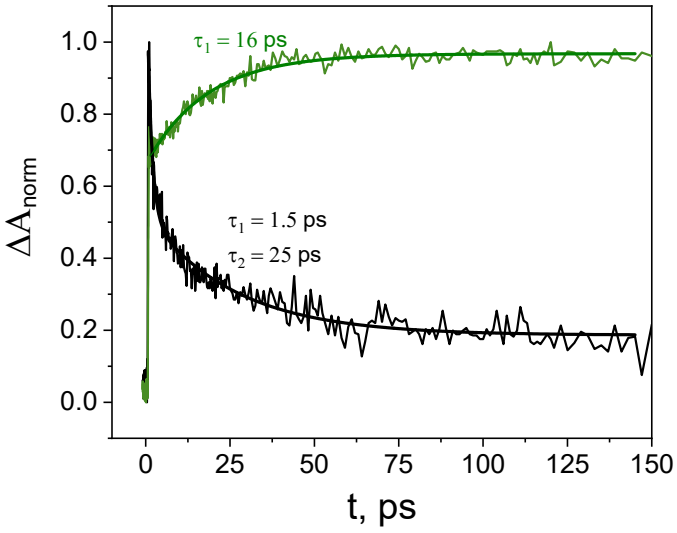

Figure 44 *Absorption time profiles at 480 nm measured for $TMPyP^{4+}$(green) and $TMPyP^{4+}$/GO (black) following the 422 nm and 437 nm laser excitation, respectively*

The comparison of the time profiles recorded for free $TMPyP^{4+}$ and $TMPyP^{4+}$ attached to the surface of the GO is shown in ***Figure* 44**. The kinetic profile at 480 nm for free $TMPyP^{4+}$ remained almost constant during 150 ps after excitation. Interestingly, at the same wavelength, $TMPyP^{4+}$/GO exhibited fast decay. The $^1S^*$ lifetime of $TMPyP^{4+}$ adsorbed on GO sheets was remarkably reduced. The decay was found to be biexponential with lifetimes of ca. 1.5 ps and 25 ps. This demonstrates a strong influence of GO on the properties of TMPyP in its photoexcited state. An electron transfer is a possible explanation for the observed fast decay of the $^1S^*$ of $TMPyP^{4+}$ attached to the GO sheet. The lack of detection of the radical cation of the porphyrin, which would constitute unambiguous evidence of any electron transfer, can be rationalize by similar rates of electron transfer and back electron transfer.

The results of the femtosecond transient absorption spectroscopy for free $ZnTMPyP^{4+}$ and $ZnTMPyP^{4+}$ bound to GO are depicted in ***Figure* 45**.

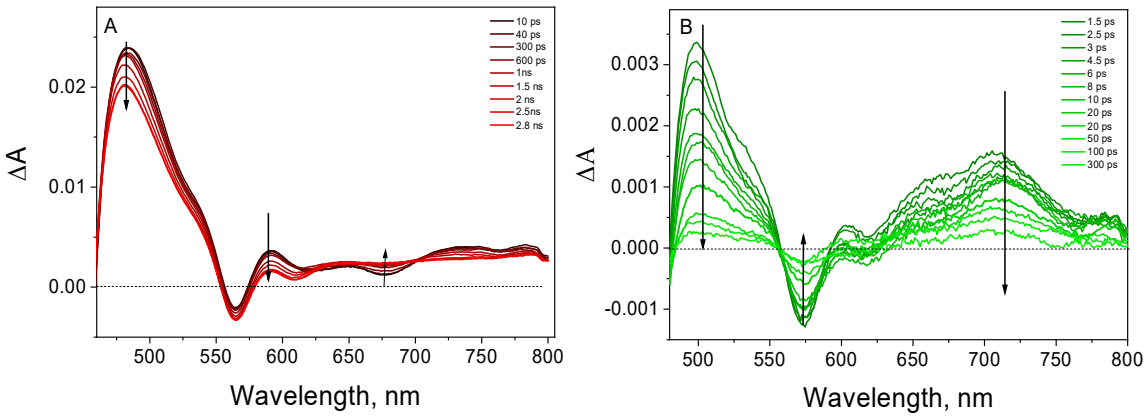

Figure 45 *Transient absorption spectra registered at various time delays for A)ZnTMPyP^{4+} (8 μM) and B) ZnTMPyP^{4+}/GO (porphyrin concentration 8.0 μM, GO concentration 10 μg mL^{-1}) in water following the 437 nm laser excitation for A) and 453 nm laser excitation for B)*

The Q-bands' apparent negative absorption band was observed at wavelengths that match the ground-state absorption spectra. The lifetime of $^1S^*$ was determined from the kinetic profile at 590 nm and was equal to 1.45 ns. This value is in excellent agreement with the value determined independently in the TCSPC experiment (***Figure 40***B). The disappearance of the transient absorption attributed to the $^1S^*$ of ZnTMPyP during 3 ns was accompanied by only small changes in the spectrum. Furthermore, the growth of a weak signal was observed around 675 nm. These changes in the absorption spectra of $^1S^*$ over time can be attributed to the triplet excited-state formation. Because of the significant similarity of both TA spectra, the spectral evolution observed in femtosecond TA spectroscopy is small.

An analogous TA experiment was conducted for a sample of the ZnTMPyP^{4+}/GO nanohybrid, i.e., porphyrin after adding GO (***Figure* 45B**). The TA spectra of ZnTMPyP^{4+}/GO look different from the TA spectrum of free ZnTMPyP^{4+} (***Figure* 45A**). ***Figure* 46** shows transient absorption spectra registered at various time delays for GO, which were used in the spectra correction. Otherwise, the observed TA spectra of the porphyrin can be falsely interpreted in terms of ET processes (see: ***Figure* 47** with uncorrected spectra).

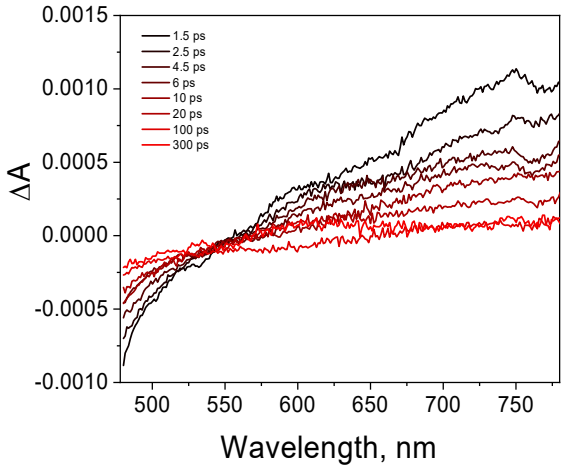

Figure 46 *Transient absorption spectra registered at various time delays for GO (10 μg mL^{-1})*

As presented in ***Figure* 45B**, an additional band was detected in the 650-800 nm region. This band has been assigned to the porphyrin radical cation ZnTMPyP$^{+\bullet}$ based on comparison to the spectra for the ZnTMPyP$^{+\bullet}$ reported previously in the literature.[81,142] Therefore the observation of ZnTMPyP$^{+\bullet}$ gives clear evidence for the photoinduced ET process from porphyrin molecule to the GO surface.

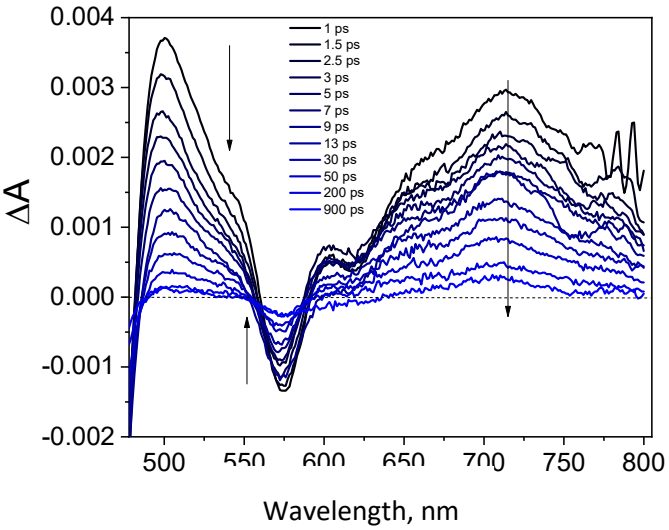

Figure 47 *Transient absorption spectra registered at various time delays for ZnTMPyP^{4+}/GO (porphyrin concentration 8.0 μM, GO – 10 μg mL^{-1}) in water following the 453 nm laser excitation without correction for the transient absorbance of the GO itself*

The time profiles for free $ZnTMPyP^{4+}$ and $ZnTMPyP^{4+}$ after GO addition were recorded at 710 nm. Their comparison reveals a significant difference in decay dynamics. In contrast to free $ZnTMyP^{4+}$, the time profiles of $ZnTMyP^{4+}$ bound to the GO sheet exhibit a very fast decay (***Figure* 48**). The time profile of $ZnTMPyP^{4+}$ attached to GO could be well fitted to the two-exponential decay function. The time constants obtained from the fit are 1.4 and 26 ps. It was previously found that back ET within the ion pair of radical cation of ZnTMPyP and graphene carboxylate occurs with a time constant of 20 ps.[80,81] Furthermore, two-time constants ranging from several to tens of picoseconds were obtained to decay the formed cation in the presence of GO.[79] Decay of the porphyrin radical cation with two-time constant can originate from various geometries of the porphyrin molecules in the nanohybrid material.

It should be noted that the radical cation of $ZnTMPyP^{4+}$ in our system was observed immediately after excitation, indicating a very fast electron transfer from $ZnTMPyP^{4+}$ to GO. Such a fast photoinduced ET can occur only when the donor and acceptor are already in a very close connection before excitation. The disappearance of the radical cation of the ZnTMPyP signal can be explained by back electron transfer. This is confirmed by comparing the bleach recovery at 575 nm, which follows the same kinetics as the kinetic decay at 710 nm. Interestingly, a residual signal (offset) of approximately 14% was present in all decay profiles. This signal is explained by a fraction of the ZnTMPyP radical cation, which did not undergo back electron transfer during our probed time window of 3 ns. The variable geometries of the $ZnTMPyP^{4+}$/GO nanohybrids may influence the rate constant of back electron transfer.

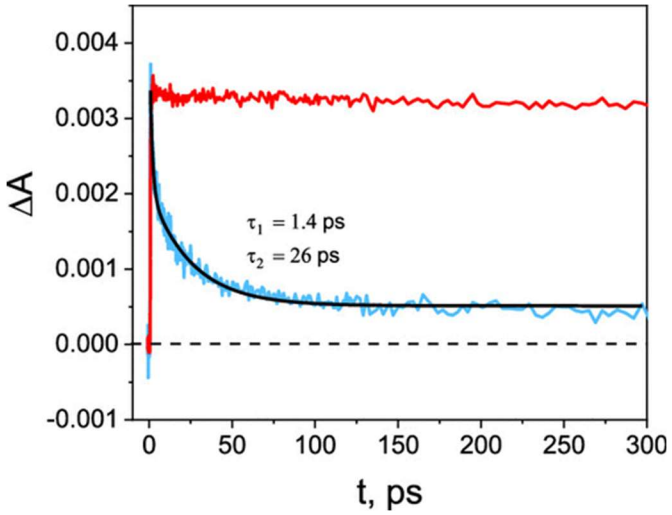

Figure 48 *Absorption time profiles at 710 nm measured for ZnTMPyP^{4+} (red) and ZnTMPyP^{4+}/GO (blue) following the 437 nm and 453 nm laser excitation, respectively (black line shows the two exponential decay fit)*

5.2.1.4 Photoelectrochemical measurements

Complementary photocurrent measurements give experimental support for the photoinduced charge separation mechanism. ***Figure 49*** shows the photoelectrical response of the SnO_2-FTO electrodes covered with: GO, TMPyP^{4+} and ZnTMPyP^{4+} (***Appendix 2***). The irradiation was switched on and off in 30-second periods to measure the electrodes' light and dark response. The photocurrent response of GO itself was negligible.

An obvious photocurrent response for the electrode was observed for electrodes covered with TMPyP^{4+}/GO and ZnTMPyP^{4+}/GO films. All experiments were carried out under the same conditions. The increase in the photocurrent provides evidence for the photoinduced charge transfer in the studied materials. The produced photocurrent was constant or decreased by 15% in the three irradiation cycles for the TMPyP^{4+}/GO and ZnTMPyP^{4+}/GO films, respectively.

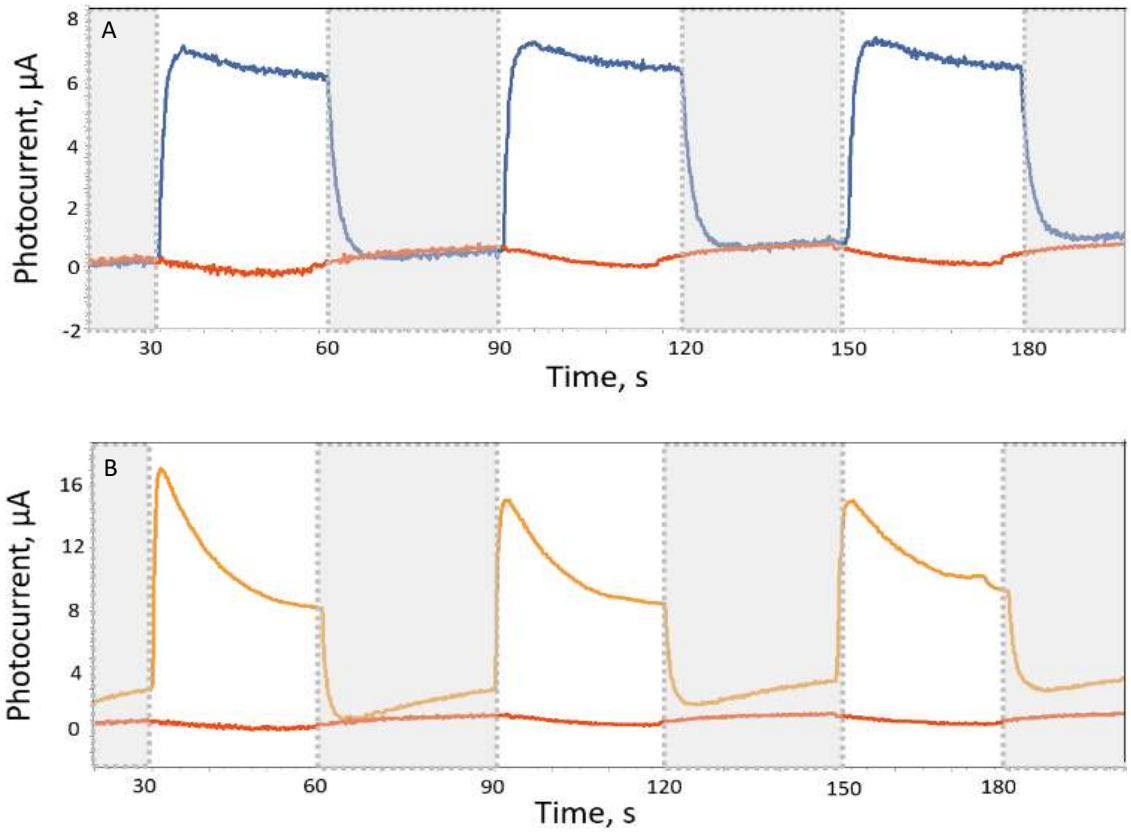

Figure 49 *Transient photocurrent in time for A) $TMPyP^{4+}$/GO and B) $ZnTMPyP^{4+}$/GO under white light illumination (electrolyte: 0.1 M LiI in acetonitrile). On both, the red line shows the photocurrent generated by GO*

The photocurrent generated by the $ZnTMPyP^{4+}$/GO sample was approximately two times higher than that produced by the $TMPyP^{4+}$/GO sample. The higher photocurrent response for zinc porphyrin might be attributed to more efficient electron-hole separations. The results obtained from the photocurrent measurements can explain the higher photocatalytic activity of the $ZnTMPyP^{4+}$/GO material (see below).

5.2.1.5 Photocatalytic activity towards RhB degradation

The photocatalytic activity of the fabricated $TMPyP^{4+}$/GO and $ZnTMPyP^{4+}$/GO nanohybrids was evaluated by degradation of the organic dye pollutant Rhodamine B (RhB) in water under visible light irradiation.

The suspension of RhB and the photocatalysts used for photolytic performance were stirred overnight to reach an absorption-desorption equilibrium. Subsequently, each sample was irradiated under visible light for 2 hours while stirring constantly. The change in RhB concentration was determined spectrophotochemically by measuring the absorbance of RhB at 554 nm at various time intervals (***Figure* 50**). Based on that, a decrease in RhB concentration was estimated. The control experiment, that is, a sample without the addition of any photocatalyst, was conducted, and very small degradation (3% after 2 hours) of RhB molecules was observed. All of the photocatalyst samples were catalytically active for the decomposition of RhB using visible-light irradiation. For a quantitative comparison of the photocatalytic performance of the hybrid materials, the absorbance of the porphyrins in both composite materials was kept constant. This ensures the absorption of the same number of photons by the samples. Obtained data were corrected for the photodegradation of RhB itself.

Interestingly, the activity of the $ZnTMPyP^{4+}$ was the highest and achieved ca. 19% of RhB decomposition after 2 hours. The free porphyrins did not show any photocatalytic activity toward RhB degradation. It was found that both porphyrins are unstable under light irradiation. It should be noted that both $TMPyP^{4+}$ and $ZnTMPyP^{4+}$ porphyrins were tested in photocatalysis as monomers. However, it was proven that porphyrins could show photocatalytic activity toward RhB degradation when they are self-assembled.[111,143] The efficiency of aggregates' photocatalytic activity depends on the morphology of the porphyrin nanostructures.[111] In addition, it was observed that the adsorption of the porphyrin molecule ($TMPyP^{4+}$ or $ZnTMPyP^{4+}$) onto the surface of GO appreciably improved the photostability of porphyrins. The decomposition of the porphyrins in the porphyrin/GO was negligible after 2 hours of irradiation.

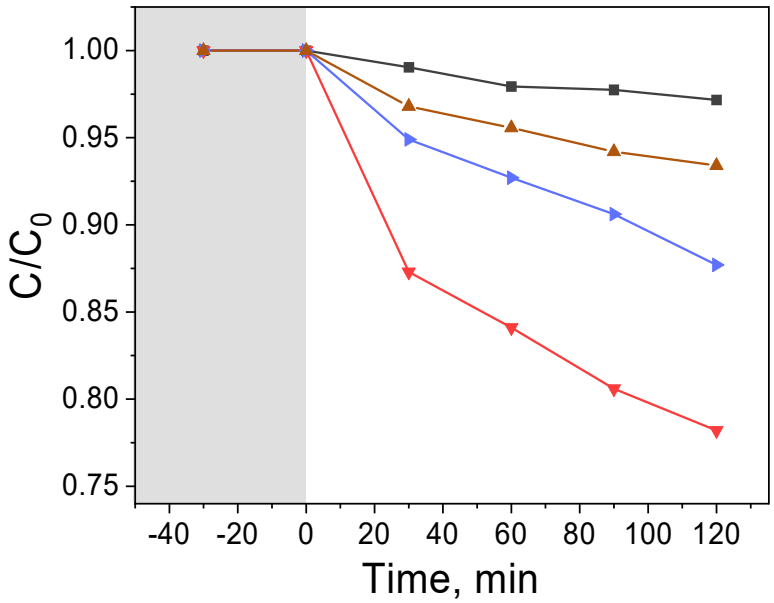

Figure 50 *RhB photodegradation under visible irradiation (λ>400 nm): control (black, ■), GO (brown, ▲), $TMPyP^{4+}$/GO composite (blue, ►) and ZnTMPyP/GO composite (red, ▼)*

The degradation of RhB could be described with a pseudo-first-order kinetic model. The experimental data were plotted as a function of $\ln(C/C_0)$ versus time to obtain the rate constants for the photocatalytic reaction. The rate constants of the reaction were found to be ca. 1.9×10^{-3} and 1.0×10^{-3} min^{-1} for $ZnTMPyP^{4+}$/GO and $TMPyP^{4+}$/GO, respectively.

A previous study reported that graphene nanoplates supported by TCPP aggregates exhibited a RhB degradation rate constant of approximately 7.3×10^{-3} min^{-1}.[143] The rate constant for RhB degradation was further increased by applying ternary nanostructure graphene@TiO_2@TCCP to 9.4×10^{-3} min^{-1}.[143] It has also been shown that supramolecular ZnTPP porphyrin-based nanofibers exhibit photocatalytic activity toward RhB degradation. The performance of the ZnTPP supramolecular assemblies was further enhanced by functionalizing with the GO sheet, with the reported rate constant of 2.6×10^{-2} min^{-1} .[144] One has to be aware that any comparison between the reported systems should be done with caution because the photocatalytic activity of these systems depends not only on the catalytic activity of the photocatalyst itself but also on experimental conditions: concentration of RhB or photocatalyst, power, and spectral pattern of the light source.

The prolongation of $ZnTMPyP^{4+}$/GO irradiation led to the degradation of 80% of RhB (***Figure* 51**).

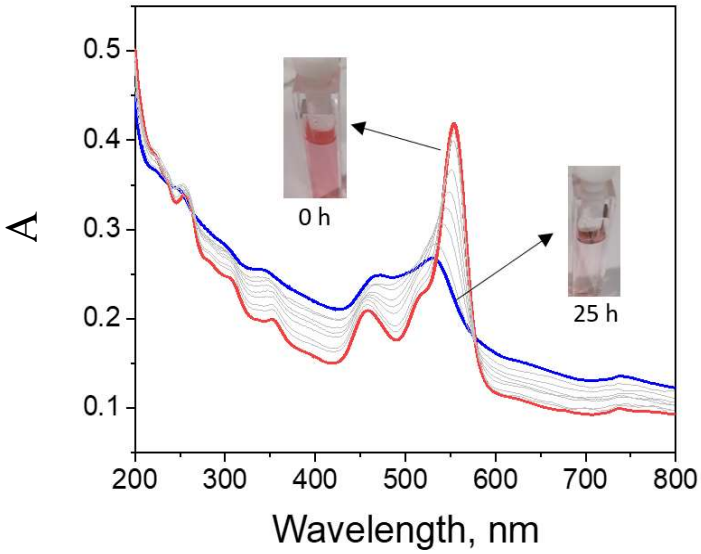

Figure 51 *UV-Vis spectra of the aqueous solution of RhB with the addition of $ZnTMPyP^{4+}$/GO as a photocatalyst during 25 h of Vis-irradiation*

Discussion of the mechanism for RhB photodegradation by $TMPyP^{4+}$/GO and $ZnTMPyP^{4+}$/GO nanohybrids

The UV-Vis maximum absorption spectra of RhB shift from 554 to 530 nm during photodegradation (***Figure* 51**). As previously reported, this effect indicated that photodegradation occurs via N-deethylation.[35,145–148] Moreover, it was found that the photodegradation of RhB was negligible if the experiment was conducted under an argon atmosphere. This indicates that the presence of oxygen is essential in this process. It is well-known that pollutants can be degraded by various reactive oxygen species (hydroxyl radical $OH^{\bullet}$, superoxide anion $O_2^{\bullet-}$) generated when a photocatalyst is irradiated by light.[147] The work function of GO was estimated to be ca. 4.2 eV. The energy levels of LUMO (-4.14 eV) and HOMO (-6.17 eV) for ZnTMPyP porphyrin were calculated and depicted in ***Scheme* 9**.

After analyzing the collected data (steady-state and time-resolved spectroscopic measurements), a possible mechanism for RhB degradation by porphyrin/GO nanohybrids was proposed (***Scheme* 9**).

The porphyrin electrons can be photoexcited from the level of S_0 to S_1^* LUMO and transferred to the GO sheet. This leads to the formation of electron-hole pairs.

The reaction between photogenerated holes on the surface of porphyrin ($TMPyP^{4+}$ or $ZnTMPyP^{4+}$) and H_2O or OH^- results in the formation of the hydroxyl radical $OH^{\bullet}$. The $OH^{\bullet}$ can oxidize RhB to degradable products. At the same time, the photogenerated electron on the GO sheet can react with oxygen molecules dissolved in H_2O and produce the superoxide oxygen anion $O_2^{\bullet-}$. Singlet oxygen ($^1O_2$) is usually formed in the energy transfer process from the triplet excited state of the molecule to the oxygen triplet ground state. On the basis of TA spectroscopy data, the formation of the triplet excited state of the porphyrin adsorbed on the GO surface is entirely suppressed. Rapid deactivation of the singlet excited state of porphyrin via ET to GO excludes the intersystem crossing process. Formation of the porphyrin in the triplet excited state does not occur. This led to the conclusion that singlet oxygen does not participate in the degradation of RhB.

In summary, ROS formation ($OH^{\bullet}$ and $O_2^{\bullet-}$) results in RhB degradation in water. The ROS formation efficiency is expected to be higher for the $ZnTMPyP^{4+}$/GO system due to the formation of longer-lived change-separated states.

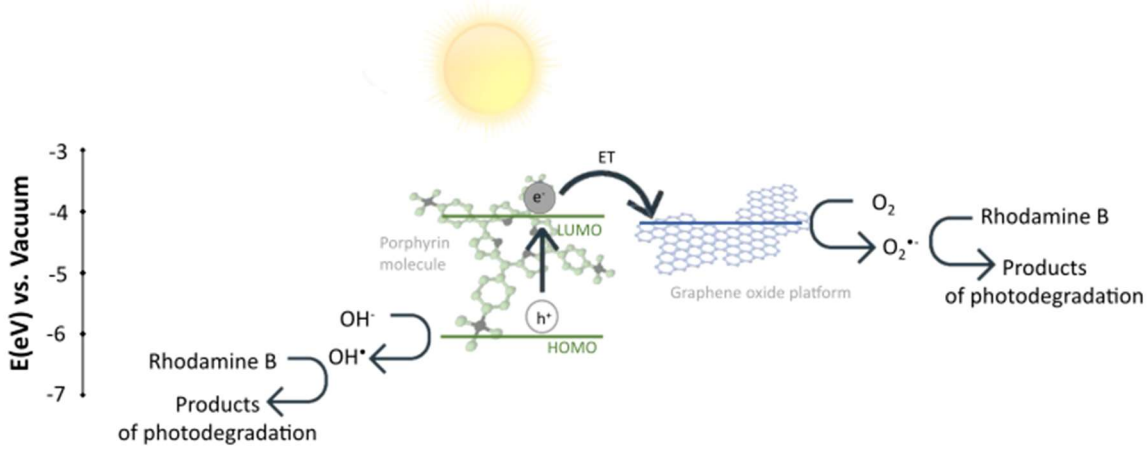

Scheme 9 *Proposed mechanism for RhB photodegradation by porphyrin/GO nanohybrids (porphyrin = $TMPyP^{4+}$, $ZnTMPyP^{4+}$)*

5.2.1.6 Summary

The comprehensive steady-state absorption and emission data analysis allowed to conclude that the metalation of $TMPyP^{4+}$ with Zn(II) increased the binding ability of the porphyrin to the GO surface. Photocurrent measurements and femtosecond TA

spectroscopy provided evidence for ET occurring in the hybrid materials. The obtained data indicate that the presence of Zn(II) in the core of the porphyrin can promote charge separation in the ZnTMPyP^{4+}/GO composites. The higher degradation rate seen with ZnTMPyP^{4+}/GO as compared to the TMPyP^{4+}/GO assemblies highlights the beneficial role of Zn(II) metalation of the porphyrin ring.

57.2.2 TMAP

5,10,15,20-tetra(4-trimethylammoniophenyl) porphyrin tetra(p-toluenesulfonate) (TMAP) is a water-soluble porphyrin. The porphyrin core is modified with four N-methylated phenyl groups, which carry a positive charge of +4 under neutral conditions. Under the acidic pH additionally, the core of the porphyrin is protonated leading to the overall increase of the molecule's charge to +6 (***Figure* 52**). The initial hypothesis was that by increasing the positive overall charge of the molecule the electrostatic interactions between the porphyrin molecule and the surface of GO can be enhanced. On the basis of the acid-base titration process of an aqueous solution of TMAP porphyrin, the acid dissociation constant (pK_a) was determined. The pK_a was found to be 2.7 (***Figure* 53**).

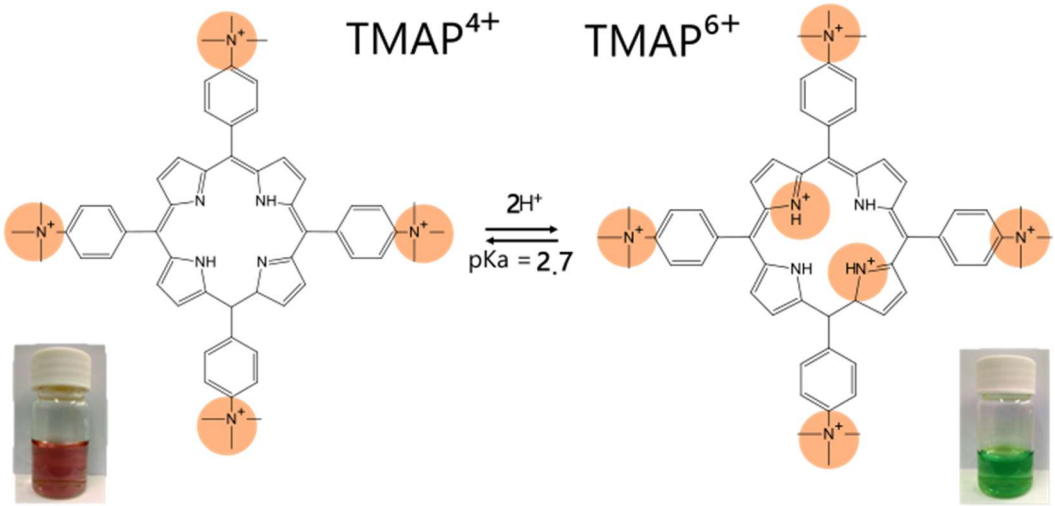

Figure 52 *Chemical structures of TMAP^{4+} and TMAP^{6+} and corresponding photograph of the porphyrin aqueous solution*

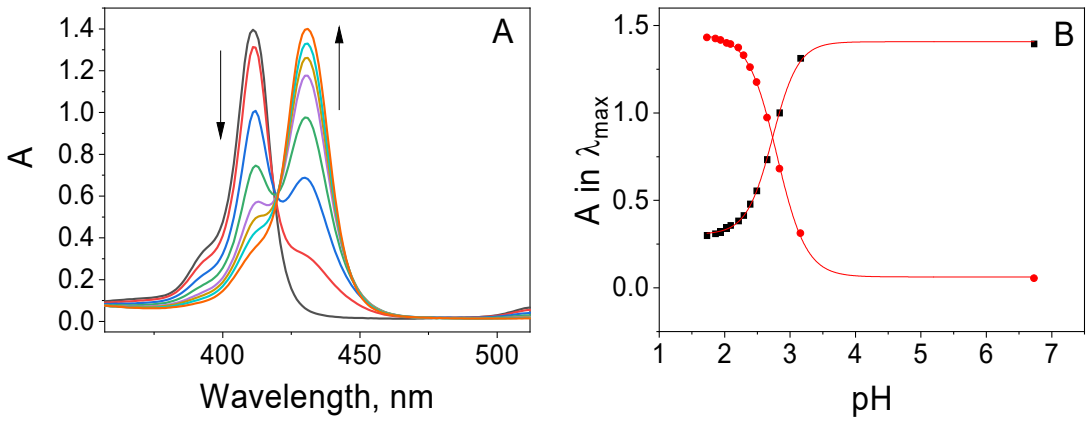

Figure 53 *A) UV-Vis absorption spectra registered for the TMAP solution (7.56 μM) during titration with 1M HCl. B) Fitting the Boltzmann function to the relationship between absorbance at 411 nm (black) or 430 nm (red), and the pH value*

The UV-Vis spectrum obtained under neutral conditions (pH 6.2) exhibited an intense Soret band centred at ca. 411 nm and the four less intense Q-bands at ca. 513, 550, 587, and 633 nm (***Figure 54***).

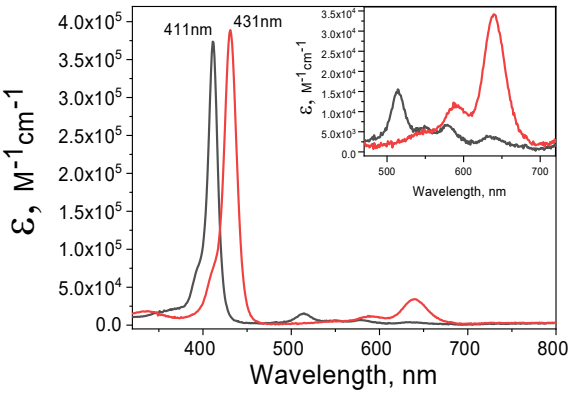

Figure 54 *Absorption spectra of $TMAP^{4+}$ (black) and $TMAP^{6+}$ (red) in water (inset: Q-band region of the same spectra)*

For acidic conditions (pH 1.8), the UV-Vis spectrum exhibited a red-shifted Soret band (at ca. 431 nm) and a decrease in the number of Q-band peaks due to the higher symmetry of the porphyrin molecule. The Q-bands change from four bands (corresponding to the D_{2h} symmetry) to two peak spectra indicative of the D_{4h} symmetry where both pyrrolic nitrogens are protonated.[63,64,66]

Based on the absorbance values of the three independent porphyrin solutions with known concentrations, the molar absorption coefficients for both forms of TMAP porphyrin were calculated. The absorption coefficients for the maximum of the Soret bands for both TMAP forms were comparable and equal to $\varepsilon_{411}=3.7 \times 10^5$ M^{-1} cm^{-1} and $\varepsilon_{431=}=3.8 \times 10^5$ M^{-1} cm^{-1} for $TMAP^{4+}$ and $TMAP^{6+}$, respectively (***Figure* 54**).

Porphyrins in solution are prone to aggregation.[110,149] Free-based porphyrins can aggregate through weak π-π interactions. However, there is still controversy about the self-aggregation of cationic porphyrins.[131,132] Doubts concerning the possible aggregation of cationic porphyrin arise from the fact that there is an electrostatic repulsion between charged substituents of the cationic porphyrin molecule. Therefore aggregation of positively charged porphyrin is still the subject of research.[131,150] To account for the possibility of the aggregation of $TMAP^{4+}$ itself, the UV-Vis spectra were measured for a series of $TMAP^{4+}$ concentrations (***Figure* 55**A). It was found that the shape of the UV-Vis spectrum obtained under neutral conditions does not change with increasing porphyrin concentration (***Figure* 55**B) and in addition, the dependence of the absorbance at the maximum of the Soret band on the $TMAP^{4+}$ concentration was found to be linear (***Figure* 55**C) This allows to conclude that in the concentration range (0.19 μM – 3.5 μM) $TMAP^{4+}$ aggregation does not occur.

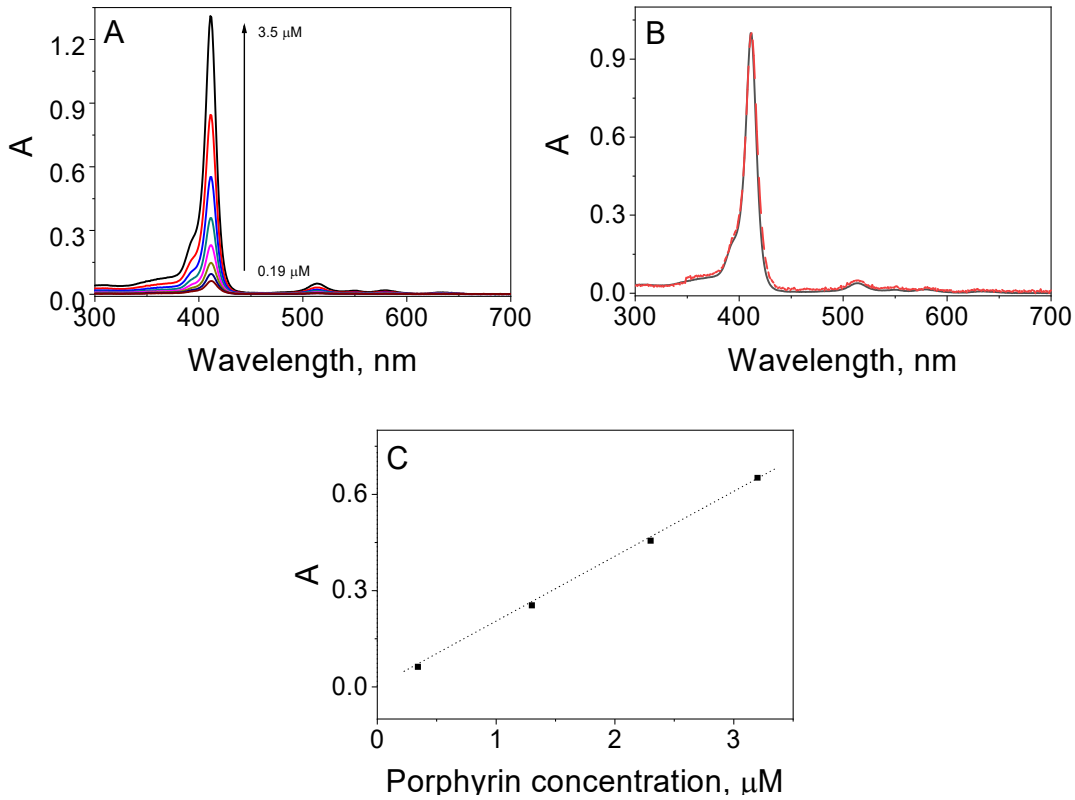

Figure 55 *A) Absorption spectra recorded for an aqueous $TMAP^{4+}$ solution for various porphyrin concentrations (ranging from0.19 μM to 3.5 μM); B) Normalized absorption spectra for aqueous $TMAP^{4+}$ solution for porphyrin concentration 3.5 μM (black) and 0.19 μM (red); C) Dependence of the absorbance at the Soret band as a function of $TMAP^{4+}$ concentration*

5.2.2.1 Steady-state absorption properties

In this part of the research, non-covalent nanohybrids between cationic TMAP and GO sheets were prepared under two different pH values (1.8 and 6.2). The TMAP molecule is positively charged, regardless of whether the environment is either almost neutral or acidic. The protonation of imino nitrogen only increases the overall charge of the porphyrin molecule from +4 to +6.

Moreover, GO sheets in an aqueous solution at neutral pH are negatively charged as a result of the deprotonation of the functional groups on their surface. Thus, cationic porphyrin derivatives are expected to functionalize the surface of GO through electrostatic forces and π-π stacking interactions.

The interactions of the TMAP porphyrin molecule with the GO oxide sheet were investigated under Ph 6.2 and 1.8. The purpose of this study was to examine which form of the TMAP molecule, $TMAP^{4+}$ or $TMAP^{6+}$, can be assembled to the GO more efficiently.

To determine whether there is an interaction between the porphyrin molecule and the surface of graphene oxide in the ground state, the experiment was carried out in which the porphyrin solution was titrated with an aqueous solution of GO followed by UV-Vis measurements.

The optical absorption spectra of the series $TMAP^{4+}$/GO nanohybrid suspension are shown in ***Figure*** **56**A. An aqueous GO solution (0.4 mg Ml^{-1}) was gradually added to the porphyrin 1.1 μM solution (pH 6.2). The addition of GO caused a stepwise disappearance of the Soret band at 411 nm accompanied by the formation of a new, red-shifted band at ca. 421 nm. The new band can be assigned to the absorption of light by a porphyrin molecule attached non-covalently to the graphene oxide sheet's surface. The shift of the Soret band between the free $TMAP^{4+}$ molecule and $TMAP^{4+}$ adsorbed on the GO surface is equal to 10 nm. An isosbestic point (at 416 nm) was observed, which

also speaks of a clear change from free $TMAP^{4+}$ to adsorbed $TMAP^{4+}$ on the surface of GO. Furthermore, Q-band peaks shifted from 513, 550, 587, and 633 nm to 519, 554, 585, and 640 nm, respectively. Furthermore, the extinction coefficient at the maximum of the Soret band of $TMAP^{4+}$ adsorbed on GO is almost twice lower ($\varepsilon_{421}=1.9 \times 10^5$ M^{-1} cm^{-1}) compared to free $TMAP^{4+}$ molecules. Only a slight broadening of the Soret band was observed for the adsorbed porphyrin. These spectral results clearly show that $TMAP^{4+}$ interacts strongly with GO in the ground state and that the $TMAP^{4+}$/GO nanohybrid can be easily obtained by simple mixing of the solutions of two components, porphyrin and graphene oxide.

Based on the spectral results described above, it is reasonable to conclude that adsorption of $TMAP^{4+}$ on the GO sheet causes significant changes in the electronic structure of the porphyrin. The bathochromic shift (10 nm) observed during nanohybrid formation could be explained by at least three different mechanisms: 1) protonation of the nitrogen in the porphyrin ring 2) J-aggregation of the porphyrin molecules, and 3) flattening of the porphyrin ring. The first possibility is highly unlikely since the protonation of the nitrogen in the ring can be achieved only in a highly acidic medium. The most plausible explanation for the observed red-shift of the Soret band in the $TMAP^{4+}$/GO is the flattening of the porphyrin structure upon adsorption on the GO sheet. This mechanism has previously been proposed for TMPyP and chemically converted graphene (CCG) or reduced graphene oxide (rGO).[78,80] In the structure of an unstrained $TMAP^{4+}$ molecule, four cationic trimethylanilinium groups are nearly perpendicular to the porphyrin plane due to a strong steric hindrance. Rotation of trimethylated pyridine substituents to the same plane as the porphyrin ring results in the extension of the π-conjugation and bathochromic shift of the Soret band. Generally, in the case of $TMAP^{4+}$ the observed red-shift (10 nm) is significantly smaller than the one observed for TMPyP/rGO (30 nm) or TMPyP/CCG (37 nm).[78,116,151] It can be attributed to the bulky cationic side groups that make it more difficult to achieve coplanar confirmation with the porphyrin macrocycle. The flattening of the porphyrin molecules is induced by a π-π stacking interaction which can be stronger for rGO or CCG sheets which have more delocalized and conjugated electron structures in comparison to GO.

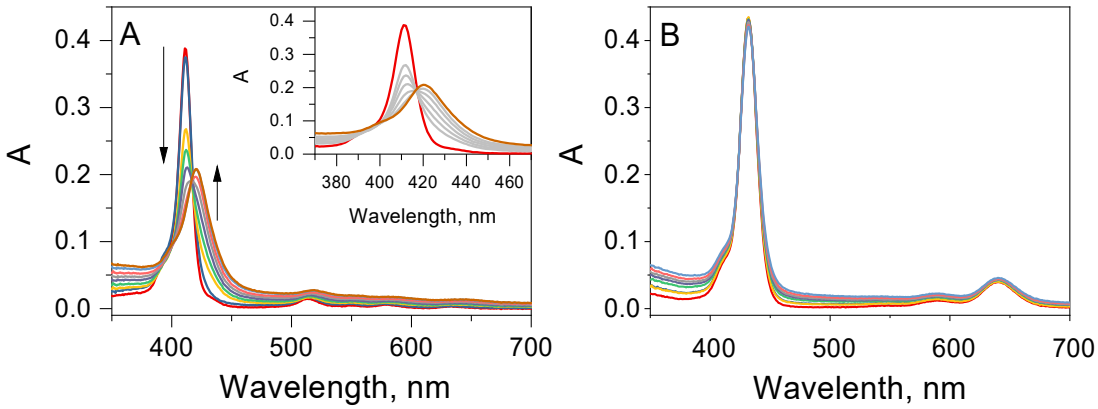

Figure 56 *Absorption spectra recorded during the process of titration of 3 mL of A) 1.1 µM aqueous solution of $TMAP^{4+}$ (pH 6.2) with 0.4 mg mL^{-1} of GO dispersion (GO concentration: 0-2.6 µg mL^{-1}); B) 1.1 µM aqueous solution of $TMAP^{6+}$ (pH 1.8) with 0.4 mg mL^{-1} of GO dispersion (GO concentration: 0-2.6 µg mL^{-1})*

An analogue titration experiment was performed under acidic pH. The experiment was carried out for the same range of GO concentration as in pH 6.2. No appreciable changes in the UV-Vis spectra of $TMAP^{6+}$ were observed (***Figure* 56**B). Only after lowering the concentration of the porphyrin molecules to 0.24 µM with a simultaneous increase in the concentration of the GO solution (the final concentration was ca. 4.6 times higher) the UV-Vis changes of $TMAP^{6+}$in the presence of GO were noticeable (***Figure* 57**).

The Soret band at ca. 431 nm has been red-shifted (25 nm) and decreased in intensity. This indicates that the interaction between $TMAP^{6+}$ and GO is largely suppressed compared to $TMAP^{4+}$.

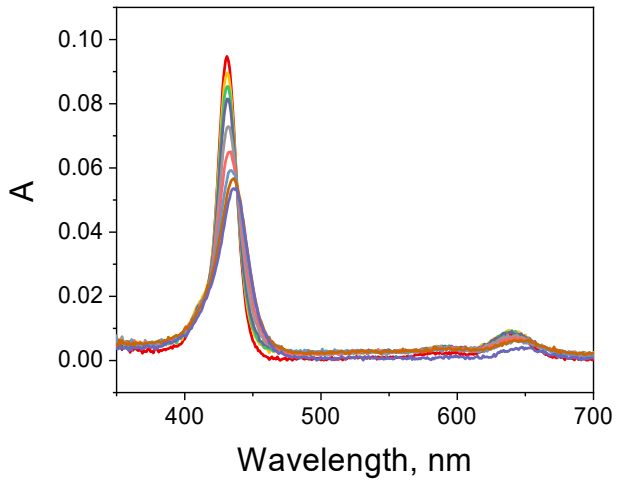

Figure 57 *Absorption spectra recorded during the titration process of 3 mL of 0.24 µM aqueous solution of* $TMAP^{6+}$ *(pH 1.8) with 3.0 mg* mL^{-1} *of GO dispersion (GO concentration: 0-12 µg* mL^{-1}*). Spectra were corrected for GO absorption*

The interaction between the porphyrin molecule and GO was examined at different pH (6.2 and 1.8) using GO films cast on glass slides. A glass slide was coated with GO (0.02 mg cm^{-2}) and immersed in aqueous solutions containing TMAP (28 µM) at pH 6.2 or 1.8 for 20 minutes. Subsequently, the films were rinsed with the solvent and dried in air. The prepared sample was measured with UV-Vis spectroscopy (***Figure* 58**). The increase in the absorption attributed to the porphyrin with a maximum at 427 and 440 nm at pH 6.2 and 1.8, respectively confirmed the successful attachment of the TMAP to GO. The Soret band of the porphyrin on the GO film was shifted by 6 nm for $TMAP^{4+}$ and 4 nm for $TMAP^{6+}$, compared to the experiments performed in solution. It is also evident that more porphyrin molecules are loaded on the film which was immersed in the porphyrin solution at pH 6.2 These results clearly show that the interaction of TMAP with the GO sheet is weaker in an acidic environment (pH 1.8).

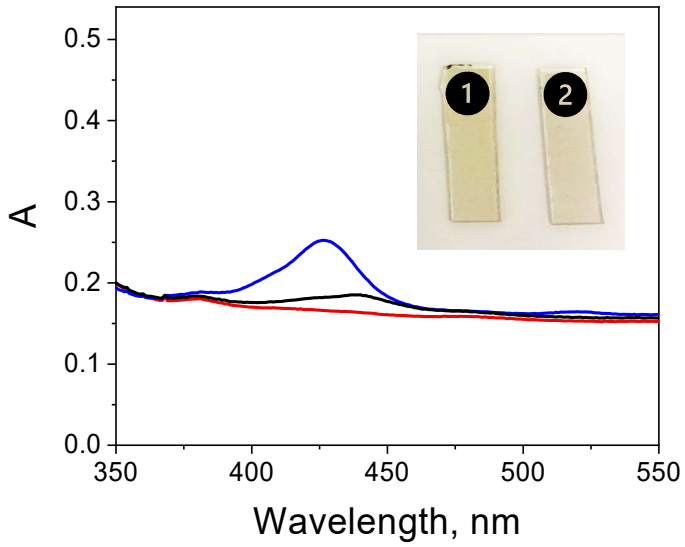

Figure 58 *Absorption spectra of the glass slide coated with GO (red), immersed in aqueous solutions of* $TMAP^{4+}$ *(pH 6.2) (blue) and* $TMAP^{6+}$ *(pH 1.8) (black) for 20 minutes. The spectra were not corrected for the absorption of the GO film itself. Inset: Images of the glass slide GO-film coated after immersion in aqueous solutions of (1)* $TMAP^{4+}$ *and (2)* $TMAP^{6+}$

To determine the pH at which the interaction between the porphyrin molecule and GO is stronger (pH 6.2 or 1.8), a centrifugation experiment followed by UV-Vis spectroscopy was conducted. First, a solution of a porphyrin/GO nanohybrid was prepared at first by mixing the two components: an aqueous solution of the GO and an aqueous solution of the porphyrin at an appropriate pH. The UV-Vis spectra of the suspension before and after centrifugation were measured (***Figure* 59**). The results obtained show that ca. 80% of the nanohybrid was successfully collected as a precipitate at pH 6.2 (12000 rpm, 45 minutes). In the analogous experiment carried out under acidic conditions (pH 1.8), the supernatant contained majority of the dye used to prepare the nanohybrid. On the basis of that, it can be assumed that under acidic pH only a small amount of porphyrin was successfully adsorbed on the GO. Therefore it can be concluded that the formation of the nanohybrid was largely suppressed under acidic pH.

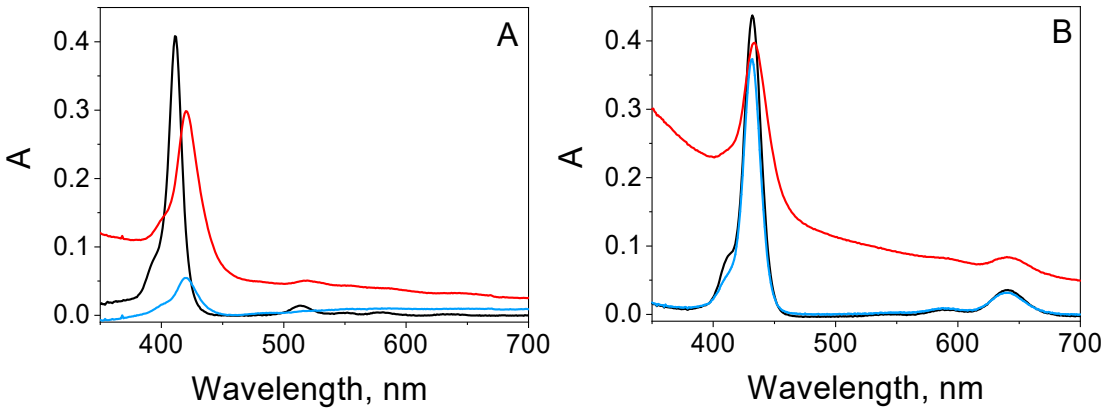

Figure 59 *Absorption spectra of A) aqueous solutions (pH 6.2) of free $TMAP^{4+}$ (black), $TMAP^{4+}$ with the addition of GO suspension (red) and spectrum of the supernatant after centrifuging (blue); B) aqueous solutions (pH 1.8) of free $TMAP^{6+}$ (black), $TMAP^{6+}$ with the addition of GO suspension (red) and spectrum of the supernatant after centrifuging (blue)*

The free energy of the electron transfer from the singlet excited state of TMAP to GO was estimated using a Rehm-Weller type calculation. First, the value of the 0-0 transition energy was calculated ($E_{0\text{-}0}$=2.1 eV), based on fluorescence results of free porphyrins. The oxidation potential (E_{ox} = 1.15 V vs. NHE) of TMAP in the ground state was taken from the literature.[137] Based on these data and the transition energy derived, the oxidation potential in the excited state was estimated (E_{ox}*= -0.95 V vs. NHE and compared to the energy of the graphene oxide conduction band (E_{CB}=-0.553 V vs. NHE).[152] The oxidation potential of porphyrin in the excited state is more negative than that of the graphene oxide conductivity band. The free enthalpy of this electron transfer (G_{ET}) was estimated to be about -0.4 eV. This means that photoinduced electron transfer is thermodynamically allowed.

Furthermore, energy transfer between two components of the hybrid ($TMAP^{4+}$ and GO or $TMAP^{6+}$ and GO) is highly unlikely due to negligible overlap of the normalized absorption spectrum of GO and the normalized spectrum of the porphyrin molecule ($TMAP^{4+}$ or $TMAP^{6+}$) (***Figure 60***).

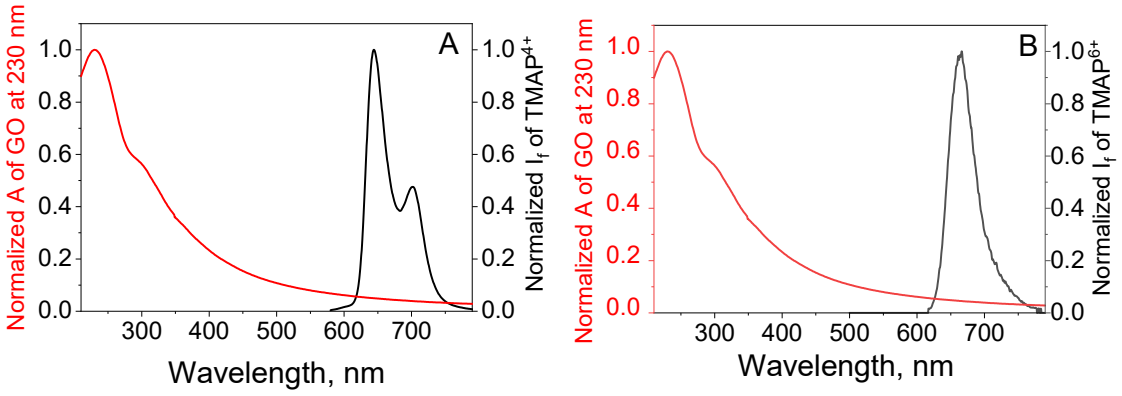

Figure 60 *Overlap of the normalized emission spectra of the A) TMAP^{4+} and B) TMAP^{6+} with the normalized absorption spectra of graphene oxide*

5.2.2.3 TMAP/GO nanohybrid characterization

As described in detail in the previous section, the aqueous solution of TMAP^{4+} was mixed with a dark brown aqueous suspension of GO, producing a light brown suspension subjected to further centrifugation. The precipitate was collected, dried, and subjected to further analysis.

The successful non-covalent functionalization of graphene oxide with cationic porphyrin – TMAP by several methods. The FTIR, TGA and elemental analysis were conducted using TMAP^{4+}/GO hybrid powder, after centrifugation and drying (***Appendix 3***). The Raman and AFM measurements were performed for TMAP porphyrin at two pH (6.2 and 1.8). Aqueous solutions of TMAP^{4+} and TMAP^{6+} were used to prepare the samples dropping diluted aqueous suspensions onto the appropriate surfaces by dropping them onto a suitable medium.

Raman Spectroscopy

Figure 61 shows the Raman spectra of TMAP^{4+} and TMAP^{6+}. The macrocycle's protonation state very slightly affected the peaks' spectral positions and intensity ratios between peaks. The most intense peaks were recorded at ca. 703 cm^{-1} (out-of-plane deformation of phenyl rings), 987 cm^{-1} (out of plane deformation of C-H bonds/pyrrole breathing vibrations), ca. 1011 cm^{-1} (symmetric stretching C_α-C_m/pyrrole breathing vibrations), ca. 1099 cm^{-1} (in-plane deformation C_β-H/ in-plane deformation C-H at phenyl rings), 1244 cm^{-1} (in-plane deformation Cm-phenyl), 1319 cm^{-1} (symmetric stretching C_α-N/asymmetric stretching C_α-C_β and in-plane deformation C_β-H), ca. 1476

cm^{-1} (asymmetric stretching C_α-C_β/stretching C_β-C_β) and 1546 cm^{-1} (symmetric stretching C_β-C_β and C_β-H/stretching C_β-C_β and C_α-C_m).

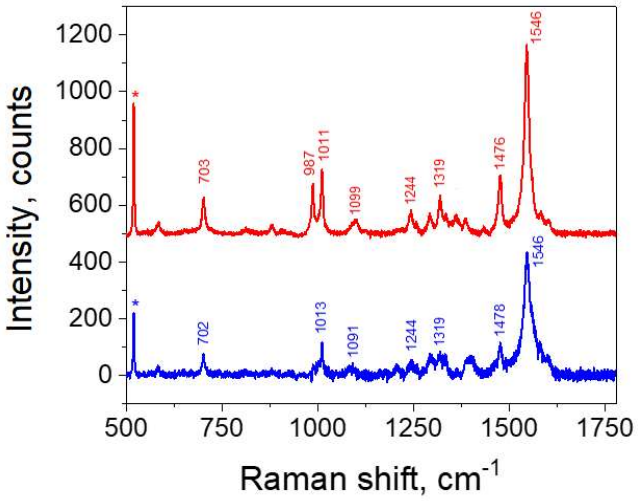

Figure 61 *Raman spectra of $TMAP^{4+}$ (blue) and $TMAP^{6+}$ (red). The asterisk denotes signals from the silicon substrate (519 cm^{-1})*

The Raman spectra of both hybrids ($TMAP^{4+}$/GO and $TMAP^{6+}$/GO) confirm the attachment of the porphyrin molecule to the surface of the graphene oxide sheet (***Figure 62***).

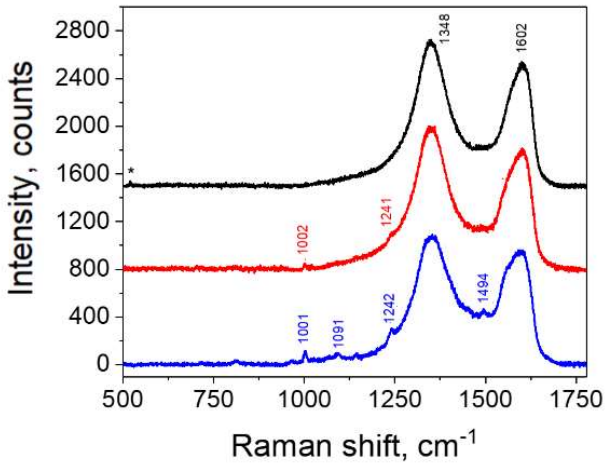

Figure 62 *Raman spectra of GO (black), $TMAP^{4+}$/GO (blue), and $TMAP^{6+}$/GO (red) hybrids excited at 532 nm. The asterisk denotes the signal from the silicon substrate (519 cm^{-1}). The spectra presented are baseline-corrected*

For both, Raman peaks characteristic of the porphyrin macrocycle are present in the spectra. Spectra. However, the signals generated by the adsorbed porphyrin molecules are more prominent in the $TMAP^{4+}$/GO hybrid, suggesting a higher porphyrin concentration in the hybrid. This observation indicates a stronger interaction between the dye and GO under neutral pH conditions than under acidic pH conditions. This result is consistent with the findings from steady-state absorption measurements. Shifts in the porphyrin signals after binding to the surface of the GO sheet appear only for peaks related to the stretching vibrations of carbon atoms in the porphyrin macrocycle itself. This is indicative of the proximity of the porphyrin core to the GO sheet.

In the hybrid spectrum, the D band typical for the GO (see: **5.1 Characteristics of 2D materials used in work**) is slightly shifted towards higher wavenumbers, by approx. 4 cm^{-1}. The D band appeared at 1353 cm^{-1} (for $TMAP^{4+}$/GO) and 1352 cm^{-1} (for $TMAP^{6+}$/GO). The G band was registered at 1597 cm^{-1} ($TMAP^{4+}$/GO) and 1602 cm^{-1} ($TMAP^{6+}$/GO). Compared to unmodified GO, only for $TMAP^{4+}$/GO, the G band was the 5 cm^{-1} downshift. However, in both nanohybrids, the broadening of the G bands can be observed. The "shoulder" appears presumably due to the overlap of the most intense porphyrin Raman peak (at ca. 1546 cm^{-1}) and the G band of GO. It provides evidence for efficient functionalization of the graphene oxide surface with the porphyrin molecules. The D-to-G intensity ratio has not changed compared to that of nonmodified GO.

Atomic Force Microscopy (AFM)

The morphology of the nanohybrids, $TMAP^{4+}$/GO and $TMAP^{6+}$/GO, was studied by AFM (***Figure* 63**). The apparent thickness of GO was found to be equal to ca. 0.9 nm which matches the thickness of one GO layer, as was described in **5.1 Characteristics of 2D materials used in work**. In comparison, the average thickness of the $TMAP^{4+}$/GO nanohybrid was determined to be approximately 1.3 nm, which gives a 0.4 nm increment. It indicated the successful decoration of the GO sheet with porphyrin molecules. Taking into account that the thickness of one TMAP porphyrin molecule is about 0.5 nm,[148] it can be concluded that the $TMAP^{4+}$ molecules were adsorbed on the GO sheet as a monolayer. However, the distribution of the porphyrin on the surface of GO was not uniform.

Under acidic conditions (pH 1.8), where the porphyrin exists as a +6 charged form, under these conditions, the determined apparent thickness value of the resulting nanohybrid

is highly variable, measuring approximately 10 nm (***Figure* 63**B). This can be explained by the formation of aggregates of GO of different thicknesses and sizes (see: **5.1 Characteristics of 2D materials used in work**).

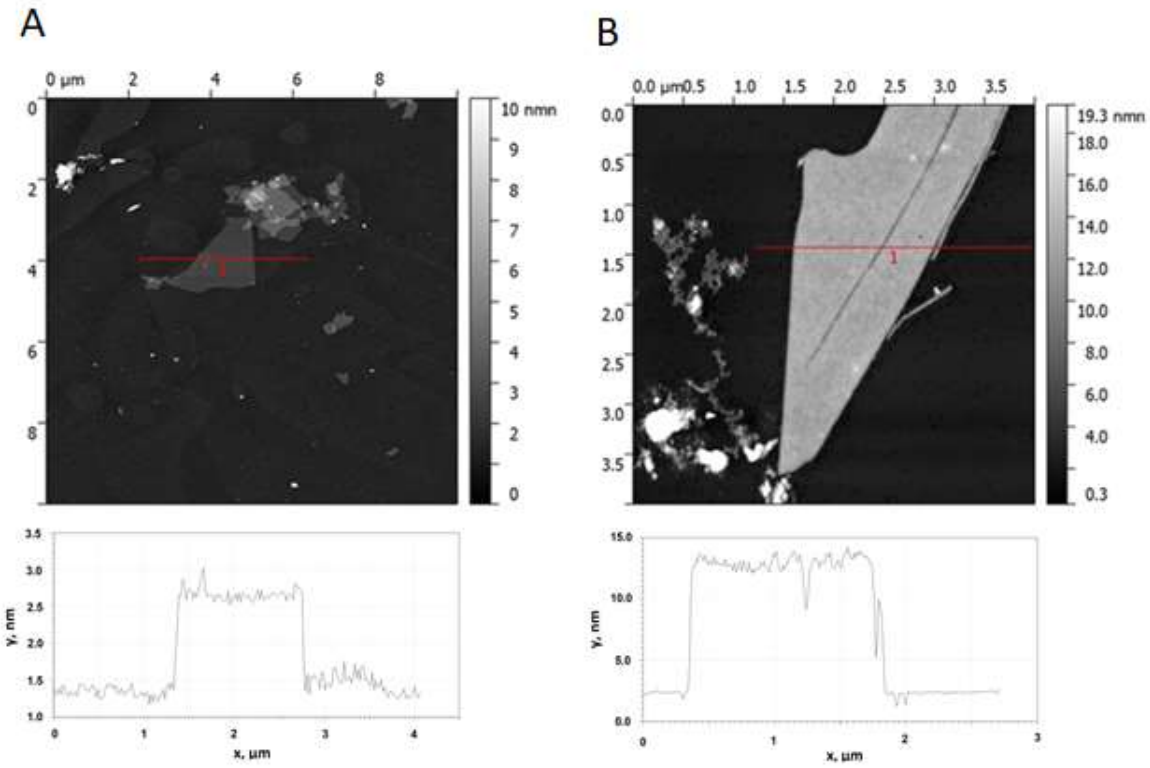

***Figure 63** AFM images of A) $TMAP^{4+}$/GO and B) $TMAP^{6+}$/GO with depth profiles*

FTIR

***Figure* 64** displays the FTIR spectra of the $TMAP^{4+}$, GO and $TMAP^{4+}$/GO nanohybrid obtained by the non-covalent interaction of the porphyrin molecule with the surface of the graphene oxide sheet. In the FTIR spectrum of GO (as described in 5.1 Characteristics of 2D materials used in work), there are numerous peaks attributed to the functional groups present in the structure of GO: a strong and broad and around 3000

cm^{-1} (O-H stretching vibration band) at 1719 cm^{-1} (carboxyl and carbonyl C=O stretching vibrations), 1590 cm^{-1} (skeletal vibrations of the C=C bonds), 1225 cm^{-1} (C-O stretching vibrations), and 1040 cm^{-1} (stretching vibrations of the C-O-C bonds in epoxy groups).

The spectrum of $TMAP^{4+}$ agrees well with the chemical structure of this porphyrin molecule. The free-base porphyrin exhibits typical bands of this class of compounds. The bands at 3410 cm^{-1} and 967 cm^{-1} correspond to N-H and C-H stretching and bending

vibrations. The bands at 846 cm^{-1} and 801 cm^{-1} referred to the out-of-plane deformation of the macrocycle ring. The bands relative to the C-H phenyl vibrations appeared at 1010 cm^{-1}, 1118 cm^{-1}, and 1175 cm^{-1}. The bands at 3036 cm^{-1} and 1475 cm^{-1} are attributed to stretching and bending vibrations $(C\text{-}H)_{methyl}$.

The FTIR spectrum of the $TMAP^{4+}$/GO nanohybrid confirms that porphyrin was successfully adsorbed on the surface of the GO sheets. The spectrum has signals typical for both graphene oxide and $TMAP^{4+}$ porphyrin. The porphyrin fingerprint region exhibits peaks at 800 cm^{-1} and 840 cm^{-1}, which were not observed in the spectrum of GO itself.

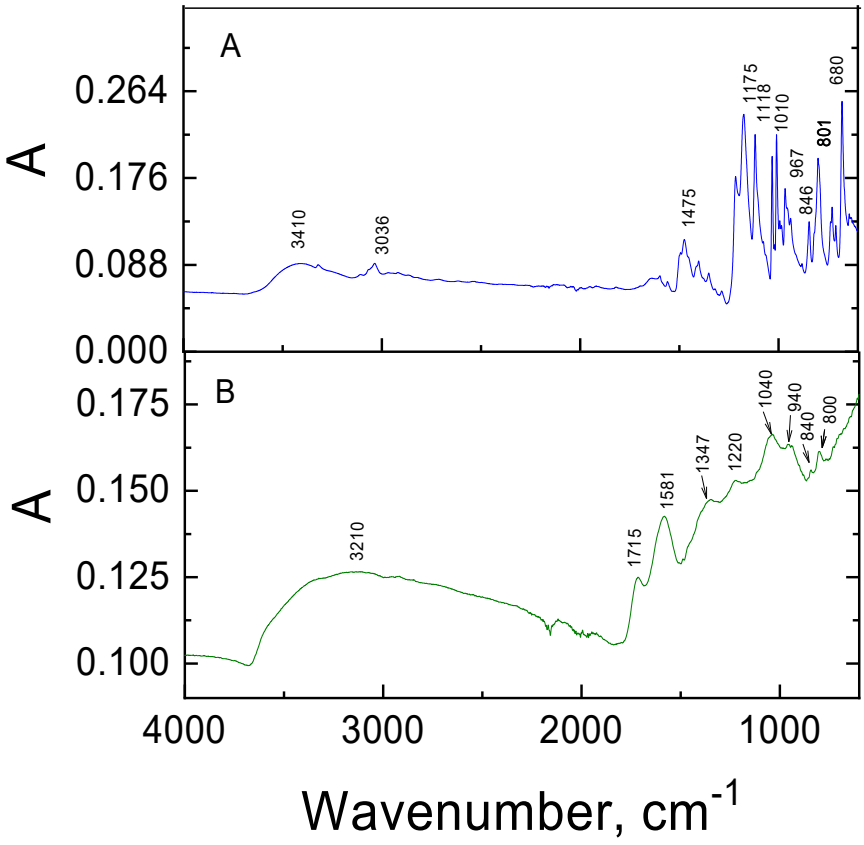

Figure 64 *The FTIR spectra of the A) $TMAP^{4+}$ and B) $TMAP^{4+}$/GO nanohybrid*

Elemental analysis

Elemental analysis was used to further confirm the adsorption of $TMAP^{4+}$ molecules on the graphene oxide sheets (***Table 9***). The nitrogen content in the $TMAP^{4+}$/GO

nanohybrid increased compared to GO. It can be attributed to the presence of porphyrin in the nanohybrid. Based on the increase in the content of the individual elements in the nanohybrid, it was estimated that the material contains ca. 18% of TMAP.

Table 9 *Results of the elemental analysis of the GO and nanohybrid $TMAP^{4+}$/GO*

Sample	C wt.%	H wt.%	N wt.%	S wt.%
GO[1]	48.43	2.21	0.0	0.20
$TMAP^{4+}$/GO	54.26	3.04	0.50	0.13

1– described in 5.1 Characteristics of 2D materials used in work

Thermogravimetric analysis (TGA)

The results obtained by thermogravimetric analysis provide additional evidence for the successful functionalization of GO with porphyrin at pH 6.2. ***Figure* 65** displays the TGA curves of GO, $TMAP^{4+}$, and $TMAP^{4+}$/GO nanohybrid. The TGA curves were recorded under an argon atmosphere from room temperature up to 900 °C.

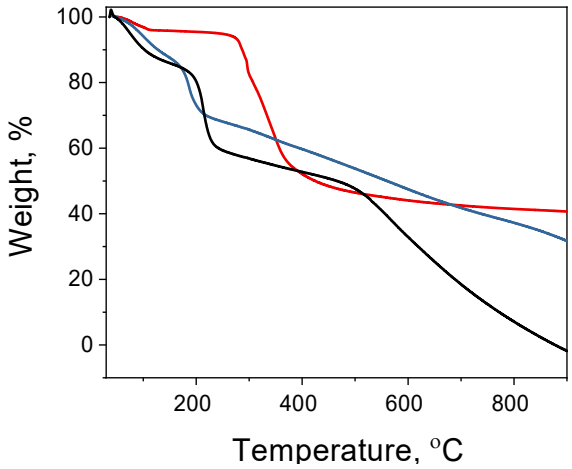

Figure 65 *The TGA curves of the GO (black), TMAP (red), and $TMAP^{4+}$/GO nanohybrid (blue)*

For the GO sample, from room temperature to 115 °C, a mass loss of about 16% is observed. This mass loss can be ascribed to the desorption of physically-adsorbed water on the surface and between the GO layers. A mass loss of approximately 24% was observed around 215 °C, attributed to unstable oxygen-containing functional groups

(such as hydroxyl, epoxy, and carboxyl) pyrolysis. The thermal decomposition of GO is completed at a temperature of 875 °C.

In the thermal decomposition of TMAP, a weight loss of approximately 4% is observed between 42 and 114 °C. It is attributed to the loss of water. In the 160-290° C range, up to 7.3% of the mass is lost due to partial removal of the $-N(CH_3)^{3+}$ groups. The decomposition of the organic moiety continues with increasing temperature, up to 900 °C, with a residue weight of 34.4%.

The TGA curve of $TMAP^{4+}$/GO shows different behavior than the TGA curves of the free components (GO and $TMAP^{4+}$), indicating that the nanohybrid is a new material with unique properties. The step attributed to the decomposition of the oxygenated groups of GO is shifted toward lower temperatures. The peak observed in the TGA of $TMAP^{4+}$ attributed to the decomposition of the cationic moiety is not observed in the TGA of $TMAP^{4+}$/GO. Electrostatic interaction of the negatively charged GO surface with the cationic groups of $TMAP^{4+}$ could increase the stability of the latter. Interestingly, the thermogravimetric analysis of the complex $TMAP^{4+}$/GO shows that the nanohybrid is more thermally stable than non-functionalized GO.

5.2.2.2. Steady-state and time-resolved emission

Photoluminescence spectroscopy is a useful tool for investigating the electronic interactions of TMAP molecules (in both forms, $TMAP^{4+}$ and $TMAP^{6+}$) in their singlet excited states with GO sheets. The correction factor for the GO absorption at the excitation wavelengths was less than 0.5% (see: **4.3.2 Inner filter effects I and II**). For comparative emission studies, the matching absorbance at the excitation wavelengths was used. To ensure the constant absorbance at the excitation wavelengths during emission measurement the solutions of porphyrins and nanohybrids were excited at the isosbestic point, that is, 416 nm and 438 nm for pH 6.2 and 1.8, respectively.

Figure* 66** shows a series of emission spectra recorded during the addition of an aqueous solution of GO to the $TMAP^{4+}$ solution and the $TMAP^{6+}$ solution both in water. First of all, it can be observed that the shapes of the spectra are different. The emission spectrum of $TMAP^{4+}$ has two unresolved bands, at ca. 645 nm and 702 nm. They can be described as Q(0,0) and Q(0,1) and are associated with the $S_1 \rightarrow S_0$ transition (Figure* 66**A). Free $TMAP^{4+}$ exhibit fluorescence with a quantum efficiency of 0.095.

Unlike the +4 form, $TMAP^{6+}$ has only one emission band, at 664 nm. The Q(0,0) band nearly vanishes, as was also reported for other porphyrins upon core protonation.[73]

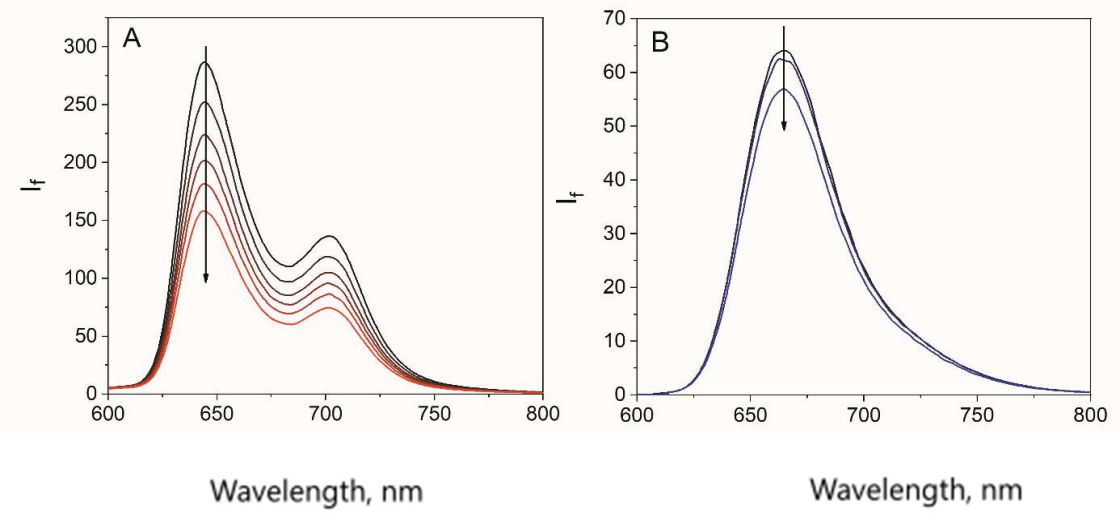

Figure 66 *A) Emission spectra recorded during addition of an aqueous suspension of GO (GO concentration: 0-0.36 μg mL^{-1}) to 0.3 μM $TMAP^{4+}$ in H_2O at pH 6.2; B) emission spectra recorded during the addition of an aqueous suspension of GO (GO concentration: 0-0.9 μg mL^{-1}) to 0.08 μM $TMAP^{6+}$ in H_2O at pH 1.8*

The emission of $TMAP^{4+}$ is successively quenched upon GO addition (***Figure* 66**A). To quench ca. 50% of the fluorescence intensity of $TMAP^{4+}$, the addition of only 0.3 μg mL^{-1} of GO is needed. The observed change in the emission intensity for $TMAP^{4+}$ is much more profound in comparison to $TMAP^{6+}$.

As shown in ***Figure* 66**B, successive addition of GO up to 0.90 μg mL^{-1} into the solution of $TMAP^{6+}$ had only a minor effect on the intensity of the emission spectra. This further confirms that the interaction between $TMAP^{6+}$ and GO is weaker compared to $TMAP^{4+}$. Only at much higher GO concetration the emission quenching was observed. With the concentration of GO 3.86 μg mL^{-1} 50% of the $TMAP^{6+}$ emission was quenched.

Two species, free $TMAP^{4+}$ and $TMAP^{4+}$/GO nanohybrid, are present in the solution during the experiment. In principle, both of them could be responsible for the observed fluorescence. $TMAP^{4+}$/GO has a different electronic structure compared to free $TMAP^{4+}$ (confirmed by UV-Vis spectroscopy – see: **5.2.2.1 Steady-state absorption properties**). Thus, it is expected that the emission of the nanohybrid should be red-shifted compared to the emission of free $TMAP^{4+}$. However, no observable changes in the emission spectra

were detected, nor was there a change in shape or a change in the position of the peaks (***Figure* 67**). As shown in ***Figure* 68**, the fluorescence excitation spectrum measured for $TMAP^{4+}$ porphyrin in the presence of GO matches the absorption spectra of free porphyrin. All the steady-state emission data obtained indicate that $TMAP^{4+}$ and $TMAP^{6+}$ are the only emissive species present in the solution. Their complexes with GO are not emissive (or their emission is below the detection capability of the apparatus used). The lack of detectable emission from the $TMAP^{4+}$/GO nanohybrid suggests that the excited state of $TMAP^{4+}$ is deactivated rapidly in other fast process. In the literature, the quenching of the emission intensity in the presence of the GBM is often considered as the evidence of electron or energy transfer. However alternative mechanisms for the observed decrease of the fluorescence intensity upon GO addition should also be considered. One possible explanation for the observed quenching of the fluorescence could be simply the static quenching i.e formation of the unemissive ground state complex between $TMAP^{4+}$ and GO.

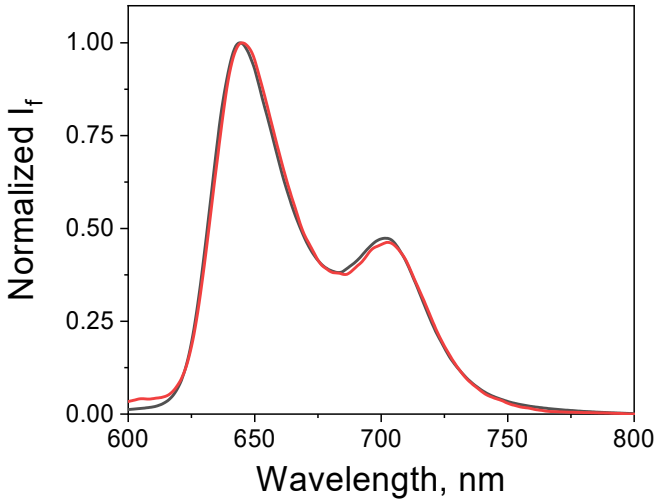

***Figure 67** Normalized emission spectra of $TMAP^{4+}$ without the presence of GO (black) and with the addition of GO (GO concentration: 0.36 μg mL^{-1}) (red)*

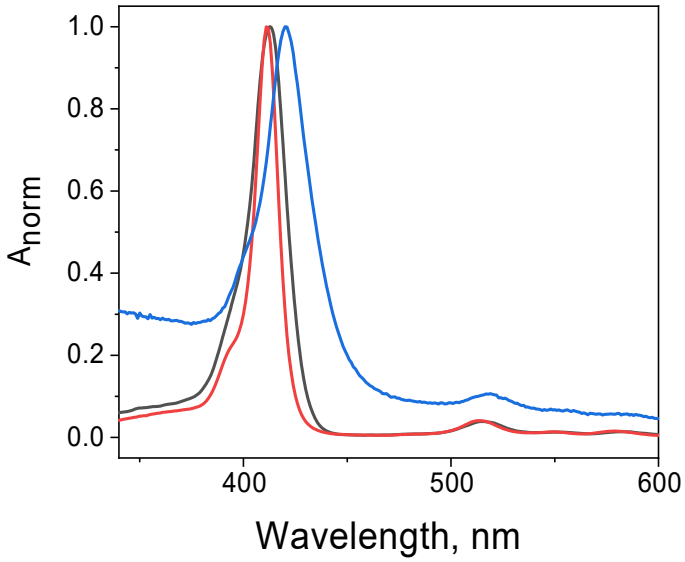

Figure 68 *The normalized fluorescence excitation spectrum of $TMAP^{4+}$ (λ_{em}=645 nm) solution recorded with the addition of an aqueous suspension of GO (black), the normalized absorption spectrum of $TMAP^{4+}$ in the absence of GO (red) and with the presence of GO (blue)*

The TCSPC method was used to conduct the lifetime measurements to get deeper insights into the emission quenching mechanism. The experiments were conducted to explore the possibility that the observed fluorescence quenching could be attributed to the interaction of the excited singlet state of unbound TMAP with GO, also known as dynamic quenching. Solutions of TMAP, at pH 6.2 and 1.8, at fixed absorbance (ca. 0.1 at the sample excitation wavelength - ***Table* 10**) were prepared. The emission decay profiles of the samples were monitored in the presence of different concentrations of GO (***Figure* 69**). The fluorescence lifetime extracted from the fluorescence decay of $TMAP^{4+}$ in the absence of GO was found to be 9.8 ns. No changes in the excited state's decay kinetics were observed with increasing concentration of GO (***Figure* 70**). For $TMAP^{6+}$, the fluorescence lifetime in the absence of GO was found to be 2.7 ns and also remained unaltered upon addition of GO.

The lack of an observable change in the lifetime of the singlet excited state of free $TMAP^{4+}$ excludes dynamic quenching by GO. Taking into account all the results discussed above, it can be stated that the observed decrease in the fluorescence intensity in the steady-state measurements can be attributed to the static quenching.[116] In summary, in the ground state an equilibrium exists between two species: fluorescent free $TMAP^{4+}$

and the non-emissive complex $TAMP^{4+}$/GO in the solution. With increasing concentration of GO the equilibrium is shifted toward the non-emissive complex, and the concentration of the unbound $TMAP^{4+}$ decreases, which is manifested by the decrease in the fluorescence intensity. It is worth emphasizing here that for the studied system, the decrease in the fluorescence intensity cannot be interpreted directly as an evidence of the electron or energy transfer. However, the lack of detectable emission of the $TMAP^{4+}$/GO complex points to the possibility of a very rapid deactivation process of the excited state of $TMAP^{4+}$ adsorbed on the GO surface, such as an electron or energy transfer.

Table 10 *Excitation and detection wavelengths and fluorescence lifetime of $TMAP^{4+}$ and $TMAP^{6+}$*

Sample	Excitation wavelength (nm)	Detection wavelength (nm)	Fluorescence lifetime (ns)
$TMAP^{4+}$	405	660	9.8
$TMAP^{6+}$	440	660	2.7

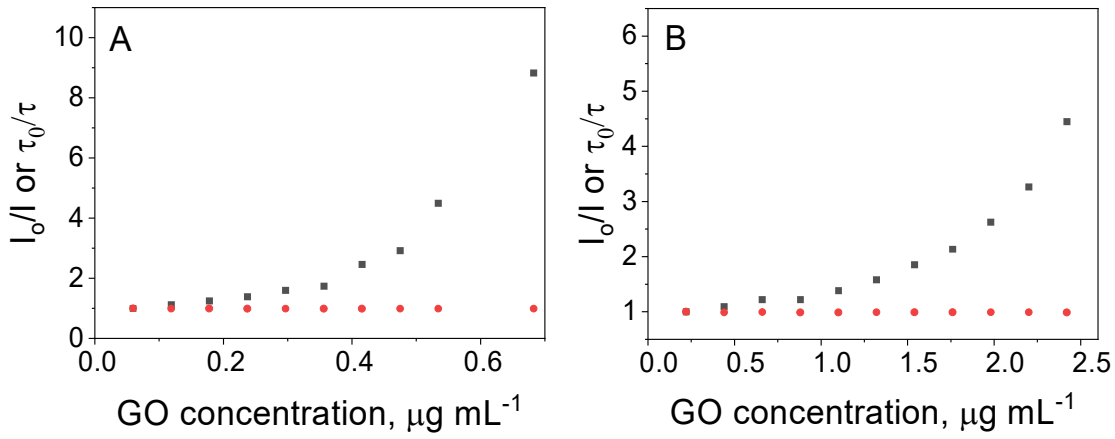

Figure 69 *The relationship between fluorescence intensities I_0/I_f (I_0 – fluorescence intensity without GO, I_f – fluorescence intensity after addition of GO) and GO concentration (black) and the relationship between fluorescence lifetimes τ_0/τ (τ_0 – fluorescence lifetime without GO, τ- fluorescence lifetime after addition of GO) and GO concentration (red) for A) $TMAP^{4+}$ and B) $TMAP^{6+}$*

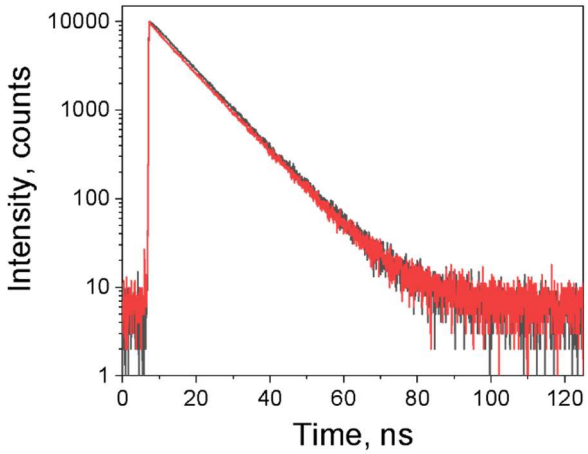

Figure 70 *$TMAP^{4+}$ fluorescence decay recorded (λ_{ex}= 405 nm, λ_{det}=660 nm) in the absence of GO (black line) and with GO (0.36 µg mL^{-1}) (red)*

5.2.2.4 Femtosecond TA Spectroscopy

Ultrafast spectroscopy experiments (femtosecond and nanosecond) were performed on free $TMAP^{4+}$ and $TMAP^{4+}$/GO nanohybrid. These measurements were performed to obtain experimental information on excited state dynamics and to determine whether the electron transfer process occurs between the photoexcited $TMAP^{4+}$ molecule and the graphene oxide sheet.

The transient absorption spectra recorded shortly after 420 nm laser pulse excitation of $TMAP^{4+}$ exhibited the characteristic spectra for singlet excited states of porphyrins (***Figure*** **71**A). The spectrum is characterized by broad and intense absorption around 450-500 nm and a Q-band bleach that match the Q-band position observed for the ground-state UV-Vis absorption spectra. The spectra underwent only a small decay over the whole time window of the experiment (3 ns). This observation is in good agreement with the singlet excited state lifetime obtained independently from the TCSPC technique (9.8 ns) (see: **5.2.2.2. Steady-state and time-resolved emission**).

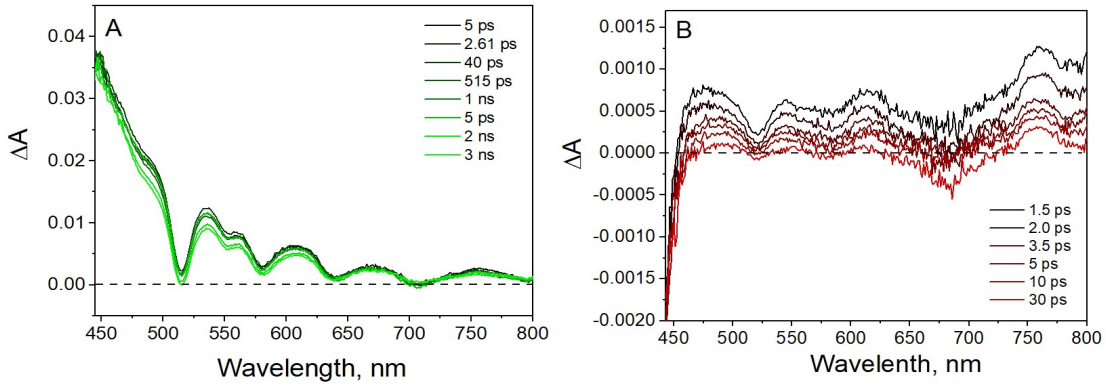

Figure 71 *Transient absorption spectra registered at various time delays for A) $TMAP^{4+}$ (2.7 μM) and B) $TMAP^{4+}$/GO ($TMAP^{4+}$ concentration 0.3 μM) in water (pH 6.2) after laser excitation at 420 nm*

Upon the addition of GO to the $TMAP^{4+}$ solution, TA shows new spectral characteristics (***Figure*** **71**B). The presence of scattered light by GO influenced the signal-to-noise ratio. The TA spectrum differs from the singlet excited state spectrum of the free $TMAP^{4+}$ molecule. New bands, observed in the range of 650 to 800 nm, were assigned to the porphyrin cation radical.[80,153,154] The radical cation detection provides proof for photoinduced electron transfer from the porphyrin molecule to the GO sheet surface.

The radical cation of $TMAP^{4+}$ was detected within the instrument's temporal resolution (80 fs), indicating that the ET from the cationic porphyrin to GO is very fast. Such a fast ET can only be possible when $TMAP^{4+}$ and GO are in very close contact before excitation. ***Figure*** **72** shows the analysis of the TA kinetics collected for free $TMAP^{4+}$ and $TMAP^{4+}$ adsorbed onto GO. Kinetic traces were collected at 755 nm, that is, at the wavelength at which maximum absorbance of the porphyrin radical cation was observed for the $TMAP^{4+}$/GO nanohybrid. A significant difference was noticed between the two investigated samples. The kinetic profile of the nanohybrid shows very fast decay dynamics (double exponential decay) compared with no decay of the excited state of free porphyrin on the same time scale of 100 ps. The time constants extracted from the decay of the $TMAP^{4+}$ radical cation are 0.4 ps and 12 ps. The fast decay of the $TMAP^{4+}$ radical cation signal can be attributed to efficient back electron transfer and recovery of the ground state complex.

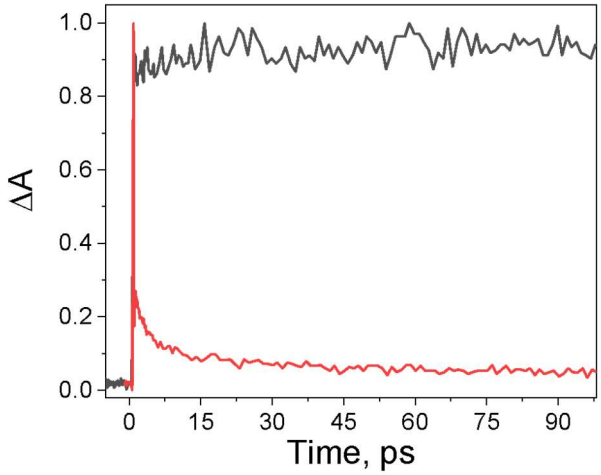

Figure 72 *Transient absorption decays recorded at 755 nm for the $TMAP^{4+}$ (black) and $TMAP^{4+}$/GO nanohybrid (red) after 420 nm excitation in water under neutral conditions (pH 6.2)*

5.2.2.5 Nanosecond TA Spectroscopy

To reveal whether the interaction between $TMAP^{4+}$ and GO is also effective in the triplet state, nanosecond transient absorption experiments were conducted. The nanosecond transient absorption spectra registered for $TMAP^{4+}$ in the absence and presence of GO after laser excitation at 532 nm are shown in ***Figure 73***. Upon laser excitation at 532 nm, the excitation of $TMAP^{4+}$ takes place rather than GO due to the latter's negligible absorbance at that wavelength. $TMAP^{4+}$ exhibited strong bleaching of the ground state at 410 nm, which was perfectly in line with the position of the porphyrin absorption spectra. Triplet-state absorption was observed with the maximum at 450 nm. The transient spectra exhibited no evolution during the decay of the triplet. For $TMAP^{4+}$, the triplet excited state band decayed simultaneously with the ground state bleach recovery. No new bands were observed, indicating that the excited state of $TMAP^{4+}$ returned to the ground state. The concentration of GO used was such that free porphyrin remained present in the solution. At a higher concentration of GO, the formation of the triplet state of $TMAP^{4+}$ was fully diminished. That can be explained by the very fast electron transfer process from the singlet excited state which prevents intersystem crossing and as consequence suppresses the triple state population.

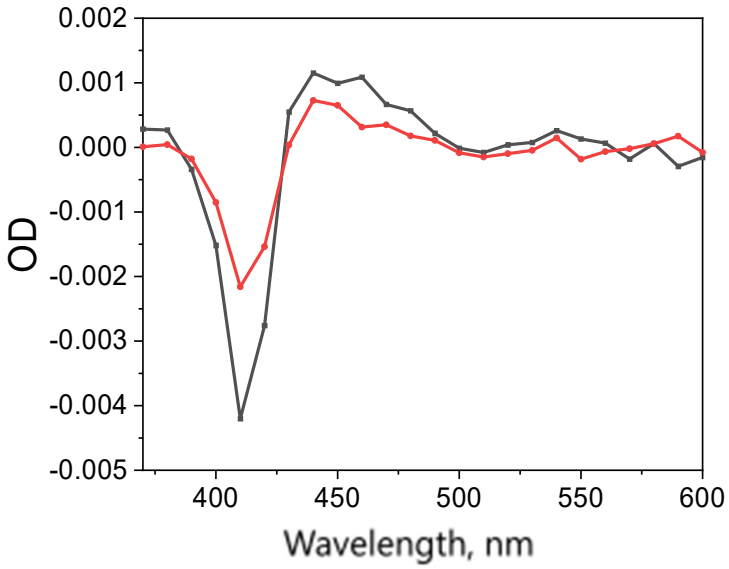

Figure 73 *Transient absorption spectra obtained during laser flash photolysis (λ_{ex}=532 nm) of deoxygenated solutions of $TMAP^{4+}$ (black) and $TMAP^{4+}$ in the presence of GO (0.3 μg mL^{-1}) (red); time delay after flash: 100 ns*

Figure 74 shows normalized recovery profiles of bleach monitored at 410 nm for the $TMAP^{4+}$ and $TMAP^{4+}$/GO nanohybrid. The triplet lifetime of the porphyrin molecule was obtained from a monoexponential fit (1.6 μs) and did not change with the addition of GO. Therefore, it can be deduced that the triplet state of $TMAP^{4+}$ does not interact with GO.

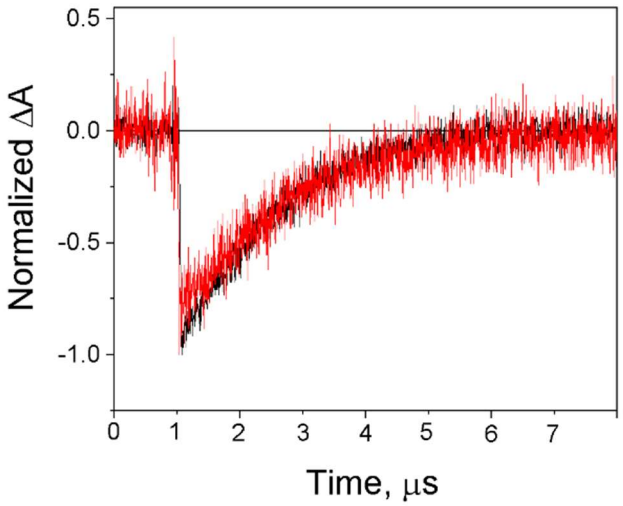

Figure 74 *Normalized recovery profiles of the bleach monitored at 410 nm for $TMAP^{4+}$ with no presence of GO (black) and $TMAP^{4+}$ with the presence of GO (concentration of GO: 0.3 μg mL^{-1}) (red)*

5.2.2.6 Discussion of possible deactivation pathways of the excited state

To sum up, all the results obtained regarding the $TMAP^{4+}$ molecule and its interaction with graphene oxide, **Scheme *10*** can be employed. The $TMAP^{4+}$/GO nanohybrid was obtained by simply mixing solutions of the two components. Upon adding GO to the porphyrin solution, the Soret band disappears, and a new band at higher wavelengths appears. This new band can be attributed to the absorption of light by a porphyrin molecule that is adsorbed non-covalently onto the surface of the graphene oxide sheet. (see: **5.2.2.1 Steady-state absorption properties**)

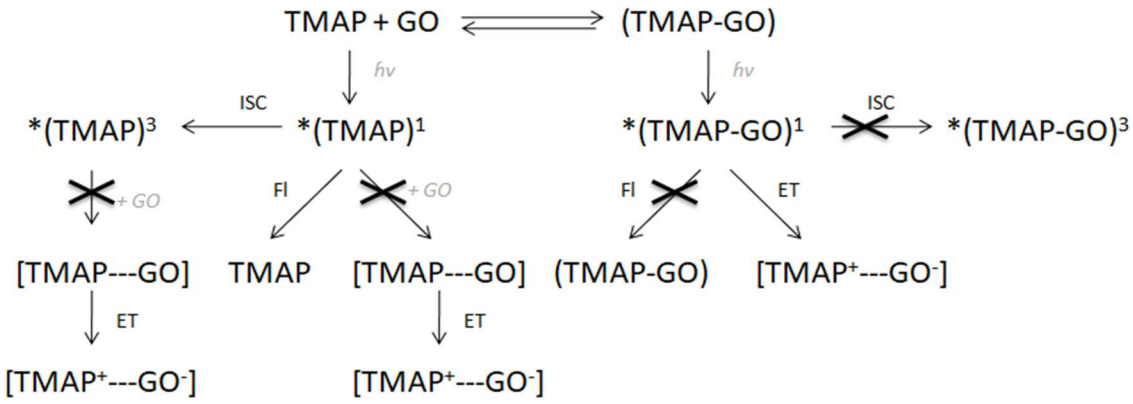

Scheme 10 *Possible deactivation paths of the excited states of free TMAP and nanohybrid TMAP/GO discussed in the text (Fl– fluorescence, ET - electron transfer)*

The interaction between porphyrin in the singlet excited state and GO was analyzed by emission measurements, both steady-state and time-resolved (see: **5.2.2.2. Steady-state and time-resolved emission**). ***Scheme* 10** presents possible deactivation paths of the excited states of the free porphyrin molecule and the $TMAP^{4+}$/GO nanohybrid. Based on the obtained results it can also be stated that the fluorescence of the porphyrin is quenched by GO solely by the static quenching mechanism. Dynamic quenching of the excited state was excluded based on TCSPC measurements in which no shortening of the fluorescence lifetime of the $TMAP^{4+}$ after the addition of GO was monitored

Interestingly, no detectable fluorescence of the excited state of the nanohybrid was observed, indicating the presence of another rapid deactivation process. The emission

of $TMAP^{4+}$ adsorbed onto the GO surface is expected to occur in a different wavelength range than that of the unbound $TMAP^{4+}$ molecule. It is due to changes in the ground state electronic structure of the porphyrin bound to the surface of the graphene oxide sheet. Moreover, no additional fluorescence decay time was detected in the TCSPC measurement that could be attributed to the decay of the singlet excited state of the porphyrin in the nanohybrid. Ultrafast time-resolved transient absorption spectroscopy confirmed the occurrence of the very fast deactivation process - electron transfer from the photoexcited $TMAP^{4+}$ singlet state to GO sheets, as proven by the formation of a porphyrin radical cation. (see: **5.2.2.4 Femtosecond TA Spectroscopy**)

5.2.2.7 Summary

This work has proven that cationic porphyrin molecules can be efficiently assembled onto the surfaces of graphene oxide sheets forming stable complexes. During the process of assembly, it is the electrostatic attraction that plays an essential role and π-π stacking cooperative interaction can only further promote the adsorption process of porphyrin. It was shown that stronger interaction with GO occurs for $TMAP^{4+}$ than for $TMAP^{6+}$ where it is largely suppressed. This can be rationalized in terms of: a) a distortion of the planarity of the porphyrin macrocycle upon protonation, b) a decrease of the Columbic interaction due to protonation of the carboxylic groups in GO, c) aggregation of the GO under acidic conditions. The non-covalent functionalization of GO with cationic porphyrin at pH 6.2 was confirmed by FTIR, Raman spectroscopy, thermogravimetric analysis (TGA), atomic forces (AFM), and elemental analysis. The nanohybrids were subjected to detailed spectroscopic characterization with several methods to probe the ground state as well as the excited state interaction between the components of the new material. It was found that the formation of $TMAP^{4+}$/GO hybrids changes porphyrin ground state electronic structure which was manifested among others by the shifts of the Soret band from 411 nm to 421 nm. Moreover, it was evidenced that the ground state interaction between $TMAP^{4+}$ and GO causes static quenching of the porphyrin emission. Surprisingly, fluorescence is not detected for the nanohybrid which indicates that a very fast deactivation process must take place. Ultrafast time-resolved transient absorption spectroscopy clearly demonstrates the occurrence of electron transfer from the photoexcited $TMAP^{4+}$ singlet state to GO sheets, as proven by the formation of a porphyrin radical cation. These results are relevant to the use of such systems

in developing energy conversion assemblies if undesired back electron transfer could be suppressed.

5.3 Neutral porphyrins

5.3.1 TAPP

In this study, 5,10,15,20-tetra(4-aminophenyl)porphyrin (TAPP) was chosen as a representative example of a neutral meso-tetra phenyl-substituted porphyrin. The TAPP has four substituents: the aminophenyl group in the outer position. The molecular structure of TAPP is depicted in ***Figure* 10**. Although this porphyrin is described in the literature as a water-soluble, in fact, its water solubility is limited to acidic pH (pH < 3). For this reason, the ethanol-water mixture was used as a solvent throughout the study.

Despite the recent advancements in the field of porphyrin/graphene nanoassemblies, there are only a few isolated reports that provide comprehensive characterization of the interaction between one porphyrin and various graphene-based materials.[62,75,78–83,93,105] In this part of the thesis, the focus was on comparison the strength of the interaction of neutral porphyrin with two types of graphene-based materials (GO and rGO) and investigating the spectroscopic properties of the obtained nanohybrid materials. Therefore two new nanohybrids of TAPP porphyrin with GO and rGO were prepared and characterized. The synthesis of the nanohybrids was carried out through non-covalent interactions between the graphene-based material and porphyrin dyes. Two newly prepared non-covalent nanohybrids, TAPP/GO and TAPP/rGO, were characterized by a number of techniques including elemental analysis, FT-IR, TGA, absorption, and emission spectroscopy.

5.3.1.1 Steady-state absorption properties

The interesting feature that attracts to this porphyrin is that the overall charge of the TAPP molecule changes between neutral and positive +2 or +6 depending on the pH of the solution (***Scheme* 11**). Each of the porphyrin forms has characteristic absorption spectra that are also reflected in a different colour of their solutions. TAPP at neutral pH does not possess a charge. The UV-Vis spectrum obtained for TAPP at pH=7.0 shows a Soret band

with a maximum at ca. 424 nm and four less intense Q-bands at ca. 521, 563, 591, and 654 nm (***Figure 75***).

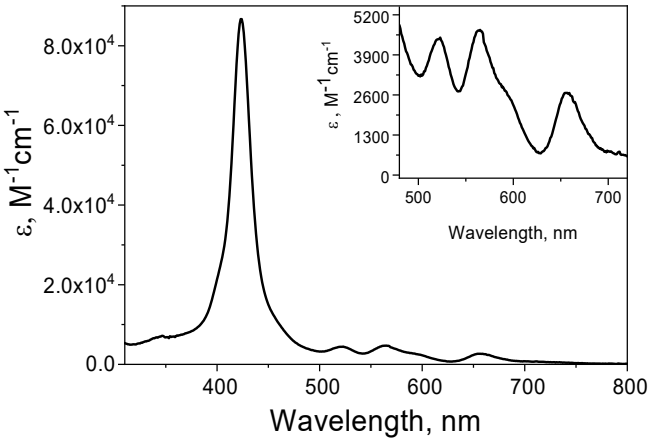

***Figure* 75** UV-Vis absorption spectrum of the ethanol-water (1:2 v/v) TAPP solution, pH=7.0. (Inset: Q-band region of the same spectrum)

However, the protonation of imino nitrogens increases the overall charge to +2 ($TAPPH_2^{2+}$). The diprotonation of the porphyrin molecule is associated with Soret band splitting (381 and 462 nm), in accordance with the presence of the conjugated amino group[155,156] (***Scheme* 11**, ***Table* 11**). The Q-band (654 nm) broadened, and red-shifted to 749 nm. The other three Q-bands disappeared under acidic conditions (***Table* 11**, ***Figure* 76**). A theoretical calculations predicted this observations.[157] The observed substantial bathochromic shift of the Q-band, accompanied by an intensified signal in the acidic solution, can be attributed to a charge transfer phenomenon occurring between the aminophenyl groups and the porphyrin core. Upon acidification, a comparable trend in behavior was observed for the TAPP porphyrin when dissolved in dimethyl sulfoxide (DMSO) as the solvent.[155] Gacka *et al.* reported similar effect of the pH-on the UV-Vis spectra for meso- (hydroxyphenyl)porphyrin (TPPH).[73] The observed changes in the spectra between neutral TPPH and protonated $TPPH^{2+}$ were explainedby theoretical calculations that predicted that the highest occupied molecular orbital (HOMO)−lowest unoccupied molecular orbital (LUMO) excitation in $TPPH^{2+}$ has a charge-transfer character.

***Table* 11** UV-Vis absorption band positions for different forms of 5,10,15,20-tatra(4-aminophenyl) porphyrin: TAPP, $TAPPH_2^{2+}$ and $TAPP^{4+}H_2^{2+}$

Porphyrin form	pH	Band positions (nm)	
		Soret	Q-bands
TAPP	5.3<	424	521, 563, 591, 654
$TAPPH_2^{2+}$	2.0-5.3	381, 462	749
$TAPP^{4+}H_2^{2+}$	<2.0	435	649

Further acidification introduces a positive charge on the four -NH_2 groups in the substituent leading to the overall increase of the porphyrin charge to +6 ($TAPP^{4+}H_2^{2+}$). It is worth mentioning that changes from neutral to cationic form increase the solubility of TAPP in water.

Spectrophotometric TAPP titration was used to determine the acid dissociation constants (pK_a) at pH < 7. The first changes in the spectra after acid addition are attributed to the attachment of two protons to imino nitrogen and the pK_a of this transition was found to be 5.3 Further acid addition causes protonation of the –NH_2 group and the pK_a of these groups in TAPP was determined to be around 2.0. In this pH range, the aggregation of GO is observed (see: **5.1 Characteristics of 2D materials used in work**).

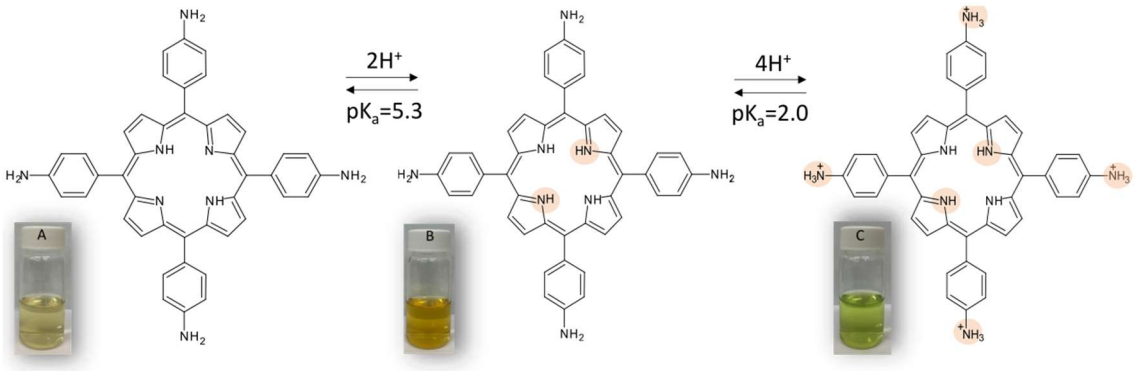

Scheme 11 *Molecular structure and ionic equilibria of 5,10,15,20-tetra(4-aminophenyl) porphyrin. pK_a' values were determined experimentally. Photographs of ethanol-water (1:2 v/v) solutions of: A) TAPP, B) $TAPPH_2^{2+}$, and C) $TAPP^{4+}H_2^{2+}$*

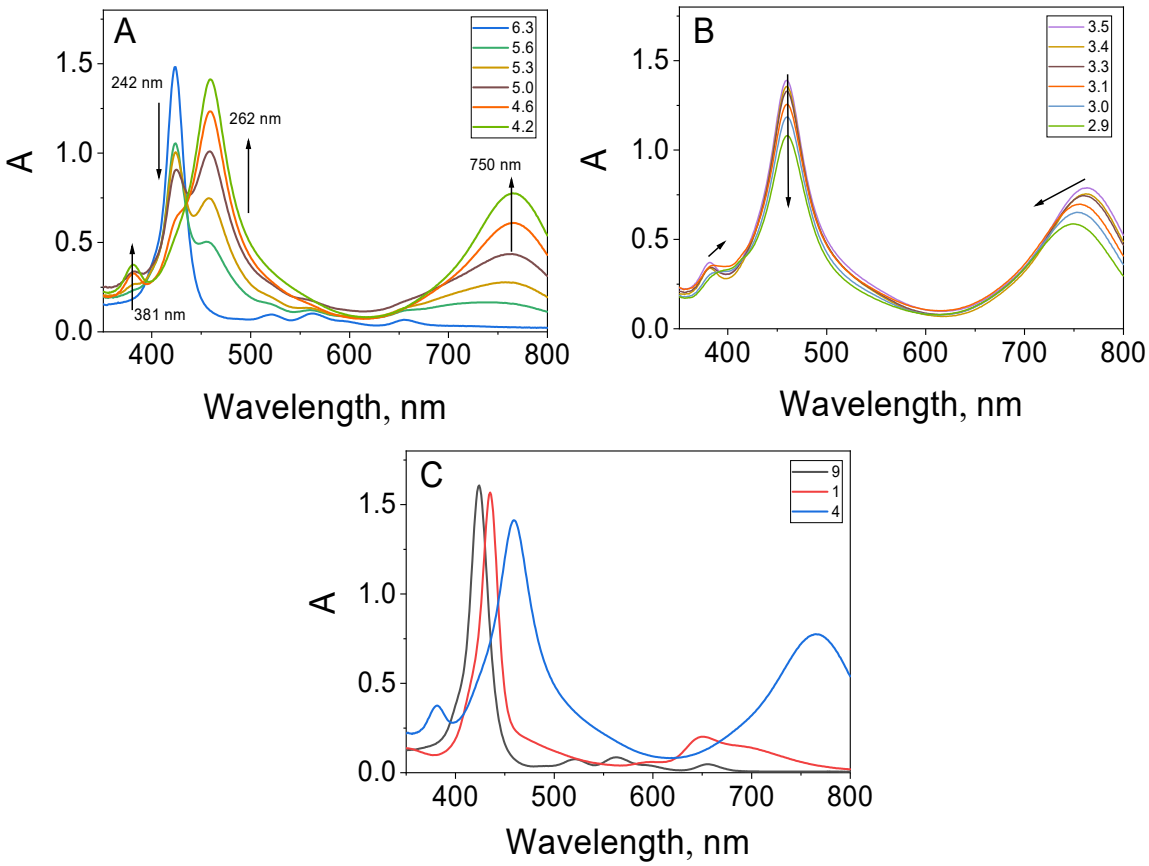

Figure 76 *Absorption spectra of 17 µM TAPP solution in ethanol-water (1:2 v/v) during acid-base titration in the range of pH values A) from 6.3 to 4.2 and B) from 3.5 to 2.9 (B). C) Absorption spectra of 17 µM TAPP solution in ethanol-water (1:2 v/v) pH equal to 9.0 (black), 4.0 (blue) and 1.0 (red)*

In this phase of the project, our main objective was to compare the strength of the π-π interactions between TAPP molecules and two GBM materials. To ensure a focused analysis without complications arising from electrostatic interactions, the neutral pH environment was selected. A. This choice was based on the pK_a values, indicating that the porphyrin exists in its neutral form at neutral pH.

Titration of porphyrin solution with GBM (GO or rGO)

The TAPP samples were titrated with 0.4 mg mL^{-1} of GO/rGO dispersion and UV-Vis spectra were recorded after each addition of GO/rGO (***Figure*** 77).

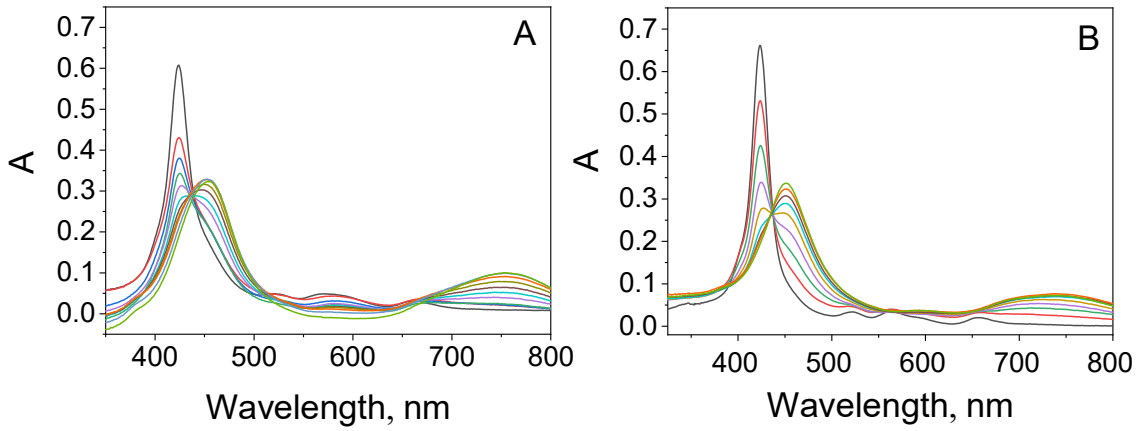

***Figure** 77 Absorption spectra recorded during the process of titration of 3 mL of A) ethanol-water (1:2 v/v, pH 7.0) solution of TAPP (7.8 μM) with 0.4 mg mL^{-1} of GO dispersion (0- 13 μg mL^{-1}), B) A ethanol-water (1:2 v/v, pH 7) solution of TAPP (8.1 μM) with 0.4 mg mL^{-1} of rGO dispersion (0- 18 μg mL^{-1}). The spectra are corrected for the GO/rGO absorption*

When the GO concentration was increased, the disappearance of the Soret band at 424 nm was observed (***Figure** 77A). Simultaneously, the intensity of the new Soret band ca. 456 nm was increasing. In the case of TAPP/rGO nanohybrids the new band was observed at 451 nm (***Figure** 77B). The newly observed bands can be attributed to the Soret band of a porphyrin molecule adsorbed onto the surface of the GBM sheet through non-covalent interactions. After titration of the TAPP solution with the GO/rGO suspension fallowing spectral changes were observed: red-shift of the Soret band, three of the four Q-bands disappeared, and the fourth band was red-shifted (750 nm) and broadened. One can notice that the Soret bands of the TAPP/GO and TAPP/rGO exhibit a significant red-shift of 32 nm and 27 nm, respectively This effect may arise from the flattening of the porphyrin molecule upon interaction with the surface of GO. The hypothesis of the flattening of the porphyrin when adsorbed on the GO/rGO sheet is supported by theoretical calculations (*vide infra*) that predict the dihedral angle between the phenyl and porphyrin planes decrease upon complexation with GO/rGO. An isosbestic point was also observed, confirming the apparent transition of free porphyrin into porphyrin adsorbed on the graphene oxide sheets (***Figure** 77, ***Table** 12).

Table 12 *Absorption properties of the free TAPP and TAPP adsorbed on GO and rGO (pH=7.0)*

	Soret band (nm)	Q-bands (nm)	Isobestic point (nm)
Free TAPP	424	521, 563, 591, 654	
TAPP/GO	456	750	437
TAPP/rGO	451	750	439

To compare the strength of the interaction of TAPP molecules with two different graphene materials (GO and rGO) the increase of the absorbance of the Soret band (after subtracting the GO/rGO absorbance) of the porphyrins adsorbed on GO or rGO as a function of their concentration was investigated. The molar absorption coefficients of TAPP adsorbed on GO and rGO are very similar and approximately half that of free TAPP with a slight broadening of the band (***Figure*** **78**).

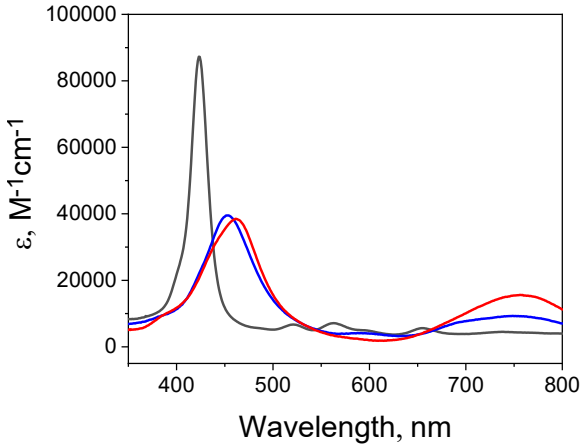

Figure 78 *Comparison of the absorption spectra of free TAPP (black), TAPP adsorbed on GO (red), TAPP adsorbed on rGO (blue) (ethanol-water 1:2 v/v, pH 7.0)*

Therefore, the increase in the absorbance is directly related to the concentration of the porphyrin molecules adsorbed on the GO/rGO sheets. The Soret band absorbance of the TAPP adsorbed on the GO/rGO surface increases linearly with the GO or rGO concentrations for both nanohybrids (***Figure*** **79**). The slope of the linear regression of the change in TAPP absorbance versus the concentration of graphene material is five times

higher for rGO than for GO. On the basis of this analysis, it can be concluded that porphyrin interacts more strongly with rGO.

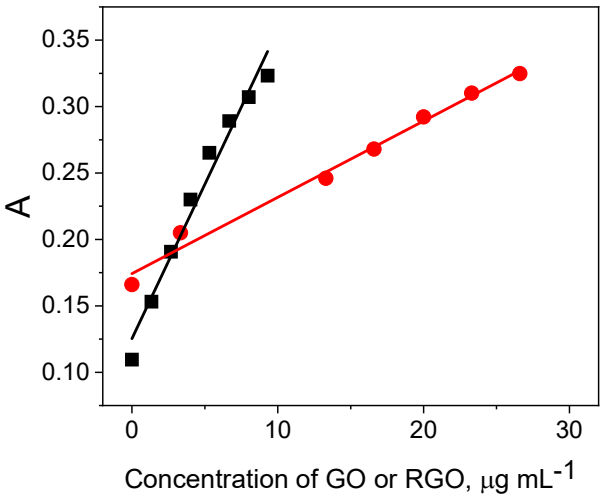

Figure 79 *Dependence of the absorbance at 451 nm (black) and 456 nm (red) of TAPP as a function of the concentration of rGO and GO, respectively*

Titration of the aqueous GO/rGO solution with the porphyrin solution was used to estimate the maximum amount of the porphyrin that can be adsorbed to the surface of GO and rGO (***Figure* 80**).

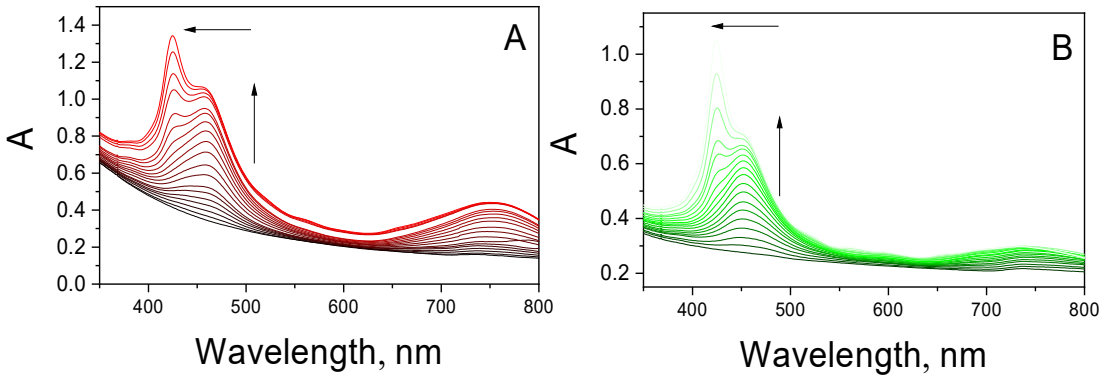

Figure 80 *Absorption spectra recorded during the addition of an ethanol-water (1:2 v/v) solution of TAPP to A) 100 μg mL^{-1} GO in H_2O (3 mL) and B) 13 μg mL^{-1} rGO in H_2O (3 mL)*

To the GO solution with a fixed concentration, different amounts of porphyrin solution were gradually added. A similar experiment was conducted for rGO. As the concentration

of TAPP increased, a corresponding rise in the absorbance of the Soret band, associated with free porphyrin, was observed. The maximum amount of TAPP in TAPP/GO is slightly above 12% (% w/w), while nearly 30% (% w/w) of TAPP can be adsorbed onto the surface of rGO (***Table* 13**).

Table 13 *Porphyrin content in the TAPP/GO and TAPP/rGO nanohybrid*

SAMPLE	Porphyrin content in the nanohybrid	
	mg of porphyrin/1 mg of GO or rGO	% of weight
TAPP/GO	0.14 mg	12.3%
TAPP/rGO	0.43 mg	30.0%

The newly obtained TAPP/GO and TAPP/rGO materials were isolated by a centrifugation experiment controlled by absorption spectroscopy. The UV−Vis spectra of the suspension of the nanohybrids before and after centrifugation are shown in ***Figure* 81**.

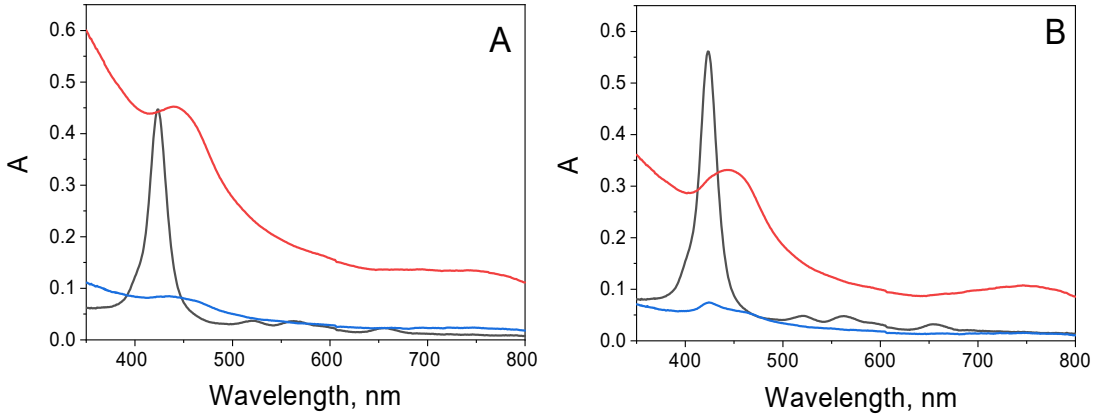

Figure 81 *UV-Vis spectra of (A) free TAPP (black), TAPP after adding GO (red), and the supernatant after centrifugation (blue); (B) free TAPP (black), TAPP after adding rGO (red), and the supernatant after centrifugation (blue)*

Based on the minor peak attributed to porphyrin in the UV−Vis of the supernatant, it can be concluded that almost the entire nanohybrid was collected as a precipitate. Based on the results, we can conclude that the interactions between GO or rGO and TAPP porphyrin are sufficiently strong to enable the formation of isolated TAPP/GO and TAPP/rGO nanohybrids, despite the absence of coulombic attraction between the neutral

TAPP and negatively charged GO (see: **2.1.1 Graphene oxide and reduced graphene oxide**).

5.3.1.2 Steady-state and time-resolved emission

To investigate interactions of the excited state of the porphyrin molecules with graphene oxide, photoluminescence spectroscopy was applied. The emission spectrum of the TAPP has one broad band centered at 675 nm. As discussed previously, the absorption spectrum of TAPP changes significantly upon the addition of a GO or rGO solution. For reliable data analysis, solutions were excited at isosbestic points (***Table* 12**). It ensures the constant absorbance of the porphyrin at the excitation wavelength during the entire quenching experiment. Moreover, the emission data were corrected for inner filter effects I and II. ***Figure* 82**A shows the emission spectra for several porphyrin/GO hybrids (with varying amounts of GO). An analogous experiment was carried out for rGO (***Figure* 82**B). The addition of GO or rGO results in a decrease in the fluorescence intensities of porphyrin. The relationships between fluorescence intensity and GO/rGO concentration for TAPP are presented in ***Figure* 83**. The fluorescence of TAPP was quenched more efficiently by rGO. The calculated quenching efficiencies for a concentration of 1.25 μg mL^{-1} of graphene-based material were approximately 17% for GO and significantly higher at 83% for rGO.

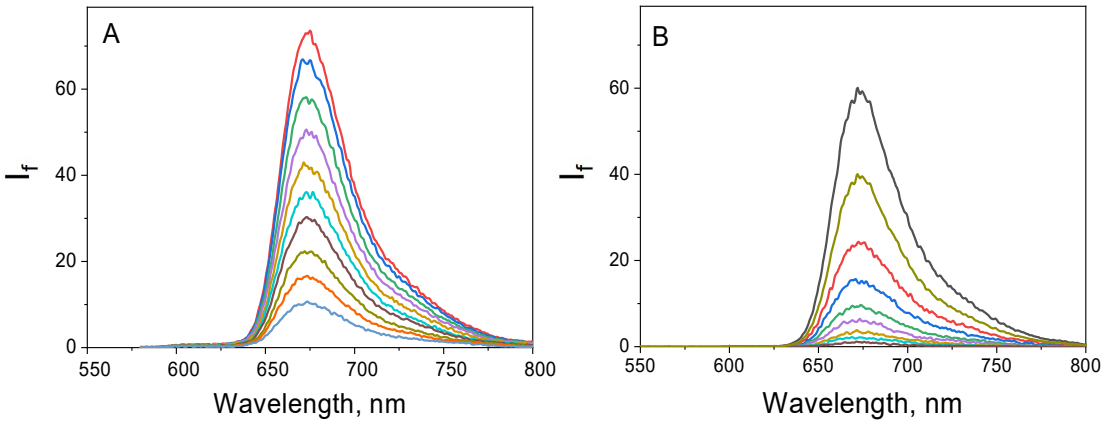

***Figure 82** Quenching of the fluorescence of the ethanol-water (1:2 v/v) solution of TAPP (pH 7.0) recorded during the addition of A) an aqueous suspension of 0.30 mg mL^{-1} GO (GO concentration: 0-8.0 μg mL^{-1}), λ_{ex}= 431 nm; B) an aqueous suspension of 0.88 mg mL^{-1} rGO (rGO concentration: 0-1.5 μg mL^{-1}), λ_{ex}= 438 nm*

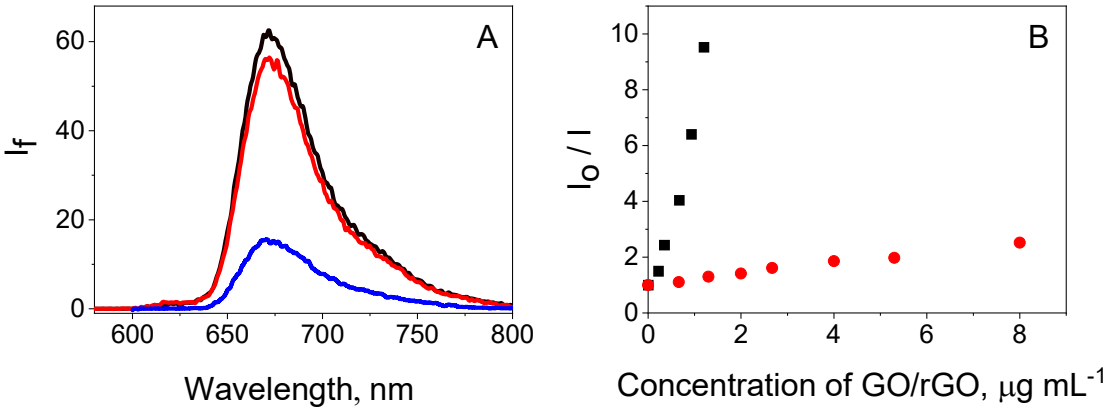

Figure 83 *A) Quenching of the fluorescence of 2.0 μM TAPP (black) recorded after the addition of 1.25 μg mL^{-1} of an aqueous suspension of GO (red) and rGO (blue). The spectra were corrected for the inner filter effect. B) Relationship between fluorescence intensity I_0/I (I_0 – I_f without GO/rGO, I – I_f after the addition of GO/rGO) and GO (red) /rGO (black) concentration for TAPP*

The lower quenching efficiency of GO provides further evidence of a weaker interaction between TAPP and GO compared to that with rGO. Relying solely on the steady-state emission measurements in the presence of a graphene-based material does not sufficiently capture the information needed to adequately describe the quenching mechanism (see: **4.3.1 Static and dynamic quenching**) Therefore the time-correlated single-photon counting technique was applied to further determine the mechanism of the emission quenching.

When the time-correlated single-photon counting technique was applied, it was found that the emission decay profiles of TAPP did not change upon the addition of either GO or rGO (***Figure* 84**). The fluorescence lifetime of the free TAPP was found to be equal to 5.7 ns and did not shorten with the addition of GO or rGO. Based on the analysis of the steady-state and time-resolved emission data, it can be concluded that the observed decrease in the emission intensity after the addition of graphene materials to the TAPP solution is solely attributed to static quenching. Static quenching as the reason for the observed decrease in the fluorescence of porphyrins in the presence of graphene-type materials has previously been reported by related systems.[74,80,158]

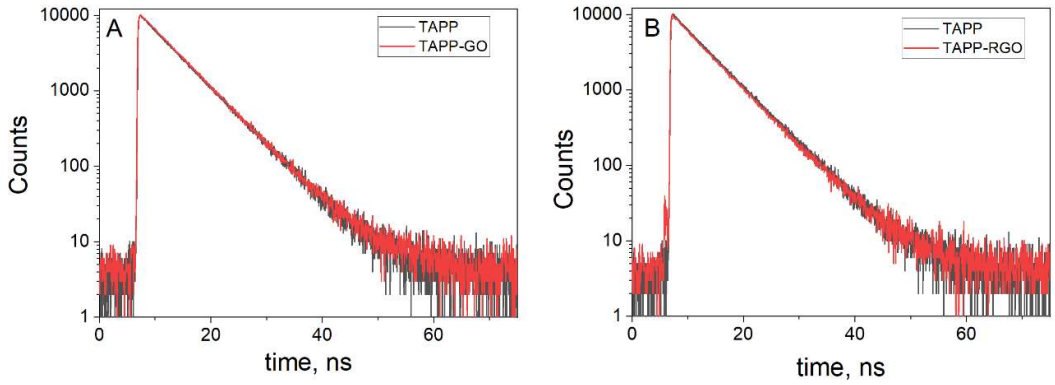

Figure 84 *Decay of (A) TAPP fluorescence recorded in the absence (black) and presence (red) of GO (2.7 μg mL^{-1}); λ_{ex}= 440 nm, λ_{em}= 672 nm, (B) TAPP fluorescence recorded in the absence (black) and presence (red) of rGO (2.7 μg mL^{-1}); λ_{ex}= 440 nm, λ_{em}= 672 nm*

5.3.1.3 Photoelectrochemical measurements for the TAPP/GO nanohybrid

Photocurrent measurements can provide evidence for photoinduced charge separation in a TAPP/GO nanohybrid. ***Figure* 85** shows the photoelectric response of the SnO_2-FTO electrodes covered with: GO and TAPP/GO.

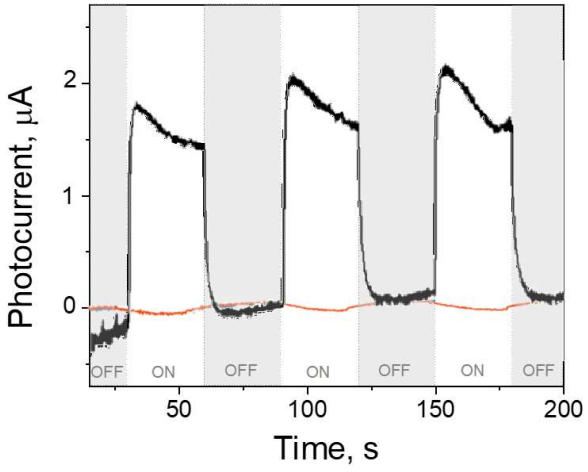

Figure 85 *Transient photocurrent in time for the TAPP/GO hybrid under white illumination (electrolyte: 0.1M LiI in acetonitrile). The red line shows the photocurrent generated by GO*

The measurement was conducted for the sample with GO for comparison with analogous hybrids of cationic porphyrins: TMPyP/GO and ZnTMPyP/GO. The conditions of the experiment were preserved. The irradiation was switched on and off in 30 second periods, which allowed the light and dark responses of the electrodes to be measured. The photocurrent response of GO was negligible.

An obvious photocurrent response for the electrode was observed for electrodes covered with TAPP/GO. Both experiments were conducted under similar conditions. The increase in photocurrent provides evidence for the photoinduced charge transfer in the studied nanohybrid material. The photocurrent response for TAPP/GO reached nearly 2 μA. The higher photocurrent response compared to pure GO might be attributed to electron-hole separation. However, the obtained photocurrent was almost 4 times lower than for $TMPyP^{4+}$/GO and 8 times lower than for $ZnTMPyP^{4+}$. This suggests that electron-hole separation in TAPP/GO is much less efficient than graphene oxide hybrids with cationic porphyrins.

5.3.1.4 Theoretical Calculations

Detailed insights into the electronic structures of the TAPP/GO and TAPP/rGO nanohybrids, as well as the tracking of structural changes occurring during their formation process, were facilitated by a series of quantum chemical calculations conducted by prof. Adam Kubas from the *Institute of Physical Chemistry, Polish Academy of Sciences*. Both GO and rGO induce similar structural changes in the TAPP molecules. The presence of GO or rGO leads to a more planar structure of the adsorbed porphyrin molecule, as evidenced by a reduction in the dihedral angle that describes the tilt of the phenyl rings relative to the plane. It is approximately 60° for the isolated porphyrin and about 49° for the TAPP/GO and TAPP/GO nanohybrids.

The calculated binding energies of TAPP to the GO and rGO systems were strongly negative and equal to -24.4 and -36.7 kcal mol^{-1}, respectively (***Table* 14**).

It is clear that TAPP tends to form a more stable complex with rGO. Furthermore, a decomposition of the binding energies was performed, separating the contributions arising from the deformation energies of the monomers (E_{deform}) and the interactions between the deformed substrates (E_{int}), as outlined in ***Scheme* 12**.

Table 14 *Binding energy related to nanohybrid formation and its decomposition according to the scheme presented (**Scheme 12**). All values are expressed in kcal mol^{-1}* [157]

Nanohybrid	E_{bind}	$E_{deform}^{graphene}$	E_{deform}^{porph}	E_{int}
TAPP/GO	-24.4	18.4	7.3	-50.1
TAPP/rGO	-36.7	8.5	5.9	-51.1

The energy of rGO deformation upon nanohybrid formation was found to be approximately 10 kcal mol^{-1} lower than that of GO. The interaction energy is higher for rGO, presumably because of the enhanced π-π stacking interactions. A higher degree of orbital mixing can be expected, which should manifest itself in the density of the excited state.

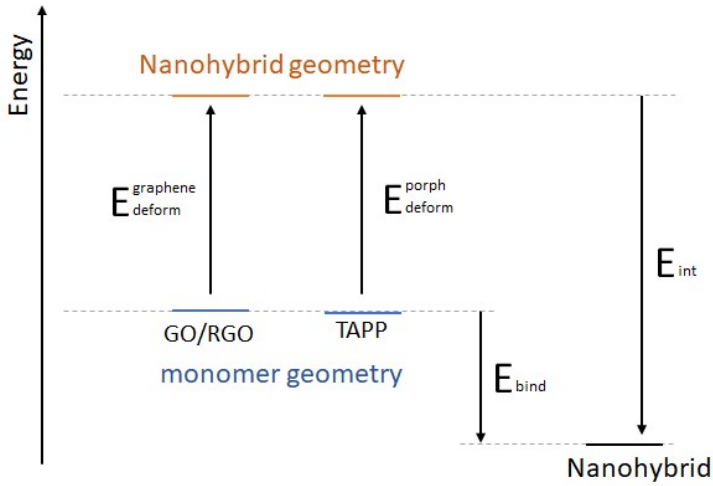

Scheme 12 *The binding energy (E_{bind}) decomposition scheme used to break down the energetic effect of nanohybrid formation into three energetic components: geometric deformation of the substrates ($E_{deform}^{graphene}$ and E_{deform}^{porp}), as well as interaction energy of the deformed substrates (E_{int})*

Experimental UV-Vis spectra were compared with the computed UV-Vis spectra. The Soret band shifts upon porphyrin adsorption on the GO/rGO sheet are well replicated in the calculations. The final nanohybrid spectrum of TAPP/GO can be relatively easily decomposed into a contribution from GO and TAPP. This is not the case for rGO, where the spectrum changes significantly upon complexation. Theoretical calculations

identified the five key transitions for each computed spectrum and traced their presence in the experimental spectral curves.[157]

5.3.1.5 Summary

Two non-covalent hybrids of TAPP porphyrin with two types of graphene-based materials (GO and rGO) were successfully synthesized. The TAPP/GO and TAPP/rGO nanohybrids were extensively characterized using various spectroscopic techniques. The conducted investigations revealed that both nanohybrids exhibit similar photophysical properties. However, TAPP/rGO exhibited a higher porphyrin content compared to TAPP/GO. These findings suggest that TAPP exhibits a stronger affinity towards rGO. Theoretical calculations carried out also strongly support this conclusions. The presence of both GO and rGO induces similar structural changes in the TAPP molecules. However, the calculated binding energies of TAPP to the GO and rGO systems were more negative for the latter graphene-based material. These results indicate that TAPP has a stronger tendency to form a stable complex with rGO. This can be attributed to the partially restored aromatic structure of rGO, which enables a stronger π-π interaction with the TAPP molecules. This section of the thesis demonstrates that the strength of the interaction between the porphyrin and GBM can be influenced not only by adjusting the structure of the porphyrin but also by modifying the GBM.

By conducting photoelectrochemical measurements on TAPP/GO, a comparison was made with other GO hybrids with cationic porphyrins. The acquired data strongly indicate the occurrence of photoinduced charge transfer in the studied nanohybrid material. However, in TAPP/GO, the efficiency of electron-hole separation is considerably lower compared to graphene oxide hybrids with cationic porphyrins such as TMPyP/GO and ZnTMPyP/GO.

5.4 Anionic porphyrins

The third group of meso-porphyrins that were investigated were anionic porphyrins represented by 5,10,15,20-tetra(4-sulfonatophenyl)porphyrin (TSPP). This research attempted to determine the interactions between this porphyrin and GO in ground-state with the ultimate goal of comparing its strength with the other groups of porphyrins, i.e., cationic (see: **5.2 Cationic porphyrins**) and neutral (see: **5.3 Neutral porphyrins**).

Since the anionic porphyrin molecules are negatively charged, electronic attraction can be excluded as a result of the type of interactions between porphyrin and graphene oxide. The interaction between porphyrin and GO can depend on of π-π stacking and van der Waals forces, which are much weaker than the columbic interaction.

Furthermore, apart from studying the interaction between TSPP monomers and GO, efforts have been made to fabricate TSPP nanostructures and utilize them for surface functionalization of GO. This approach was motivated by the literature report that well-organized porphyrin nanostructures often exhibit enhanced photocatalytic performance compared to their monomeric counterparts.[159] They are therefore promising candidates for photocatalysis, photovoltaics, and electronics applications where photoinduced electron transfer occurs. This is because porphyrin aggregates with clearly defined molecular arrangement exhibit superior charge separation properties than monomeric porphyrins. Accordingly, the self-assembly of porphyrins was demonstrated to be a powerful tool enabling the fabrication of nanostructured materials with tunable morphologies and properties.[159] Moreover, further exciton characterization of porphyrin self-assembly may serve for a better understanding of aggregates in photosynthetic organisms. In order to prepare nanohybrids of GO with aggregates of TSPP an attempt was made to prepare TSPP nanorods. The method used previously for TCPP was employed[159], namely: the acid-base neutralization-based surfactant-assisted self–assembly method. The method was modified by elongating the time between the acid-base neutralization process and the centrifugation. Thus, the nucleation time has been extended.

It has been demonstrated, that the growth of porphyrin nanoassemblies on an rGO surface improves the electronic interaction by shortening the interfacial distance between graphene and porphyrin,[160] thereby enhancing in the presence of rGO upon the photoexcitation of porphyrin nanoassemblies, which eventually generate a photocurrent.

Recently, Bera *et al.* demonstrated a composite one-dimensional (1D) nanostructure of 5,10,15,20-tetra(4-carboxyphenyl)porphyrin (TCPP) and rGO for to improve photoinduced charge separation.[161] They observed a very fast decay of TCPP NR in the TCPP NR/rGO composite due to the electron transfer process that enhances the photocurrent under visible light illumination. This study reveals that photoinduced charge separation of porphyrin nanorods occurs in the presence of rGO. Thus, the growth of porphyrin aggregates on the rGO surface is interesting for versatile applications.

5.4.1 TSPP

TSPP was selected for this study as a model of anionic meso-tetra phenyl substituted porphyrin. The molecular structure of TSPP is shown in ***Figure* 10** (**4.1 The compounds used in the doctoral dissertation**). The TSPP is a water-soluble porphyrin.[162] The porphyrin core is substituted with four phenyl sulfonate groups, which, under neutral conditions, bear a charge of -4. The presence of a negative charge plays a crucial role in the interaction with charged molecules or materials.[163] Moreover, sulfonic groups have electron withdrawing effects.[164] Modification of pH can change the total charge of the molecule (***Scheme* 13**). However, it should be kept in mind that it is known that this porphyrin tends to self-assemble at a pH lower than ~4.6 at 25°C and under ambient conditions.[137] In an aqueous solution, two or more chemical forms of TSPP may exist in equilibrium, depending on the pH of the solution. At lower pH, due to the protonation of the two pyrrole nitrogens of the ionic porphyrin the biprotonated form ($TSPP^{4-}H_2^{2+}$) predominates, while an increase in pH results in the conversion of the biprotonated form into the monomeric base form ($TSPP^{4-}$).[165] In the pH range of 1.0 – 4.6 TSPP porphyrin molecules exist as a binary ionic molecule (in some literature reports even up to 4.8).[166,167] The dual nature enables intermolecular attractions between the negative charges of the peripheral groups and the positively charged porphyrin cores and is responsible for the observed aggregation of TSPP at acidic pH. Therefore, only $TSPP^{4-}$ is suitable for studies of the interaction of monomeric porphyrin with GO.

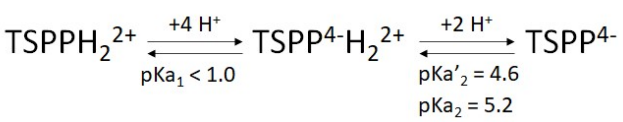

Scheme 13 *Ionic equilibria of TSPP porphyrin. pKa' values were taken from the literature*[162]

Most scientific reports on porphyrins and their complexes with graphene-based materials, i.e., GO or rGO, apply to cationic porphyrins.[50,79,80,108] If the report includes anionic porphyrin, it is focused on its 3D-structure form or aggregates[76,108,143], rather than on the monomeric form. This research examined the interaction between the monomeric form of TSPP and GO sheets. All experiments were carried out at a pH=7.0 to ensure that only the monomeric form was present. Spectroscopic methods (steady-state absorption and emission, time-resolved emission), and photoelectrochemical measurements (transient photocurrent and photovoltage) were used to analyze TSPP and its nanoassemblies with GO.

5.4.1. Steady-state absorption measurements

The absorption spectrum for free TSPP porphyrin in water, pH=7.0 was measured and presented in ***Figure* 86**. The UV-Vis spectrum exhibits peaks typical for the high symmetry (D_{2h}) porphyrin group. The main intense band at ca. 413 nm is the characteristic Soret band, whereas the four less intense bands at ca. 516 nm, 553 nm, 579 nm, and 634 nm are assigned as Q-bands. The Soret band has a weak shoulder at about 396 nm, corresponding to n→π transition of electrons in the core of the free base.[63,64] The absorption coefficient was determined spectroscopically using the Beer-Lambert relationship (see: **4.2 UV-Vis absorption measurements**) and is equal to 5.1×10^5 $M^{-1}cm^{-1}$ at $\lambda = 413$ nm.

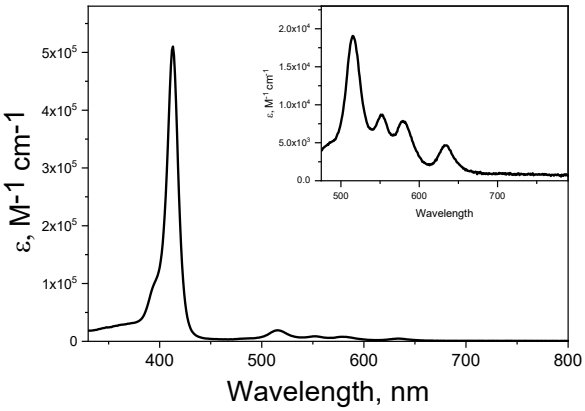

Figure 86 *Absorption spectrum of the aqueous solution of $TSPP^{4-}$, pH=7.0 (inset: Q-band region of the same spectrum)*

It is known that the presence of graphene-based materials can have a significant effect on the UV-Vis spectra of porphyrin.[73,80,95,133] UV−Vis spectroscopy was therefore used

to study the ground-state interaction between both components: GO and $TSPP^{4-}$ under pH 7.0 (***Figure* 87**).

The optical absorption spectra of the series $TSPP^{4-}$/GO nanohybrid suspension are shown in ***Figure* 87**. At first sight, there is no clear evidence of any interaction between the GO and $TSPP^{4-}$ molecules in the ground state (***Figure* 87**A). However, upon closer examination, it becomes evident that a weak interaction exists between these two chemical moieties, as indicated by the observed changes in UV-Vis absorption. With increasing concentration of GO, the intensity of the porphyrin Soret band at 413 nm decreases (the absorbance of the weak shoulder at about 396 nm also decreases) and a new band at ~435 nm appears (marked by an asterisk) (***Figure* 87**B). It can be seen that the Soret band of $TSPP^{4-}$/GO exhibited a red-shift (ca. 22 nm). This significant change in the position of the absorption band can be explained by the flattening of the porphyrin molecule driven by π-π stacking between the porphyrin moiety and the GO sheet.[73,74,80,157,158] Comparison of the literature data on the UV-Vis spectra of the TSPP aggregates suggest that adsorption of $TSPP^{4-}$ to GO occurs in the form of a monomer, no aggregates are formed. The B-bands attributed to H-aggregates of $TSPP^{4-}$ are known to be much more redshifted (peaks occur at 422 nm and 490 nm).[168] An isosbestic point was also observed at 420 nm. However, the observed interaction between porphyrin molecules and GO is rather weak. This is confirmed by the fact that despite the addition of a large amount of GO (final GO concentration: 48 μg mL^{-1}), free porphyrin still remains in an equilibrium with porphyrin adsorbed on the surface of GO.

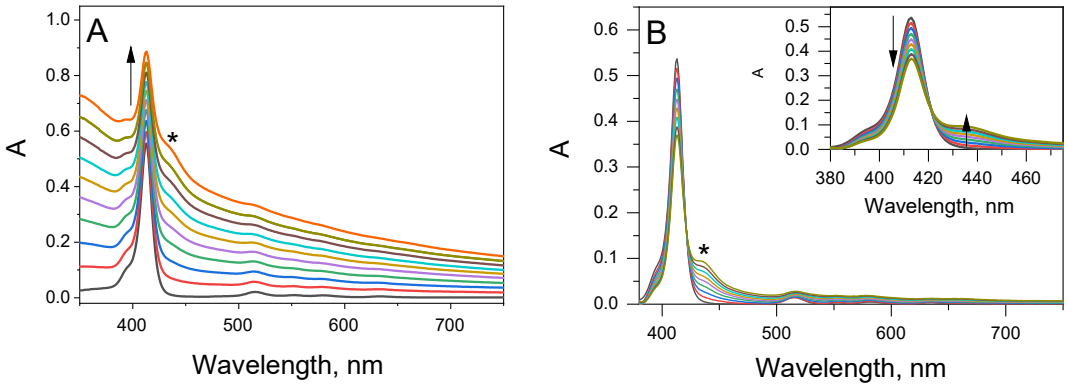

Figure 87 *Absorption spectra recorded during the process of titration of 3 mL of 1.7 μM aqueous solution of $TSPP^{4-}$ (pH=7.0) with 5.1 mg mL^{-1} of GO dispersion (0 – 48 μg mL^{-1}) A) uncorrected and B) corrected for the GO absorption. The inset shows the same spectra presented only in the Soret band region*

5.4.1.2 Steady-state and time-resolved emission

The interaction of the excited state of $TSPP^{4-}$ with the GO sheets was investigated by emission spectroscopy. Fluorescence measurements require matching of the absorbances at the excitation wavelength. Excitation at the isosbestic point, that is, 420 nm, ensured constant absorbance.

The fluorescence emission spectra of the investigated samples are shown in ***Figure* 88**. Upon excitation at 420 nm in the absence of GO (black line), $TSPP^{4-}$ exhibited a broad fluorescence band in the range of 625 to 750 nm. As expected, $TSPP^{4-}$ emission spectra of the monomeric form of porphyrin were observed with the Q(0,0) and Q(0,1) bands at 644 nm and ca. 702 nm. The peak ratio (644 to 702 nm) is equal to 2.5 and was kept constant throughout the titration with the GO experiment. The measured fluorescence quantum yield equals to 0.062, which is in agreement with the values reported in the literature.[166]

As shown in ***Figure 88***A, the addition of GO causes fluorescence quenching. With a concentration of GO equals to 0.01 mg mL^{-1}, the intensity of porphyrin fluorescence was reduced by a half. The most interesting observation from the steady-state emission experiment was that the Stern-Volmer plot I_0/I *versus* the concentration of the graphene oxide was not linear. It can be seen that the experimental data could be better fitted if two concentration regimes were taken into account. For the regime with a lower concentration

of GO, the rate of fluorescence quenching was estimated to be approximately 137.5 mg^{-1} mL.

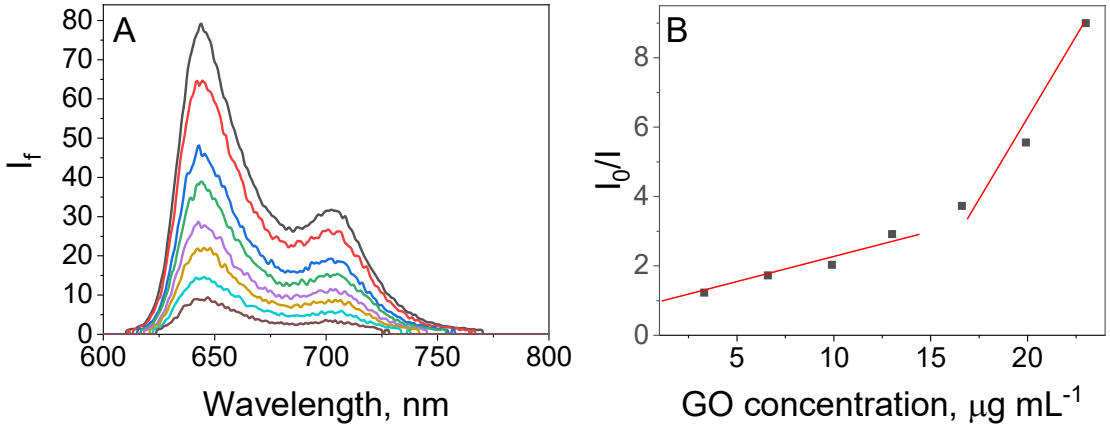

Figure 88 *A) Quenching of the fluorescence of 0.2 μM $TSPP^{4-}$ in water recorded during the addition of an aqueous suspension of 0.14 mg mL^{-1} GO (concentration of GO in solution 0- 23 μg mL^{-1}), λ_{ex}= 420 nm; B) Relationship between fluorescence intensity I_0/I ($I_0 - I_f$ without GO, $I - I_f$ after the addition of GO) and GO concentration for $TSPP^{4-}$*

The fluorescence spectrum of $TSPP^{4-}$ with a GO concentration of 23 μg mL^{-1} was normalized and compared to the fluorescence spectrum of $TSPP^{4-}$ in the absence of GO (***Figure* 89**). No changes in the spectrum shape, peaks ratio, or additional peaks were observed. Therefore is no evidence for the formation of an emissive $TSPP^{4-}$/GO nanohybrid. The results discussed demonstrate that the observed fluorescence in ***Figure* 89** originates solely from the free $TSPP^{4-}$ in the suspension. The possible explanation for the lack of measurable emission from the $TSPP^{4-}$/GO complex is the existence of a non-radiative process that leads to a very quick deactivation of the singlet excited state. The recorded decrease in the fluorescence intensity upon the addition of GO to the $TSPP^{4-}$ solution could be attributed to the dynamic or static quenching (***Figure* 88**A).

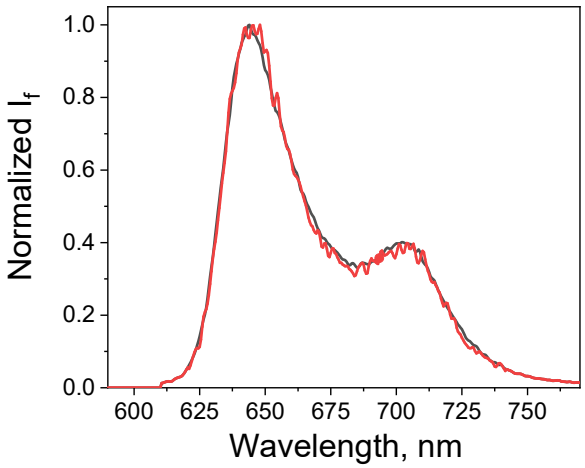

Figure 89 *Normalized steady-state fluorescence spectra of $TSPP^{4-}$ without the addition of GO (black) and with GO at concentration of 23 μg mL^{-1} (red)*

If dynamic quenching is taking place, a decrease in the observed fluorescence lifetime would be expected. Conversely, this phenomenon is not anticipated in the case of static quenching. (see: **4.3.1 Static and dynamic quenching**) The TCSPC technique was applied to determine which mechanism is responsible for the observed decrease of the fluorescence intensity upon the addition of GO. The emission decay profiles of $TSPP^{4-}$ were monitored in the absence and presence of varying concentrations of GO. The fluorescence lifetime evaluated from the emission decay in the absence of GO was equal to 9.9 ns (excitation at 440 nm and monitoring at 644 nm) (***Figure* 90**). After the addition of GO, no detectable change in the kinetic profiles of the excited state was recorded. One would normally have expected a shortening of the singlet excited state of unbound $TSPP^{4-}$ if the quenching was the result of a dynamic process induced by GO. There might also be a possibility to see the appearance of a second decay associated with any fluorescence of the nanohybrid. Neither of these decays was detected during the TCSPC experiment. ***Figure* 91** presents a comparison of the data obtained from steady-state and time-resolved emission measurements. With the increase of the GO concentration up to 23 μg mL^{-1}, increases the I_0/I (I_0 - I_f without GO, I - I_f after the addition of GO). The relationship between fluorescence lifetime and GO concentration remains unchanged. On the basis of the above time-resolved emission experiments, the possibility of dynamic quenching of the singlet excited state of free $TSPP^{4-}$ by GO can be excluded.

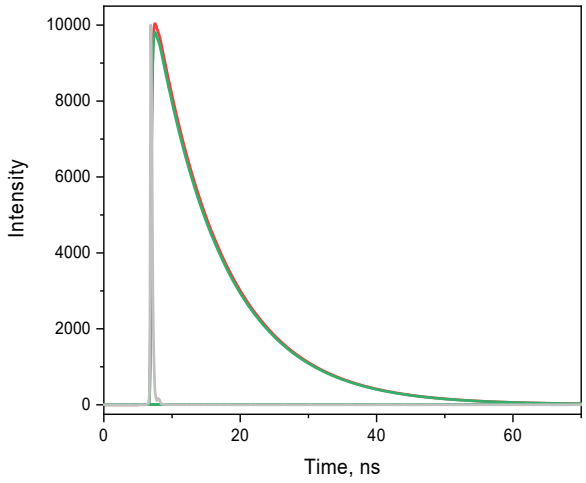

Figure 90 *Decay of the fluorescence of $TSPP^{4-}$ (0.3 μM) in water (pH=7.0) recorded in the absence (red) and presence (green) of GO, prompt (grey); λ_{ex} = 420 nm, λ_{em} = 644 nm*

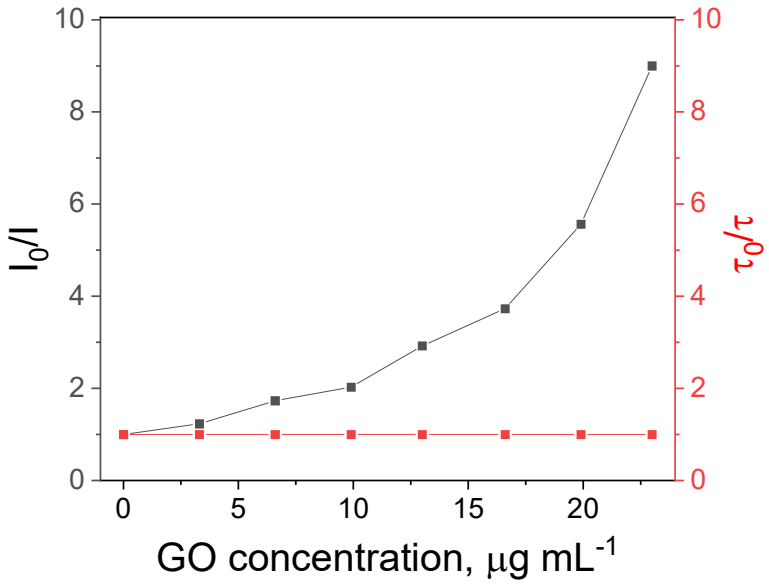

Figure 91 *Relationship between fluorescence intensity I_0/I (I_0 - I_f without GO, I - I_f after addition of GO) and GO concentration for $TSPP^{4-}$ (black) and the relationship between fluorescence lifetime τ_0/τ (τ_0 - fluorescence lifetime without GO, τ - fluorescence lifetime after addition of GO) and GO concentration for $TSPP^{4-}$ (red)*

The lack of measurable emission from the $TSPP^{4-}$/GO complex indicates that there is a possibility of a very rapid deactivation process of the excited state, such as an electron or energy transfer. This process could be responsible for the quenching of the singlet

excited state ($^1S^*$) of porphyrin in the $TSPP^{4-}/^4GO$ complex. The free energy of ET was calculated to probe the possibility of ET from the singlet excited state ($^1S^*$) of the porphyrin to GO. For this purpose, the Rehm-Weller equation was applied. The data used for the calculations of free energy of the ET process were summarized in ***Table* 15**. The conduction band edge of GO was found to be equal to -0.55 V vs. NHE.[130] Using values from ***Table* 15**, the free energy of the electron transfer from the singlet excited state of TSPP to GO was estimated to be -0.355 eV. The negative value of the free energy of ET for TSPP indicates that photoinduced electron transfer could occur in the $TSPP^{4-}$/GO system.

Table 15 *Zero-zero transitions of the singlet excited state of TSPP, its oxidation potential, and the driving force of the electron transfer reaction values*

Porphyrin	$E_{0\text{-}0}$ (eV)	E_{ox} (V vs. NHE)[100,169]	E^*_{ox} (V vs. NHE)	ΔG_{ET} (eV)
TSPP	2.03	1.34	-0.69	-0.355

Based on the negligible overlap of the emission spectra of $TSPP^{4-}$ with the absorption spectra of graphene oxide (***Figure* 92**), energy transfer between the donor-acceptor compound of the TSPP/GO hybrid is highly unlikely.

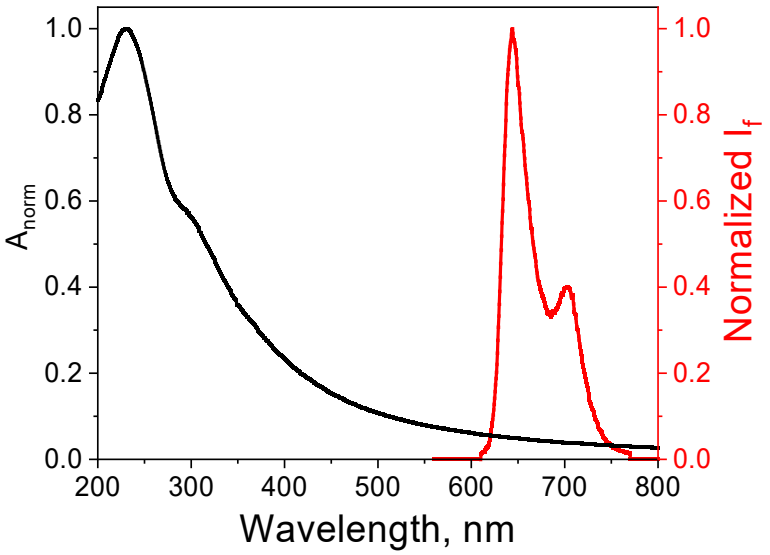

Figure 92 *The overlap of the $TSPP^{4-}$ emission spectrum (red) with the graphene oxide absorption spectrum (black)*

5.4.1.3 Photoelectrochemical measurements

The experimental support for the photoinduced charge separation mechanism comes from photocurrent measurements. ***Figure* 93** shows the photoelectric response of the SnO_2-FTO electrode covered with GO or $TSPP^{4-}$/GO films. The irradiation was switched on and off in 30-second periods to measure the light and dark current responses. It can be seen that the photocurrent response of the GO film was relatively small. However, an obvious photocurrent response was observed for the electrode covered with $TSPP^{4-}$/GO under similar experimental conditions. This increase in photocurrent provides evidence for the photo-induced charge transfer in the studied materials. The produced photocurrent was not constant and decreased nearly in half during those 30 seconds of illumination. However, it was repeatable in three irradiation cycles.

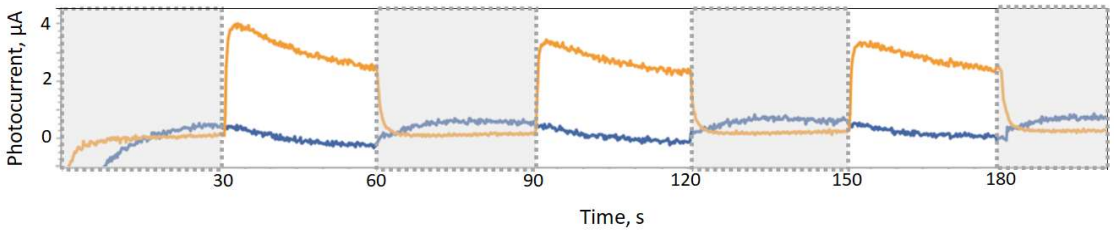

Figure 93 *Transient photocurrent in time for TSPP/GO under white light illumination (electrolyte: 0.1 M LiI in acetonitrile). The blue line shows the photocurrent generated by GO alone*

The photovoltage response is shown in ***Figure* 94**. The build-up of the photovoltage is rather slow and attains a steady state in about 100 s. The decay of the photovoltage upon stopping the illumination shows the small loss of accumulated electrons in the recombination with the redox couple. Such losses have been reported earlier in photovoltage measurement for FTO/rGO/TMPyP as a working electrode and for photoelectrochemical cells employing the nanostructured semiconductor films.[80,170,171]

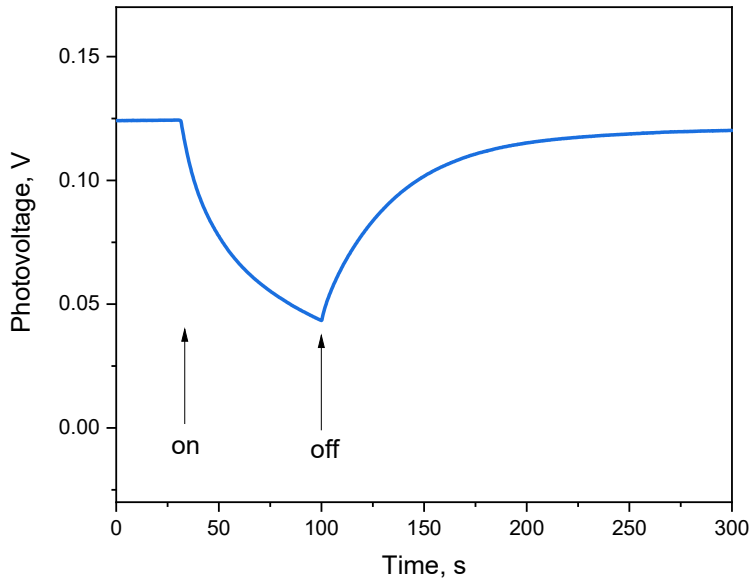

Figure 94 *Photovoltage response SnO_2-FTO electrode covered with TSPP/GO film under white light illumination (electrolyte: 0.5 LiI in a can)*

5.4.1.4 Nanostructures of TSPP

J-aggregated porphyrin molecules offer a promising approach in the development of light-harvesting systems due to their ability to mimic natural light-harvesting systems.[172,173] Hasobe *et al.* have reviewed the supramolecular architecture of porphyrin with changing size and shape for solar energy conversion.[148] Emerging research has highlighted the significant impact of porphyrin nanoaggregate shapes, such as spheres, rods, flakes, and flowers, on photocatalytic properties.[85] Rod-shaped assemblies of TCPP porphyrin exhibit 81% photocatalytic activity (calculated degradation rate of RhB) due to stronger intermolecular π–π interactions which act as a photosemiconductor due to coherent electronic delocalization and facilitate the electron transfer process.[85] Therefore, considerable research efforts have been recently directed toward graphene–porphyrin nanoassembly hybrid materials for light-harvesting.[2,40,76,144]

In the preceding paragraphs, the discussion focused on the $TSPP^{4-}$/GO hybrid, featuring porphyrin in the form of monomers. However, the utilization of well-defined organic structures of porphyrin holds great promise for applications such as photocatalysis, photovoltaics, and electronics, where photoinduced electron transfer plays a crucial role. Therefore, the investigation into the possible formation of functionalized GO with nanostructured TSPP was undertaken.

The overall charge and its localization influence the possibility of aggregation of the TSPP porphyrin. The TSPP has a binary ionic nature that enables intermolecular attraction between the negative charges of the peripheral groups and the positively charged porphyrin cores. Therefore, TSPP tends to self-assemble at lower pH.[174] At a pH lower than 4.6 the TSPP exist in the $TSPP^{4-}H_2^{2+}$ form (***Scheme* 13**). Due to protonation at low pH (that is, at pH < 4.6) the symmetry of the porphyrin increases to D_{4h} and is manifested through a dramatically changed absorption pattern, which shows that the Soret band is bathochromically shifted.

In general, porphyrins can form two types of aggregates: J-type (edge-to-edge arrangement) and H-type (face-to-face arrangement)[167] (***Figure* 95**). According to Kasha's exciton theory, J-aggregates are formed when the transition dipole moments of the monomer molecules are aligned parallel to the line that joins the molecular centers in the aggregate ('head-to-tail'). By contrast, in the case of H-aggregates, the transition dipole moments of the monomer molecules are perpendicular to the line of centres of the molecules.[175] The aggregation occurs during the self-assemble porphyrins nanostructure formation, which results in a shift of their corresponding UV-Vis and fluorescence spectrum.[167] It is generally accepted that a red-shift in the electronic absorption spectra relative to that of the monomer is attributed to the formation of J-aggregate, whereas a blue shift is observed for H-aggregates.

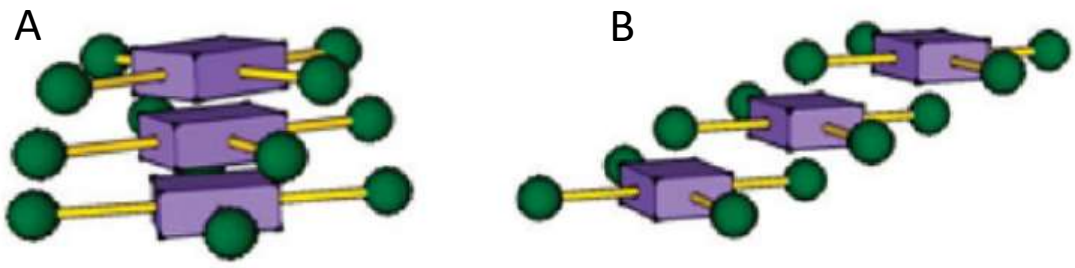

***Figure 95** Structural models for (a) H-type and (b) J-type aggregates*[167]

While the literature predominantly focuses on reporting J-aggregates in carbocyanine dye family molecules[176–178], there is also a substantial amount of research dedicated to exploring the water-soluble ionic TSPP.[149,174,179] The aggregation of TSPP can be induced by decreasing the pH or increasing the ionic strength of the solution, which can be effectively monitored by observing the variations in absorption peaks

corresponding to different species. Under certain conditions, which involve very acidic media and high ionic strength, TSPP has been shown to form highly ordered molecular aggregates.[166] It has been found that the counterion of inorganic salts, surfactant assemblies, microemulsions, metal ions, proteins, polypeptides, dendrimers, nucleic acids, cyclodextrins and myoglobin could promote TSPP aggregation in an acidic medium.

To fabricate nanohybrids of GO with TSPP aggregates, an initial step involved the synthesis and characterization of TSPP nanorods. The acid-base neutralization-based surfactant-assisted self-assembly method was used. The method was adapted from the previously reported synthesis of TCPP nanostructures.[159] Nevertheless, the modification involved elongating the duration between the acid-base neutralization process and centrifugation, thereby extending the nucleation time. In brief, the 4 mg of TSPP powder was dissolved in 0.5 mL of NaOH water solution (0.2 M). In the alkaline solution, porphyrin molecules form an anion $TSPP^{4-}$ (**Błąd! Nie można odnaleźć źródła odwołania.**), forming a homogeneous red solution. Subsequently, the $TSPP^{4-}$ solution was rapidly added to the previously prepared cetrimonium bromide (CTAB) solution, which is a cationic surfactant (0.036 g in 9.5 mL of water with the addition of 0.085 mL of conc. hydrochloric acid). An immediate colour change was observed. Subsequently, the solution was stirred vigorously for 25 minutes and then centrifuged (10000 rpm, 10 min). The sediment was washed with water and centrifuged once again (10000 rpm, 10 min) (**Błąd! Nie można odnaleźć źródła odwołania.**). Detailed synthesis conditions for each batch are summarized in ***Table* 16**.

A useful method for determining the morphology of the obtained structure was transmission electron microscopy. The TEM images were taken after each synthesis batch. Samples for TEM measurements were prepared by adding the minimum amount of water to the precipitate after a second centrifugation, without prior drying.

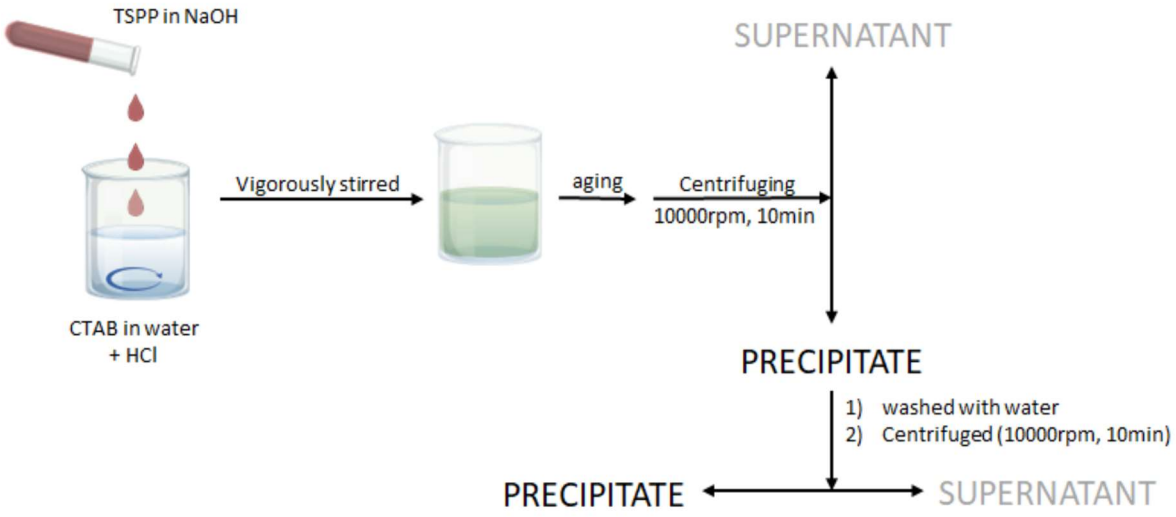

Scheme 14 *Schematic illustration of the acid-base neutralization-based surfactant-assisted self-assembly method for the TSPP nanorod synthesis process*

Table 16 *Detailed synthesis conditions for each sample of TSPP nanostructures*

Sample	pH	Stirring time (minutes)	Ageing time (hours)	TEM Figure
1	7.0	10	19	***Figure* 96**
2	7.0	60	19	***Figure* 97**
3	7.0	90	19	***Figure* 98**

In all three cases, the final pH after mixing TSPP solution with CTAB solutions was 7.0. Their synthesis process differs in stirring time, which was 10, 60 or 90 minutes (***Table* 16**). TEM analysis confirmed that the nanostructures obtained using the procedure described in sample 1 were rod-shaped (see: ***Figure* 96**). However, these rod-shaped structures exhibited a tendency to cluster together. Prolonging the stirring time to 60 minutes led to the formation of extensive flat structures (***Figure* 97**). After 90 minutes of stirring, the structures were short and dense (***Figure* 98**).

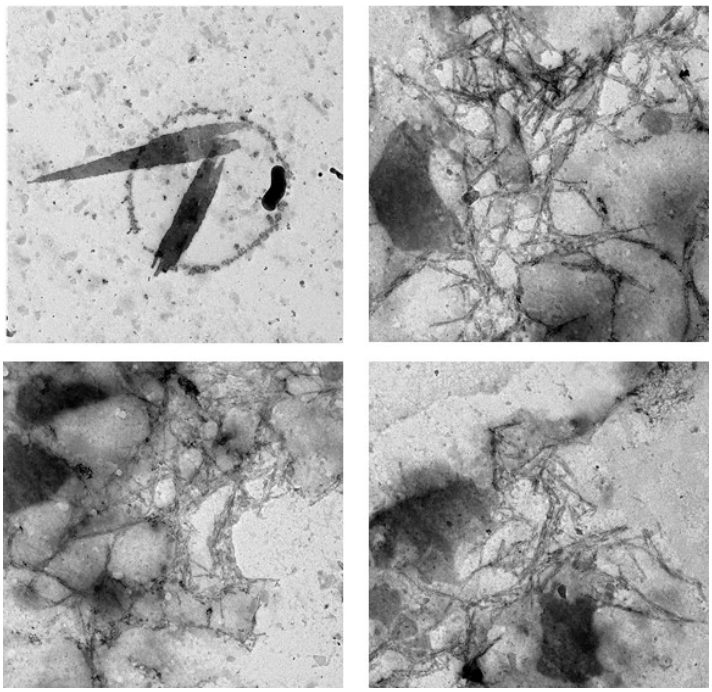

Figure 96 *TEM images of sample 1*

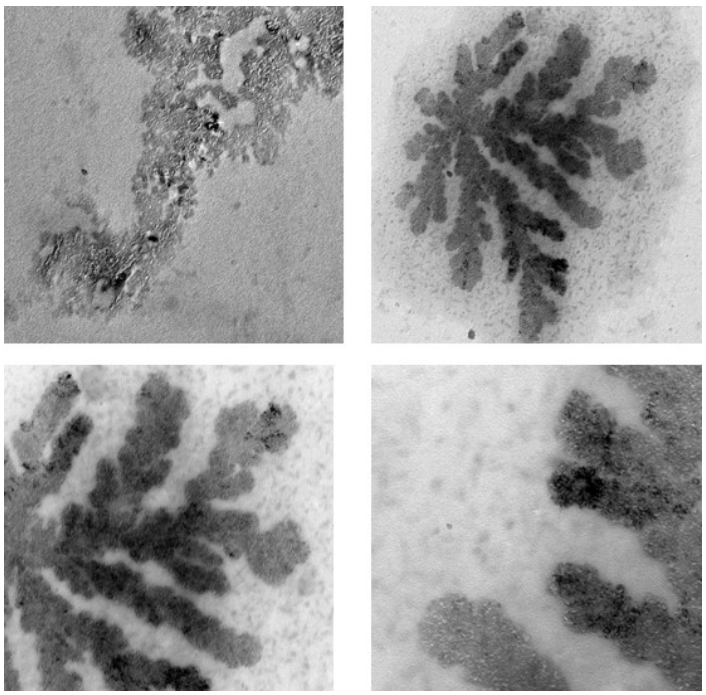

Figure 97 *TEM images of sample 2*

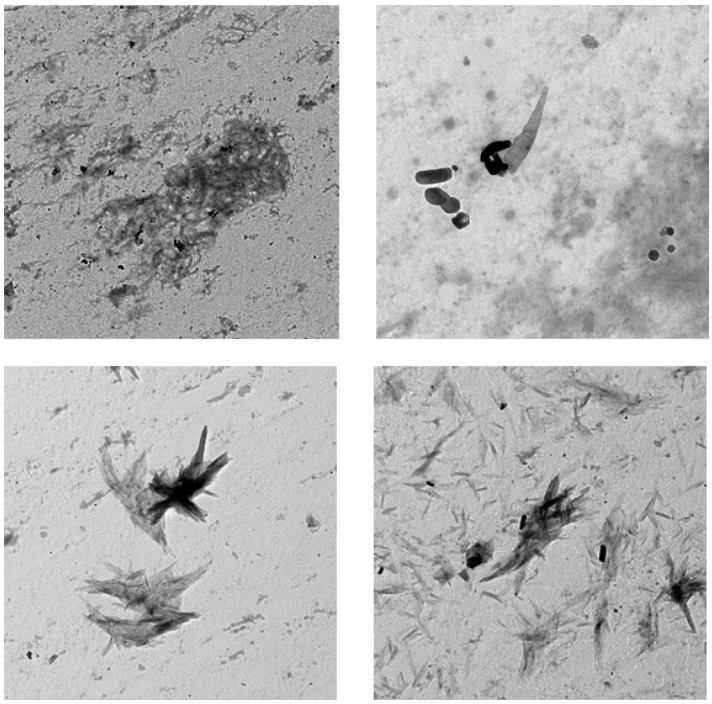

Figure 98 *TEM images of sample 3*

With no doubt, the longest and most rod-shaped structures were obtained when the stirring time was 10 minutes and the sample was left overnight before centrifugation. The experiment was repeated to verify the method's repeatability. ***Figure* 99** shows the TEM images of the structures obtained in two independent batches of synthesis (the same pH, and stirring time). It can be observed that the TSPP structures obtained from the first process are much longer. Therefore, the method and process conditions were re-examined. The variations in the lengths of the obtained nanostructures may be attributed to temperature differences among individual synthesis batches. To check the influence of temperature, the process was repeated for three different temperatures: 4°C, 22°C and 50°C. Temperatures were maintained throughout the ageing process. The TEM images of the structures obtained under these three temperature conditions are presented in ***Figure* 100**A-***Figure* 102**A. In all three cases, the formation of structures were observed. However, at lower temperatures, these structures appeared shorter and less regular. The structures obtained in the individual batches were repetitive, which is confirmed by the UV-Vis spectra (***Figure* 100**B- ***Figure* 102**B). TEM images of TSPP structures (sample 1 procedure) obtained at 50 °C showed formation of a rod-shaped structures. The average length of the structures is about 250-300 nm (up to 500 nm) with a diameter of about 35 nm.

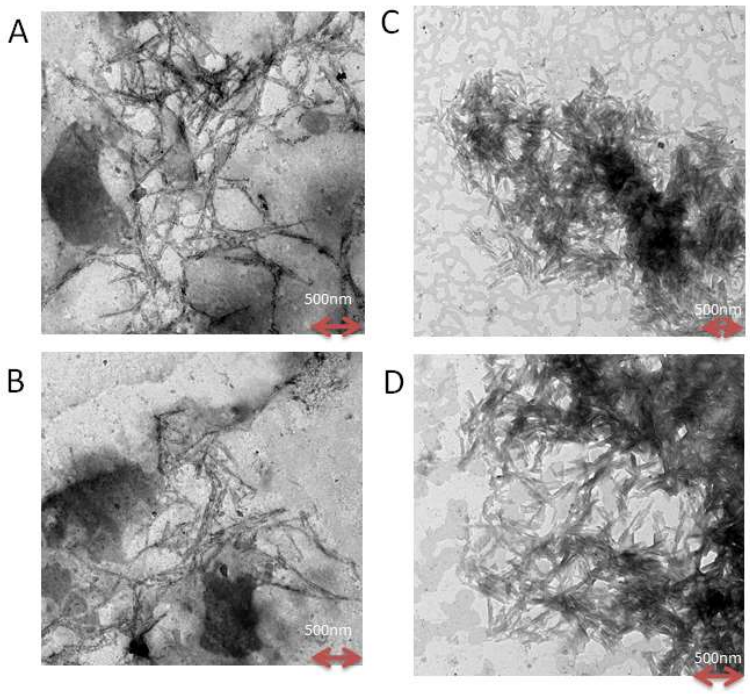

Figure 99 *TEM images of rod-shaped structures of TSPP obtained in two separate synthesis processes (sample 1 conditions; pH=7.0, stirring time: 10 minutes, sample was left over the night after centrifuging): A,B) first batch and C,D) second batch*

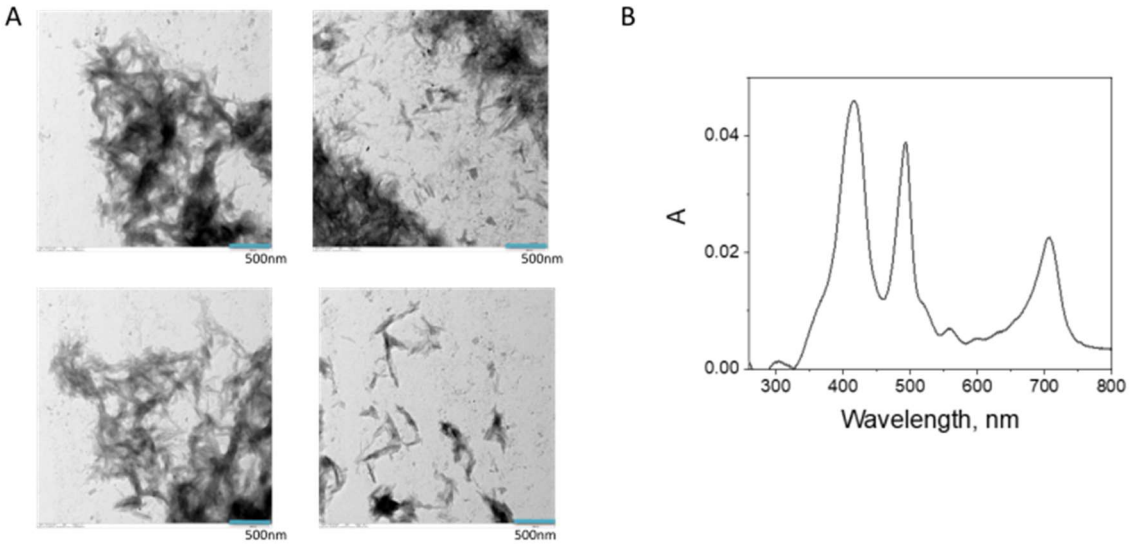

Figure 100 *A) TEM images of the TSPP nanostructures synthesized under temperature conditions: 4°C and B) the UV-Vis spectrum of their solution in THF*

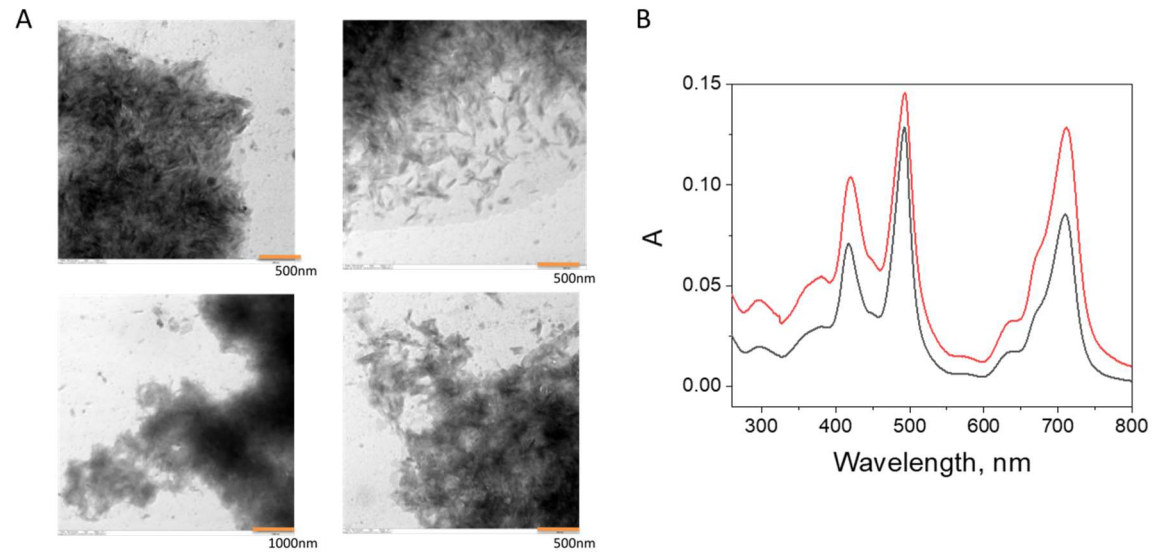

Figure 101 *A) TEM images of TSPP nanostructures synthesized under temperature conditions: 22°C and B) UV-Vis spectra of two independent prepared samples in THF*

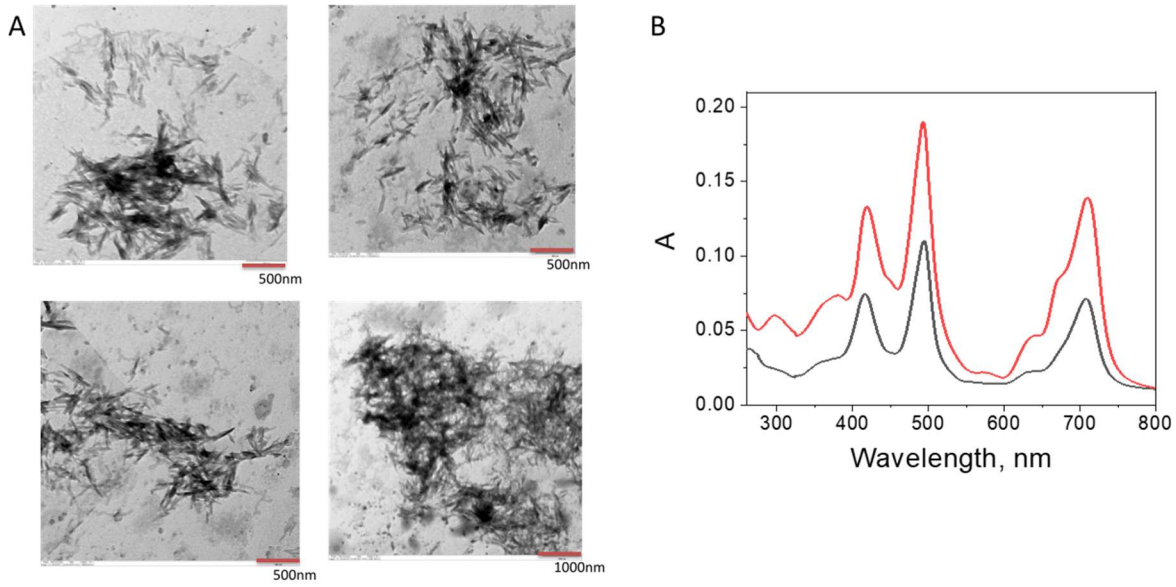

Figure 102 *A) TEM images of TSPP nanostructures synthesized under temperature conditions: 50°C and B) UV-Vis spectra of two independently prepared samples in THF*

***Figure* 103** shows the absorption spectra of the obtained TSPP nanostructures in THF. It has two strong bands in the Soret region at 420 and 493 nm which is in agreement with previous reports for TSPP nanostructures.[174] The 421 nm transition is due to the non-aggregated porphyrin and the red-shifted maximum (at 493 nm) is due to the presence of aggregated form. A red-shift in the electronic absorption spectra relatively to that of the monomer is a proof of J-aggregate. The head-to-tail alignment might be typical

molecular arrangements for the structure defining a J-aggregate leading to a red-shifted absorption band. In addition, a very intense band above 700 nm is observed. The UV-Vis spectra of the TSPP nanostructures in THF do not change after 1 h pointing to the stability of the nanostructures in THF.

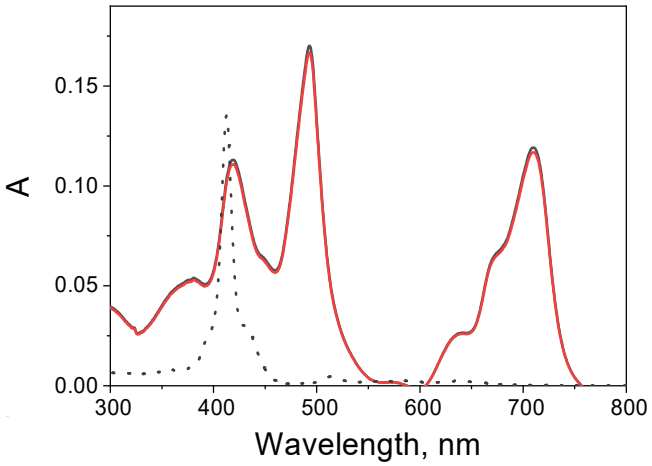

Figure 103 *Absorption spectra of obtained TSPP nanostructures in THF. The red lines show the spectra recorded after 1 hour and the dotted line shows the absorption spectrum of the molecular form* $TSPP^{4-}$ *for comparison*

To check the possibility of depositing the obtained TSPP nanostructures on the surface of GO, a titration process was carried out. The 3 mL of THF solution of the obtained TSPP structures placed in a quartz cuvette with a 10 mm light path was titrated with 0.2 mg mL^{-1} of GO solution in THF. In ***Figure* 104** are shown the optical absorption spectra recorded during the titration process. The intensity of the band at 420 nm increased with a simultaneous decrease in the intensity of the band at 493 nm. The positions of B-bands agree with the literature of the TSPP monomer.[168] The intensity of the band above 700 nm also decreased. It can be concluded that the addition of GO to the porphyrin-structure solution causes the destabilization of TSPP structures.

Taking the above into consideration further research on the assemblies of TSPP nanostructures with GO was not continued.

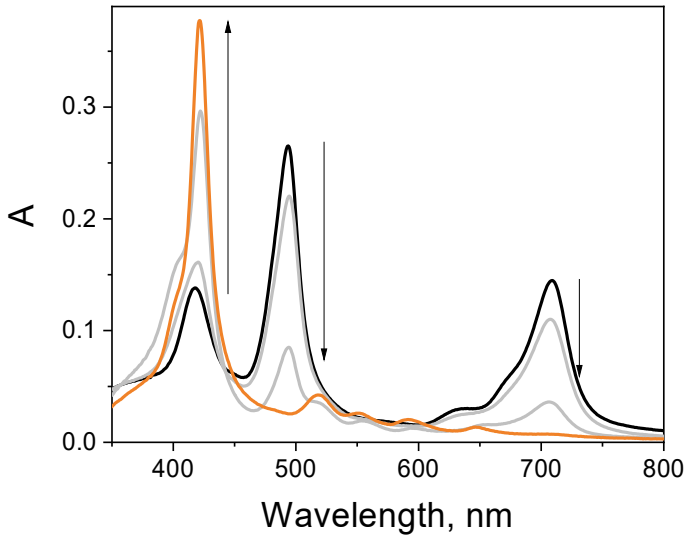

Figure 104 *Absorption spectra recorded during the titration process of 3 mL of THF solution of TSPP-structures with 0.2 mg mL^{-1} of GO dispersion in THF (0 – 8 µg mL^{-1}) uncorrected for the GO absorption*

5.4.1.5 Summary

The TSPP porphyrin, in its $TSPP^{4-}$ form, was chosen as a representative model of anionic meso-tetra phenyl substituted porphyrin for the purpose of later comparison with other porphyrin groups (such as cationic and anionic). Its interaction with GO was investigated by steady-state absorption and emission (both steady-state and time-resolved). The measurements carried out indicate that the interaction between $TSPP^{4-}$ and GO is largely suppressed in comparison to neutral and cationic porphyrin. The interaction of the excited state of $TSPP^{4-}$ with the GO sheets was investigated by emission spectroscopy. The addition of GO causes fluorescence quenching which was attributed to the static mechanism. They are characterized by different quenching rates. Moreover, experimental support for the photoinduced charge separation mechanism comes from complementary photocurrent measurements. The increase in the photocurrent provides evidence for the photo-induced charge transfer in the studied materials.

In an effort to prepare nanohybrids of GO with TSPP aggregates, a synthesis and characterization process for TSPP nanorods was pursued using an acid-base neutralization-based surfactant-assisted self-assembly method. The thermal conditions of the synthesis were refined and rod-shaped structures were obtained. The average length of these structures ranged from approximately 250-300 nm (up to 500 nm) with a diameter

of about 35 nm. Unfortunately, the addition of GO to the porphyrin-structure solution causes destabilization of TSPP structures which resulted in the restoration of the TSPP in the monomeric form.

6. Conclusive summary

In this doctoral thesis, seven newly developed nanohybrids were investigated: $TMPyP^{4+}$/GO, $ZnTMPyP^{4+}$/GO, $TMAP^{4+}$/GO, $TMAP^{6+}$/GO, TAPP/GO, TAPP/rGO, and $TSPP^{4-}$/GO. These nanohybrids were carefully synthesized and characterized. The synthesis process involved combining a solution of the porphyrin with a suspension of graphene-based materials (either GO or rGO). To gain a deeper understanding of the structure-property relationship, each nanohybrid underwent a thorough and comprehensive characterization, primarily focusing on spectroscopic analysis. This approach allowed to investigate and elucidate the intricate relationship between the porphyrin structure and its corresponding nanohybrid with GBM properties. This characterization provided valuable insights into how the structural features of porphyrin influenced the strength of the interaction with GBM. This work paved the way for a more comprehensive understanding of porphyrin/GBM hybrids properties and potential applications.

Below, a concise summary of the key findings from this thesis is provided.

First of all during the titration process, in all cases, the intensity of the original Soret bands in the UV-Vis spectra gradually decreased. Additionally, new red-shifted Soret bands emerged, indicating significant changes in the electronic structure of the porphyrin upon adsorption on the GBM.

The positions of the Soret bands, along with their corresponding molar absorption coefficients, as well as the values of their shifts and the positions of the isosbestic points, were collected in ***Table* 17.** These observed shifts in the absorption band positions are noteworthy and can be attributed to the flattening of the porphyrin molecules, induced by the π-π stacking interactions between the porphyrin moiety and the GO/rGO sheets. The smallest change in the position of the Soret band (6 nm) was observed for $TMAP^{6+}$, which may be related to the large substituent hindering flattening.

Table 17 *Summary of the absorption properties of $TMPyP^{4+}$, $ZnTMPyP^{4+}$, $TMAP^{4+}$ $TMAP^{6+}$, TAPP and $TSPP^{4-}$ in water as a free molecule and adsorbed on the surface of GBM (GO or rGO)*

Porfiryna	GBM	Free porphyrin molecule		Adsorbed on GBM		Shift of Soret (nm)	Isosbestic point (nm)
		λ_{max} (nm)	ε (M^{-1} cm^{-1})	λ_{max} (nm)	ε [2] (M^{-1} cm^{-1})		
$TMPyP^{4+}$	GO	422	2.0×10^5	440	1.2×10^5	18	434
$ZnTMPyP^{4+}$	GO	437	1.2×10^5	453	0.8×10^5	16	447
$TMAP^{4+}$	GO	411	3.7×10^5	421	1.9×10^5	10	416
$TMAP^{6+}$	GO	431	3.8×10^5	436	-	6	-
TAPP [1]	GO	424	0.85×10^5	456	0.37×10^5	32	437
	rGO			451	0.37×10^5	27	439
$TSPP^{4-}$	GO	413	5.1×10^5	435	-	22	420

1- ethanol-water (1:2 v/v) solution; 2- were determined assuming that 100% of the porphyrin bound to GO

On the basis of the spectral results described above, it is reasonable to conclude that the adsorption of the porphyrins on the GBM sheets causes significant changes in the electronic structure of these porphyrins.

Photoluminescence spectroscopy serves as a valuable tool for investigating the electronic interactions occurring between porphyrin molecules in their singlet excited states and GO sheets. In order to conduct comparative emission studies, that the excitation wavelengths matched the absorbance of the samples were ensured. To maintain a consistent absorbance at the excitation wavelengths during emission measurements, the solutions of porphyrins and nanohybrids were excited at the isosbestic points, as documented in ***Table*** **17**.

An increase in the amount of GO in the sample results in a decrease in the fluorescence intensity of the porphyrin. To quantify this effect, the GO concentration required to decrease the emission intensity by 50% was determined and recorded in ***Table*** **18**.

This data provides insights into the quenching behaviour of the porphyrin fluorescence as a function of GO concentration.

Table 18 *The GBM (GO or rGO) concentration required to quench 50% of the intensity of porphyrin emission in the investigated nanohybrids*

Nanohybrid	GBM	Concentration of GO (μg mL^{-1})
$TMPyP^{4+}$	GO	0.42
$ZnTMPyP^{4+}$		0.19
$TMAP^{4+}$		0.30
$TMAP^{6+}$		1.50
TAPP		3.68
TAPP	rGO	0.75
$TSPP^{4-}$	GO	10.00

Among the porphyrins ($TMPyP^{4+}$, $ZnTMPyP^{4+}$, $TMAP^{4+}$), the concentrations required to induce fluorescence quenching were found to be the lowest for cationic porphyrins ($TMPyP^{4+}$, $ZnTMPyP^{4+}$, $TMAP^{4+}$). However, an exception to this trend was observed with the porphyrin $TMAP^{6+}$, which exhibited a relatively higher concentration for achieving the same quenching effect. The concentrations of GO necessary to quench 50% of the emission intensity for the neutral (TAPP) and anionic ($TSPP^{4-}$) porphyrins were found to be significantly higher compared to the cationic porphyrins. Specifically, in comparison to ZnTMPyP4+, the concentrations of GO required for quenching were 50 times higher for the neutral porphyrin and 19 times higher for the anionic porphyrin. The interaction between TAPP and rGO was found to be stronger than the interaction between TAPP and GO. Based on the above data, it can be concluded that the strength of the porphyrin emission quenching by GO increases follows the order: $ZnTMPyP^{4+}$ > $TMAP^{4+}$ > $TMPyP^{4+}$ > $TMAP^{6+}$ >TAPP > $TSPP^{4-}$.

***Table* 19** shows the fluorescence lifetime of the porphyrins along with the excitation and detection wavelength. Interestingly no change in the fluorescence decay kinetics of porphyrins was observed with increasing GO concentration or rGO. The lack of a detectable change in the fluorescence lifetime of the free porphyrins excludes

dynamic quenching of the singlet excited state of porphyrins within investigated nanohybrids.

Table 19 *fluorescence time (together with excitation and detection wavelength for investigated porphyrins ($TMPyP^{4+}$, $ZnTMPyP^{4+}$, $TMAP^{4+}$ $TMAP^{6+}$, TAPP and $TSPP^{4-}$)*

Porphyrin	fluorescence lifetime (ns)	λ_{ex} (nm)	λ_{det} (nm)
$TMPyP^{4+}$	5.7	440	693
$ZnTMPyP^{4+}$	1.3	440	650
$TMAP^{4+}$	9.8	405	660
$TMAP^{6+}$	2.7	440	660
TAPP	5.7	440	672
$TSPP^{4-}$	9.9	440	644

The comprehensive steady-state absorption and emission data analysis allowed to conclude that the metalation of TMPyP with Zn(II) increased the binding ability of the porphyrin to the GO surface. The porphyrin content in the $ZnTMPyP^{4+}$/GO (4.9%) is higher compared to $TMPyP^{4+}$/GO (3.7%). Photocurrent measurements and femtosecond TA spectroscopy provided evidence for ET occurring in the hybrid materials ($ZnTMPyP^{4+}$/GO and $TMPyP^{4+}$/GO) (see: **5.2.1.3 Femtosecond TA Spectroscopy** and **5.2.1.4 Photoelectrochemical measurements**). Both hybrid materials, $TMPyP^{4+}$/GO and $ZnTMPyP^{4+}$/GO, demonstrated higher photocatalytic activity toward RhB degradation as compared to GO alone (see: **5.2.1.5 Photocatalytic activity towards RhB degradation**); however, $ZnTMPyP^{4+}$/GO exhibited significantly more efficient performance. The data obtained indicate that the presence of Zn in the porphyrin core can promote charge separation in the $ZnTMPyP^{4+}$/ GO compounds. The higher degradation rate seen with $ZnTMPyP^{4+}$/GO as compared to the $TMPyP^{4+}$/GO assemblies highlights the beneficial role of Zn(II)-metalation of the porphyrin ring.

Conducted measurements allow also to establish the effect of the pH on the formation of the hybrid material. It has been proven that stronger interaction with GO occurs for $TMAP^{4+}$ than for $TMAP^{6+}$ where it is largely suppressed. This can be rationalized in terms of: a) a distortion of the planarity of the porphyrin macrocycle upon protonation, b) a decrease of the Columbic interaction due to protonation of the carboxylic groups

in GO, and c) aggregation of the GO under acidic conditions. The non-covalent functionalization of GO with cationic porphyrin at pH 6.2 was confirmed by FTIR, Raman spectroscopy, thermogravimetric analysis (TGA), atomic forces (AFM), and elemental analysis (see: **5.2.2.3 TMAP/GO nanohybrid characterization**). The nanohybrids were subjected to detailed spectroscopic characterization with several methods to probe the ground state as well as the excited state interaction between the components of the new material. It was found that the formation of $TMAP^{4+}$/GO hybrids changes the electronic structure of the porphyrin ground state, which was manifested among others by the shifts of the Soret band from 411 nm to 421 nm (***Table* 17**). Moreover, it was evidenced that the ground state interaction between $TMAP^{4+}$ and GO causes static quenching of the porphyrin emission (***Table* 18**). Surprisingly, fluorescence is not detected for the nanohybrid, indicating that a very fast deactivation process must take place. Ultrafast time-resolved transient absorption spectroscopy clearly demonstrates the occurrence of electron transfer from the photoexcited $TMAP^{4+}$ singlet state to GO sheets, as proven by the formation of a porphyrin radical cation. (see: **5.2.2.4 Femtosecond TA Spectroscopy**) These results are relevant to the use of such systems in developing energy conversion assemblies if undesired back electron transfer could be suppressed.

Also the effect of GBM oxidation level on the spectroscopic properties of the porphyrins was determined by comparing the TAPP/GO and TAPP/rGO properties. The conducted investigations revealed that both nanohybrids exhibit similar photophysical properties. However, TAPP/rGO exhibited a higher porphyrin content compared to that of TAPP/GO. These findings suggest that TAPP exhibits a stronger affinity for rGO. Theoretical calculations carried out also strongly support this conclusions. (see**:** **5.3.1.4 Theoretical Calculations**) The presence of both GO and rGO induces similar structural changes in the TAPP molecules. However, the binding energies calculated for TAPP to the GO and rGO systems were significantly lower for the latter graphene-based material. These results indicate that TAPP has a stronger tendency to form a stable complex with rGO. This can be attributed to the partially restored aromatic structure of rGO, which enables a stronger π-π interaction with the TAPP molecules. This section of the thesis demonstrates that the strength of the interaction between the porphyrin and GBM can be influenced not only by adjusting the structure of the porphyrin but also by modifying the GBM. During the photoelectrochemical

measurements of TAPP/GO, a comparative analysis was performed with other GO hybrids incorporating cationic porphyrins. The obtained data provided evidence for the presence of photoinduced charge transfer within the investigated nanohybrid material. However, it was observed that the efficiency of electron-hole separation in TAPP/GO was notably lower in comparison to graphene oxide hybrids containing cationic porphyrins, such as TMPyP/GO and ZnTMPyP/GO. Lastly, the measurements of the interaction of $TSPP^{4-}$ with GO indicate that this interaction is largely suppressed in comparison to neutral and cationic porphyrin. The addition of a much higher concentration of GO causes fluorescence quenching, which was attributed to the static mechanism (***Table* 18**). Experimental support for the photoinduced charge separation mechanism comes from complementary photocurrent measurements. The increase in the photocurrent provides evidence for the photo-induced charge transfer in the studied materials.

In an effort to prepare nanohybrids of GO with TSPP aggregates, a synthesis and characterization process for TSPP nanorods was pursued using an acid-base neutralization-based surfactant-assisted self-assembly method. The thermal conditions of the synthesis were refined and rod-shaped structures were obtained. The average length of these structures ranged from approximately 250-300 nm (up to 500 nm) with a diameter of about 35 nm. Regrettably, the addition of GO to the porphyrin-structure solution causes the destabilization of TSPP structures which resulted in the restoration of the TSPP in the monomeric form.

To summarize, very detailed research on porphyrin/GO nanohybrids allowed for a better understanding of the relationship between the porphyrin structure and the strength and nature of the interaction with GO. Time-resolved absorption spectroscopy allowed to observe photoinduced electron transfer, which can potentially be used in photovoltaics, artificial photosynthesis or photodegradation of pollutants. Thus results discussed in the thesis are relevant to the use of such systems in developing energy conversion assemblies.

7. Abstract

7.1 Abstract in English

The increasing demand for new safe functional materials with more effective, specific properties is expanding the horizons of current research worldwide. Graphene-based materials (GBM) have attracted interest because of their outstanding properties, such as large surface area, mechanical stability, and optical transmittance. The conjugated aromatic system has made these materials ideal candidates for use as charge carriers or promoters. Additionally, the oxidized structure of graphene, namely - graphene oxide (GO), which includes various oxygen-based functional groups opens up the possibilities for its functionalization with other materials or molecules. Unlike graphene, GO can form stable aqueous suspensions, which makes it more suitable for some applications e.g. water splitting or dye photodegradation.

One promising approach to functionalize GBM involves surface coverage with light-harvesting molecules capable of capturing photons from solar light especially in the UV-Vis region. Porphyrins are an excellent example of such molecules due to their high molar absorption coefficients in the visible region.

Bringing these two individual components, graphene-based material and porphyrin molecule, into new hybrid materials may lead to important synergies. The formation of the hybrid material can be achieved through the formation of covalent bonds between the components of the nanostructure or through non-covalent interactions (π-π, electrostatic, hydrogen bonding, van der Waals). In recent years, particular attention has been paid to porphyrin hybrids with GBM that rely on non-covalent interactions. This interest results from the ease with which they can be prepared and the high efficiency of this process.

The main aim of this doctoral dissertation was to synthesize a hybrid system that contains a graphene oxide or reduced graphene oxide and porphyrin molecule and to conduct a detailed spectroscopic analysis of their properties in terms of potential use for the photocatalytic degradation of organic dyes. The research included 1) photochemical and photophysical characterization of selected porphyrins or metalloporphyrins and their hybrids with graphene oxide (or its reduced form), 2) comparison of the spectroscopic properties between various newly obtained hybrid materials, and 3) investigation of the

possible phenomenon of photoinduced electron transfer from the exited porphyrin molecule to a graphene oxide sheet.

This dissertation allows to fully understand the non-covalent interaction of porphyrin-graphene oxide nanostructures. One of the key elements of this study were parameters, which control the strength of the interaction of the hybrids components. Therefore the main purposes of this doctoral dissertation are:

1. synthesis and characterization of novel nanohybrids based on GBM (GO and rGO) and porphyrins,

2. define a correlation between porphyrin structure (anionic, neutral, cationic and free-base vs metalated) and its interaction in the ground-state and excited state with GBM,

3. comparison of the spectroscopic properties of free porphyrins and porphyrins adsorbed on the surface of GBM,

4. determination of the effect of GBM oxidation level on the strength of the interaction with porphyrin and its spectroscopic properties following adsorption of the GBM sheet,

5. establishment of the effect of pH on the formation of the hybrid materials.

These scientific goals are discussed for different types of porphyrins: cationic, neutral, and anionic.

In this doctoral dissertation various research methods were used to determine the spectroscopic and photophysical properties of the hybrids materials including: steady-state absorption, time-resolved emission spectroscopy, nanosecond and femtosecond transient absorption spectroscopy, and photoelectrochemical measurements. In addition for characterization of the nanohybrid FTIR, Raman spectroscopy, thermogravimetric analysis (TGA), atomic force microscopy and elemental analysis were employed.

The part of the doctoral dissertation which concerns cationic porphyrins, includes two major directions. In the first part, two noncovalent porphyrin-graphene oxide nanohybrids were synthesized by mixing the solution of the cationic porphyrin 5,10,15,20-tetra(1-methyl-4-pyridino) porphyrin tetra(p-toluenesulfonate) (TMPyP) or its zinc(II) derivative (ZnTMPyP) with a graphene oxide suspension and were subsequently characterized in view of their spectroscopic properties and applications in Rhodamine B (RhB)

photodegradation. The main objective was to determine how the presence of a Zn(II) atom in the porphyrin core affects the photocatalytic activity toward RhB degradation. Obtained data indicated that the presence of metal atoms could promote charge separation in the ZnTMPyP^{4+}/GO composites. Metalation of the porphyrin with the Zn(II) atom was found to increase the binding ability of the porphyrin to the graphene oxide surface. Ultrafast time-resolved transient absorption spectroscopy and photocurrent measurements strongly suggested the occurrence of an electron transfer process from photoexcited porphyrin to graphene oxide. Hybrid materials showed higher photocatalytic activity toward RhB degradation in comparison to that of pure GO. The ZnTMPyP^{4+}/GO exhibited higher efficiency, ca. 19% RhB decomposition after 2 hours of irradiation in comparison to TMPyP^{4+}/GO. This observation was attributed to more efficient charge separation.

In the second part, the non-covalent nanohybrid composed of cationic 5,10,15,20- tetra(4-trimethylammoniophenyl)porphyrin tetra(p-toluenesulfonate) (TMAP) and graphene oxide sheets were prepared at two pH values (6.2 vs. 1.8). The main objective was to investigate the pH-dependent behaviour of a non-covalent cationic porphyrin–graphene oxide nanohybrid. The TMAP molecule is positively charged, regardless of the pH of the solution. However, the protonation of imino nitrogens increased the overall charge of the porphyrin molecule from +4 to +6 (TMAP^{4+} and TMAP^{6+}). Therefore by modulation of the pH, the electrostatic interaction between porphyrin and GO could be changed. However, surprisingly it was found that at acidic pH, the interaction of TMAP^{6+} with GO was largely suppressed. The TMAP^{4+}/GO hybrid was fully described by spectroscopic technique as well as several compositional and morphological characterization methods. It was found that the formation of TMAP^{4+}/GO hybrid changes the porphyrin ground state electronic structure which was manifested among others by the Soret band shift in the UV-Vis spectra. Moreover, it was evidenced that the ground state interaction between porphyrin and GO causes static quenching of the porphyrin emission. In addition, fast quenching of the singlet excited state of the porphyrin adsorbed on the GO sheet occurred, which could be presumably attributed to the electron transfer process.

The part of the dissertation about neutral porphyrins was focused on the comparison of the strength of the interaction of neutral porphyrin with two types of graphene-based materials (GO and rGO) and investigating the properties of the obtained nanohybrid

materials. The data obtained indicated that both nanohybrids have similar photophysical properties. However, rGO can be functionalized with TAPP molecules more efficiently. Moreover, photocurrent measurements strongly suggest the occurrence of an electron transfer process from photoexcited porphyrin to graphene oxide in the TAPP/GO nanohybrid.

The third and last part of the dissertation presents the results obtained for the 5,10,15,20-tetra(4-sulfonatophenyl)porphyrin (TSPP). The TSPP was selected for this study as a model of anionic meso-tetra phenyl substituted porphyrin. This research attempted to determine the interactions between this porphyrin and GO in ground-state with the ultimate goal of comparing its strength with the other groups of porphyrins, i.e. cationic and neutral Since the anionic porphyrin molecules are negatively charged the electronic attraction can be excluded as a type of interaction between porphyrin and graphene oxide. The interaction between porphyrin and GO can be based on the stacking of π-π stacking and van der Waals forces, which are much weaker than the columbic interaction.

In summary, the research on nanohybrids presented in the doctoral dissertation involved the synthesis and spectroscopic characterization of novel porphyrin/graphene oxide nanohybrids. The conducted studies provided a better understanding of the relationship between the porphyrin structure and the strength and nature of interactions with GO. Time-resolved absorption spectroscopy allowed for the observation of photo-induced electron transfer, which has potential applications in photovoltaics, artificial photosynthesis, and photocatalytic degradation of pollutants. Therefore, the results discussed in the dissertation are significant for the utilization of such materials in designing energy conversion systems.

7.2 Streszczenie pracy w języku polskim

Zaspokojenie rosnącego zapotrzebowania na materiały o zaawansowanych zastosowaniach wymaga poszerzenia horyzontów obecnych badań na całym świecie. Materiały na bazie grafenu (GBM) wzbudziły zainteresowanie ze względu na swoje wyjątkowe właściwości, takie jak duża powierzchnia właściwa, stabilność mechaniczna i przepuszczalność optyczna. Sprzężony układ aromatyczny sprawia, że materiały te są idealnymi kandydatami do wykorzystania jako nośniki ładunku. Dodatkowo utleniona forma grafenu, czyli tlenek grafenu (GO), zawiera różne tlenowe grupy funkcyjne,

co otwiera możliwości jego funkcjonalizacji innymi indywiduami chemicznymi. W przeciwieństwie do grafenu GO może tworzyć stabilne wodne zawiesiny, co czyni go bardziej odpowiednim do niektórych zastosowań wymagających środowiska wodnego np. rozkładu wody czy fotodegradacji barwników.

Jedno z obiecujących podejść do funkcjonalizacji GBM obejmuje pokrycie powierzchni cząsteczkami zdolnymi do absorpcji światła słonecznego, w szczególności w zakresie UV-Vis. Doskonałym przykładem takich cząsteczek są porfiryny, ze względu na ich wysokie molowe współczynniki absorpcji w obszarze widzialnym.

Połączenie tych dwóch rodzajów komponentów: materiału na bazie grafenu i cząsteczki porfiryny, może prowadzić do ważnych synergii. Syntezy takiego materiału hybrydowego można dokonać na drodze funkcjonalizacji kowalencyjnej (poprzez tworzenie wiązań między składnikami nanostruktury) lub poprzez oddziaływania niekowalencyjne (oddziaływania π-π, elektrostatyczne, van der Waalsa, wiązania wodorowe). W ostatnich latach szczególną uwagę zwrócono na hybrydy porfiryny z GBM, które opierają się na oddziaływaniach niekowalencyjnych. Zainteresowanie to wynika między innymi z łatwości, z jaką można je przygotować i wysokiej wydajności tego procesu.

Głównym celem niniejszej pracy doktorskiej była synteza nowych układów hybrydowych zawierających GO lub rGO (zredukowany tlenek grafenu) i cząsteczki porfiryny oraz przeprowadzenie szczegółowej analizy spektroskopowej ich właściwości pod kątem potencjalnego zastosowania do fotokatalitycznej degradacji barwników organicznych. Badania obejmowały: 1) fotochemiczną i fotofizyczną charakterystykę wybranych porfiryn lub metaloporfiryn i ich hybryd z tlenkiem grafenu (lub jego zredukowaną formą), 2) porównanie właściwości spektroskopowych różnych nowo otrzymanych materiałów hybrydowych oraz 3) zbadanie możliwego zjawiska fotoindukowanego przeniesienia elektronów z cząsteczki porfiryny na arkusz GO/rGO.

Rozprawa ta pozwala w pełni zrozumieć niekowalencyjne oddziaływanie nanostruktur porfiryny i tlenku grafenu. Jednym z kluczowych elementów tych badań była analiza parametrów, które kontrolują siłę oddziaływania pomiędzy składnikami hybryd. Podsumowując głównymi celami tej rozprawy doktorskiej są:

1. synteza i charakterystyka nowych niekowalencyjnych nanohybryd opartych na GBM (GO i rGO) i porfirynach,

2. zdefiniowanie korelacji między strukturą porfiryny (anionową, neutralną, kationową oraz porfiryną i jej cynkową pochodną) a jej oddziaływaniem w stanie podstawowym i wzbudzonym z GBM,

3. porównanie właściwości spektroskopowych wolnych porfiryn i porfiryn zaadsorbowanych na powierzchni GBM,

4. określenie wpływu stopnia utlenienia GBM na siłę oddziaływania z porfiryną i jej właściwości spektroskopowe po adsorpcji do arkusza GBM,

5. ustalenie wpływu pH na tworzenie materiału hybrydowego porfiryna/tlenek grafenu.

Te cele naukowe zrealizowano dla różnych rodzajów porfiryn: kationowych, obojętnych i anionowych.

W pracy doktorskiej wykorzystano różne metody badawcze do określenia właściwości spektroskopowych i fotofizycznych materiałów hybrydowych, w tym: absorpcję w stanie podstawowym, czasowo-rozdzielczą spektroskopię emisyjną, nanosekundową i femtosekundową spektroskopię absorpcji przejściowej, pomiary fotoelektrochemiczne. Dodatkowo, do scharakteryzowania otrzymanych nanohybrid zastosowano spektroskopię fourierowską w podczerwieni (FTIR), spektroskopię Ramana, analizę termograwimetryczną (TGA), mikroskopię sił atomowych i analizę elementarną.

Część rozprawy doktorskiej, która dotyczy porfiryn kationowych, obejmuje dwa główne kierunki. W pierwszej części zsyntetyzowano dwie niekowalencyjne nanohybrydy tlenku grafenu i porfiryny poprzez zmieszanie roztworu kationowej porfiryny 5,10,15,20-tetra(1-metylo-4-pirydyno)porfiryny tetra(p-toluensulfonianu) ($TMPyP^{4+}$) lub jej pochodnej cynkowej ($ZnTMPyP^{4+}$) z zawiesiną tlenku grafenu. Następnie scharakteryzowano je pod kątem właściwości spektroskopowych i zastosowań do fotodegradacji Rodaminy B (RhB). Głównym celem było ustalenie, w jaki sposób obecność atomu Zn(II) w rdzeniu porfiryny wpływa na aktywność fotokatalityczną w kierunku degradacji RhB. Uzyskane dane wskazują, że obecność atomów metalu może sprzyjać separacji ładunków w nanohybrydzie $ZnTMPyP^{4+}$/GO. Stwierdzono, że wprowadzanie Zn(II) do porfiryny zwiększa zdolność wiązania porfiryny z powierzchnią tlenku grafenu. Ultraszybka, czasowo rozdzielcza spektroskopia

absorpcyjna i pomiary fotoprądowe wskazały na występowanie procesu przenoszenia elektronu z fotowzbudzonej porfiryny do tlenku grafenu. Materiały hybrydowe wykazały wyższą aktywność fotokatalityczną w kierunku degradacji RhB w porównaniu z czystym GO. ZnTMPyP^{4+}/GO wykazywał wyższą wydajność, ok. 19% rozkładu RhB po 2 godzinach naświetlania w porównaniu do TMPyP^{4+}/GO. Obserwację tę przypisano bardziej wydajnej separacji ładunków.

W drugiej części przygotowano niekowalencyjną nanohybrydę złożoną z kationowej 5,10,15,20-tetra(4-trimetyloamoniofenylo)porfiryny tetra(p-toluenosulfonianu) (TMAP) i arkuszy tlenku grafenu. Syntezy dokonano w dwóch rożnych pH (6.2 i 1.8). Głównym celem było zbadanie zależności wydajności tworzenia niekowalencyjnej nanohybrydyny kationowej porfiryny z tlenkiem grafenu od pH roztworu. Cząsteczka TMAP jest naładowana dodatnio, niezależnie od pH roztworu. Jednak protonacja azotu iminowego zwiększa całkowity ładunek cząsteczki porfiryny z +4 do +6 (TMAP^{4+} i TMAP^{6+}). Poprzez zmianę pH możliwa jest zatem zmiana siły oddziaływania elektrostatycznego między porfiryną a GO. Zaskakująco, stwierdzono, że przy kwaśnym pH odziaływanie TMAP^{6+} z GO było w dużej mierze ograniczone. Hybryda TMAP^{4+}/GO została w pełni opisana kilkoma metodami charakteryzacji kompozycyjnej i morfologicznej oraz technikami spektroskopowymi. Wszystkie te badania pozwoliły uzyskać obraz oddziaływania porfiryn z GO zarówno w stanie podstawowym, jak i wzbudzonym. Stwierdzono, że powstawanie hybrydy TMAP^{4+}/GO zmienia strukturę elektronową stanu podstawowego porfiryny, co przejawiało się .in.. przesunięciem pasma Soreta. Ponadto wykazano, że oddziaływanie stanu podstawowego między porfiryną a GO powoduje statyczne wygaszanie emisji porfiryny. Ponadto wykazano, że oddziaływanie stanu podstawowego między porfiryną a GO powoduje statyczne wygaszanie emisji porfiryny.Część rozprawy doktorskiej dotycząca porfiryn neutralnych skupiła się na porównaniu siły oddziaływania neutralnej porfiryny 5,10,15,20-tetra(4-aminophenyl)porphyrin
z dwoma rodzajami materiałów na bazie grafenu (GO i rGO) oraz zbadaniu właściwości otrzymanych materiałów nanohybrydowych. Uzyskane dane wskazują, że obie nanohybrydy mają podobne właściwości fotofizyczne. Jednak rGO może być funkcjonalizowany za pomocą cząsteczek TAPP bardziej efektywnie. Ponadto pomiary fotoprądowe sugerują wystąpienie procesu przenoszenia elektronów z fotowzbudzonej porfiryny do tlenku grafenu w nanohybrydzie TAPP/GO.

W trzeciej i ostatniej części rozprawy przedstawiono wyniki uzyskane dla 5,10,15,20-tetra(4-sulfonianofenylo)porfiryny (TSPP), wybranego jako model porfiryny anionowej. Badania te miały na celu określenie oddziaływania między tą porfiryną a GO w stanie podstawowym, a ostatecznym celem było porównanie jej siły z innymi grupami porfiryn, tj. kationowymi i obojętnymi. Ponieważ anionowe cząsteczki porfiryny są naładowane ujemnie, przyciąganie elektronowe można wykluczyć jako rodzaj interakcji między porfiryną a tlenkiem grafenu. Oddziaływanie pomiędzy porfiryną a GO może opierać się na odzdziaływaniach π-π aromatycznych pierścieni obu komponentów i siłach van der Waalsa, które są znacznie słabsze niż oddziaływanie kolumbowskie.

Podsumowując, badania nad nanohybrydami przedstawione w rozprawie doktorskiej obejmowały syntezę i charakterystykę spektroskopową nowych nanohybryd porfiryna/materiał grafenowy. Przeprowadzone badania pozwoliły na lepsze zrozumienie zależności między strukturą porfiryny a siłą i charakterem interakcji z GO. Spektroskopia absorpcyjna z rozdzielczością czasową pozwoliła zaobserwować fotoindukowane przeniesienie elektronów, który potencjalnie może być wykorzystane w fotowoltaice, sztucznej fotosyntezie czy fotodegradacji zanieczyszczeń. Tak więc wyniki omówione w pracy są istotne dla wykorzystania takich materiałów w projektowaniu układów do konwersji energii.

8. Personal Data

8.1 Publication Record

8.1.1 Articles related to the dissertation

1. Lerf–Klinowski-Type Models of Graphene Oxide and Reduced Graphene Oxide Are Robust in Analyzing Non-Covalent Functionalization with Porphyrins.,
A. Siklitskaya, E. Gacka, D. Larowska, M. Mazurkiewicz-Pawlicka, A. Malolepszy, L. Stobiński, B. Marciniak, A. Lewandowska-Andrałojć, A. Kubas
Sci. Rep. 2021 11, 7977
15 Citations, (IF=4.997)
DOI:10.1038/s41598-021-86880-1

2. Graphene Oxide Functionalized with Cationic Porphyrins as Materials for the Photodegradation of Rhodamine B
D. Larowska, J .M.O'Brien, M. O. Senge, G. Burdzinski, B. Marciniak, A. Lewandowska-Andralojc
J. Phys. Chem. C 2020 124 (29), 15769-15780
23 Citations, (IF=4.177)
DOI: 10.1021/acs.jpcc.0c03907

3. **Cationic Porphyrin-Graphene Oxide Hybrid: Donor-Acceptor Composite for Efficient Photoinduced Electron Transfer**
D. Larowska, A. Wojcik, M. Mazurkiewicz-Pawlicka, A. Malolepszy, L. Stobiński, B. Marciniak, A. Lewandowska-Andralojc,
ChemPhysChem, 2019, 20, 1054.
15 Citations, (IF=3.52)
DOI: 10.1002/cphc.201900040

8.1.2 Other publication

4. Novel Purine Alkaloid Cocrystals with Trimesic and Hemimellitic Acids as Coformers: Synthetic Approach and Supramolecular Analysis
M. R. Gołdyn, D. Larowska, E. Bartoszak-Adamska
Crystal Growth & Design 2021 21 (1), 396-413
DOI: 10.1021/acs.cgd.0c01242

5. How Eosin Y/Graphene Oxide-Based Materials Can Improve Efficiency of Light-Driven Hydrogen Generation: Mechanistic Aspects

A. Lewandowska-Andrałojć, D. Larowska, E. Gacka, T. Pedzinski, B. Marciniak

J. Phys. Chem. C 2020 124 (5), 2747-2755

DOI: 10.1021/acs.jpcc.9b09573

6. Synthon Hierarchy in Theobromine Cocrystals with Hydroxybenzoic Acids as Coformers

M. R. Gołdyn, D. Larowska, W. Nowak, E. Bartoszak-Adamska

CrystEngComm 2019 21,(48)

DOI: 10.1039/C9CE01195A

7. Theobromine Cocrystals with Monohydroxybenzoic Acids – Synthesis, X-ray Structural analysis, Solubility and Thermal Properties

M. R. Gołdyn, D. Larowska, W. Nowak, E. Bartoszak-Adamska

CrystEngComm 2019, 21(3)

DOI: 10.1039/C9CE01020C

8.2 International Internships

- Friedrich-Alexander-Universitat Erlangen (Nurnberg, Erlangen, Germany) 07.2018-09.2018 | Department of Chemistry and Pharmacy (prof. Dirk Guldi)
  during the internship, the TEM measurements included in this work were carried out
- University of Notre Dame (South Bend, IN, United States of America) 06.2019 | Radiation Laboratory (prof. Prashant Kamat)
  during the internship, the photoelectrochemical measurements included in this work were carried out
- Institut de Science et d'Ingénierie (Strasburg, France) | 10.2019-02.2020 | Nanochemistry Laboratory (prof. Paolo Samori)
  during the internship, the studies related to photocatalytic activity toward RhB included in this work were carried out

8.3 Contribution at Conferences

1. **The European Conference Physics of Magnetism** (07.2017, Trzebaw, Poland)
   • BLS examination of electron-phonon interaction in Bi_2Te_3-semiconductor heterostructures (poster, ENG)
2. **XI Copernican International Young Scientists Conference** (06.2017, Toruń, Poland)
   • Comparative investigations of the spectroscopic properties of the cationic porphyrins and its zinc analog and their non-covalent functionalization with graphene oxide (poster, ENG)
   • Bismuth(III) telluride (Bi_2Te_3) as a representative component of topological insulators (poster, ENG)
3. **Sekcja Młodych Polskiego Towarzystwa Chemicznego** (12.2017, Bydgoszcz, Poland)
   • Comparative investigations of the spectroscopic properties of the cationic porphyrins and their non-covalent functionalization with graphene oxide (poster, ENG)
4. **Analitycal methods to study oxidative damage, antioxidants and drugs" Advanced analytical chemistry for life science** (05.2018, Białystok, Poland)
   • Cationic porphyrin-GO hybrids as a complexes with potential application in photodynamic therapy - their photophysical and photochemical properties (poster, ENG)
5. **First European Congress on Photosynthesis Research** (06.2018, Uppsala, Sweden) • Investigations of the spectroscopic properties of the TMAP-porphyrin and its non-covalent functionalization with graphene oxide (poster, ENG)
6. **2nd International Workshop on Functional Nanostructured Materials (FuNaM-2)** (10.2018, Kraków, Poland)
   • Non-covalent interaction between TMAP-porphyrin and graphene oxide (poster, ENG)
7. **Women in Science – 1st Erlangen Symposium** (10.2018, Erlangen, Germany)
   • Porphyrin TMPyP on graphene oxide for the enhanced photocatalytic performance (oral, ENG)
8. **Poznańskie Mikrosympozjum Grafenowe** (03.2019, Poznań, Poland)
   • Niekowalencyjna funkcjonalizacja tlenku grafenu barwnikami porfirynowymi (oral, PL)

• Fotoindukowane przeniesienie elektronu w niekowalencyjnej hybrydzie porfiryna TMAP-GO (poster, PL)

9. **V Krajowa Konferencja „Grafen i inne materiały 2D”** (09.2019, Szczecin, Poland)

   • Supramolecular complexes of graphene oxide with porphyrins (oral, ENG)

10. **28th IUPAC Symposium on Photochemistry** (07.2022, Amsterdam, Holland)

    • GO-Porphyrin hybrids as materials for dyes photodegradation (poster, ENG)

11. **17th conference in the MAF (Methods and Applications in Fluorescence** (09.2022, Gothenburg, Sweden)

    • Spectroscopic characterization of non-covalent porphyrin-graphene oxide nanohybrids (poster, ENG)

9. References

(1) Kielmann, M.; Prior, C.; Senge, M.O. *New J. Chem.* **2018**, *42* (10), 7529–7550.

(2) Kamat, P.V. *J. Phys. Chem. Lett.* **2011**, *2* (3), 242–251.

(3) Bai, S.; Shen, X. *RSC Adv.* **2012**, *2* (1), 64–98.

(4) Luo, B.; Liu, S.; Zhi, L. *Small* **2012**, *8* (5), 630–646.

(5) MacHado, B.F.; Serp, P. *Catal. Sci. Technol.* **2012**, *2* (1), 54–75.

(6) Li, X.; Chen, Y.; Tao, Y.; Shen, L.; Xu, Z.; Bian, Z.; Li, H. *Chem Catal.* **2022**, *2* (6), 315–1345.

(7) Geim, A.K.; Novoselov, K.S. *Nat. Mater.* **2007**, *6*, 183–191.

(8) Morris, J.E.; Iniewski, K. *Graphene, Carbon Nanotubes and Nanostructures*; CRC Press, **2013**.

(9) Proctor, D.; Melendrez Armada D.A *An Introduction to Graphene and Carbon Nanotubes*; **2019**.

(10) Novoselov, K.S.; Jiang, D.; Schedin, F.; Booth, T.J.; Khotkevich, V.V; Morozov, S.V; Geim, A.K. **2005**, *102* (30), 10451–10453.

(11) Khomenko, O.V.; Prodanov, M.V.; Sherback, Y.V. *J. Nano- Electron. Phys.* **2009**, *1*, 66–78.

(12) Grima, J.N.; Winczewski, S.; Mizzi, L.; Grech, M.C.; Cauchi, R.; Gatt, R.; Attard, D.; Wojciechowski, K.W.; Rybicki, J. **2014**, 1–5.

(13) Iijima, I.S.; Yudasaka, M.; Yamada, R.; Bandow, S.; Suenaga, K.; Kokai, F.; Takahashi K. M. *Chem. Phys. Lett.* **1999**, *309* (August), 165–170.

(14) Kroto, H.W.; Heath, J.R.; O'Brien, S.C.; Curl, R.F.; Smalley, R.F. *Nature* **1985***.,* 318(6042), 162–163.

(15) Iijima, S. *Nature* **1991**, *354(6348).*

(16) Ichihashi, T.; Iijima, S. *Nature* **1993**, *363(6430).*

(17) Bethune, D.S.; Kiang, C.H.; de Vries, M.S.; Gorman, G.; Savoy, R.; Vazquez, J.; Beyers, R. *Nature* **1993**, *363* (6430), 605–607.

(18) Taha, M.H.F.; Ashraf, H.; Caesarendra, W. *Appl. Syst. Innov.* **2020**, *3* (3), 1–33.

(19) Singh, V.; Joung, D.; Zhai, L.; Soumen D.; Khondaker S.I.; Seal, S. *Prog. Mater. Sci.* **2011**, *56* (8), 1178–1271

(20) Khan, M.; Tahir, M.N.; Adil, S.F.; Khan, H.U.; Siddiqui, M.R.H.; Al-warthan A.A.; Tremel W. *J. Mater. Chem. A* **2015**, *3* (37), 18753–18808.

(21) Yun, Y.S.; Yoon, G.; Park, M.; Cho, S.Y.; Lim, H-D.; Kim, H.; Park, Y.W.; Kim, B.H.; Kang, K.; Jin, H.-J. *NPG Asia Mater.* **2016**, *8* (12), 338.

(22) Shao, Y.; Wang, J.; Wu, H.; Liu, J.; Aksay, I.A.; Lin, Y. *Electroanalysis* **2010**, *10*, 1027–1036.

(23) Kim, J.T.; Choi, S.-Y. *Opt Express* **2011**, 19 (24), 1291–1294.

(24) Shen, H.; Zhang, L.; Liu, M.; Zhang, Z. *Theranostics* **2012**, 2 (3), 283–294.

(25) Romanchuk, A.Y.; Slesarev, A.S.; Kalmykov S.N.; Kosynkin, D.V.; Tour J.M. *Phys. Chem. Chem. Phys.* **2013**, 15, 2321–2327.

(26) Choi, H.-J.; Jung, S.-M.; Seo, J.-M.; Chang D.-W.; Dai L.; Baek J.-B. *Opt Express* **2011**, *19* (24), 1291–1294.

(27) Joshi, A.; Bajaj, A.; Singh, R.; Alegaonkar, P.S.; Balasubramanian, K.; Datar, S.; *Nanotechnology* **2014**, *25*, 239501.

(28) Kausar, A.; Rafique, I.; Muhammad B. *Polym. Plast. Technol. Eng.* **2017**, *56* (13), 1438–1456.

(29) Avouris, P. *Nano Lett.* **2010**, *10*, 4285–4294.

(30) Llatser, I.; Kremers, C.; Cabellos-aparicio, A. *Photonics Nanostructures - Fundam. Appl.* **2012**, *10*, 353–358.

(31) Suk, J.W.; Kirk, K.; Hao, Y.; Hall, N.A.; Ruoff, R.S. *Adv. Mater.* **2012**, 1–6.

(32) Wu, J.; Agrawal, M.; Becerril, A.; Bao, Z.; Liu, Z.; Chen, Ḱ.Y.; Peumans, P. *ACS Nano* **2010**, *4* (1), 43–48.

(33) Nine, J.; Cole, M.A.; Tran, D.N.H.; Losic, D. *J. Mater. Chem. A Mater. energy Sustain.* **2015**, *3*, 12580–12602.

(34) Zhu, Y.; Murali, S.; Cai, W.; Li, X.; Suk, J.W.; Potts, J.R.; Ruoff, R.S. *Adv. Mater.* **2010**, *22* (35), 3906–3924.

(35) Morín, M. E. Z.; Torres-Martínez, L.; Sanchez-Martínez, D.; Gómez-Solís, C.; *Mater. Res.* **2017**, *20* (5), 1322–1331.

(36) Krishnamoorthy, K.; Mohan, R.; Kim, S.J. *Appl. Phys. Lett.* **2011**, *98* (24), 2013–2016.

(37) Dreyer, D.R.; Todd, D.; Bielawski, C.W. *Chem. Soc. Rev.*, 43(15), 5288.

(38) Lerf, A.; He, H.; Forster, M.; Klinowski, J. *J.Phys.Chem. B* **1998**, *5647* (97), 4477–4482.

(39) Loh, K.P.; Bao, Q.; Eda, G.; Chhowalla, M. *Nat. Chem.* **2010**, *2* (12), 1015–1024.

(40) Hsu H.-C.; Shown, I.; Wei, H.-Y., Chang, Y.-C.; Du, H.-Y.; Lin, Y.-G.; Tseng, C.-A.; Wang, C.-H.; Chen, L.-C.; Lind Y.-C.; Chen, K.-H. *Nanoscale* **2013**, *5* (1), 262–268.

(41) Stankovich, S.; Dikin, D.A.; Piner, R.D.; Kohlhaas, K.A.; Kleinhammes, A.; Jia, Y.; Wu, Y.; Nguyen, S.B.T.; Ruoff, R.S. *Carbon N. Y.* **2007**, *45* (7), 1558–1565.

(42) Hummers W.S.; Offeman R.E. *J. Am. Chem. Soc* **1958**, *80(6)*, 1339–1339.

(43) De Silva, K.K.H.; Huang, H.-H.; Yoshimura, M. *Appl. Surf. Sci.* **2018**, *447*, 338–346.

(44) Stankovich, S.; Piner, R.D.; Chen, X.; Wu, N.; Nguyen, S.T.; Ruoff, R.S. *J. Mater. Chem.* **2006**, *16* (2), 155–158.

(45) Paredes, J.I.; Villar-Rodil, S.; Solís-Fernández, P.; Martínez-Alonso, A.; Tascón, J.M. D. *Langmuir* **2009**, *25* (10), 5957–5968.

(46) Ma, L.; Niu, H.; Cai, J.; Zhao, P.; Wang, C.; Bai, X.; Lian, Y.; Wang, W. *Carbon N. Y.* **2013**, *67*, 488–499.

(47) Li, S.; Zhong, X.; Yang, H.; Hu, Y.; Zhang, F.; Niu, Z.; Hu, W.; Dong, Z.; Jin, J.; Li, R.; Ma J. *Carbon N. Y.* **2011**, *49* (13), 4239–4245.

(48) Li, Z.; He, M.; Xu, D.; Liu, Z. *Journal Photochem. Photobiol. C Photochem. Rev.* **2014**, *18*, 1–17.

(49) Georgakilas, V.; Otyepka, M.; Bourlinos, A.B.; Chandra, V.; Kim, N.; Kemp, K.C.; Hobza, P.; Zboril, R.; Kim, K.S. *Chem. Rev.* **2012**, *112*, 6156–6214.

(50) Xu, Y.; Liu, Z.; Zhang, X.; Wang, Y.; Tian, J.; Huang, Y.; Ma, Y.; Zhang, X.; Chen, Y. *Adv. Mater.* **2009**, *21* (12), 1275–1279.

(51) Nguyen, B.H.; Nguyen, V.H. *Adv. Nat. Sci. Nanosci. Nanotechnol.* **2015**, *6* (4).

(52) Orth, E.S.; Ferreira, J.G.L.; Fonsaca, J.E.S.; Blaskievicz, S.F.; Domingues, S.H.; Dasgupta, A.; Terrones, M.; Zarbin, A.J.G. *J. Colloid Interface Sci.* **2016**, *467*, 239–244.

(53) Panagiotopoulos, A.; Ladomenou, K.; Dongyue, S.; Artero, V. *Dalt. Trans.* **2016**, *45* (15), 6732–6738.

(54) Rao, H.; Schmidt, L.C.; Bonin, J.; Robert, M. *Nat. Lett.* **2017**, *548* (7665), 74–77.

(55) Amanullah, S.; Saha, P. *Faraday Discuss.* **2022**, *234*, 143–158.

(56) Cheng, N.; Kemna, C. *Electrocatalysis* **2012**, 238–251.

(57) Chen, Y.; Li, A.; Huang, Z.-H.; Wang, L.-N.; Kang, F. *Nanomaterials* **2016**, *6* (3), 51.

(58) Walter, M.G.; Rudine, A.B.; Wamser, C.C. *J. Porphyr. Phthalocyanines* **2010**, *14* (09), 759–792.

(59) Cong, M.; Chen, X.; Xia, K.; Ding, X.; Zhang, L.; Jin, Y.; Gao, Y.; Zhang, L. *J. Mater. Chem. A* **2021**, *9*, 4673–4678.

(60) Shepherd, M.; Hunter, C.N. *Biochem. J.* **2004**, *382* (3), 1009–1013.

(61) Zhang P.; Hu J.; Liu B.; Yang J. *Chemosphere* **2019**, *219*, 617–635.

(62) Wang Y.T.; Chang X.Y.; Zhang Y. *J. Nanosci. Nanotechnol.* **2017**, *17* (12), 9027–9035.

(63) Gouterman, M.; Wagnière, G.H.; Snyder, L.C.S *J. Mol. Spectrosc.* **1963**, *11* (1–6), 108–127.

(64) Gouterman, M. *J. Mol. Spectrosc* **1961**, *6*, 138–163.

(65) Uttamlal, M.; Sheila Holmes-Smith, A. *Chem. Phys. Lett.* **2008**, *454* (4–6), 223–228.

(66) Giovanetti R. *Macro To Nano Spectroscopy*; Uddin, J., Ed. **2012**; 460.

(67) Nasri, H. **2020**. Conference Abstract: 2020 IEEE International Conference on Design & Test of Integrated Micro & Nano-Systems (DTS)

(68) Seybold, P.G. *J. Mol. Spectrosc.* **1969**, *13*, 1–13.

(69) Andrade, S.M.; Teixeira, R.; Costa, S.M.B. Sobral Abílio J.F.N., *Biophys. Chem.* **2008**, *133*, 1–10.

(70) Gust D., Moore T.A. *Acc. Chem. Res.* **2001**, *34* (1), 40–48.

(71) Sajadi, S.M.S.; Khoee, S. *Sci. Rep.* **2021**, *11* (1), 1–14.

(72) Bala Murali Krishna M., Venkatramaiah N., Venkatesan R., *J. Mater. Chem.* **2012**, *22 (7)*, 3059–3068.

(73) Gacka, E.; Wojcik, A.; Mazurkiewicz-Pawlicka, M.; Malolepszy, A.; Stobiński, L.; Kubas, A.; Hug, G. L.; Marciniak, B.; Lewandowska-Andralojc, A. *J. Phys. Chem. C* **2019**, *123* (6), 3368–3380.

(74) Gacka, E.; Burdzinski, G.; Marciniak, B.; Kubas, A.; Lewandowska-Andralojc, A. *Phys. Chem. Chem. Phys.* **2020**, *22* (24), 13456–13466.

(75) Wang, Y.; Zhang, Y.; Chen, J.; Dong, Z.; Chang, X.; Zhang, Y. *Electrochemistry* **2015**, *83* (11), 950–955.

(76) Zhu, M.; Li, Z.; Xiao, B.; Lu, Y.; Du, Y.; Yang, P.; Wang, X. S *ACS Appl. Mater. Interfaces* **2013**, *5* (5), 1732–1740.

(77) Chen, Y.; Huang, Z.H.; Yue, M.; Kang, F. *Nanoscale* **2014**, *6* (2), 978–985.

(78) Xu, Y.; Zhao, L.; Bai, H.; Hong, W.; Li, C.; Shi, G. *J. Am. Chem. Soc.* **2009**, *131*, 13490–13497.

(79) Aly, S. M.; Parida, M.R.; Alarousu, E.; Mohammed, O.F. *Chem. Commun.* **2014**, *50* (72), 10452–10455.

(80) Wojcik, A.; Kamat, P.V. *ACS Nano* **2010**, *4* (11), 6697–6706.

(81) Masih, D.; Aly, S.M.; Usman, A.; Alarousu, E.; Mohammed, O.F. *Phys. Chem. Chem. Phys.* **2015**, *17* (14), 9015–9019.

(82) Sun, J.; Meng, D.; Jiang, S.; Wu, G.; Yan, S.; Geng, J.; Huang, Y. *J. Mater. Chem.* **2012**, *22* (36), 18879–18886.

(83) Liu, Z.; Zhao, H.X.; Huang, C.Z. *PLoS One* **2012**, *7* (12), 1–8.

(84) Zhang, X. *Carbon N. Y.* **2011**, *49* (12), 3842–3850.

(85) Mandal, S.; Nayak, S.K.; Mallampalli, S.; Patra, A. *ACS Applied Materials & Interfaces* **2014** Jan 6(1), 130-136

(86) Bajjou, O.; Bakour, A.; Khenfouch, M.; Baitoul, M.; Faulques, E.; Maaza, M. *Synth. Met.* **2016**, 211, 247–252.

(87) Zheng, L.; Ye, D.; Xiong, L.; Xu, J.; Tao, K.; Zou, Z.; Huang, D.; Kang, X.; Yang, S.; Xia, J. *Anal. Chim. Acta* **2013**, *768*, 69–75.

(88) Ge, R.; Wang, X.; Zhang, C.; Kang, S. Z.; Qin, L.; Li, G.; Li, X. *Colloids Surfaces A Physicochem. Eng. Asp.* **2015**, *483*, 45–52.

(89) Lightcap, I.V.; Kamat, P.V. *Acc. Chem. Res.* **2012**, *46* (10), 2235–2243.

(90) Cao, S.; Yu, J. *J. Photochem. Photobiol. C Photochem. Rev.* **2016**, *27*, 72–99.

(91) Zhang, X.; Peng, T.; Song, S. *J. Mater. Chem. A Mater. energy Sustain.* **2016**, *4*, 2365–2402.

(92) Lewandowska-Andralojc, A.; Marciniak, B. *ACS Energy Lett.* **2019**, *4* (8), 1898–1901.

(93) Ye, T.X.; Ye, S.L.; Chen, D.M.; Chen, Q.A.; Qiu, B.; Chen, X. *Spectrochim. Acta - Part A Mol. Biomol. Spectrosc.* **2012**, *86*, 467–471.

(94) Min, S.; Lu, G. *Int. J. Hydrogen Energy* **2012**, *37* (14), 10564–10574.

(95) Gacka, E.; Burdzinski, G.; Marciniak, B.; Kubas A.; Lewandowska-Andralojc, A. *Phys. Chem. Chem. Phys.* **2020**, *19*.

(96) Aydin, M.; Akins, D.L. *Appl. Mol. Spectrosc. to Curr. Res. Chem. Biol. Sci.* **2016**.

(97) Wang, P.; Cheng, M.; Zhang, Z. *J. Saudi Chem. Soc.* **2014**, *18* (4), 308–316.

(98) Lewandowska, K.; Rosiak, N.; Bogucki, A.; Cielecka-Piontek, J.; Mizera, M.; Bednarski, W.; Suchecki, M.; Szaciłowski, K. *Molecules* **2019**, *24* (4).

(99) Shu, J.; Qiu, Z.; Wei, Q.; Zhuang, J.; Tang, D. *Sci. Rep.* **2015**, *5* (September), 1–11.

(100) Kathiravan, A.; Kumar, P. S.; Renganathan, R.; Anandan, S. *Colloids Surfaces A Physicochem. Eng. Asp.* **2009**, *333* (1–3), 175–181.

(101) De Miguel, M.; Aílvaro, M.; Garciía, H. *Langmuir* **2012**, *28* (5), 2849–2857.

(102) Karolczak, J.; Kowalska, D.; Lukaszewicz, A.; Maciejewski, A. *J. Phys. Chem.* **2004**, *108* (21), 4570–4575.

(103) Tripathy, U.; Kowalska, D.; Liu, X.; Velate, S.; Steer, R.P. *J. Phys. Chem.* **2008**, *112* (26), 5824–5833.

(104) Iwase, A.; Ng, Y.H.; Ishiguro, Y.; Kudo, A.; Amal, R. **2011**, 11054–11057.

(105) Yuan, Y.J.; Chen, D.; Zhong, J.; Yang, L.X.; Wang, J.J.; Yu, Z.T.; Zou, Z.G. *J. Phys. Chem. C* **2017**, *121* (39).

(106) La, D.D.; Rananaware, A.; Salimimarand, M.; Bhosale, S.V. *ChemistrySelect* **2016**, *1* (15), 4430–4434.

(107) La, D.; Hangarge, R.; Bhosale, S.V.; Ninh, H.; Jones, L.; Bhosale, S.V. *Appl. Sci.* **2017**, 7(6), 643.

(108) El-Shafai, N.; El-Khouly, M.E.; El-Kemary, M.; Ramadan, M.S.; Masoud, M.S. *Photochem. Photobiol. Sci.* **2019**, *18* (8), 2071–2079.

(109) Kielmann, M.; Prior, C.; Senge, M.O. *New J. Chem.* **2018**, *42* (10), 7529–7550.

(110) De Napoli, M.; Nardis, S.; Paolesse, R.; Vicente, M.G.H.; Lauceri, R.; Purrello, R. *J. Am. Chem. Soc.* **2004**, *126* (19), 5934–5935.

(111) Guo, P.; Chen, P.; Ma, W.; Liu, M. *J. Mater. Chem.* **2012**, *22* (38), 20243–20249.

(112) Szczepaniak, W. *Metody Instrumentalne w Analizie Chemicznej*; Wydawnictwo Naukowe PWN, **2004**.

(113) Kęcki, Z. *Podstawy Spektroskopii Molekularnej*; Wydawnictwo Naukowe PWN, **2013**.

(114) Gispert, R. J. *Coordination Chemistry*; Wiley-VCH, Weinheim, **2008**.

(115) Marciniak, B. *J. Chem. Education* **1986** 63, 998-1000.

(116) Lakowicz, J. R. *Principles of Fluorescence Spectroscopy*; Springer New York, NY, **2006**.

(117) Stobinski, L.; Lesiaka, B.; Malolepszy, A.; Mazurkiewicz, M.; Mierzwa, B.; Zemek, J.; Jiricek, P.; Bieloshapka, *J Electron Spectros Relat Phenomena* **2014**, 195, 145–154.

(118) Chen, J.; Yao, B.; Li, C.; Shi, G. *Carbon N. Y.* **2013**, *64* (1), 225–229.

(119) Marcano, D.C.; Kosynkin, D.V; Berlin, J.M.; Sinitskii, A.; Sun, Z.; Slesarev, A.; Alemany, L.B.; Lu, W.; Tour, J.M. *ACS Nano* **2010**, *4* (8), 4806–4814.

(120) Abulizi, A.; Okitsu, K.; Zhu, J. *Ultrason. - Sonochemistry* **2014**, *21* (3), 1174–1181.

(121) Cuong, T.V.; Pham, V.H.; Tran, Q.T.; Hahn, S.H.; Chung, J.S.; Shin, E.W.; Kim, E.J. *Mater. Lett.* **2010**, *64* (3), 399–401.

(122) Luo, Z.; Lu, Y.; Somers, L.A.; Johnson, A.T.C. *J. Am. Chem. Soc.* **2009**, *131* (3), 898–899.

(123) Zhang, J.; Yang, H.; Shen, G.; Cheng, P.; Zhang, J.; Guo, S. *Chem. Commun.* **2010**, *46* (7), 1112–1114.

(124) Gilje, S.; Kaner, R.B.; Wallace, G.G.; Li, D.A. N.; Mu, M.B. Li, D., Müller, M.B., *Nature Nanotechnology*, **2008**, 3(2), 101–105.

(125) Becerril, H.A.; Mao, J.; Liu, Z.; Stoltenberg, R.M.; Bao, Z.; Chen, Y. *ACS Nano* **2008**, *2* (3), 463–470.

(126) Gacka, E.; Majchrzycki, Ł.; Marciniak, B.; Lewandowska-Andralojc, A. *Sci. Rep.* **2021**, *11* (1), 1–11.

(127) Gudarzi, M.M. *Langmuir* **2016**, *32* (20), 5058–5068.

(128) Whitby, R.L.D.; Korobeinyk, A.; Gun'Ko, V.M.; Busquets, R.; Cundy, A.B.; László, K.; Skubiszewska-Ziba, J.; Leboda, R.; Tombacz, E.; Toth, I.Y.; Kovacse K.; Mikhalovsky S.V.; *Chem. Commun.* **2011**, *47* (34), 9645–9647.

(129) Szabó, T.; Tombácz, E.; Illés, E.; Dékány, I. *Carbon N. Y.* **2006**, *44* (3), 537–545.

(130) Yeh, T.F.; Chan, F.F.; Hsieh, C.Te; Teng, H.G *J. Phys. Chem. C* **2011**, *115* (45), 22587–22597.

(131) Kano, K.; Minamizono, H.; Kitae, T.; Negi, S. *J. Phys. Chem. A* **1997**, *101* (34), 6118–6124.

(132) Kano, K., Nakajima, T., Takei, M., & Hashimoto, S. *Bull. Chem. Soc.Jpn.* **1987**, *60*, 1281–1287.

(133) Chernia, Z.; Gill, D. *Langmuir* **1999**, *15* (5), 1625–1633.

(134) Khurana, R.; Kakatkar, A.S.; Chatterjee, S.; Barooah, N.; Kunwar, A.; Bhasikuttan, A.C.; Mohanty, J. *Front. Chem.* **2019**, *7* (JUN), 1–11.

(135) Rehm, D.; Weller, A. *Ber. Bunsenges. Phys. Chem.* **1969**, *73*, 834.

(136) Rehm, D.; Weller, A. *Isr. J. Chem* **1970**, *8*, 259.

(137) Kalyanasundaram, K.; Neumann-Spallart, M. *J. Phys. Chem.* **1982**, *86* (26), 5163–5169.

(138) Laermer, F.; Elsaesser, T.; Kaiser, W. *Chem. Phys. Lett.* **1989**, *156* (4), 381–386.

(139) Retsek, J.L.; Gentemann, S.; Medforth, C.J.; Smith, K.M.; Chirvony, V.S.; Fajer, J.; Holten, D. *J. Phys. Chem. B* **2000**, *104* (29), 6690–6693.

(140) Enescu, M.; Steenkeste, K.; Tfibel, F.; Fontaine-Aupart, M.P. *Phys. Chem. Chem. Phys.* **2002**, *4* (24), 6092–6099.

(141) Barbosa Neto, N.M.; Correa, D.S.; De Boni, L.; Parra, G.G.; Misoguti, L.; Mendonça, C.R.; Borissevitch, I.E.; Zílio, S.C.; Gonçalves, P.J. *Chem. Phys. Lett.* **2013**, *587*, 118–123.

(142) Kaniyankandy, S.; Achary, S.N.; Rawalekar, S.; Ghosh, H.N. *J. Phys. Chem. C* **2011**, *115* (39), 19110–19116.

(143) La, D.D.; Bhosale, S.V.; Jones, L.A.; Revaprasadu, N.; Bhosale, S.V. *ChemistrySelect* **2017**, *2* (11), 3329–3333.

(144) Guo, P.; Chen, P.; Liu, M. *ACS Appl. Mater. Interfaces* **2013**, *5* (11), 5336–5345.

(145) Wang, Q.; Li, J.; Bai, Y.; Lu, X.; Ding, Y.; Yin, S.; Huang, H.; Ma, H.; Wang, F.; Su, B. *J. Photochem. Photobiol. B Biol.* **2013**, *126*, 47–54.

(146) Pica, M.; Calzuola, S.; Donnadio, A.; Gentili, P.L.; Nocchetti, M.; Casciola, M. *Catalysts* **2019**, *9* (1), 3.

(147) Yu, K.; Yang, S.; He, H.; Sun, C.; Gu, C.; Ju, Y. *J. Phys. Chem. A* **2009**, *113* (37), 10024–10032.

(148) Hasobe, T. *J. Phys. Chem. Lett.* **2013**, *4* (11), 1771–1780.

(149) Ohno, O.; Kaizu, Y.; Kobayashi, H. *J. Chem. Phys.* **1993**, *99* (5), 4128–4139.

(150) Leighton, P.; Cowan, J.A.; Abraham, R.J.; Sanders, J.K.M. *J.Org.Chem* **1988**, *53*, 733–740.

(151) Sasaki, K.; Li, H.-W.; Hayashi, A.; Yamabe, J.; Ogura, T. *Hydrogen Energy Engineering*. Springer **2016**, 593.

(152) Latorre-Sanchez, M.; Lavorato, C.; Puche, M.; Fornøs, V. *Chem. - A Eur. J.* **2012**, *18* (52), 16774–16783.

(153) Neta, P. *J. Phys. Chem.* **1981**, No. 12, 3678–3684.

(154) Nahor G.S.; Neta P.; Hambright P.; Robinson L.R., *J. Phys Chem.* **1991**, *95* (11), 4415–4418.

(155) Conradie, J.; Wamser, C.C.; Ghosh, A. *J. Phys. Chem. A* **2021**, *125* (46), 9953–9961.

(156) Zurita A.; Duran A.; Ribó J.M.; El-Hachemi Z.; Crusants J. *RCS Adv.* **2017**, *7*, 3353–3357.

(157) Siklitskaya, A.; Gacka, E.; Larowska, D.; Mazurkiewicz-Pawlicka, M.; Malolepszy, A.; Stobiński, L.; Marciniak, B.; Lewandowska-Andrałojć, A.; Kubas, A. *Sci. Rep.* **2021**, *11* (1), 1–14.

(158) Larowska, D.; Wojcik, A.; Mazurkiewicz-Pawlicka, M.; Malolepszy, A.; Stobiński, L.; Marciniak, B.; Lewandowska-Andralojc, A. *ChemPhysChem* **2019**, *20* (8).

(159) Lu, J.; Li, Z.; An, W.; Liu, L.; Cui, W. *Nanomaterials* **2019**, *9* (9), 1321.

(160) Mondal, B.; Bera, R.; Nayak, S.K.; Patra, A. *J. Mater. Chem. C* **2016**, *4* (25), 6027–6036.

(161) Bera, R.; Mandal, S.; Mondal, B.; Jana, B.; Nayak, S.K.; Patra, A.; *ACS Sustain. Chem. Eng.* **2016**, *4* (3), 1562–1568.

(162) Sobczyński, J.; Tønnesen, H. H.; Kristensen, S. *Pharmazie* **2013**, *68* (2), 100–109.

(163) Carlos, J.; Louro, T. Conference Abstract, **2004**.

(164) McMurry, J. Organic Chemistry. *Brooks/Cole Publ.* **2000**, *5th Edition*.

(165) Ali, M.; Pandey, S. *J. Photochem. Photobiol. A Chem.* **2009**, *207*, 288–296.

(166) Andrade, S.M.; Costa, M.B. *Biophys. J.* **2002**, *82* (3), 1607–1619.

(167) Hollingsworth, J.V; Richard, A.J.; Grac, M.; Vicente, H.; Russo, P.S. *Biomacromolecules* **2011**, *13*, 60–72.

(168) Boda, D.; Neagu, M.; Constantin, C.; Diaconeasa, A.; Ianosi, S.; Amalinei, C.; Stanoiu, B.; Crauciuc, E.; Toma, O.; Ion, R. A CASE REPORT; **2009**, 61–69.

(169) Kathiravan, A.; Anbazhagan, V.; Jhonsi, M.A.; Renganathan, R.I *J. Mol. Struct.* **2009**, *919* (1–3), 79–82.

(170) Gratzel, M. *Inorg. Chem.* **2005**, *44* (20), 6841–6851.

(171) Thavasi, V.; Renugopalakrishnan, V.; Jose, R.; Ramakrishna, S. *Mater. Sci. Eng. R* **2009**, *63*, 81–99.

(172) Berova N.; Di Bari L.; Pescitelli. G. *ChemInform* **2007**, *38* (33).

(173) Akins, D.L.; Zhu, H.; Guo, C. *J. Phys. Chem.* **1996**, *100* (13), 5420–5425.

(174) Akins, D.L.; Zhu, H.; Guo, C. *J. Phys. Chem.* **1994**, *98* (14), 3612–3618.

(175) McRae, E.G.; Kasha, M. *J. Chem. Phys.* **1958**, *28* (4), 721–722.

(176) Higgins, D.A.; Barbara, P.F. *J. Phys. Chem.* **1995**, *99*, 3–7.

(177) Tatikolov, A.S.; Costa, M.B. *Chem. Phys. Lett.* **2001**, *346* (3–4), 233–240.

(178) Spitz, C.; Knoester, J.; Daehne, S. *Chem. Phys.* **2002**, *275* (1–3), 271–284.

(179) Maiti, N.C.; Ravikanth, M.; Mazumdar, S. *J. Phys. Chem.* **1995**, *99* (47), 17192–17197.

Appendix 1

Reduced graphene oxide (rGO) was obtained by a chemical reduction of GO (0.1 mg mL^{-1} water) using an excess of ascorbic acid (0.1 M) at pH 10 adjusted by NaOH. The reaction mixture was stirred and kept at 70 °C for 5 h until the brown suspension turned black. Subsequently, the suspension obtained was centrifuged at 12000 rpm (14986 rcf) for 30 min and washed with water several times in order to remove any excess of ascorbic acid. The wet solid was transferred into a Petri dish and dried in an oven for 24 h at 60 °C. Under mild sonication, the obtained rGO could be re-dispersed in water.

Appendix 2

The method of preparation of the GO-SnO_2-FTO, TMPyP-GO-SnO_2-FTO or ZnTMPyP-GO-SnO_2-FTO electrodes was as follows: A layer of SnO_2 was placed on a fluorine-doped tin oxide (FTO) glass electrode *via* a doctor blading method and received thermal treatment under an air atmosphere. The prepared samples were covered with graphene oxide via electrophoretic deposition. GO-SnO_2-FTO electrodes were left overnight in porphyrin baths (60 μM) and dried in air to achieve porphyrin functionalization on their surface.

Appendix 3

Preparation of the TMAP/GO hybrid

3 ml of $TMAP^{4+}$ (1.1 µM) aqueous solution (pH 6.2) was mixed with 10 µl aqueous GO suspension (3 mg mL^{-1} GO) resulting in a light brown suspension. The mixture was centrifuged at 12000 rpm (14986 rcf) for 2 hours. The obtained supernatant was light yellow and a precipitate of dark brown $TMAP^{4+}$/GO powder was obtained by drying the wet precipitate in an oven for 14 h at 80 °C.

Table of Figures

Table of Schemes

Table of Tables